

BLL ID NO. - D 67336/86

LOUGHBOROUGH  
UNIVERSITY OF TECHNOLOGY  
LIBRARY

AUTHOR/FILING TITLE	
CHEIKH - MERI, H	
ACCESSION/COPY NO.	
010542/01	
VOL. NO.	CLASS MARK
	T
<del>FOR REFERENCE ONLY</del>	
C1 JUL 1988	
- 3 OCT 1997	
28 NOV 2000	
FOR REFERENCE ONLY	

001 0542 01

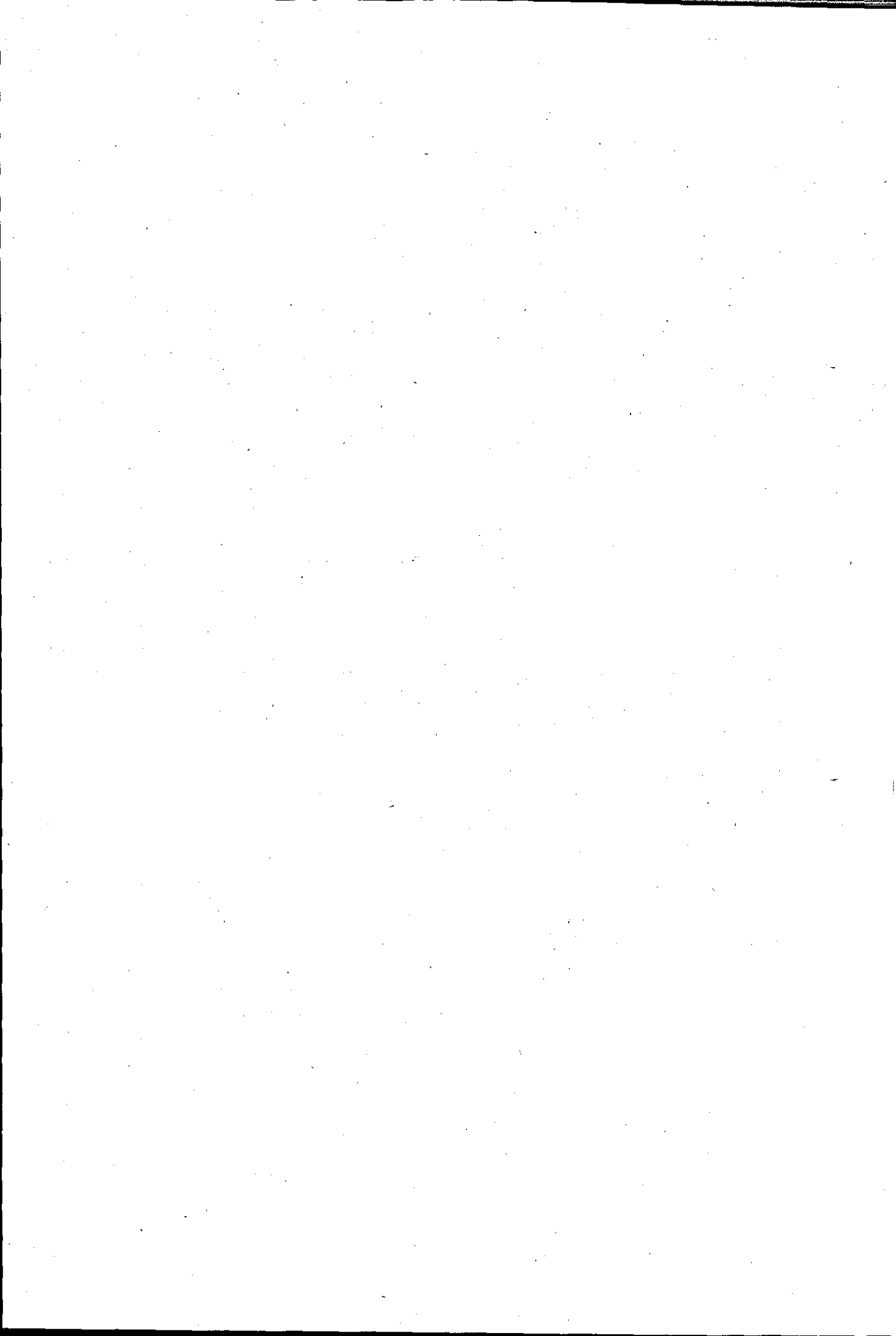


This book was bound by

**Badminton Press**

18 Half Croft, Syston, Leicester, LE7 8LD

Telephone: Leicester (0533) 602918.



THE PRODUCTION AND EVALUATION OF A PRESSURE DIECAST,  
GRAPHITIC, HYPEREUTECTIC ALUMINIUM-SILICON ALLOY

by

H. CHEIKH-MERI

B.Sc, M.Tech.

A Doctoral Thesis submitted in partial fulfilment of the  
requirements for the award of Doctor of Philosophy of the  
Loughborough University of Technology

Loughborough University of Technology Library
Date April '86
Class T
Acc. No. 010542/01

## SYNOPSIS

The principal aim of this research was to utilize the newly-developed technology of processing partially solid alloys as a means of dispersing untreated graphite particles in a hypereutectic aluminium-silicon alloy. The optimum conditions for the dispersion and retention of graphite particles in the alloy were evaluated together with the suitability of cold chamber pressure diecasting as a method of producing castings from the alloy composite. The second aim of the research was to obtain information and data on the mechanical and tribological properties of the hypereutectic aluminium-silicon alloy (LM30) containing graphite particles, since the presence of graphite was expected to contribute low frictional losses and improved wear resistance to the already exploited properties of excellent corrosion resistance and thermal conductivity. By introducing the graphite particles into a vigorously stirred, partially-solid alloy slurry the particles were readily dispersed within the slurry. Providing that there was a sufficient volume fraction of solid, the particles of graphite were mechanically entrapped within the slurry preventing their rejection from the melt. The equipment used for production of the alloy composite consisted of a rheocasting unit mounted on the tie bars of a EMB No. 10 cold chamber pressure diecasting machine.

The LM 30 alloy used for the investigation was designed specifically for a diecast aluminium alloy automobile-engine cylinder block capable of operating without the usual cast iron cylinder liners. Potentially its application extends to a wide range of castings in which a combination of wear resistance with lightness is required. Such alloys possess the valuable characteristics of high fluidity and freedom from hot-shortness. The alloy used in this investigation was obtained in the form of commercial ingots.

A commercially-available synthetic graphite was used to evaluate the influence of both graphite particle size and addition level on the mechanical properties and wear characteristics of the alloy. Successful dispersion of the

graphite was obtained for particles in the size range 75 $\mu$ m to 355 $\mu$ m. Sufficient alloy for each experiment was melted in an electric-resistance heated furnace then transferred to the preheated rheocasting unit and stirred until the temperature of the alloy in the slurry zone reached the predetermined temperature. The graphite particles were then introduced to the alloy slurry through the base of the hollow stirring rotor. The composite alloy slurry was discharged from the rheocasting unit and transferred via the heated launder to the shot chamber of the pressure die casting machine. The slurry was injected immediately and the casting allowed to solidify completely before ejection from the die.

The mechanical properties evaluation showed that strength and ductility were reduced in an alloy which contained graphite. Pin on disc wear tests showed that graphite additions resulted in less wear, reduced coefficient of friction, reduced steady running temperature and reduced damage to mating components.

## ACKNOWLEDGEMENTS

The author wishes to record his acknowledgements to the following:

Professor R.J. Sury, Head of the Department of Engineering Production and Director of Research, for providing the opportunity and facilities necessary to carry out this work.

Dr. A.J. Clegg and DR. A.A. Das, Research supervisors, for their kind encouragement and guidance throughout the course of this investigation.

Mr. R. Pearson, Research technician, for engineering skills and technical support.

Mr. B.J. Goodman, Mr. R. Abrey, Mr. A. Haigh and Mr. R. Parker, technical staff for their assistance with experimental work.

Dr. D.H. Ross, Experimental Officer in the Department of Materials Engineering and Design, for conducting the Electron Probe Microanalysis.

## CONTENTS

	<u>PAGE NO.</u>
CHAPTER ONE: Introduction	1
CHAPTER TWO: Background And Literature Survey	
2.1 - Aluminium-Silicon Alloys And Their Applications.	9
2.2 - Pressure Die Casting.	13
2.3 - Methods Of Cast Composite Production.	16
2.4 - Rheocasting And Compocasting.	23
2.5 - Significance Of Wear And Methods Of Testing Alloys.	31
2.6 - Summary And Proposed Approach To Research.	44
CHAPTER THREE: Design Of Equipment	
3.1 - Compocasting Unit: Design Modification, Manufacture And Evaluation.	60
3.2 - Die Casting Equipment.	64
CHAPTER FOUR: Materials And Experimental Procedures	
4.1 - Materials Used.	71
4.2 - Alloy Preparation.	73
4.3 - Composite Alloy Production.	73
4.4 - Composite Alloy Evaluation.	96
CHAPTER FIVE: Results And Observations	
5.1 - Results Of Composite Alloy Production.	110
5.2 - Results Of Composite Alloy Evaluation.	110
5.3 - Qualitative Analysis Of Graphite Content.	123
5.4 - Observations Of Composite Alloy Production.	124
5.5 - Observations Of Composite Alloy Evaluation.	126

## CONTENTS

	<u>PAGE NO.</u>
CHAPTER SIX: Discussion	
6.1 - Discussion-Composite Alloy Production.	156
6.2 - Discussion-Composite Alloy Evaluation.	167
CHAPTER SEVEN: Conclusions	185
CHAPTER EIGHT: Suggestions For Further Work	188
REFERENCES:	191
APPENDICES:	
Appendix 1: Design And Manufacture Of Equipment Used In Compocasting.	205
Appendix 2: Design And Manufacture Of The Pressure Diecasting Die.	210
Appendix 3: Semi-Solid Alloy Processing Variables And Their Calculation.	214
Appendix 4: Mechanical Properties Calculations.	218
Appendix 5: Tribological Properties Calculations.	220
Appendix 6: Graphite Calculation.	222
Appendix 7: Figures.	223

## LIST OF TABLES

<u>TABLE NO.</u>	<u>PAGE NO.</u>
1 - Relationship between power consumed and time for three phase induction motor on free load.	79
1A - Relationship between rheocasting process variables and viscosity observations.	82
1B - Relationship between the compocasting parameters and viscosity observations.	88
1C - Relationship between pressure diecasting parameters and casting integrity.	92
2 - Primary silicon particle counts.	98
3 - Tensile test results for control castings.	148
4 - Tensile test results for graphitic alloy castings.	149
5 - Hardness test results for control castings.	150
6 - Hardness test results for graphitic alloy castings.	151
7 - Pin on disc wear test results for control castings (dry friction).	152
8 - Pin on disc wear test results for graphitic alloy castings (dry friction).	153
9 - Pin on disc wear test results for control castings (lubricated friction).	154
10 - Pin on disc wear test results for graphitic castings (lubricated friction).	154
11 - Quantitative analysis of graphite content.	155

12 - The effect of graphite addition level on the increase in load applied.	182
13 - The effect of graphite addition level on the tribological properties of LM30 alloy.	183
14 - The effect of poor lubrication conditions on the tribological properties of LM30 alloy.	184

## CHAPTER ONE

### INTRODUCTION

The widening of markets and the increasing demands for goods as the affluent society progresses will favour mass production methods that can be fully automated, keeping the processing time and finishing costs to a minimum. From the knowledge of the modern manufacturing processes for metal products, the logical trend must therefore be the search for a process capable of converting liquid metal directly into the finished product conforming as closely as possible to the final configuration, accuracy and the surface finish necessary and maximising mechanical properties. The process should also be adaptable to differences in casting design and common metallurgical features.

#### 1.1 PRESSURE DIE CASTING OF SEMI-SOLID SLURRY

Conventional pressure die casting meets most of the above requirements of high productivity which enables it to compete with stamping and forging processes. Furthermore it has the capability of producing more detailed components with much closer dimensional control and less subsequent machining in comparison with sand castings and permanent mould castings. Conversion costs from basic ingot are lower and the pressure die casting process is more tolerant of input metal having higher levels of impurity and therefore lower cost. The tooling costs for pressure die casting are usually much higher than for either sand or permanent mould but tools can usually be amortized over hundreds of thousands of castings <sup>(1)</sup>.

The new developments in the pressure die casting process, such as the use of disposable cores, broaden the basis for the use of pressure die casting in the automobile industry <sup>(2)</sup>.

Components which require disposable cores such as intake manifolds and cylinder heads, currently made by either the sand or semi-permanent mould processes, could be produced by pressure die casting.

Pressure die casting is used when <sup>(3)</sup>: a large quantity of identical components is needed (the minimum to be economic

is 5,000 to 10,000 depending on the complexity of the die); the design of component is complex and is expensive to machine; machining, assembly or surface finishing accounts for an appreciable amount of the final cost; a reduction in investment in machine tools and floor space is needed; and undercuts and intricate holes can be produced by means of sliding permanent cores.

The metals most often die cast are zinc alloys, aluminium alloys and magnesium alloys. All use steel moulds which last for hundreds of thousands of castings in the case of zinc alloys, and about 50,000 to 250,000 shots for aluminium and magnesium alloys. Dies used for higher melting point alloys may only last for 15,000 to 50,000 shots <sup>(4)</sup>.

While pressure die casting is certainly desirable from an economic point of view, the process does have its limitations. These are <sup>(3)</sup>: Thermal die fatigue due to the injection of superheated liquid metal which results in a sudden increase in die temperature; die design is complex due to the need to incorporate a weir in the die to prevent the liquid metal in the shot sleeve entering the die cavity prematurely; and the most important is that castings produced are porous internally and die castings cannot be heat treated without blistering the casting skin, which explains why pressure die cast components are not as strong as forgings.

These deficiencies had led to the development of a new technique which is claimed to overcome the above disadvantages. The technique utilizes semi-solid alloy slurry instead of superheated liquid alloy. This can be achieved by heating the alloy to a temperature between the solidus and liquidus and then agitating it vigorously. This converts the material into a slurry in which the dendrites are broken down and globularise to form rounded particles (this technique is known as "rheocasting"). If agitation ceases, the rounded particles tend to form agglomerations surrounded by liquid phase and the resultant slurry has a relatively high viscosity enabling it to be handled as an apparent solid. The semi-solid slurry is thixotropic and

when sheared as it passes through the gate in a die casting machine will flow like a viscous liquid. When it is injected into the die cavity less turbulence occurs and die castings of improved soundness may be produced. The absence of porosity allows heat treatment operations to be carried out without blistering of the casting skin. In the new process the slurry can be cast in the form of bars of accurate weight which can later be reheated to a temperature at which they are half molten (soft solid). When placed in the shot sleeve of the die casting machine and pressurised the billet is converted to a slurry which flows in a non-turbulent manner into the die. This technique is known as "thixocasting".

## 1.2 THE SEARCH FOR ECONOMIC MATERIALS

Another demand is for light weight, energy efficient materials and this has increased activity in the material community to develop specific alloys and processing techniques to meet this new challenge.

The increasing use of aluminium alloy castings, albeit at the expense of ferrous castings, in the automobile industry is a response to this demand. Whilst aluminium alloy castings are supplied to most sectors of the market, the transport sector consumes about 60% of the UK output and other countries are equally dependant on this market <sup>(5)</sup>. It has been estimated that every 250lb (113kg) weight saving will improve a car's fuel consumption figure by 1 mpg (0.35km/litre) <sup>(6)</sup>. Although the greatest potential for weight saving exists in the body shell, aluminium alloy castings can and do contribute to a weight saving in the power train and wheels. During the past thirty years almost every possible cast iron component in the power train has been tried and proven in aluminium alloy castings. With few exceptions diecast parts have proven functionally adequate, even though the economic advantage may at the time have been marginal in some cases <sup>(7)</sup>. However, the continued emphasis on fuel economy and the almost mandatory requirement to use aluminium alloy transmission parts to ensure proper weight distribution in front-wheel drive cars <sup>(7)</sup> will ensure an increase in the demand for aluminium alloy castings in the current decade.

The weight saving potential of aluminium alloy castings over cast iron is demonstrated by the following examples <sup>(6)</sup>. A typical cylinder block and head in cast iron weigh about 250lb (113kg), in aluminium alloy they would weigh about 80lb (36kg). A gear case and clutch housing in cast iron weigh about 50lb (22½kg), in aluminium alloy they would weigh about 15lb (7kg). In the USA it was estimated that there was only 61½lb (28kg) of aluminium alloy castings/vehicle in 1973, by 1979 this figure had risen to 75lb(34kg) and in 1982 it was 89lb (40kg). This trend is expected to continue, in 1985 it is expected to be 102lb (46kg) and by 1990 120lb (54½kg). All these figures exclude the possible introduction of aluminium alloy cylinder blocks <sup>(8)</sup>. The cylinder block represents the heaviest iron casting in the power train and consequently the greatest weight saving potential. However, whilst aluminium alloy cylinder blocks have been used in production, they have generally featured cast iron cylinder liners with an associated manufacturing cost penalty. The combination of Reynolds Metals alloy 390 (BS 1490: 1970: LM30) technology and the General Motors Acurad Process resulted in the use of an aluminium alloy cylinder block in the Chevrolet Vega 2.3 litre engine in the USA <sup>(9)</sup>. Although the engine was withdrawn in the USA the technology is being used successfully in European cars such as the Porsche 928, Daimler Benz 450 SLC and Rolls-Royce Camargue <sup>(10)</sup>. However, attainment of the necessary cast structure <sup>(11)</sup> and the special surface etching of the bore, together with the piston coating procedure <sup>(12)</sup>, have resulted in an increased manufacturing cost which can only be accepted in expensive luxury and performance cars.

### 1.3 BEARING MATERIALS

Light weight bearing materials have been sought since at least the 1930s. Much of the development during this period has been of aluminium alloys which exhibit a high strength-to-weight ratio and excellent resistance to wear, corrosion and scoring. A relatively soft alloy is required to ensure good characteristics and this criterion has contributed to the development of Al-Sn and Al-Cu-Sn alloys containing very high percentages of alloying elements <sup>(13)</sup>. Recent emphasis placed on the conservation of scarce materials such as tin,

lead, copper and zinc has diverted the search to newer bearing materials based on more abundantly available materials such as silicon which is cheap and commercially available. As a result, certain Al-Si, Al-Cu and Al-Zn alloys containing relatively lower percentages of alloying elements such as copper, magnesium, nickel...etc. and higher percentages of silicon such as hypereutectic aluminium-silicon alloys have been developed for bearing applications. Bearings made of these alloys performed well under normal conditions but were found unsuitable for limiting lubrication conditions <sup>(14)</sup>. Composite materials such as copper alloy-graphite <sup>(15)</sup> and iron alloy-tungsten disulphide made by powder metallurgical techniques, have been successfully used in bearings, but their commercial exploitation remains strictly limited due to the dimensional limitation of the production techniques. In addition, the powder metallurgy route is expensive. These limitations have been overcome by the recent development of techniques such as "compcasting" for making as-cast metal particulate composites. In compocasting the slurry nature of rheocast metal alloy (see 1.1) permits the addition and retention of particulate material. The composites are made starting with a vigorously agitated, partially solidified metal alloy. Then, particulate materials (eg. graphite, silicon carbide, glass beads...etc.) are added whilst agitation continues. Providing that there is a sufficient volume fraction of primary solid particles in the alloy, the added particles will be mechanically entrapped within the alloy slurry which will prevent their rejection from the melt. The resultant composite slurry has a low viscosity in comparison to the superheated liquid alloy normally used for casting. The composite alloy slurry can be successfully shaped by pressure-assisted processes such as squeeze casting or pressure die casting, in addition to the conventional casting processes.

Using this technique, several aluminium-based composites have been developed, such as aluminium alloy-graphite <sup>(16)</sup> and aluminium alloy-ceramic <sup>(17)</sup>. From these new materials, aluminium-graphite composites have created considerable interest because of their resistance to wear and scuffing <sup>(18,19)</sup>. Work on such composites has indicated that bearings

made of graphitic aluminium alloys can work satisfactorily even under marginal lubrication conditions (20).

#### 1.4 BEARINGS IN AUTOMOBILE INDUSTRY

A bearing can be regarded as a mechanism for transmitting a load between two surfaces in relative motion. Thus, ever since the invention of the wheel, bearings have played a key role in transport. The wide spectrum of loads and speeds and the high reliability which is demanded from modern motor vehicles make bearing performance a key factor in the overall behaviour of the engine or system.

The widespread introduction of the automobile provided a spur to bearing development and led to the introduction of bearing systems capable of sustaining higher speeds and loads to meet the requirements of modern engines. Reliability has increased dramatically; most car owners would feel aggrieved if their car bearings or pistons had to be replaced during their period of ownership, whilst running-in procedures demanded by modern engines are far less critical and irksome to the driver than in the past. The major need for change in current technology over the last 20 years came as a response to both economical and social demands (21).

The general trends in engine technology require component surfaces to run under more difficult conditions, particularly as the quality of fuel decreases. There is also a requirement to reduce friction and oil consumption with no accompanying loss in wear resistance. Castings are widely used for applications in the internal-combustion engine that require good friction and wear resistance and their use is expanding as the diesel engine becomes even more widely used. Critical components which are cast include: piston rings; cylinder liners; the camshaft and tappets; and the crankshaft and its associated bearings (19). Cast iron in one form or another is by far the most widely used material and specific treatments have been applied to extend the life and operating efficiency of these components. Piston rings are quite commonly electroplated with chromium or plasma sprayed with chromium carbide, cylinder liners are finished by cross

honing to produce a plateau/groove finish that enhances oil retention. The situation is becoming even more complex as other materials, including sintered iron rings cast aluminium alloy liners, and special surface treatments, including laser treatments, are becoming more widespread (10). The use of aluminium alloy bores in automotive engines dates back many years and their development has followed two main paths based on providing either the piston or the liner with a hard, more wear resistance overlay. In the first of these technologies the liner is made in a material with a high silicon content (17-20%) and machined on its inside diameter using a special technique to display the primary silicon polyhedra, so that they act as a hard and wear-resistant support against the abrasive action of the rings (22). Aluminium-silicon alloys fulfil this requirement, in combination with good casting characteristics and freedom from hot shortness. However, a limitation exists in their tribological performance in the form of a tendency to scuff in conditions where lubrication is sparse or intermittent (23).

The principal aim of this research was to produce a bearing material which will permit direct piston/liner contact, the use of traditional piston alloys and the use of conventional liner finishing methods. This is very important as it allows those who undertake engine conversions to enlarge the bores by a simple diamond boring operation without chemical finishing, which is not possible with a hard overlay.

It has been reported that the inclusion of evenly dispersed graphite particles in hypereutectic aluminium-silicon alloys improves their tribological properties by providing solid lubrication (24). The primary silicon polyhedra provide the support and the graphite provides the lubrication to enable a direct piston/liner contact to be obtained.

The major difficulty in the preparation of cast aluminium-graphite particle composites by a liquid metallurgy process is the apparent non-wettability of graphite by liquid aluminium alloys and hence the rejection of graphite particles from the melt. Several attempts have been made by other

researchers to solve the problem of non-wetting between graphite and liquid aluminium alloys, but most of these methods have proved costly since they require either a regular supply of metal coated graphite particles, or very high power ultrasonic probes. The research reported in this thesis utilized the newly-developed technology of processing a partially solid hypereutectic aluminium-silicon alloy as a method of dispersing uncoated and untreated graphite particles in the alloy. The optimum conditions for the dispersion and retention of graphite particles in the alloy were evaluated together with the suitability of cold chamber pressure die-casting as a method of producing castings from the alloy composite.

The results of an exploratory investigation to establish the effect of graphite particle size and the level of graphite additions on the mechanical properties and wear characteristics of LM30, the hypereutectic aluminium-silicon alloy, has been presented and discussed in this thesis.

## CHAPTER TWO

### BACKGROUND AND LITERATURE SURVEY

#### 2.1 ALUMINIUM-SILICON ALLOYS AND THEIR APPLICATIONS

The growth in consumption of aluminium during the last thirty years has been faster than that of many other metals including iron and copper. The reasons for this are numerous but the major ones are: its high strength to weight ratio; excellent corrosion resistance; ease of fabrication; high electrical and thermal conductivities; low cost in comparison with other non-ferrous materials (Foundry Trade Journal price list) and high scrap value. These properties, together with its relatively stable price and virtually inexhaustible supply in the foreseeable future, are encouraging metallurgists and engineers to find new ways by which the full potential of this versatile metal may be realised. One example of this is the continued research and development efforts in applications where the bearing properties are of primary importance.

The commercial aluminium alloys employed for casting purposes contain various percentages of one or more alloying elements, depending on the casting process and the mechanical and physical properties required. The alloying elements such as copper, magnesium and silicon are partially dissolved in aluminium to form a solid solution of  $\alpha$ -Al, whilst the surplus forms a eutectic mixture of  $\alpha$ -Al and  $\text{CuAl}_2$ ,  $\text{Al}_3\text{Mg}_2$  and silicon respectively (25). Silicon is probably one of the least expensive alloying additions commonly made to aluminium. Silicon improves castability, increases strength to weight ratio, decreases the coefficient of thermal expansion and imparts wear resistance to aluminium (23). Aluminium-silicon alloys form the largest family of the aluminium base casting alloys, ranging from simple binary to more complex alloy systems. Structurally, aluminium-silicon alloys can be divided into three groups (26):

- (a) hypoeutectic, in which the matrix  $\alpha$ -Al is the major constituent, with smaller amounts of dispersed eutectic and/or intermetallic compounds in the matrix;

- (b) eutectic, in which the eutectic mixture constituent predominates and contains smaller volumes of excess  $\alpha$ -Al and of the other compounds;
- (c) hypereutectic, in which the hypereutectic phase and other compounds are dispersed in the eutectic.

An important group of aluminium-silicon alloys has been formed for the automotive industry. A380, BS1490 (1970) LM24 for die casting, A332, BS1490 (1970) LM13 for pistons and 319, BS1490 (1970) LM25 for sand and permanent mould (27).

The hypereutectic aluminium-silicon alloy 390, BS1490 (1970) LM30 has been developed recently for casting aluminium monoblocks. This alloy has good fluidity over its wide solidification range, and provides large numbers of primary silicon polyhedra on solidification. These precipitates, when brought into bas-relief, by any of several methods, provide a surface with excellent sliding friction properties (28). The silicon surface is extremely wear resistant and from four to five times as long-lasting as traditional cast iron cylinder surfaces (22). In addition this alloy has a low coefficient of thermal expansion, superior fluidity in thin sections and high thermal conductivity (29). The alloy strength can be increased with T<sub>6</sub> and T<sub>7</sub> Tempers, and little loss of strength occurs at temperatures up to 400°F (205°C), even after holding at temperature for extended periods of time (29).

The application of aluminium-silicon alloys for cylinder liners is expanding because of attempts to reduce the weight of automobiles to improve fuel efficiency. Aluminium-silicon cylinder blocks have been used in many production automobiles from as early as 1960. The development of the Reynolds 390  $\approx$  LM30 alloy for the Chevrolet Vega and the use of an etch treatment to leave the silicon particles standing proud of the load-bearing surface was the first success, making it possible to omit a cast iron liner. Considerable economic savings are possible if the aluminium alloy surface itself can be used directly as the bearing surface (6). It has been reported that the effect of cooling rate during solidification or structural modification do not significantly affect the wear

resistance of the hypereutectic aluminium-silicon alloy but the silicon content exerts a significant influence on wear rate and transition load<sup>(23,30)</sup>, see Figs. 1 and 2.

For many engineering applications, such as piston and cylinder arrangements, it is necessary to run aluminium-silicon alloys in sliding contact with each other. However, unless lubricating conditions are ideal, they tend to seize or gall. The problem becomes more intense in conditions of boundary lubrication<sup>(23)</sup>. Such conditions can occur in almost all cases of sliding contact. Various solutions have been tried to solve this problem using surface treatments and coatings<sup>(22)</sup>, these methods have proved effective but expensive.

The 390 alloy  $\cong$  LM30 with a silicon content of 16-18% was developed for aluminium cylinder blocks. This composition provides large and well distributed quantities of primary silicon on solidification. Although the silicon surface provided by this alloy is extremely wear resistant the most significant problem was that of scuffing of the bore on cold start<sup>(31)</sup>.

An alternative approach was undertaken by Bruni and Iguera<sup>(24)</sup> whereby nickel-coated graphite particles were incorporated into a hypereutectic aluminium-silicon alloy. Cylinders were produced from this alloy as a substitute for cast iron cylinder liners. Pistons and rings were identical to those used with the original cast iron cylinder liner. All Components were finished using a standard diamond boring operation with no special chemical treatment required. The authors stated that the graphitic aluminium-silicon alloy displayed superior wear and friction characteristics in all cases. A scuffing test was carried out and it was found that the properties of aluminium-graphite cylinders allowed the test to be extended to three times their normal duration. A further observation was that average power outputs were increased as a direct result of improved friction properties. Krishnan et al.<sup>(32)</sup> have stated that an aluminium-silicon-3wt% graphite particle composite piston in a 5hp single cylinder diesel engine could withstand an

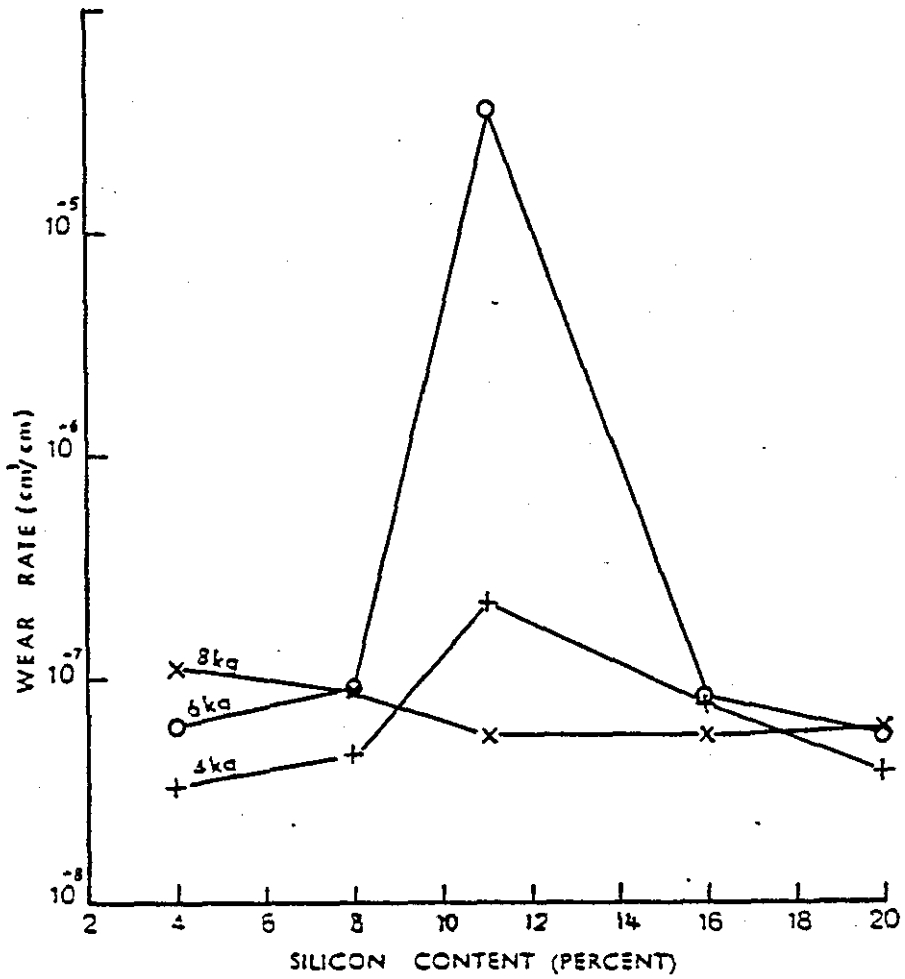


Fig. 1 - effect of silicon content on wear rate (Ref.23)

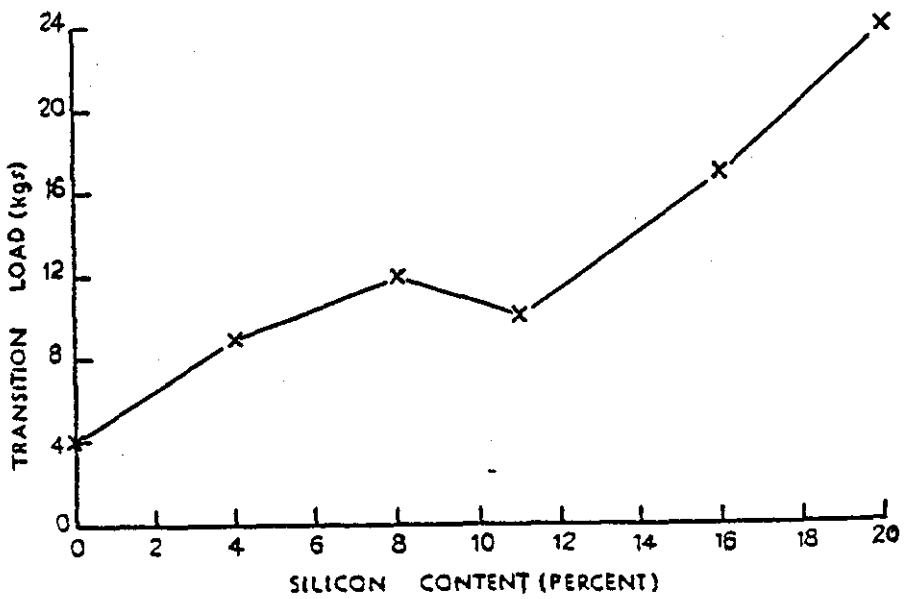


Fig. 2 - effect of silicon content on transition load (Ref.23)

endurance test of 500 hours without any apparent deterioration. The use of such a composite as a piston material resulted in: a reduction in the specific fuel consumption; considerable reduction in the wear of piston rings; reduction in the wear of the piston; and reduction in frictional horsepower losses, due to the continuous lubrication provided by graphite particles which were smeared on the bearing surface. Also higher damping capacity of the composite pistons and reduction in the coefficient of thermal expansion were achieved. The authors also stated that the wear test results indicate that graphitic aluminium-silicon alloys offer a promising material for automotive pistons. However, adoption of graphitic aluminium-silicon alloys in production engines may not have occurred as a result of difficulties in manufacturing components from such composites and the methods available at present for dispersing graphite may not be suitable for volume production.

## 2.2 PRESSURE DIE CASTING

One of the oldest methods of casting molten metal is by gravity pouring into sand moulds and this method, with many refinements, is still the single most important casting process. Methods for producing more precise castings, such as plaster casting or investment casting, are available but like sand casting they have the disadvantage that the mould must be destroyed to remove the casting.

The permanent mould processes, such as diecasting, enable the mould or die to be reused many times. Whilst the metal may be gravity poured into a permanent die, improvements in appearance and accuracy and reduced section thickness can be obtained by the application of pressure to force the metal into the die. Considerable improvement has been made in the evolution from the first manually operated plunger type die casting machine to the modern automatic plunger machines. Steel for dies has been refined to the stage at which economical die life is obtained with all the die casting alloys and rapid strides are being made in perfecting even more suitable die materials. Much progress has also been made in die casting techniques during the last five decades.

The control of casting variables, such as metal and die temperatures, pressures and shot speeds, is much advanced.

Pressure die casting is undoubtedly capable of mass producing components requiring little or no machining, an advantage which none of the other metal die processes can offer. The most serious matter is that conventional pressure die casting produces castings which are porous internally, much of the porosity in die castings is die cavity atmosphere (nitrogen and/or volatilized lubricants...etc.) compressed under the high pressure imposed during solidification. When a die casting is solution heat treated the compressed gasses in the pores expand at the same time that the metal surrounding them is softening and the casting blisters <sup>(2)</sup>. Much attention has been paid to avoiding defects like air entrapment and shrinkage porosity, inherent to the process. Methods have included flushing the die cavity with inert gas or oxygen and evacuating the die cavity prior to injection <sup>(33)</sup>. However, these are only partially successful, owing to capital cost and difficulties in operation <sup>(2)</sup>.

Acurad is a process developed by the General Motors Company for pressure die casting. The process utilizes two concentric plungers Fig.3. The first plunger, which is relatively slow speed, squeezes the molten metal into the die cavity. At this stage the alloy is partially solidified and most of the shrinkage and porosity holes has already formed, the other plunger now operates to complete the action of the first plunger by forcing more molten metal into the die cavity to fill these holes and produce sound castings <sup>(34)</sup>.

Research carried out at M.I.T. in the USA <sup>(35)</sup> and Fulmer Research Laboratories in the UK <sup>(3)</sup> has showed that it is possible to deform and shape metal in the semi-solid state between the liquidus and solidus provided the structure of the metal is controlled. Semi-solid metal injection casting is a new process for making precision die castings which, it is claimed, overcomes the defects associated with conventional pressure die castings produced from superheated liquid metal. The process uses a semi-solid aluminium alloy slurry in a

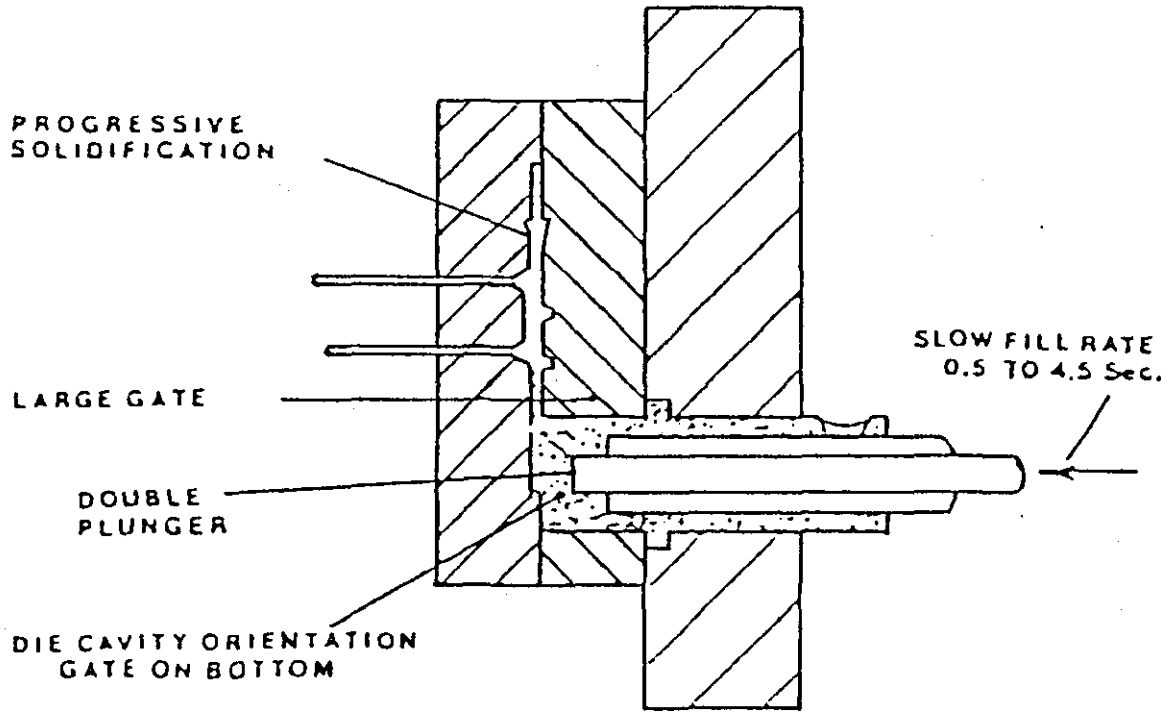


Fig. 3 - Principle of the ACURAD process (Ref.34)

thixotropic condition, such an alloy can be handled as if it is a rather soft solid, but when sheared by the runner and the ingate of the die it will flow without turbulence as a non-newtonian fluid. This would allow the entrapped gasses in the die cavity to escape through the die vents and hence sound castings can be obtained.

The design of dies can be simplified and the lower temperature of the slurry compared to liquid metal means that half of the Latent heat and all the superheat has been removed, thus the lower die temperature results in less thermal shock and faster cycle times, so improving the productivity of the die casting process<sup>(1)</sup>.

Comparison between semi-solid pressure die casting and the "ACurad Process" shows no difference at all in the way they process the alloy, except in the first method, most of the shrinkage occurred before injection, whilst in the latter, the shrinkage occurred after the first injection (ie. in the shot chamber of the die casting machine). From the economic point of view, the semi-solid pressure die casting process appears to be less expensive than the "ACurad Process", since there is no need for superheating the alloy and conventional pressure die casting machines can be used. The semi-solid casting process is considered in greater detail at a later stage in this review.

### 2.3 METHODS OF CAST COMPOSITE PRODUCTION

The most direct route for the production of graphitic particulate aluminium composites would seem to be to add graphite powder to the molten metal and cast the resulting composite melt. The major difficulty with such an addition has been reported to be the lack of wetting between graphite and aluminium leading to the rejection of graphite as soon as it is introduced into the melt. The contact angle of aluminium with graphite is  $160^\circ$  and it is reported to remain non-wetting between the melting point of aluminium and  $1080^\circ\text{C}$ <sup>(36)</sup>.

Attempts have been made to solve the problem of non-wetting

between graphite and molten aluminium through several approaches. The main methods are:

- (1) Nickel and copper coated graphite particle injection by gas stream.
- (2) The vortex method.
- (3) Pellet method.
- (4) Ultrasonic method.
- (5) The briquette method.
- (6) Infiltration of coated graphite by molten aluminium alloy.
- (7) Compcasting method.
- (8) Other methods.

### Review of Process for the production of graphitic aluminium alloys

- 1 - Injection into the melt of nickel coated graphite powder in a stream of nitrogen gas.

This method was first described by Badia et al.<sup>(37)</sup> in 1969. A nickel coated powder was used which allowed nickel to be wetted by molten aluminium alloy. A special gun was developed with a hopper to contain coated powder and allow it to fall by gravity into a nitrogen gas stream. The melt, at a temperature of 676-732 °C, was stirred whilst the nozzle of the gun was placed beneath the melt surface. The authors described a mechanism whereby a nitrogen bubble formed in the melt.

The bubble rose slowly to the surface whilst its size increased due to the decreasing pressure head. Coated graphite particles came into contact with the bubble-melt interface and either dispersed into the melt or were rejected. Transfer of graphite took place if conditions were energetically favourable and if graphite came to the interface. The necessary condition for transfer was said to be a function of surface energy and density. After transfer, the nickel dissolved in the molten aluminium, at this point vigorous stirring of the melt was necessary to ensure that the graphite did not float. Casting the composite in a permanent mould was essential to ensure a high cooling rate and so prevent graphite flotation. Badia<sup>(37)</sup> gave examples of automobile

pistons which were cast in this way and indicated, with photographs, a regular dispersion of graphite. He also stated that castings could be remelted but that graphite tends to be lost after successive remelts. This phenomenon has been confirmed by Krishnan et al.<sup>(32)</sup>.

However, the nitrogen stream had useful secondary effects in degassing the melt and protecting the nickel coated graphite powder from oxidation. The authors also claimed that stirring and mixing were sufficient to prevent graphite segregation in the melt, but subsequent publications did not confirm this finding<sup>(38-40)</sup>. Later work reported that the gas injection method led to a large proportion of rejected graphite<sup>(16)</sup>, and the use of nickel coated particulate resulted in the formation of an intermetallic compound ( $\text{Ni Al}_3$ ) within the casting which caused embrittlement<sup>(41)</sup>. The copper coated method follows the same route. Surappa and Rohatgi<sup>(41)</sup> have reported that up to 15wt% of graphite particles could be introduced. In addition to the disadvantages mentioned above, the presence of copper in large quantities in the melt resulted in inferior corrosion resistance and, with both copper and nickel coating, both elements tend to oxidise by exposure to air (due to the flotation of graphite particles during the injection) which resulted in the rejection of the oxidized particles, because both copper and nickel oxides are not wet by molten aluminium.

## 2 - The vortex method

This involves stirring the melt to create a vortex into which the coated graphite particles could be placed and so dispersed. Work published in 1971 and carried out by Badia et al.<sup>(16)</sup> concerned the development of the "vortex method" and also the use of copper-coated graphite particles. The process for copper coating was described by Pai et al.<sup>(42)</sup>

The "vortex method" consisted of heating the aluminium alloy to a completely liquid temperature. Stirring was then introduced using an impeller powered by an electric motor. The driving shaft of the impeller was usually inclined at an angle of  $20^\circ$  to accenuate the formation of a vortex within

the liquid. Graphite powder, normally nickel coated, was then introduced to the vortex and was pulled down into the melt and subsequently dispersed evenly throughout the melt by the stirring action. To optimise the performance of the impeller a simulation was used which involved using a mixture of red polypropylene powder in water. These two substances offered a similar density relationship to liquid aluminium alloy and graphite. The extent of mixing could be easily seen because the powder was red. Examples were given of pistons, bearings, and other components, all having been cast in permanent moulds. The vortex method was claimed to offer better graphite recovery than the gas injection method and also the impeller could be controlled to ensure predictable graphite content and dispersion. Graphite segregation, due to flotation, could be put to good use to provide areas of high graphite content within a casting which would also contain more ductile, graphite free areas. This could be achieved by control of cooling rates and mould orientation. Surappa et al.<sup>(41)</sup> published details of the use of copper coated graphite for the production of graphitised aluminium alloys.

A later development of the vortex technique was described by Krishnan et al.<sup>(43)</sup> in 1981 and termed the "UPAL" process. The mixing technique was similar to that described before, but the graphite did not require a metallic coating because of the special heat treatment for the graphite particles which made this unnecessary. This consisted of heating the graphite particles to 400° C for one hour prior to stirring and was thought to remove all traces of adsorbed gases and moisture from the graphite surface and in doing so, improve wettability. The authors also stated that if temperature exceeds 400° C, severe oxidation is encountered. However, there is no indication for graphite oxidation at 400° C. Alloying elements such as silicon, copper and magnesium have been reported to aid the dispersion of graphite particles in aluminium alloy melts and significantly increase the recoveries of graphite particles in the castings. Examples of cast pistons and liners were shown which were produced by this technique. The UPAL process was claimed to offer a reduction in cost of composite production, although producing the

composite material by this method required an additional process (graphite treatment). Furthermore heat treatment of graphite might affect its lubrication property as a solid lubricant especially in dry friction.

### 3- The Pellet Method

The process involves the use of a pellet compact of aluminium alloy powder and coated graphite powder. This method was put forward by Pai and Rohatgi<sup>(44)</sup> in 1978. In this paper the authors stated that both the gas injection method and the "vortex method" suffered a problem during the transfer of the graphite particles from the air or the gas bubbles into the bath of the molten metal. Using the pellet method this problem was overcome since the pellet was already under the surface of the molten metal, being held there in a metal cup. The pellets were prepared by producing a powder compact of aluminium and coated graphite powder in the ratio of 1:2, with a green density of between 2.4 and 2.6g/cm<sup>3</sup>. The pellets, 20mm in diameter and 50mm in length, were produced at a pressure between 3 and 5 kg/mm<sup>2</sup>. Several pellets were plunged into the melt using an inverted cup whilst stirring. Expanding gases entrapped between the powder particles and expanding aluminium powder become heated to the melt temperature resulting in disintegration of the pellet and dispersion of graphite throughout the melt. The authors also stated that the presence of silicon in the melt was found to give higher recoveries of graphite, probably as a result of silicon forming a metastable phase with graphite, or alternatively, silicon may have become adsorbed on the surface of the graphite particles reducing their flotation rate in the melt. It was also found that occasionally places in castings were found where graphite was not evenly dispersed, perhaps due to incomplete disintegration of the pellets. The authors also stated that the pellet contains a layer of oxide of 1.5µm thick on aluminium powder which gets dispersed in the melt. The formation of the oxide layer is due to the contact between aluminium powder and air. However, the authors claimed that the oxide layer may be removed, but they did not say how since degassing is not permissible after graphite

injection and, bearing in mind that the density of aluminium oxide is about the same as molten aluminium, so aluminium oxides would be expected to stay suspended in the melt<sup>(33)</sup>. It was concluded that the pellet technique was suitable for use in foundries because less skill was required and good results were obtained. However, the use of copper or nickel coated graphite particles has been considered costly for producing composite materials.

#### 4 - The Ultrasonic Method

This method has been widely used for the production of aluminium alloy graphite fibre composites<sup>(45)</sup> and stems from the idea that graphite will not be wet by aluminium alloys due to the effect of adsorbed oxygen and water on the surface of the graphite particles..

Gorbunov et al.<sup>(46)</sup> subjected the melt to ultrasonic vibrations using a probe 2-5mm below the surface oscillating at a frequency of 15-20kHz. Uncoated graphite was introduced into a bath at a temperature of 20-25°C above the liquidus temperature resulting in a pasty mix. The temperature was then increased whilst the ultrasonic probe was slowly lowered to the full depth of the bath and left for 2-3 minutes to obtain additional degassing and to distribute the graphite particles more uniformly. Wetting was thought to be due to the combined action of cleaning by ultrasonic vibrations and surface and interface active elements, resulting in the formation of strong bonds. The graphite particles were claimed to be free from adsorbed gasses and various impurity films, and so the wetting was improved. The temperature of the composite had to be limited to ensure that graphite remained suspended within the melt which may have limited viscosity because it was stated that the most effective means of forming was semi-liquid stamping or pressure die casting with an enlarged ingate. However, the use of a high power ultrasonic probe make this process expensive for the production of composite materials.

#### 5 - The Briquette Method<sup>(47)</sup>

The General Motors Corporation of USA have patented a method

for producing graphitic aluminium castings. It consists of reacting nickel coated graphite particles with aluminium alloys at elevated temperatures in a non-oxidising environment to form a briquette consisting essentially of graphite particles and a discrete nickel-aluminium intermetallic phase in an aluminium matrix. The briquette can be immersed in an aluminium alloy melt where it melts and the graphite particles become suspended in the molten aluminium alloy by the convective forces in the melt. Although the author did not state that good graphite distribution was obtained by this method, he showed a microphotograph with some graphite particles distributed in the melt.

#### 6 - Infiltration of Coated Powder by Molten Aluminium Alloy

The Teikoku Piston Ring Company of Japan has patented a method for making "Lubricated" aluminium alloys<sup>(48)</sup>. In this method, graphite or boron nitride powder coated with nickel or copper, by vapour deposition or electroless plating, was infiltrated with molten aluminium and solidified to make "Self Lubricated Aluminium Alloys".

#### 7 - Compocasting

The process involves adding non-metals to a partially solidified, vigorously agitated slurry. The high viscosity of the slurry prevents particles floating, settling or agglomerating. This process will be described in detail later.

#### 8 - Other Methods

Singer<sup>(49)</sup> described a process involving the production of composite materials by co-depositing the matrix metal and the composite particles entrained in an inert gas. The principle of this method is that molten metals or alloys are atomised in an inert atmosphere to give a spray of liquid particles. The atomised liquid particles and the composite particles, such as graphite were directed onto a cooler surface where they impinge and flatten into the form of thin discs or plates. Although the author did not give much detail about the mechanisms of depositing the graphite particles or about the equipment used he stated that good interfacial contact

between the metal matrix and composite material was obtained.

Another method has been developed by Pechiney<sup>(50)</sup>. In this method cylinder liners of hypereutectic alloys were produced by powder metallurgy. In this method the optimum size of primary silicon can be achieved together with the addition to the matrix of a solid lubricant such as graphite. These liners can then be inserted in engine blocks produced from conventional alloys.

The reason that such methods are not common is because of the difficulties associated with them. The first method appears to be very slow and the components made by this method have limited dimensions and applications. In the powder metallurgy route the difficulties associated with the process are:

- (a) the lack of strength and the inferior wear properties due to the rapid oxidation of aluminium powder by air and
- (b) the difficulties in obtaining an even distribution of graphite in aluminium powder due to the difference in density between the two materials.

#### 2.4 RHEOCASTING AND COMPOCASTING

The methods described so far for producing composite material, required either coated graphite particles or special treatment of the melts or particles. This has led to processes which are costly or excessively time consuming and complicated for large scale production of components made from graphitic aluminium alloys.

At the M.I.T. in the USA, Flemings and his group developed a compocasting technique from their investigations into rheocasting. They found that metal alloys held at a temperature between the solidus and the liquidus and vigorously agitated exhibited an unusual non-dendritic structure<sup>(51)</sup>. Alloys in this condition could be cast at a temperature lower than their melting points. Compocasting<sup>(52)</sup> was a development in which particulate non-metallic material could be added to, dispersed and retained in a semi-solid alloy slurry. Reports make no specific reference to the inclusion of graphite particles in aluminium-silicon alloys by compocasting, but

it has been claimed that anthracite (carbon based material) can be included and so this method may offer a potential means of adding graphite. The advantage of there being no need to use coated or specially treated particles could be offered together with the established advantages of rheocasting<sup>(51)</sup>.

#### 2.4.1 Principle of Semi-Solid Processing

Until recently, almost all commercial metal-forming processes were carried out either in the fully solid or fully liquid condition. This is because solidification in most castings and ingots is dendritic. The growing dendrites form a continuous skeleton in the liquid-solid zone when the volume fraction of solid exceeds approximately 20%. Therefore, the alloy can neither be poured successfully, to allow solidification processing, nor can it be deformed homogeneously without cracking<sup>(53)</sup>. However, if the alloy in this state is vigorously agitated the structure tends to degenerate, converting the material into a low viscosity slurry due to the breakdown of the dendrites to form rounded particles. If the alloy is held without further agitation the rounded particles agglomerate and are surrounded by liquid phase. The slurry viscosity rapidly increases so that it can be handled as a solid. However, if vigorous shearing is again introduced the material regains its liquid-like properties.

Rheological slurries are thixotropic in nature so the increase in shear rate results in lower viscosity. It is possible to shape such slurries by a variety of casting processes including low and high pressure die casting.

#### 2.4.2 The Production and Casting of Semi-Solid Aluminium Alloys

Rheocasting as described by Flemings<sup>(51)</sup>, has been developed as a means of utilizing the rheological properties of vigorously agitated semi-solid slurries. Flemings achieved vigorous agitation by stirring semi-solid alloys in such a manner that they became "sheared". The rheocasting process is shown in (Fig.4). Rheocast slurry has been produced continuously at fraction solids ranging up to 70%. The semi-solid slurry was fed directly into a casting machine such as a cold chamber pressure die casting machine and formed into

parts. A development from the rheocasting process which has become known as "thixocasting"<sup>(51)</sup>, is shown in (Fig.5). In this process the metal slurry was fully solidified as an ingot after leaving the rheocasting unit and could be cut into convenient lengths or shapes. When the metal is required to be formed it is simply necessary to reheat the thixotropic slugs to the required semi-solid temperature, retaining the non-dendritic structure, where the material can be handled as a solid. The slug could be placed directly into the shot chamber of the die casting machine and shaped.

Fundamental work on vigorously agitated, partially solidified alloys has shown that the structure and rheological behaviour of an alloy slurry are a function of three process variables. These variables are: the average rate of agitation (shear rate); the average cooling rate during primary solidification; and the volume fraction of solid particles within the slurry<sup>(53)</sup>. The general trends established, relating process variables to structure and viscosity of partially solid alloys, were found to be:

- 1 - The increase in shear rate generally reduced the amount of entrapped liquid in solid particles resulting in a corresponding decrease in viscosity and reduction in the size of primary solid particles (at slow cooling rate).
- 2 - For a given shear rate, the increase in average cooling rate during primary solidification reduced the size of primary solid particles, but increased the amount of entrapped liquid in the primary solid particles. This increased the volume fraction solid in the slurry and hence increased viscosity.
- 3 - The increase in volume fraction solid in the slurry increased its viscosity.
- 4 - For a given average shear and cooling rate, the relative viscosity ( $\eta_r$ ) of a partially solid metal slurry at volume fraction solid higher than 0.20 could be described by an exponential equation:

$$\eta_r = A \exp B g_s$$

where: A and B are constants depending on average shear and cooling rates.  $g_s$  is the volume fraction solid in the slurry.

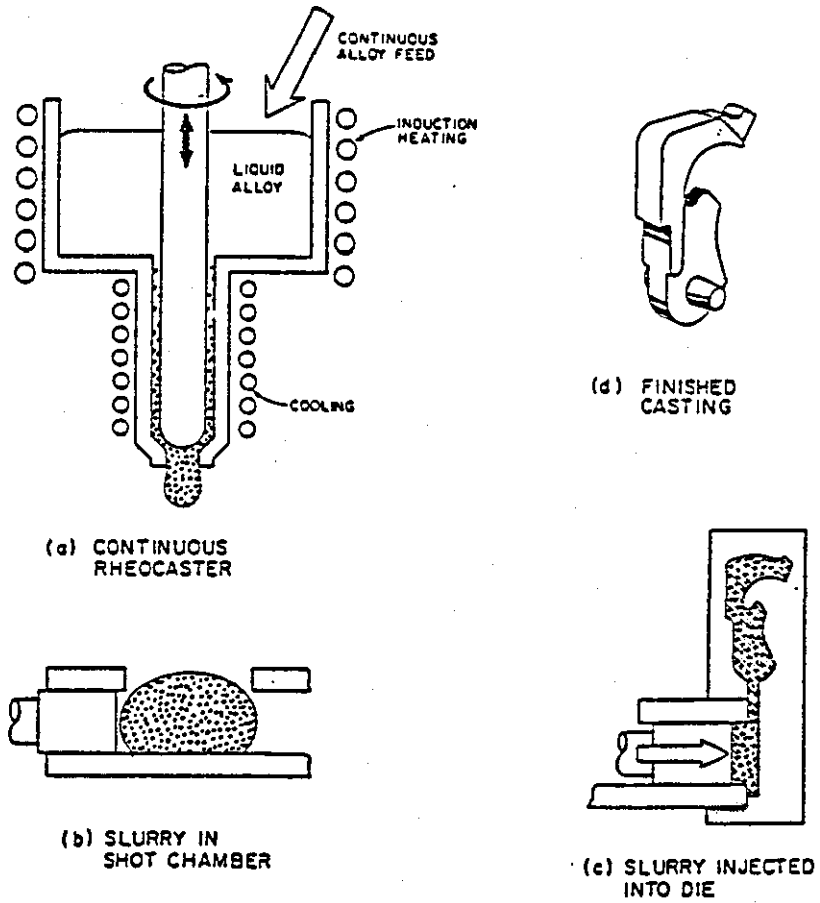


Fig. 4 - Rheocast Process (Ref.51)

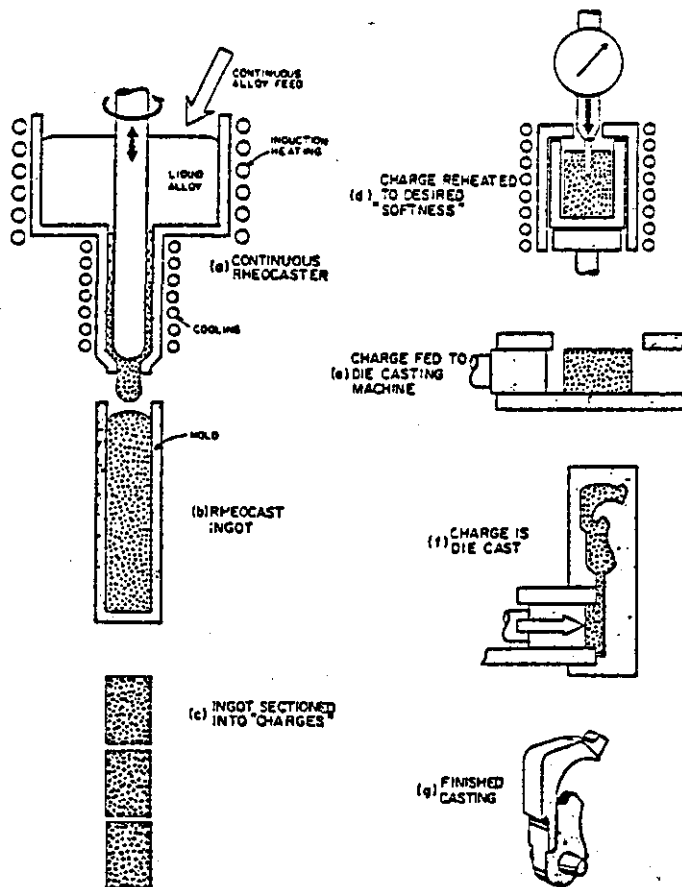


Fig. 5 - Thixocast Process (Ref.51)

The relative viscosity of a suspension is defined as  $\eta_r = \eta_a / \eta_o$ , where  $\eta_a$  is apparent viscosity of the suspension and  $\eta_o$  is the viscosity of the liquid.

- 5 - Metal slurries are thixotropic (their viscosity decreases with an increase in rate of shear and is time dependent and reversible) and show a hysteresis loop phenomenon similar to other well known thixotropic systems, see Fig.6. Measured areas of hysteresis loops (a quantitative measure of thixotropy) increase with increasing volume fraction solid, initial viscosity and time at rest. Thixotropic hysteresis loops were obtained by increasing shear rate continuously whilst torque (which reflected viscosity) was measured. At some point, shear rate was maintained constant and then reduced in the exact reverse to the increase in speed of rotation. The down curve was then obtained. If the two curves did not coincide the behaviour was thixotropic.

#### 2.4.3 Compocasting

Compocasting would appear to offer a means of dispersing non-metallic substances in aluminium alloys. Mehrabian and Flemings<sup>(54)</sup> stated that particulate or fibrous non-metallic substances could be added to and retained in vigorously agitated slurries. Development of abrasion resistant and low friction materials, or perhaps dilution of expensive metals are possible areas of application.

In general when adding non-metals to partially solidified vigorously agitated slurries, it appeared that the high effective viscosity of the slurry prevents particles floating, settling or agglomerating. Increasing the mixing time promoted interaction between particles and the semi-liquid matrix and so improved bonding. Particles of graphite, silicon-carbide, aluminium oxide, magnesium oxide, boron, mica and anthracite have been dispersed by this method. Particle size varied from sub-micron up to 0.1mm. The resulting composite could be cast when partially solid or after allowing it to completely solidify and then reheating to semi-solid temperature before shaping (thixocasting). Compocasting was thought to bring the alloy close enough to the non-metal

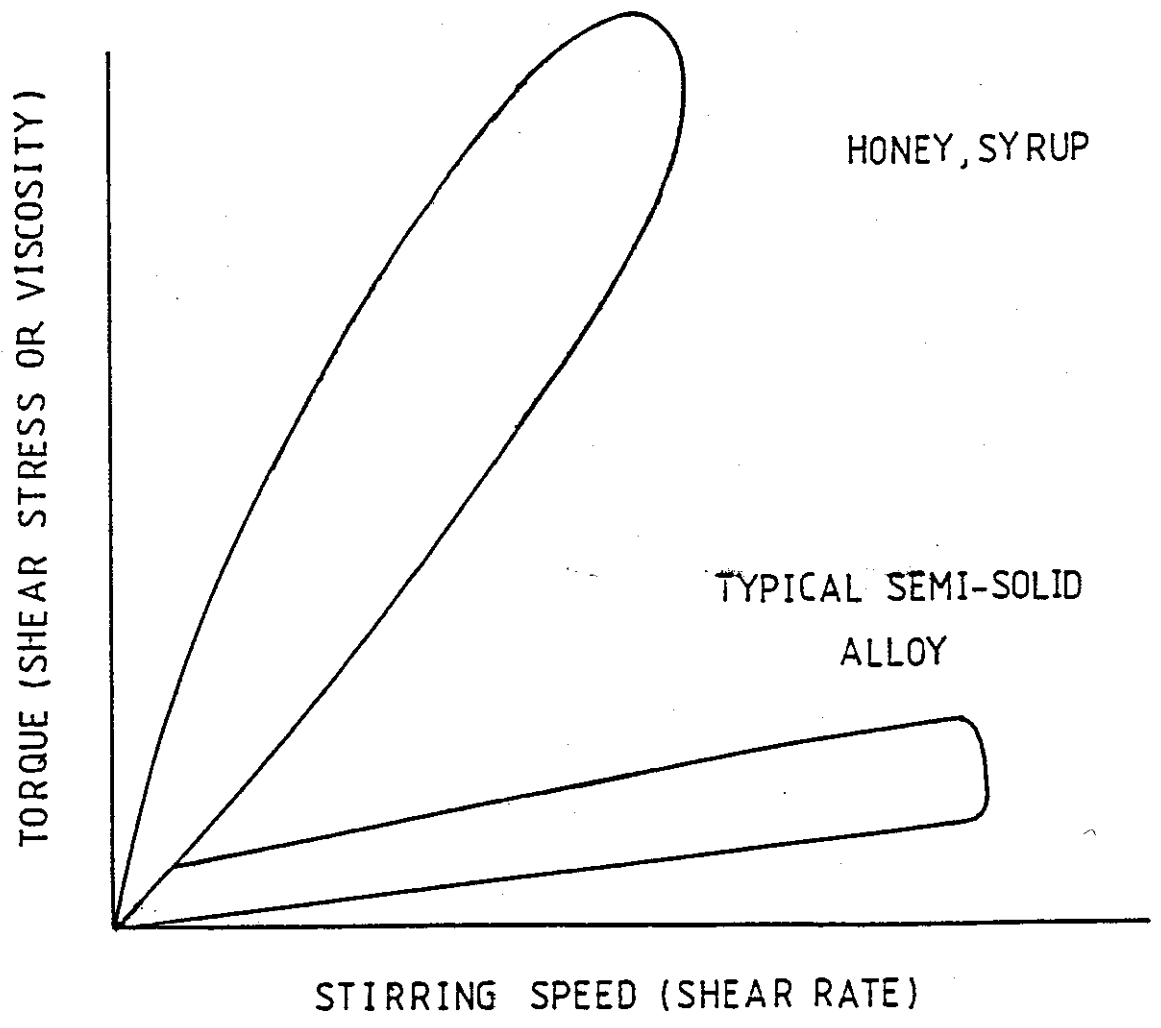


Fig. 6 - Qualitative Thixotropic Hysteresis Loops(Ref.53)

surface to permit bond formation by continuous agitation of the liquid portion of the slurry, despite the fact that molten metal did not wet the non-metal by simple contact<sup>(51)</sup>. The type of bond between non-metal particles and the metal matrix was stated to be one of five types classified by Metcalfe<sup>(55)</sup>, but was thought to be peculiar to the composite system, conditions, time and temperature. The five bond types were: dissolution and wetting bond; reaction bond; exchange reaction bond; the oxide bond; and mixed bonds.

The compocasting process may be particularly economical if it is desired to manufacture strip for bearings. Here the thixocasting route would appear to offer advantages..

If the partially solid material is held at a constant temperature after shearing ceased, a large increase in viscosity takes place as a result of growth and welding of the primary particles in the liquid. At this stage the composite could be handled as a solid. Research has been carried out into rolling the material in this state<sup>(56)</sup> to produce strip. Therefore an aluminium alloy containing graphite particles in a thixotropic state may be in a useful form for roll bonding onto a steel backing prior to the forming of bearings.

Compocasting in aluminium graphite bearing production seems to be attractive for the following reasons:

- (I) No need for expensive metallic coatings on graphite powder.
- (II) Useful material form for bonding to steel strip (no need for two casting operations)
- (III) Lower casting temperature resulting in lower energy usage.
- (IV) Fewer problems with graphite rejection and segregation.

However West<sup>(57)</sup> reported that rheocasting tended to have an adverse effect on fatigue life which may be undesirable in terms of bearing performance

#### 2.4.4 METHODS OF CASTING GRAPHITIC COMPONENTS

Having dispersed and retained graphite within an aluminium alloy melt or slurry, the next stage to be considered is the manufacture of actual castings. Published works on graphitic aluminium alloys appear to refer to bearings as a prime target for graphitic aluminium alloys<sup>(32,44,46)</sup>. However, for bearing production to be as economical as possible casting may not be viable. Most shell bearings are produced by blanking and forming operations. Thus if aluminium-graphite bearings are found to exhibit useful bearing properties, it is likely that special attention will have to be given to production by this method. Krishnan et al.<sup>(41)</sup> have shown that centrifugal casting is a viable technique for producing circular bearings. The density difference between aluminium alloy and graphite particles was put to good advantage, since the graphite particles tended to segregate at the inner bearing surface, resulting in a high graphite content at the bearing surface with a stronger backing. Centrifugal casting of aluminium alloys with graphite particles may prove to be an economical means of producing bearing shapes, especially if it can be shown that graphitic aluminium alloys offer similar properties to centrifugally cast tin Babbit whose constituents are considerably more expensive. The author also gave data concerning optimum particle size, casting temperature and spinning speeds.

Badia et al.<sup>(37)</sup> also reported that segregation of graphite particles could occur in large sand castings due to the flotation during a slow solidification in the sand mould. This disadvantage can be turned to advantage by including high graphite content at selected areas, as in the case of the sand cast alloy 356 BSI490; 1970: LM25 Journal bearing, by the placement of a copper chill in the drag a fairly uniform graphite dispersion was obtained. The author also stated that certain sand castings could be made of graphitic aluminium by the use of chills and control of pouring temperature<sup>(16)</sup>.

Semi-solid graphitic aluminium alloys have been reported to be suitable for a variety of casting processes including low and high pressure die casting<sup>(51)</sup>.

## 2.5 SIGNIFICANCE OF WEAR AND METHODS OF TESTING ALLOYS

The wear literature reveals a confusing variety of wear phenomenon and proposed wear mechanisms. Part of the problem is the very large number of variables which can influence wear behaviour, such as test geometry, load, interaction rate and time, materials properties and environmental factors, including temperature. Even when investigators carefully hold some of these variables constant, the resulting data may be useless for other combinations of these variables. Thus the territory is only partially, and some times imperfectly, mapped.

Wear is one of the three most commonly encountered industrial problems leading to the replacement of components and assemblies in engineering, the others being fatigue and corrosion. Wear is rarely catastrophic, but it reduces operating efficiency by increasing the power losses, oil consumption, and the rate of component replacement<sup>(58)</sup>.

Wear can be defined as the progressive loss of substance from the operating surface of a body occurring as a result of relative motion at the surface (O.E.C.D.)<sup>(59)</sup>.

Whilst in the past it was considered that two basic types of wear, adhesive and abrasive, predominated research has shown that almost every material failure mechanism plays some part in wear behaviour. The literature now makes reference to: adhesion; abrasion; erosion; fatigue; impact; plastic deformation and fracture; and corrosion, including oxidation. It can be seen, therefore, that almost every physical, mechanical, and chemical characteristic of a material is likely to play some part in wear behaviour. It is for these reasons that there are no simple, well defined theories of wear and that there is very little correlation between friction (cause) and wear (effect). Eyre<sup>(60)</sup> has reviewed some of the more common mechanisms of wear. These are:

### 2.5.1 Abrasive Wear

Abrasive wear occurs when hard particles penetrate a surface and displace material in the form of elongated chips or slivers.

An otherwise smooth surface becomes roughened with fairly regular grooves, with or without loosely attached metallic debris. This type of damage is described as scratching, scoring, or gouging, the difference being mainly in the degree of severity.

In practice, abrasive wear occurs under two conditions. The first operates under low stress conditions and the latter under high stress conditions. Under low stress conditions particles are transported across the surface with little breakdown in particle size of abrasive. Under high stress conditions particles are reduced in size or are trapped between two bearing surfaces. In both cases, only a small fraction of the particles cause wear, owing to variations in the angle of the attack and the fact that those particles which roll or slide contribute little to wear. Wear volume usually increases linearly with both load and sliding distance. If deviations do occur they are usually due to a reduction in particle size, clogging of the surface or changes in surface conditions at the interface.

Abrasive wear is claimed to account for 50% of wear in industrial situations<sup>(60)</sup>.

### 2.5.2 Adhesive Wear

Adhesive wear occurs when surfaces slide against each other, and the pressure is high enough to cause local plastic deformation and adhesion. Adhesion is favoured by clean surfaces, non oxidising conditions and by chemical and structural similarities between the bearing couple. With increasing motion, the size of the asperities increases and transfer of material from one surface to another occurs because the asperities rupture at their weakest points. Adhesive wear increases where the contact area is larger, this usually occurs in soft materials. Chemically clean surfaces promote bonding and welding and so result in increased wear, particularly when the couple is mutually soluble. Transferred material may become considerably harder due to strain hardening and phase hardening which may cause associated abrasive wear<sup>(60)</sup>. Adhesion is claimed to depend on the ability of pure metals within a bearing couple

to form solid solutions (61). Lead for example has a very low solubility in iron and therefore would represent a good choice for a counterface. Other constraints must however, be considered, the low strength of lead making it unsuitable for bearings other than in alloyed or mixed form. Adhesive wear should in theory be avoided where a metal slides against a non-metal, such as a ceramic or polymer. The solid solution theory is difficult to apply in practice because information is available only for pure metals under certain sliding conditions.

Variations in load and speed have been found to bring about marked changes in wear behaviour. Transition from mild wear to severe wear has been found to result in the breakdown of an oxidised surface at the sliding couple (62,63). The transition is referred to as the oxidative to metallic transition. The oxidative layer helps prevent adhesion. Very severe adhesion wear results in gross surface damage, this sort of damage is known as "scuffing" (64).

Adhesive wear is claimed to account for 15% of wear in industrial situations. (60).

### 2.5.3 Fretting

Fretting is defined as: "a wear phenomenon occurring between two surfaces having oscillatory relative motion of small amplitude" (60). Fretting usually appears as reddish brown debris on ferrous material. Surfaces are rarely completely out of contact due to the small amplitude of oscillations and so there is little opportunity for the products of the action to escape. This can result in blockage of lubrication and may even cause seizure. Two main processes appear to be involved in fretting these are:

- (I) A mechanical action which removes oxide films resulting in rapid reoxidation followed by further removal of oxide with each successive cycle.
- (II) The removal of fine particles by mechanical abrading or by the formation and subsequent shearing of welds at points of contact.

The particles are then broken up by direct shearing or fatigue . Fretting is always characterised by minute reciprocating motion between the wearing materials which are held together by a normal force, and therefore can be eliminated, or at least reduced, by preventing the relative motion between parts by designing a more rigid mount, or by loading the area with lubricant and increasing the abrasion resistance by nitriding, chrome plating...etc.<sup>(65)</sup> .

Fretting is claimed to account for 8% of wear in industrial situations<sup>(60)</sup> .

#### 2.5.4 Corrosive Wear

The introduction of high-sulphur fuels and contaminated lubricants caused considerable increase in the wear rates of internal combustion engines which is attributed to acidic formations. Modern lubricants have been developed which contain alkaline additions to neutralise the acidity. The problem of corrosive wear in modern engines is not serious and is usually only evident after a long operation life<sup>(58)</sup> .

Increases in wear rate due to corrosion are difficult to describe in a specific sense. No set corrosion model can be applied universally to bearing situations. A typical individual example of impaired resistance occurs in white metal bearings where the formation of tin oxide by corrosion, can seriously reduce the strength of the bearing. The presence of the hard tin oxide particles produced increases abrasive wear. Corrosion can be reduced by changes in the structure and composition of the bearing couple material<sup>(60)</sup> .

#### 2.5.5 Fatigue

Fatigue occurs on bearing surfaces which come into repeated contact at stresses in excess of the specified fatigue stress for the materials concerned. This type of damage is particularly common in cams, ball bearings and gear teeth. Damage may be initiated at or near the surface, in both cases resulting in a pitted mating surface. Corrosion or defects within the body of the material may promote early fatigue failures. Fatigue problems can be seen as striations

extending radially from the fatigue source. Fatigue striations may become obscured by products of corrosion or where surfaces continue to rub against each other after the initiation of fracture. Surface treatments such as thermal treatment (flame hardening, laser hardening, spark hardening...etc.) which increase hardness and leave the surface in a condition of residual compressive stress are used to improve fatigue failure resistance<sup>(21)</sup>.

#### 2.5.6 Delamination

Delamination is a recently characterised mechanism of wear thought to occur in "scuffing" in the internal combustion engines. It is also thought to be present in many other bearing applications and is indicated by the production of plate like debris. Discovery of delamination followed observations that the debris produced in many situations did not have the appearance of debris produced in abrasion or adhesion<sup>(66)</sup>. Wear debris from delamination appears as plate-like debris with a length to thickness ratio in excess of 10:1. Cylinder liners previously thought to fail by abrasion have been known to fail by delamination<sup>(67)</sup>. Delamination is indicated by a ploughed surface appearance. Both flat and coiled plates of debris may be produced. The effects of deformation are highly localised and it is sometimes possible to see plates originating at discontinuities in material structures.

#### 2.5.7 The Relationship Between Material Type and Wear Mechanisms

The choice of materials for oil-film lubricated bearings is determined mainly by the requirements to avoid damage during start-up or momentary periods of interruption of the oil-film and a nice balance is required between the strength to support the load and deformability to ensure the maximum degree of conformability with the opposing surface. Another property of considerable importance is embedability i.e. the ability to absorb hard contaminant particles within the body of the material so that they do not score the other bearing surface<sup>(68)</sup>.

The Construction of bearing materials has a major influence on

their dominant mechanisms of wear. For example hard particles in a soft matrix, such as vanadium carbide in steel acts as a load carrying element which resists abrasive wear. This is due to the hard particles standing proud of the matrix which allows a differential wear process to occur. Abrasive wear resistance is inversely proportional to overall hardness<sup>(60)</sup>. The greater the number of hard particles the greater the resistance to abrasive wear. However, work hardening may also have some effect. Cast irons do not work harden and so there is a good correlation between hardness and abrasive wear. Some steels, for example Hadfield's manganese steel, offer better abrasive wear resistant above certain loads, when surface pressure is high enough to drastically work harden the surface. Resistance to abrasive wear is also dependent of the hardness of the abrasive particles. Aluminium alloys are comparatively soft and so in the presence of hard abrasive particles tend to suffer a high rate of abrasive wear. However, few wear interface conditions produce sufficient particles to cause major problems. Softer materials also allow a small number of abrasive particles to be embedded without major abrasive wear damage. Because adhesive wear is caused by welding and deformation of contacting asperities it is encouraged if the wear couple is mutually soluble. Bearing materials which consist of a soft material dispersed throughout a hard matrix resist adhesive wear by allowing the soft material to smear over the hard matrix. The softer material (eg. lead in copper-lead alloys) forms a layer of material which is not mutually soluble with the material of the mating component and so adhesive wear is avoided. This in turn can also reduce abrasive wear by preventing the formation of small particles of debris which may abrade the mating surfaces. Bearing materials which operate in this manner are also associated with sharp transition in wear behaviour. For example, some aluminium alloys tend to wear at a mild rate due to the formation of a tenacious oxide layer on the surface. However, above a certain load, the layer breaks down and wear becomes considerably more severe. The use of tin in aluminium-tin alloys is a similar example.

Single phase materials are used to produce bearings which are toughened and resistant to fatigue, allowing high loads to be carried at high speeds. The lack of a secondary phase helps to prevent the initiation of cracks, which may eventually cause the material to become fragmented. This helps prevent wear by abrasion and delamination. However, single phase materials may be soluble in the material of their mating components, which can result in adhesive wear. Therefore, an insoluble overlay is usually required (eg. the use of lead on silver). The use of non-metallic bearings usually eliminates adhesive wear because they are rarely soluble in metals. However their low dimensional stability, hardness and strength can result in severe abrasive wear and delamination.

#### 2.5.8 Wear Testing Objectives and Approaches

The selection of a wear test depends not only on the mode of wear being investigated but also on the objective of the test. Wear tests are run for a variety of reasons, however, they generally fall into one of the following four categories: fundamental understanding; determination of the effect of variables; characterisation of materials and lubricants; and selection of materials for specific application. The type of test rig will be dictated by the following: the type of wear; the specimen geometry; the selected operating conditions; the type of motion desired; and the need for multiple testing<sup>(69)</sup>.

A number of approaches have been used in evaluating the performance of bearing materials. This has led to problems in comparing the properties of different materials. The available information concerning the actual performance in service of different bearing materials and their comparative usefulness is by no means always so reliable and much of the published information is a matter of opinion rather than scientific data. The problem has arisen due to a lack of working standards.<sup>(70)</sup>

Bearing materials should have a number of properties to ensure that the function of the bearing is maintained under various

operating conditions. These properties are interdependent and also they depend on the properties of the mating component, lubrication (if any) and on operating conditions. This makes it difficult to design an adequate standard test method. However, various proposals have been and are being put forward as a suitable means of assessing the tribological properties of bearing materials, but a problem of inconsistency of results appears to exist<sup>(71)</sup>. As yet, no firm recommendations have been made. Some of the assessment and test methods available for consideration are:

#### (P.V.) VALUE

Attempts have been made to classify performance in terms of a p.v. value, which is the product of pressure and linear velocity. This is of little practical use in view of the number of variables unaccounted for and speed dependant properties in bearings. Nevertheless, the analysis is widely used in bearing literature and applied in many bearing configurations.

#### ZN/P Evaluation

The quantity ZN/P is also widely used as a criterion, where:

Z = lubricant viscosity

N = rotational speed

P = bearing pressure

In theory this relationship produces a straight line passing through the origin<sup>(70)</sup>. However, the relationship is valid only to a certain level, below which the coefficient of friction increases sharply due to the breakdown of the lubricant film. Below this the bearing becomes unsuitable because the increased coefficient of friction causes increased temperature, which in turn decreases the viscosity value and further increases the coefficient of friction. The minimum value of ZN/P changes with the material in question. Softer materials tend to give lower values. In practice, differences in material may be swamped by differences in bearing design<sup>(70)</sup>. Low ZN/P is useful for starting when hydrodynamic lubrication may not be adequate. In these cases the minimum value of ZN/P must inevitably be passed through.

A wear test which appears to be in widespread use for obtaining the quantity ZN/P is the "Hohman Wear Test"<sup>(72,73)</sup>. The principle of the test is shown in Fig. 7 and the type of result obtained is shown in Fig. 8.

The whole device is immersed in an oil bath of given viscosity. Referring to Fig. 8, the sudden increase in coefficient of friction can be seen as demonstrated by Forrester<sup>(70)</sup>. This is in the region of boundary lubrication where the fluid film is breaking down and the qualities of the bearing material are most important. Unfortunately the analysis is not reliable in this region.

### Independent Assessments

Many research workers in tribology have realised that little standardisation in bearing test methods exists and that most established methods of assessment are limited. A few such workers have therefore embarked upon their own research projects using methods of test and assessment which have evolved and been found to offer suitable comparisons within individual projects.

Two approaches of this type are described below:

#### 1 - Neyman<sup>(74)</sup>

Four basic tests were evolved as a means of comparing four bearing materials. The materials compared were three different steel backed bronze and one aluminium-tin alloy without backing. The tests consisted of:

- (I) Radially loading the bearing in increments until a transition from hydrodynamic to mixed lubrication was reached (load capacity test).
- (II) Constant radial load, but with an incrementally applied lateral load.
- (III) As test (I), except the lubricant contained iron powder. This test was stopped when the bearing temperature reached 90° C.
- (IV) Constant frictional torque was applied under mixed lubrication conditions. Load, bush temperature and frictional torque were continuously monitored until

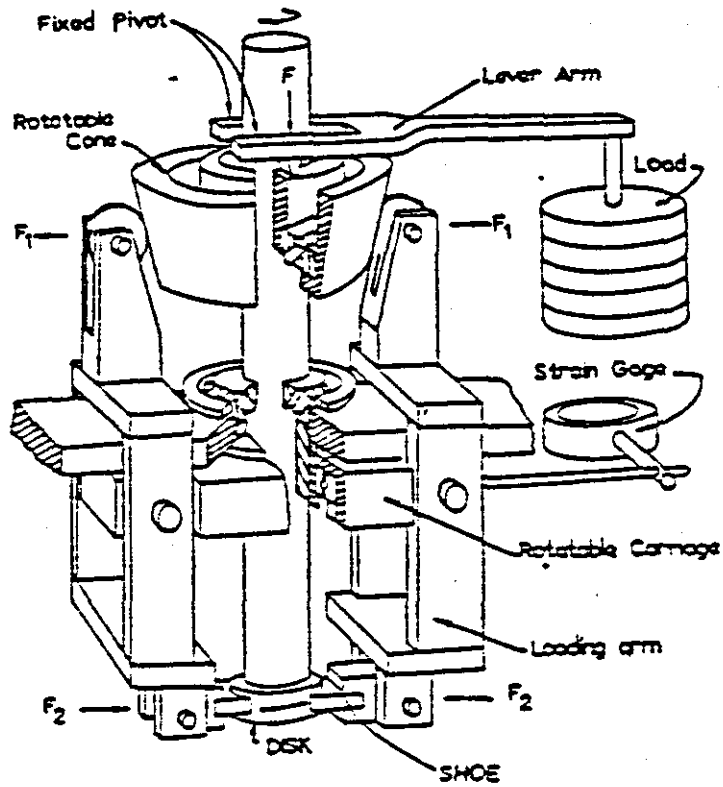


Fig. 7 - Hohman Wear Tester (Ref. 73)

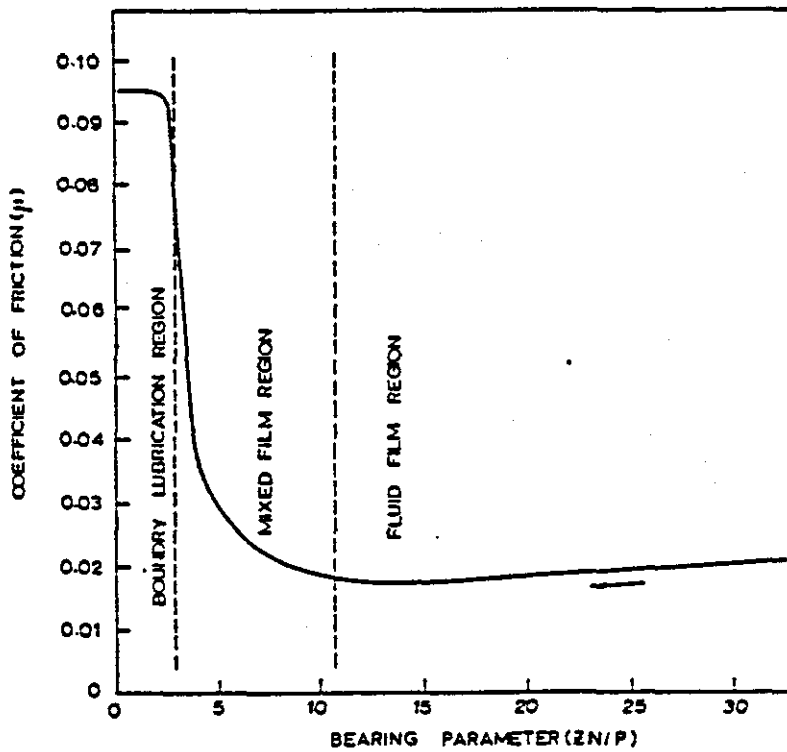


Fig. 8 - Typical Result - Hohman Wear Test (Ref. 73)

steady state conditions were obtained. A curve was then drawn for load vs. time and hence a comparative running-in characteristic obtained.

To summarise the results, the bronzes exhibited superior performance to the aluminium-tin alloy in all but test (I). Here the aluminium-tin alloy gave results similar to the most superior bronze (which was a 70% copper-lead alloy). The results appear to conflict with claims from other sources but may not be directly comparable as the aluminium-tin was not used in backed form. However, few reports give such detailed experimental data, but tend to rely on subjective discussion rather than quantitative results.

## 2 - Brunel University Tribology Group

The Tribology Group in the Metallurgy Department of Brunel University has established a number of interests in the field of tribology. One such interest is in the development of bearing materials, with a particular interest in aluminium alloys. To assess bearing materials two principle methods are used, these being the reciprocating diamond scratch test and the pin on disc test. The reciprocating diamond scratch test is described by Razavizadeh and Davies<sup>(52)</sup> and was designed to simulate wear by abrasion and delamination. A single point diamond rockwell indenter with an included angle of 120° is used to produce tracks of various lengths. The speed of the diamond can be changed by adjusting motor speed. Tests can be carried out with different loads and different numbers of passes.

Assessment of performance is then carried out by comparing scratch width with the aid of travelling microscope. A formula may then be applied to convert scratch width into abraded wear volume.

Data is usually presented in the form of graphs of wear volume vs. applied load and wear volume vs. number of passes. Wear rate may also be computed. The test is usually supplemented by the use of scanning electron microscope (SEM) examination to show the amount of plastic flow, delamination and abrasion which may explain changes in wear volume.

The reciprocating diamond scratch test is shown schematically in (Fig.9).

The Pin on Disc test is used extensively in evaluating bearing materials and has been described by Shivanath et al.<sup>(23)</sup>. The test is shown schematically in (Fig.10). A pin of bearing material is loaded in contact with the flat surface of a hardened steel or cast iron disc. The speed of the disc is carefully controlled to ensure a constant linear sliding velocity. Change in wear distance (ie. the length of pin lost) is continuously recorded with the aid of a linear displacement transducer. This can give useful indications of wear and also the point at which any transition may have occurred. Coefficient of friction measurements may be obtained by accurately measuring the deflection of the pin in the direction of rotation of the disc. The force required to cause such a deflection is determined and from this the coefficient of friction is calculated. The values obtained are not absolute because coefficient of friction is dependent on speed<sup>(71)</sup> but provided speed is controlled values are comparable between tests.

Further data may be obtained from temperature measurements obtained by attaching thermocouples to the pin.

Scanning electron microscopy may be used to provide supporting evidence about modes of wear and indications of the reasons behind any transitions which may have occurred and been indicated by transition in wear distance, coefficient of friction or temperature. There are many wear mechanisms present in pin on disc testing and so the test may be considered to be a simulation of the type of conditions which may be met in service. The SEM has been instrumental in identifying and explaining the wear mechanisms present<sup>(75)</sup>.

#### 2.5.9 Fatigue Testing

Fatigue is a very common mechanism of bearing material failure. Various machines are available to test bearing fatigue life, a typical example being the Glacier fatigue tester<sup>(76)</sup>. This consists of a shaft running in a bearing

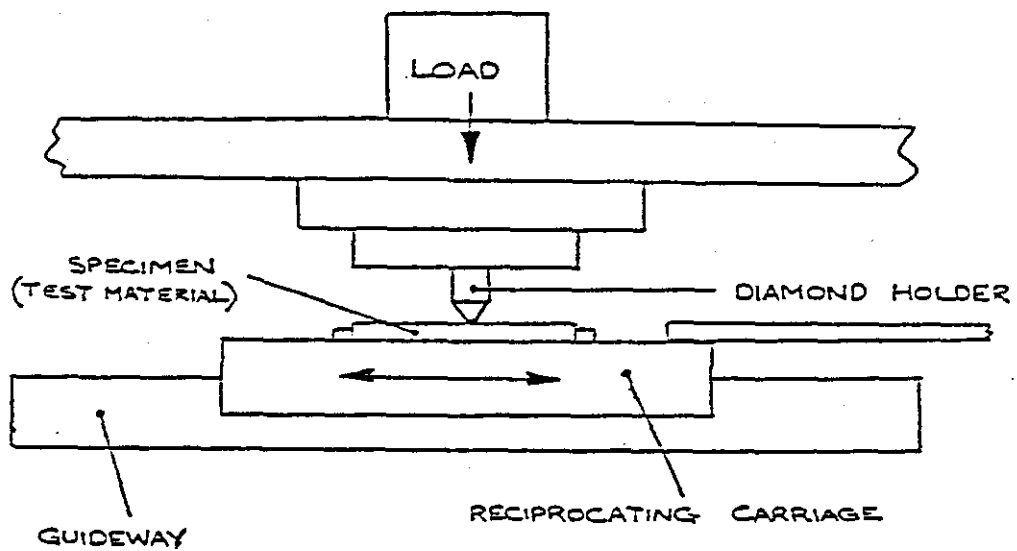


Fig. 9 - Diamond Scratch Test (Ref. 62)

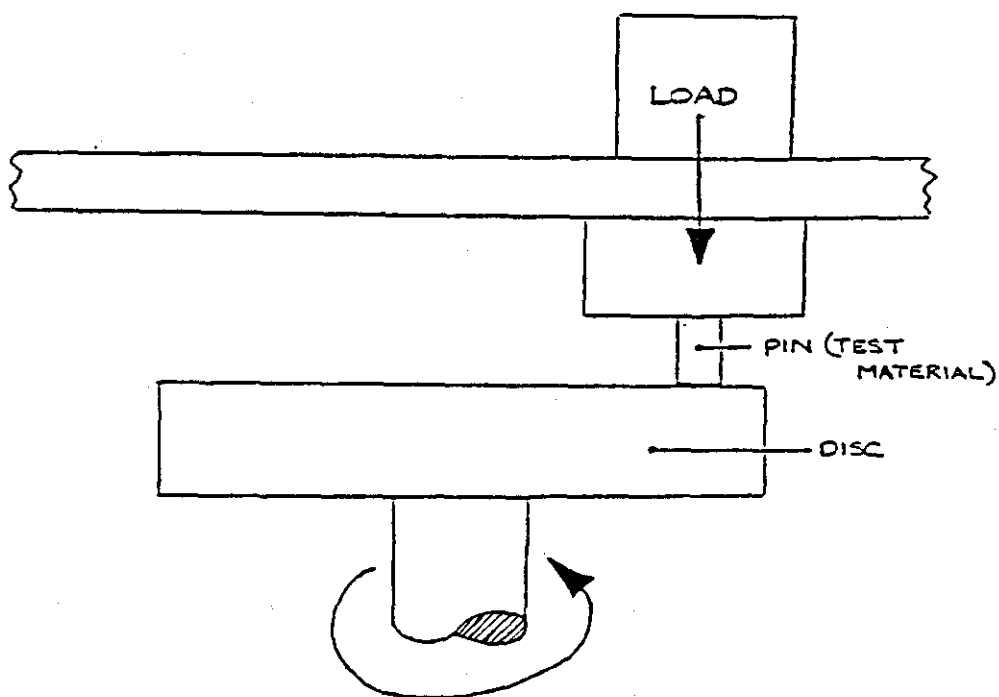


Fig. 10 - Pin on Disc Test (Ref. 23)

under test, with an eccentric weighting applied to induce cyclic stresses.

In common with other methods of assessing bearing materials, standardisation of fatigue testing does not exist and so results from different sources are not comparable. Standardisation of test conditions is particularly important when evaluating the fatigue life of any material.

#### 2.5.10 Corrosion Testing

For the results to be relevant, corrosion testing should take place under the conditions in which the bearing is likely to operate. Bearing materials must be tested in likely lubricants and coupled with the materials with which they will be in contact under operating conditions. Common means of evaluating corrosion performance, such as salt spray tests, have little relevance to bearing applications.<sup>(77)</sup>

#### 2.6 SUMMARY AND PROPOSED APPROACH TO RESEARCH

In plain bearing applications, aluminium alloy-graphite particulate composites have been found to offer: resistance to seizing and galling; low coefficient of friction; and resistance to wear. Load carrying capacity has been indicated to be similar to bronze materials and the composites offered outstanding performance in conditions of boundary lubrication due to a thin layer of graphite becoming smeared on bearing surfaces. It has been also reported that aluminium-silicon alloys containing dispersed graphite particles have been shown to offer an outstanding performance when used for pistons and cylinders in reciprocating internal combustion engines, and it may offer an economical solution to lubrication problems encountered in the all-aluminium engine.

Special techniques are required to disperse and retain graphite particles in aluminium alloys because the former will not be wet by the latter.

Several techniques have been developed to solve this problem which involve the use of coated or specially treated graphite particles. Methods involving completely liquid alloys,

described by various sources, for the preparation and casting of graphitic aluminium alloys appear to suffer from the following limitations:

- (a) special treatments have been required either to the melt or to the graphite particles (or both) in order to ensure that wetting takes place. Metal coated graphite particles are costly to produce, and melt treatment may result in means of production which are time-consuming and/or expensive for industrial exploitation. In addition, in both cases, new elements are introduced to the alloy under investigation and this will result in changes in the alloy's properties.
- (b) Constant stirring for the composite produced in such methods has been widely reported to be necessary to ensure that graphite particles remain evenly dispersed. In addition the composites are usually cast into permanent moulds. This appears to be an attempt to avoid segregation and agglomeration due to the flotation of the graphite particles. The permanent mould provides a fast cooling rate which does not give the graphite particles the time to segregate.

The inclusion of graphite in aluminium alloys has been widely claimed to reduce the strength of the alloy in comparison with a similar alloy without included graphite. In bearing materials a need has been established to optimise mechanical properties in order to obtain good load carrying capacity and fatigue properties. Therefore, there may also be a need to ensure that the casting process used for the production of components manufactured from graphitic aluminium alloys provides high casting integrity so that mechanical properties are not impaired by inherent casting defects.

Published data on mechanical and tribological properties of graphitic aluminium alloys does not include a fundamental appraisal of the effect of graphite content, graphite particle size and alloying elements. Many sources have reported results of graphite additions to aluminium alloys. However, graphite contents investigated and base aluminium alloys used, have varied widely. There appears to be a requirement to

produce a fundamental knowledge on the mechanical and tribological performance of graphitic aluminium alloys with particular reference to the effect of various graphite contents and graphite particle size on aluminium alloys and in particular aluminium-silicon alloys.

#### 2.6.1 Work Programme

In finalizing the work programme the following was proposed;

The use of compocasting, as a method for incorporating uncoated and untreated graphite particles in a hypereutectic aluminium-silicon alloy (LM30), to produce a bearing material which contains graphite as a solid lubricant and is resistant to wear.

This material could have the potential for the production of monoblocks for automobile engines. The proposed technique appears to offer the following advantages:

- (a) no need for specially coated or heat treated graphite particles and no extraneous elements introduced;
- (b) lower casting temperature resulting in longer die life and lower heat input;
- (c) graphite dispersion without rejection, flotation, agglomeration or segregation;
- (d) the potential for taking advantage of the rheological benefits of rheocasting and thixocasting (eg. improved die filling properties) in commercial processing of the composite.

After evaluation of the optimum conditions for the dispersion and the retention of graphite particles in the alloy the pressure diecasting process was used as the method of shaping the composite so that the following could be achieved:

- (a) high casting integrity resulting in a minimum loss of properties due to the graphite inclusion;
- (b) the use of a process suitable for industrial production of components which might benefit by manufacture from semi-solid aluminium alloys with a dispersed graphite particles (eg. automotive pistons and bearings);

(c) heat treatable components due to the absence of gas porosity and reduction in shrinkage cavities.

Finally the production of specimens by the above technique and a comprehensive evaluation to promote understanding and knowledge of mechanical and tribological properties of the graphitic hypereutectic aluminium-silicon alloy, in comparison with the same alloy without graphite addition.

## CHAPTER THREE

### DESIGN OF EQUIPMENT

In early publications rheocasting equipment was described as simply stirring paddles, bobs or rotors rotated by an electric motor in a crucible containing the semi-solid alloy. Much fundamental work was carried out using systems of this type. At M.I.T. Spencer et al.<sup>(78)</sup> made many discoveries which characterised the rheocasting process using a high temperature viscometer based on a simple design (Fig.11).

Later designs became more sophisticated with multiple contra-rotating stirring paddles, Campbell, at Fulmer Research<sup>(79)</sup> and Mehrabian et al. at M.I.T.<sup>(51,80)</sup> reported similar designs of this type which allowed larger quantities of semi-solid alloy to be sheared. Early work on compocasting was carried out using designs of this type. The design used by Mehrabian et al. for compocasting is shown in (Fig.12)

As research in rheocasting moved towards production of components from semi-solid material, design of equipment progressed towards machines which were more practical in terms of the amounts and quality of material produced. Ramati et al.<sup>(81)</sup> reported a design for continuous production of rheocast material. The equipment was designed with commercial exploitation in mind. The production, at high speed, of rheocast ingots was required and the design to achieve this is shown in (Fig.13). The alloy was continuously cooled from above the liquidus and agitated as it passed through the lower semi-solid temperature zone. The liquid zone in the equipment allowed a continuous supply of liquid metal to be added to the machine and prevented contact of the semi-solid zone with air. The upper liquid zone remained undisturbed and so prevented air penetrating the semi-solid. This design was developed at the University of Illinois.

Later work at Fiat SPA, Italy<sup>(82)</sup>, resulted in the patent for a new rheocaster in which it is claimed that very high volume fraction solid, of up to 80%, can be sheared. This was achieved by replacing the stirring mechanism by a system of

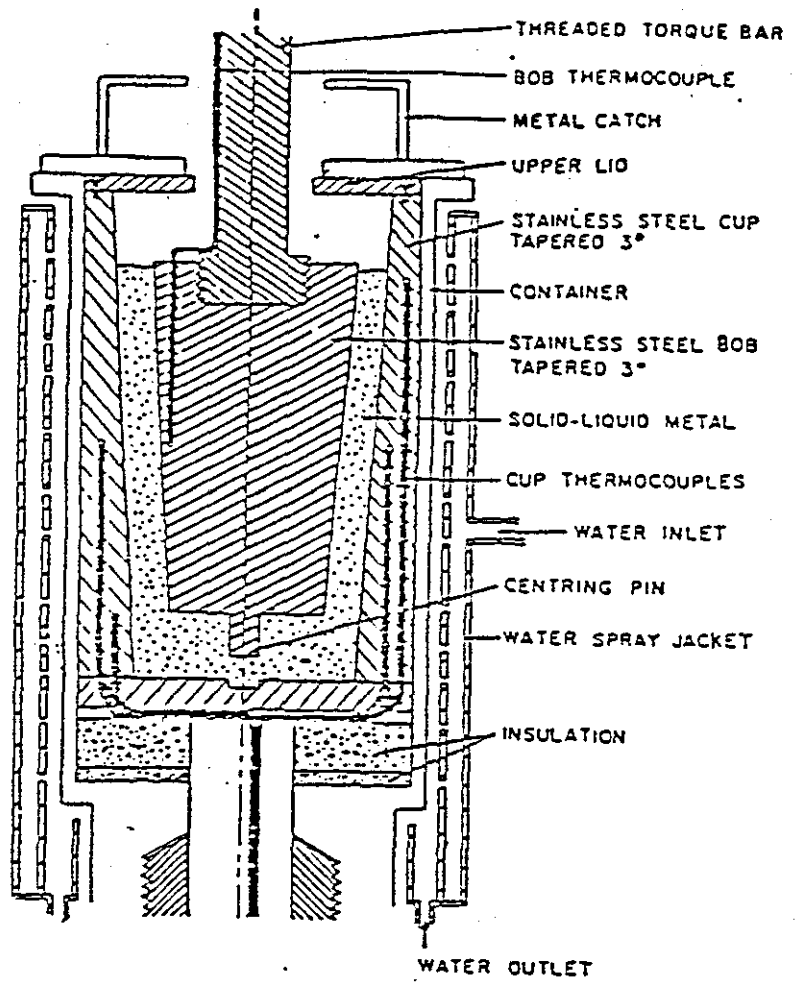


Fig. 11 - VISCOMETER (Ref. 78)

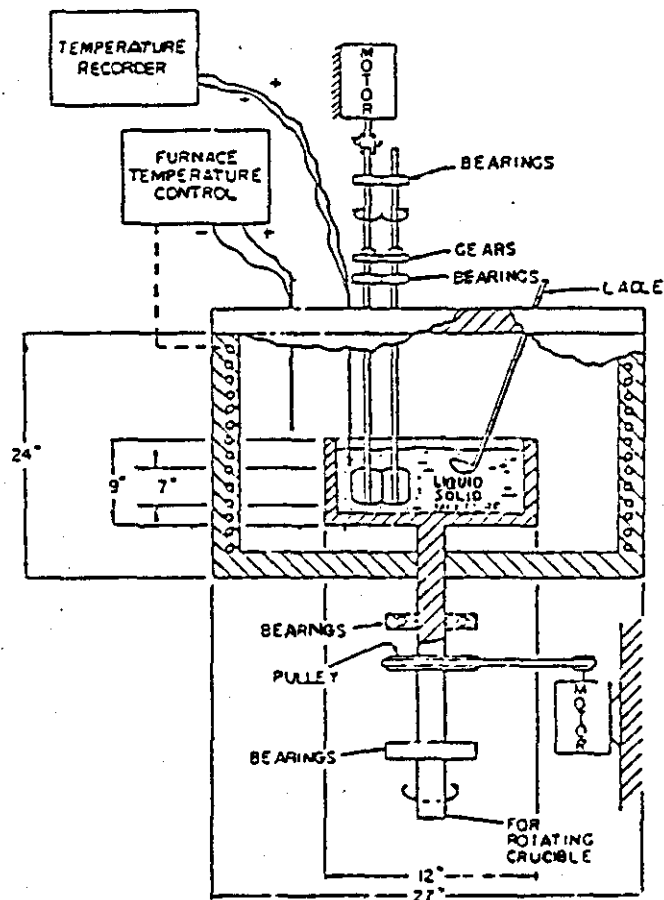


Fig. 12 - COMPOCASTING EQUIPMENT (Ref. 80)

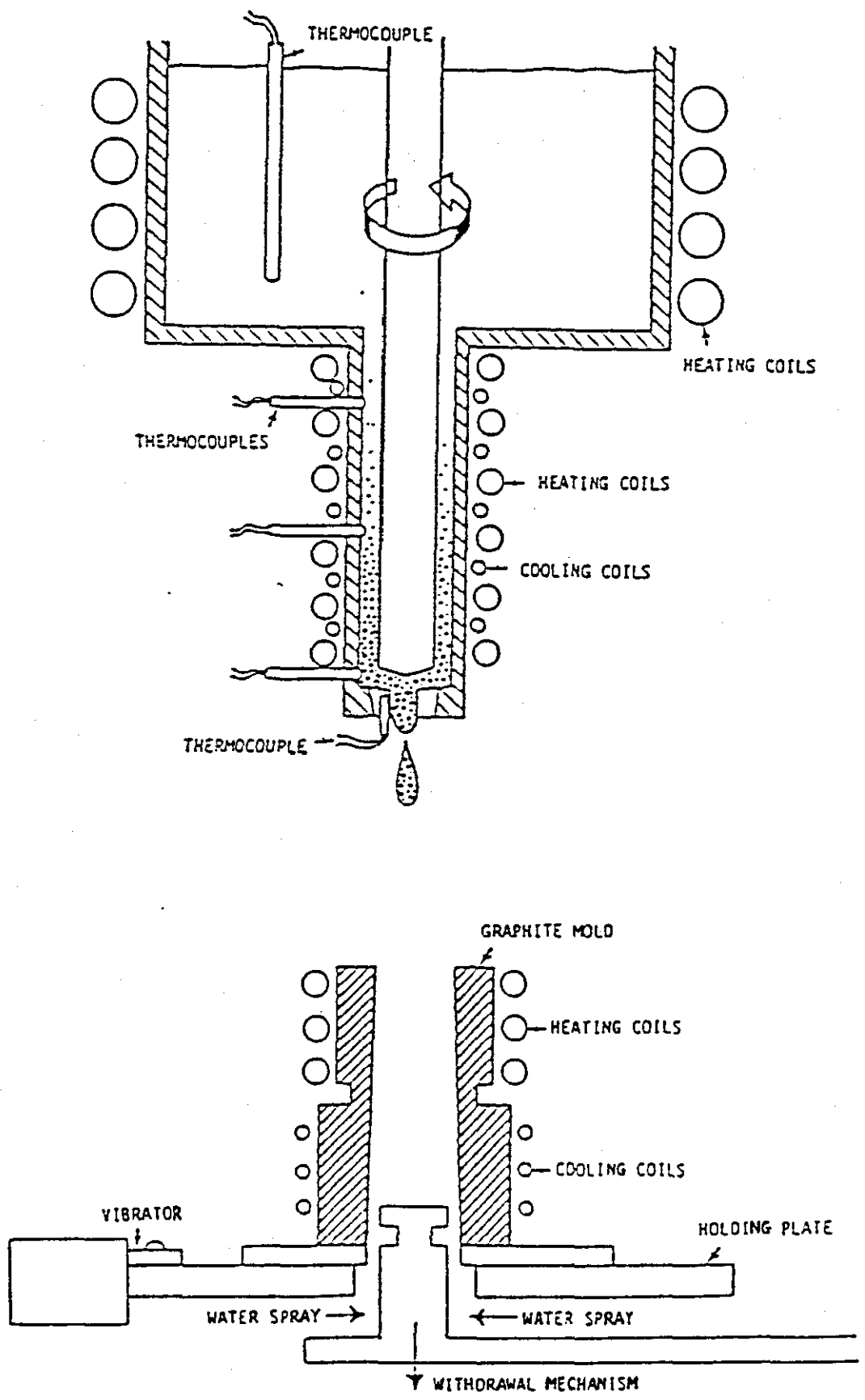


Fig. 13-CONTINUOUS RHEOCASTING UNIT (Ref. 81 )

stationary baffles through which the semi-solid alloy was forced to pass by mechanical pressure. In this way, shear rates far in excess of those associated with previous designs can be obtained see Fig.14. Such a design could provide a solution to the segregation of solid particles associated with high rotor speeds, due to the difference in density between the solid particles and liquid metal and it could be used as a continuous rheocaster for mass production in industry

At Loughborough University of Technology, Gibson<sup>(83)</sup> produced a rheocaster which is similar to that described by Ramati<sup>(51)</sup> and West<sup>(57)</sup>, with some modifications to make it suitable for compocasting requirements. The rotor in this design, shown in Fig.15, involves four splines placed along the length of the rotor which operates in the semi-solid zone. The section of the rotor which operates in the liquid zone was left smooth to ensure that the minimum of disturbance occurred in this region. The graphite was stored within the shearing rotor so that the graphite particles could be injected into the melt by mechanical pressure when the required volume fraction solid and shear rate had been established. Gibson also reported that graphite particles needed to be at the same temperature as the semi-solid slurry to prevent the sudden reduction in slurry temperature due to the addition of cold graphite which resulted in a rapid increase in the volume fraction solid and hence increased the slurry's viscosity. The general arrangement of this design is shown in Fig.16. The compocaster was designed to operate as a batch rather than a continuous rheocaster. A plug was incorporated in the base of the crucible which when removed allowed the composite slurry to be ejected through the crucible base.

Whilst Gibson's design was adapted for manufacturing the rheocasting unit for production of the graphitic, hypereutectic alloy, the modifications to the design necessary to enable the unit to be used in conjunction with the pressure diecasting machine were extensive. It was necessary to construct a new compocasting unit exclusively for use with the pressure diecasting machine and designed to fulfil the following requirements :

- (a) The compocasting unit should have dimensions appropriate to the requirement for it to be mounted on the tie bars of the pressure die casting machine. These were dictated by the distance between the injection head and the fixed platen.
- (b) Provision should be made to prevent porosity due to air entrapment.
- (c) The resulting composite slurry should be directly cast after the rheocasting operation, eliminating the need to produce and remelt ingots.
- (d) The addition of graphite should be achieved with minimal variations of the volume fraction solid and shear rate.
- (e) There should be provision for monitoring volume fraction solid, shear rate and viscosity.
- (f) The output should be in a suitable form for transferring to the shot chamber of the pressure diecasting machine.

Those features of the continuous rheocaster design which met these requirements were incorporated in the research equipment. For example the two zone crucible arrangement was incorporated with the expectation that the upper layer of liquid would prevent oxidation of the slurry formed in the lower zone. The temperatures of the upper and the lower zones were monitored using Newtronic temperature controllers in conjunction with chromel-alumel thermocouples. The shearing rotor was powered by an induction motor with a hydraulic speed drive. Different rotor speeds were required to obtain different shear rates. The hydraulic variable speed drive coupled to the induction motor provided speed variation from 0 to 1500 rpm in both clockwise and anti-clockwise directions. However, in order to achieve higher speed, i.e. higher shear rates, the pulleys used to transmit the movement from the induction motor to the rotor were chosen to provide an increase in the speed by the ratio of 1.78. This was achieved by using a driving pulley with 32 and a driven pulley with 18 teeth.

The compocasting unit mounted on the tie bars of the cold chamber pressure diecasting machine is shown pictorially in Fig.17 and schematically in Fig.19. The equipment design is shown in Fig.20 and the design details are described in Appendix 1.

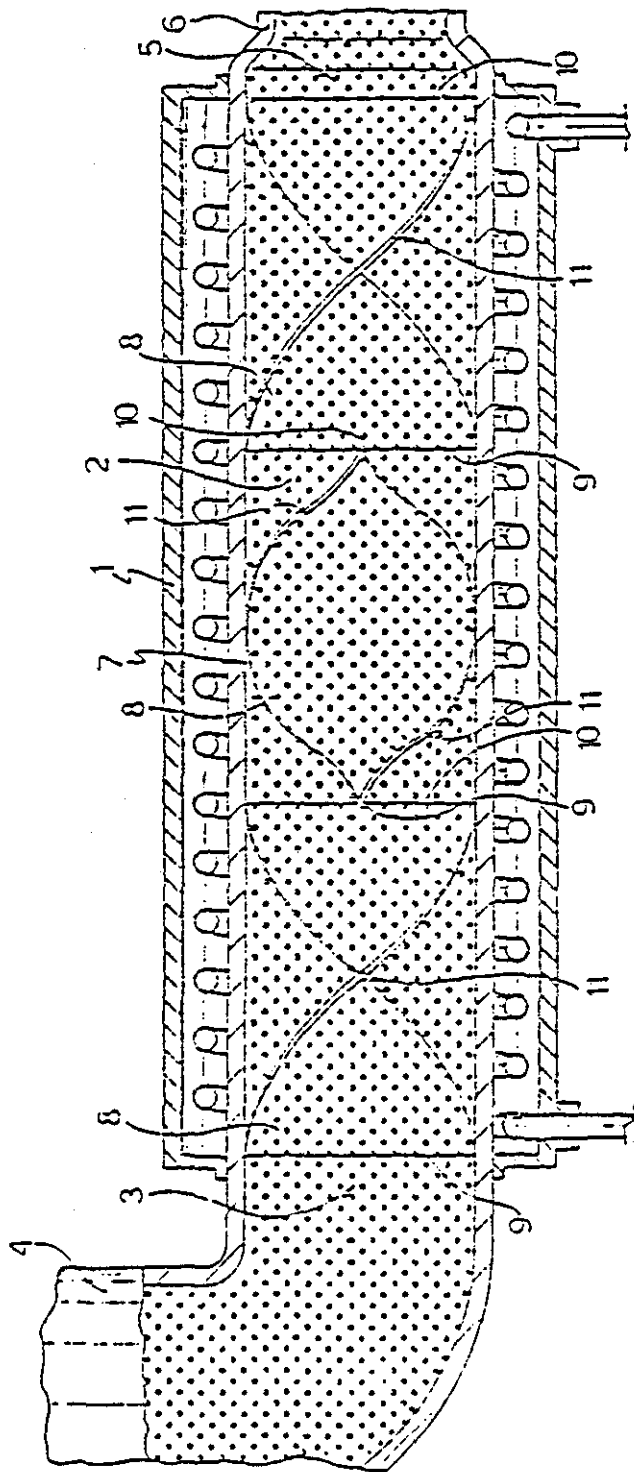


Fig.14 -Continuous Rheocasting Unit ( Ref. 82 )

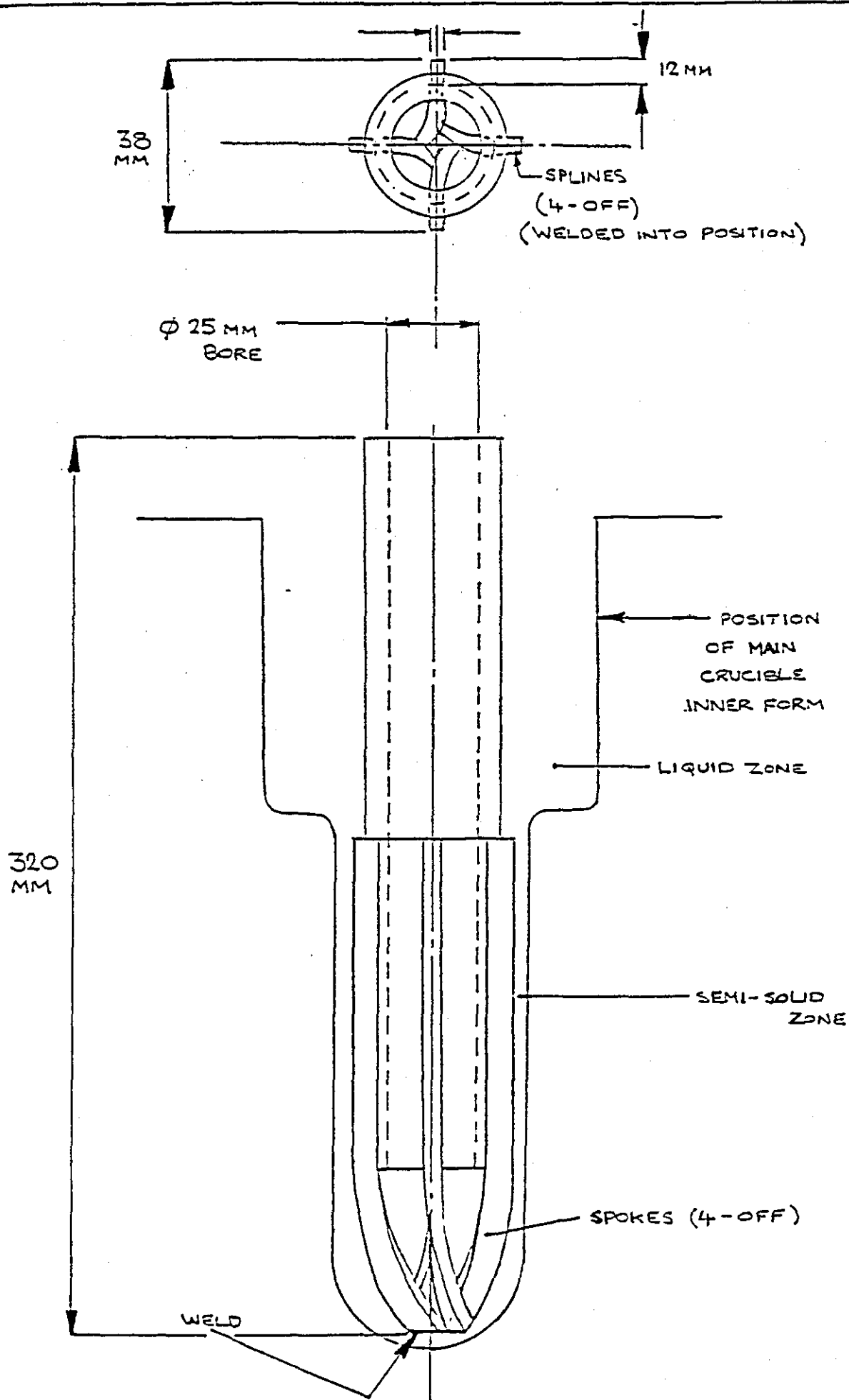


Fig.15 - ROTOR DESIGN (Ref. 83 )

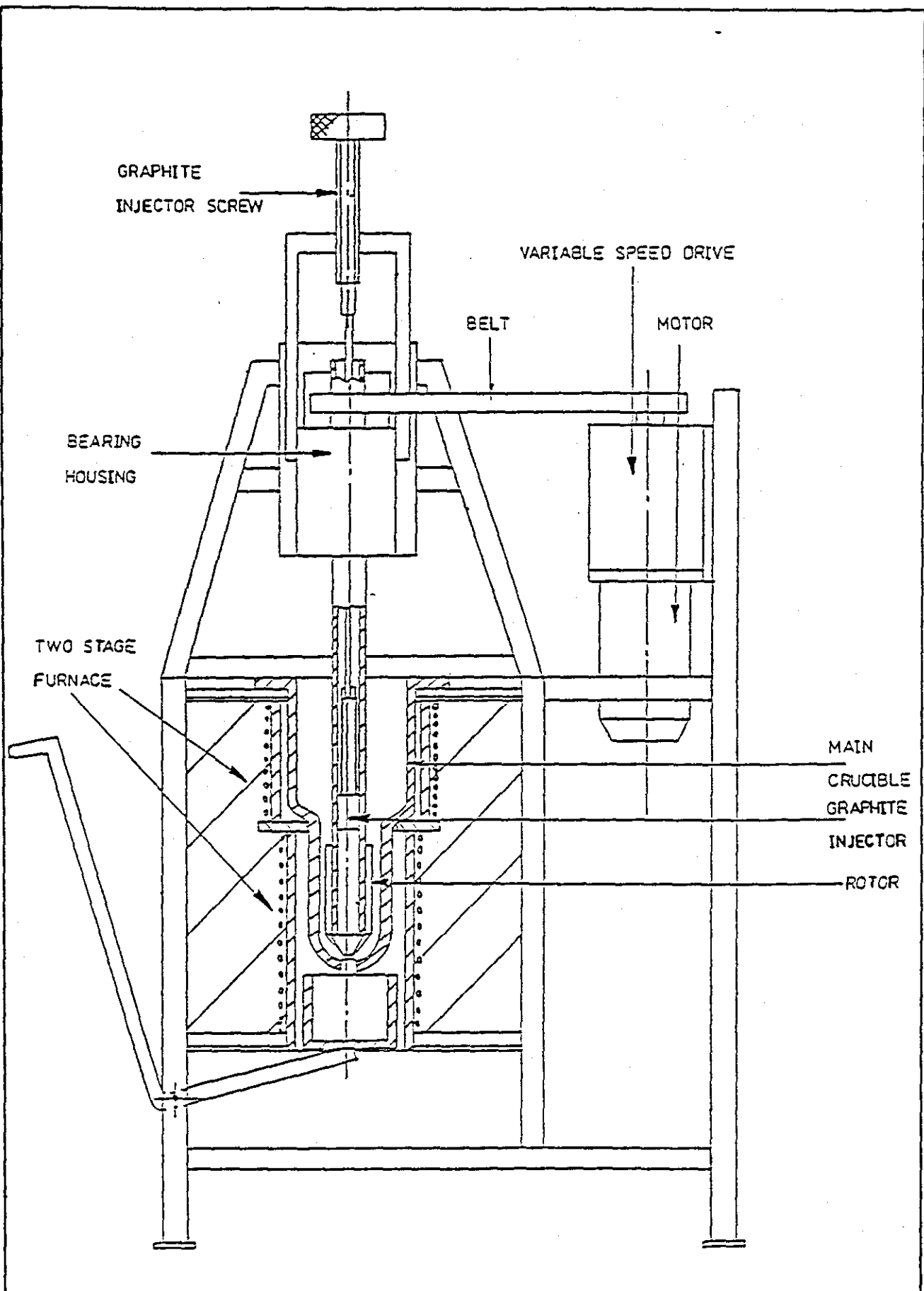


Fig.16- Comopocasting Unit ( Ref. 83 )

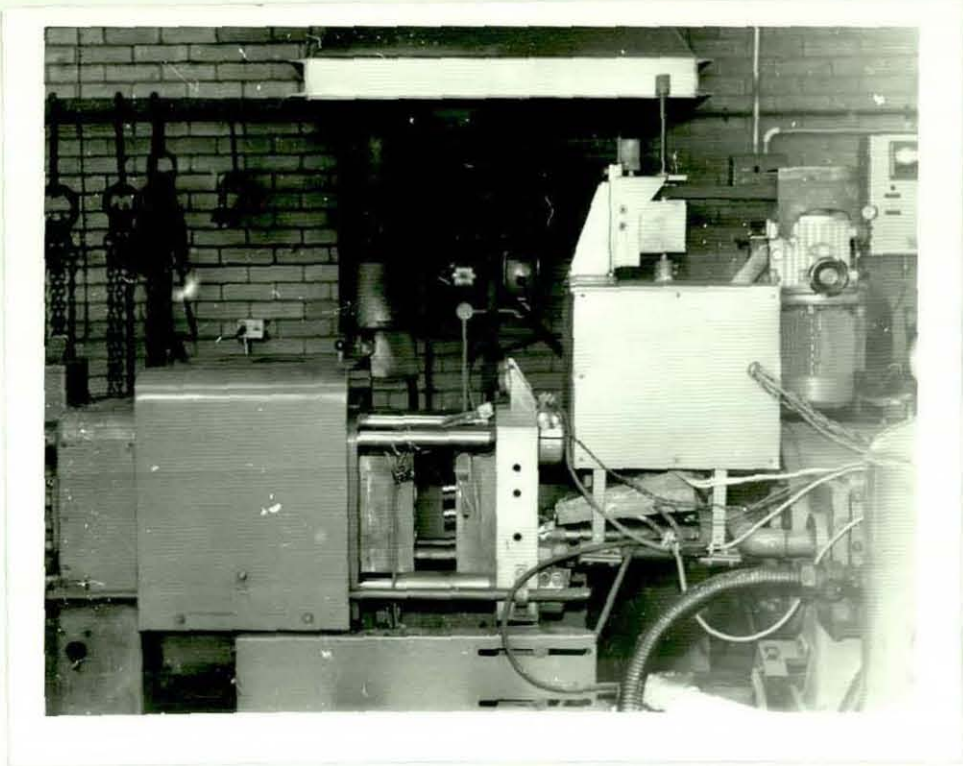


Fig. 17 - Compoasting unit mounted on the tie-bars of EMB No.10 cold chamber pressure die casting machine.



Fig. 18 - Test casting design.

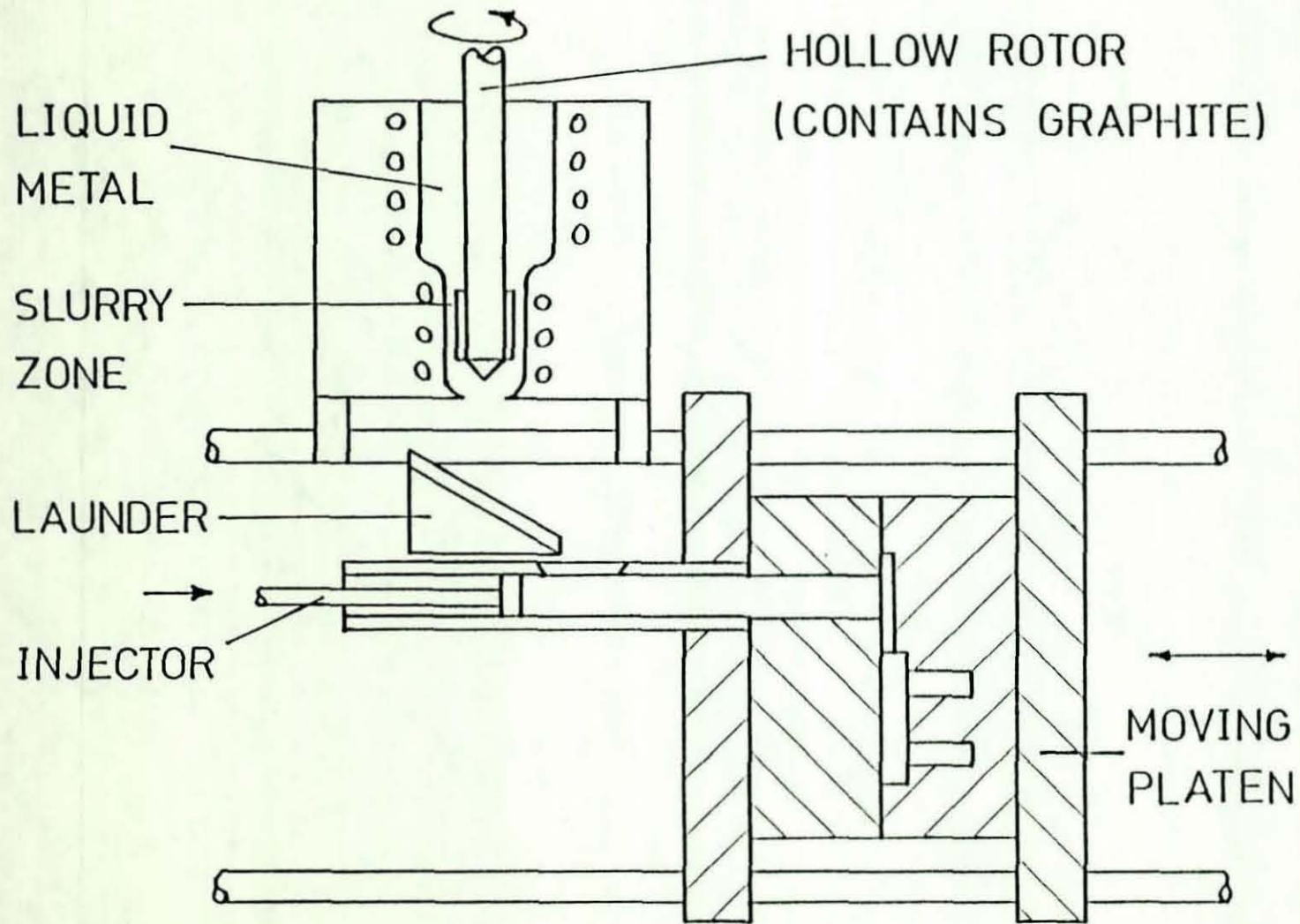
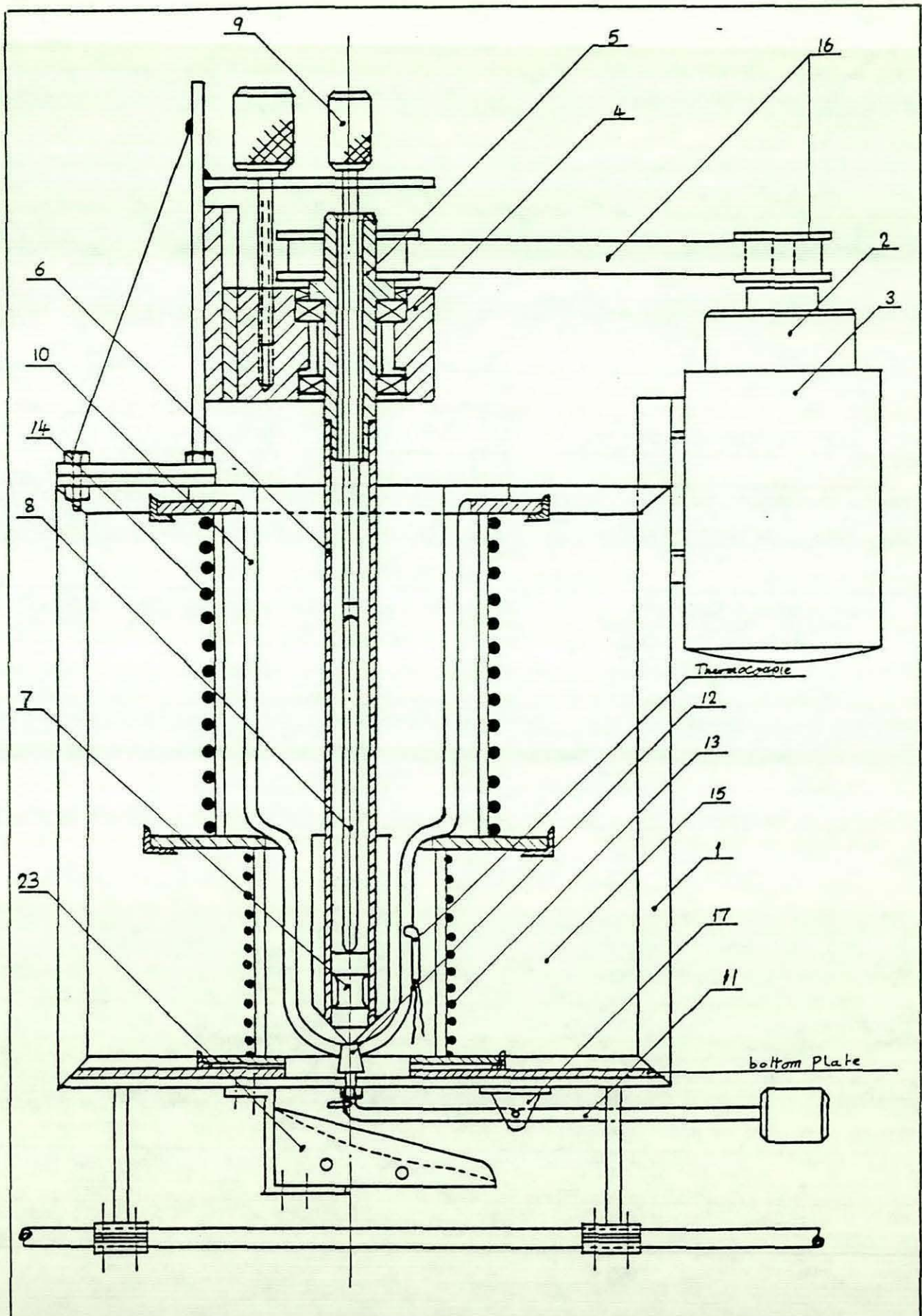


Fig. 19 - The comocasting Unit Mounted on the Pressure Die Casting Machine



DRAWING NO. 20

SCALE : 1/4

DIMENSIONS:

DESCRIPTION : compocasting unit - general arrangement

Detail No.	Description
1	Frame work
2	Variable speed drive
3	Electric motor
4	Bearing housing assembly
5	Rotor drive shaft
6	Rotor
7	Graphite injector piston
8	Push rod
9	Graphite injection screw
10	Crucible
11	Fork arrangement
12	Plug
13	Semi-solid zone heater
14	Liquid zone heater
15	Insulation material
16	Timing belt and pulleys
17	Fork arrangement swivel joint
23	Launder
Items not shown	
18	Liquid zone temperature controller
19	Semi-solid zone temperature controller
20	Thermocouples
21	Temperature readout
22	Tachometer

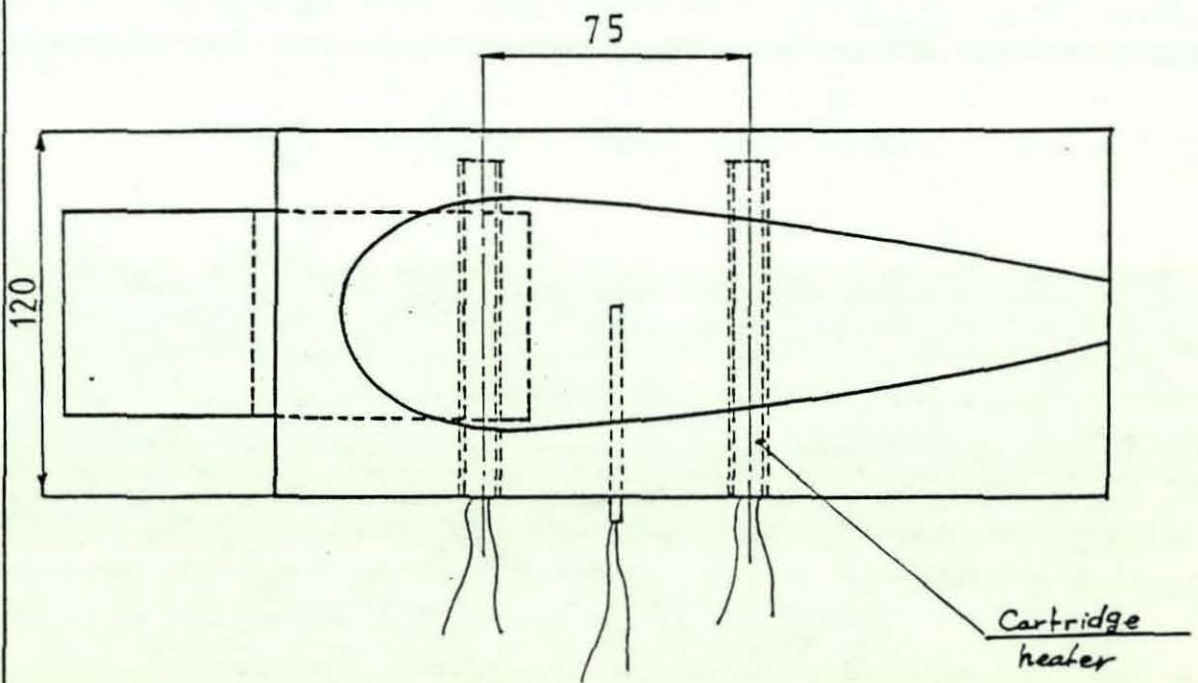
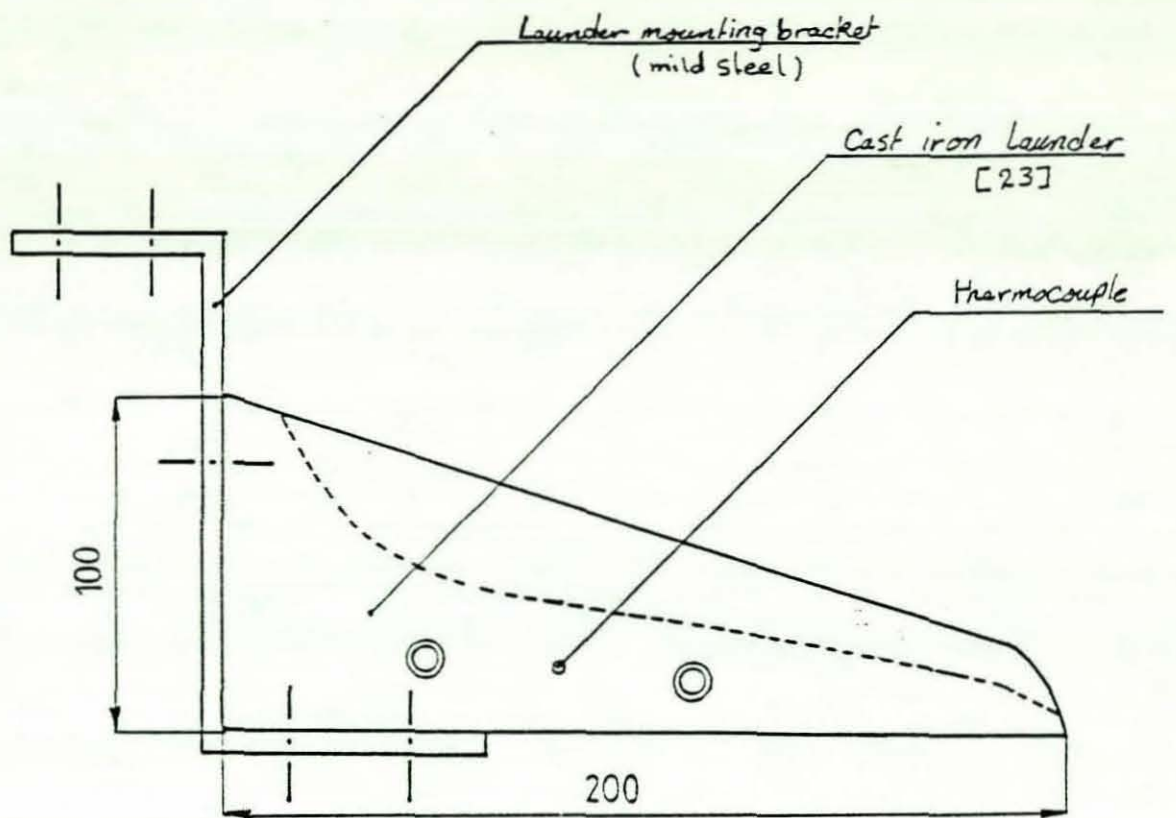
Fig. 20A - General Arrangement - Parts List

It was considered preferable that the composite slurry should fall directly into the shot chamber of the die casting machine. However, the design of the die casting machine imposed a restraint in respect of the method of transferring the composite alloy slurry from the compocasting unit to the shot sleeve due to the limited distance between the injection head and the fixed platen, and the position of the shot chamber in the pressure die casting machine. It was necessary in practice to transfer the slurry via a heated launder Fig.21.

The test casting design Fig.18 was evolved to provide the required specimens for mechanical properties and wear characteristics evaluation rather than to evaluate the degree of casting complexity attainable when pressure-diecasting a composite slurry. Provision was included in the die-design to enable different gate dimensions to be used. It was considered that, in addition to die temperature, injection pressure and injection speed the gate dimensions would be an important factor in the successful processing of the composite slurry. The dies shown in Fig.22 were preheated using thermostatically-controlled electric cartridge heaters. The design details are described in Appendix 2.

### 3.1 COMPOCASTING UNIT: DESIGN MODIFICATION, MANUFACTURE AND EVALUATION

As mentioned, the design of the pressure die casting machine, imposed a restraint on the design of the compocasting unit, due to the limited area between the injection head and the fixed platen. To make the compocasting unit as compact as possible, the temperature controllers for the upper and lower portions of the crucible were removed from the compocasting unit, stored in a separate box and fixed to the wall near the die casting machine. The plug was provided with a "T" junction, Fig.23, and the fork arrangement, Fig.24, was fixed to the bottom of the compocasting unit. When the slurry reached the desired volume fraction solid, the fork operates to pull the plug down so the slurry can be ejected from the crucible. The other side of the fork arrangement was provided

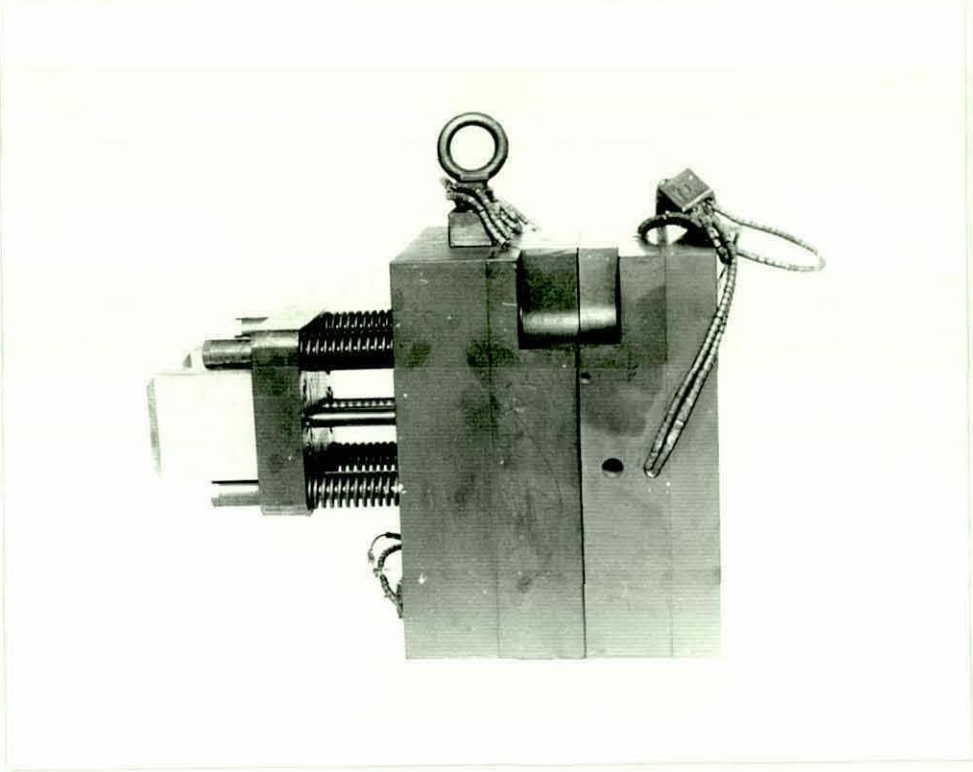


DRAWING NO: 21

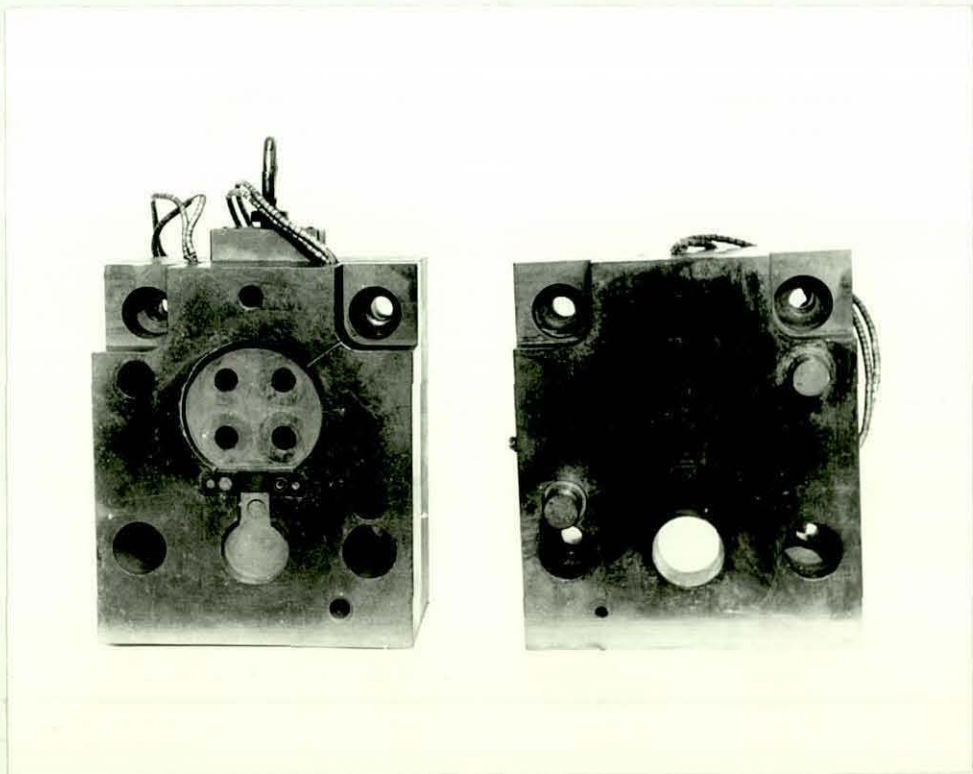
SCALE:

DIMENSIONS: mm

DESCRIPTION : cast iron launder



a - assembled die



b - the two die halves

Fig. 22 - Pressure Die Casting Die Design

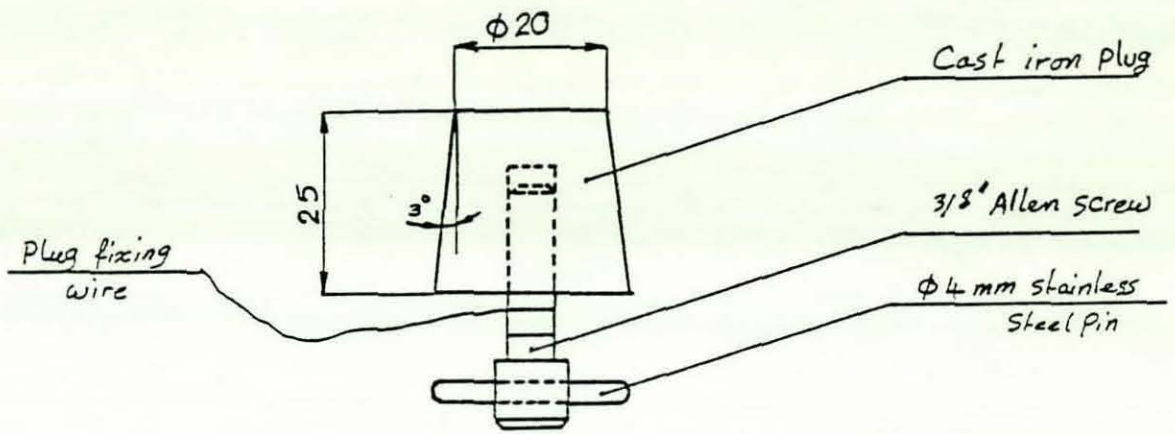


FIGURE 23

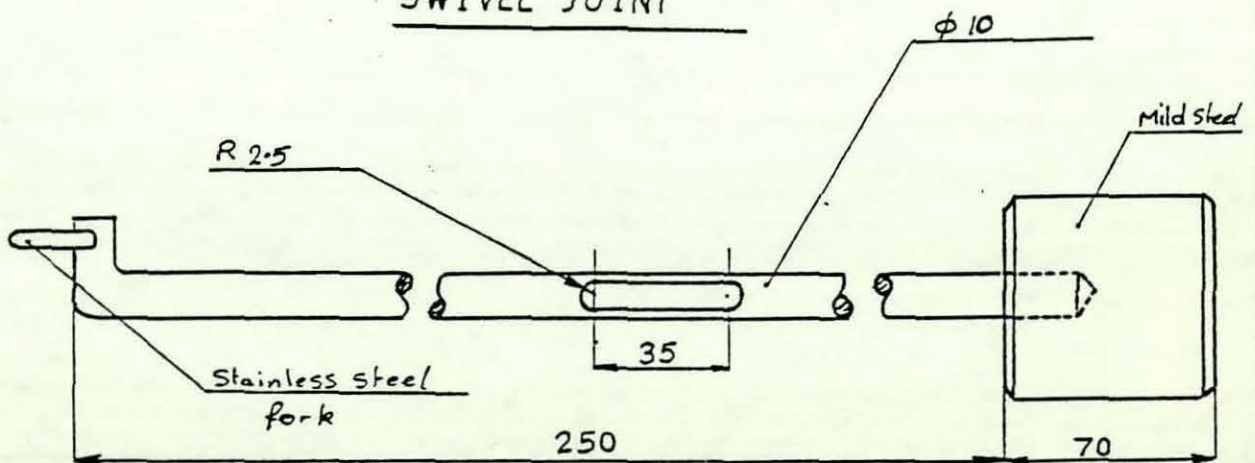
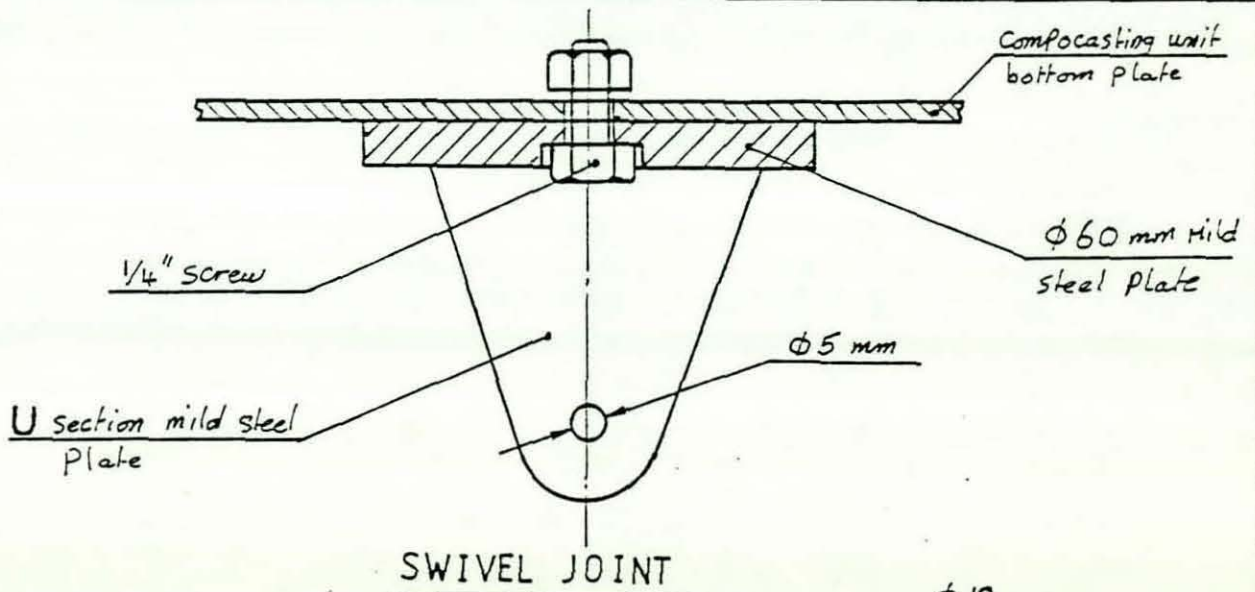


FIGURE 24

DRAWING NO : 23, 24

SCALE :

DIMENSIONS : mm

DESCRIPTION : fig. 23 - plug , fig. 24 - fork arrangement

with a counterbalance to ensure that the plug stayed in position in order to prevent the unscheduled departure of the slurry. A wire was used to connect the plug to the compocasting unit to prevent the plug running down with the slurry to the shot chamber of the die casting machine when the ejection takes place. A thermocouple was fixed to the crucible through a little hole made in the wall of the semi-solid portion to allow accurate measurement of the temperature of the slurry in the semi-solid zone Fig.20. The compocasting unit was manufactured and assembled as shown in Figs.20,21,23-26. Initial testing was carried out to evaluate the performance of the compocasting unit, and it was found that the unit performed well.

## 3.2 DIE CASTING EQUIPMENT

### 3.2.1 Gravity Die Casting Equipment

A copper die shown in fig.27 was employed as a means of producing gravity die castings from which the mechanical and tribological properties could be determined and compared with similar properties of castings produced by pressure die casting. The die was preheated to  $130^{\circ}\text{C}^{(84)}$  and the castings were made of fully liquid LM30 alloy without graphite addition.

### 3.2.2 Pressure Die Casting Equipment

The pressure die casting process has been used to investigate it's suitability for making castings of the LM30 semi-solid composite slurries, and to assess the mechanical properties which might be achieved by using this process.

The EMB No.10 cold chamber pressure die casting machine which existed at Loughborough University has been used. The machine is supposed to operate at 150 psi (10.21 Bar) air pressure, but the compressor which is connected to that machine does not permit more than 90 psi (6.13 Bar) maximum. From the outset this presented a limitation because the production of castings of reduced soundness was inevitable.

Height adjustment

Pin

Drive Pulley

Bearing housing  
holding bracket

Graphite injection screw [9]

Seal

Bearing

Rotor drive  
shaft [5]

Bearing

Bearing housing

Seal

150

105

185

Dovetail  
slide

30°

130

100

80

13

38

100

DRAWING NO: 25

SCALE: 1/2

DIMENSIONS: mm

DESCRIPTION: bearing housing assembly

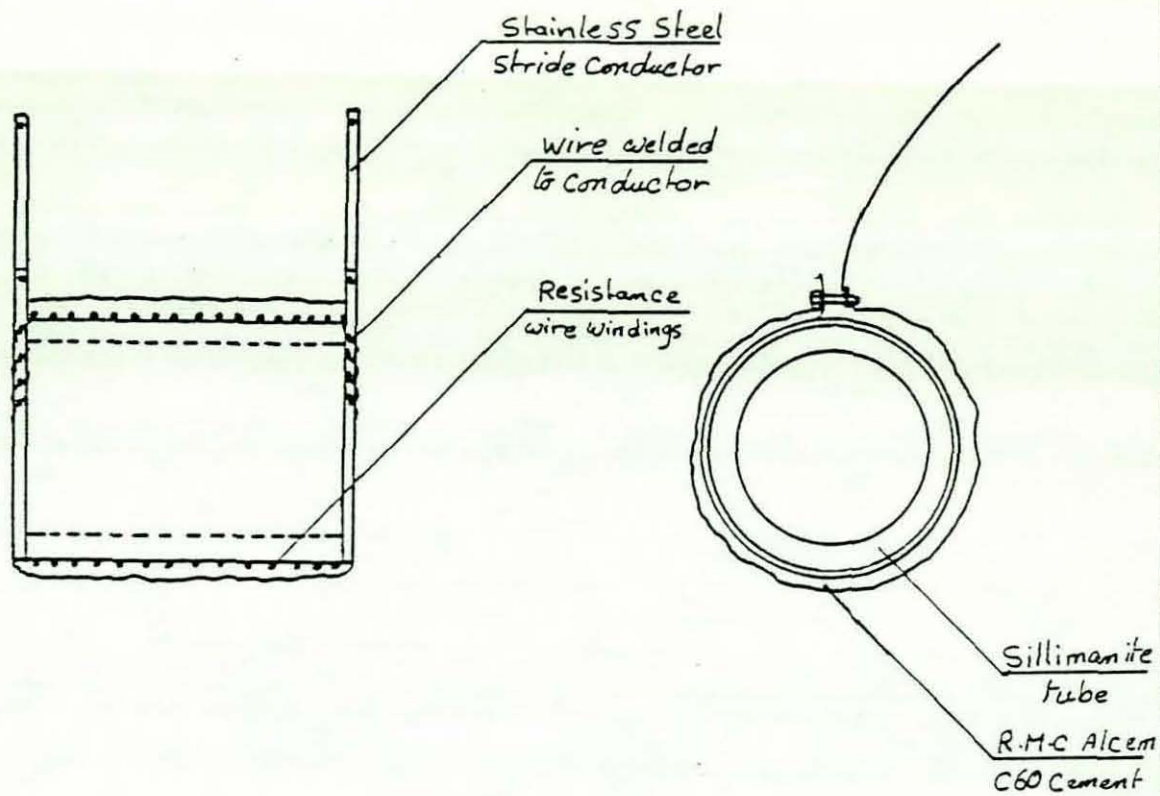


FIGURE 26

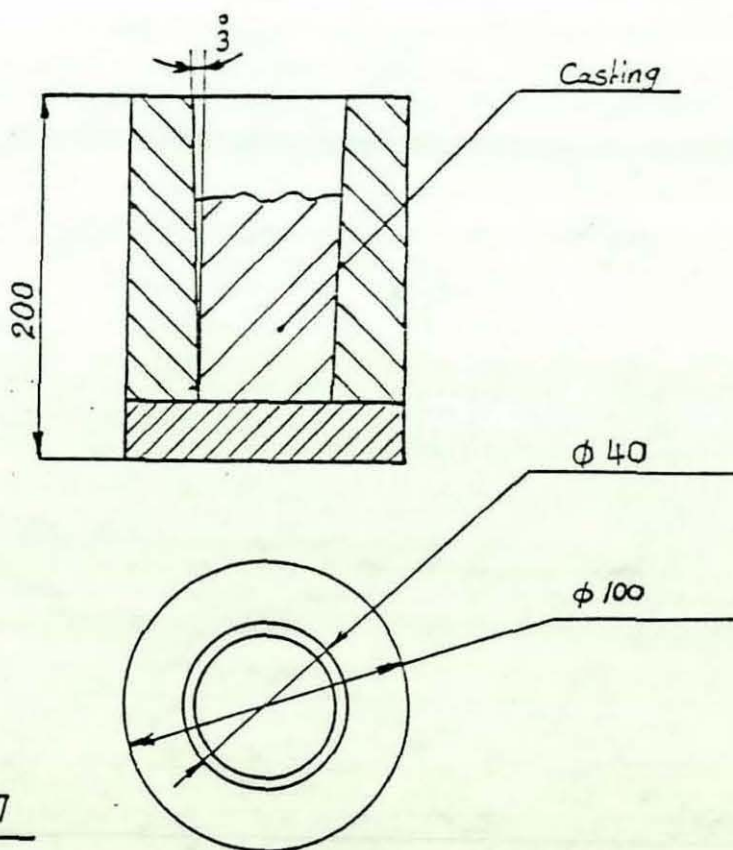


FIGURE 27

DRAWING NO: 26 , 27

SCALE:

DIMENSIONS: mm

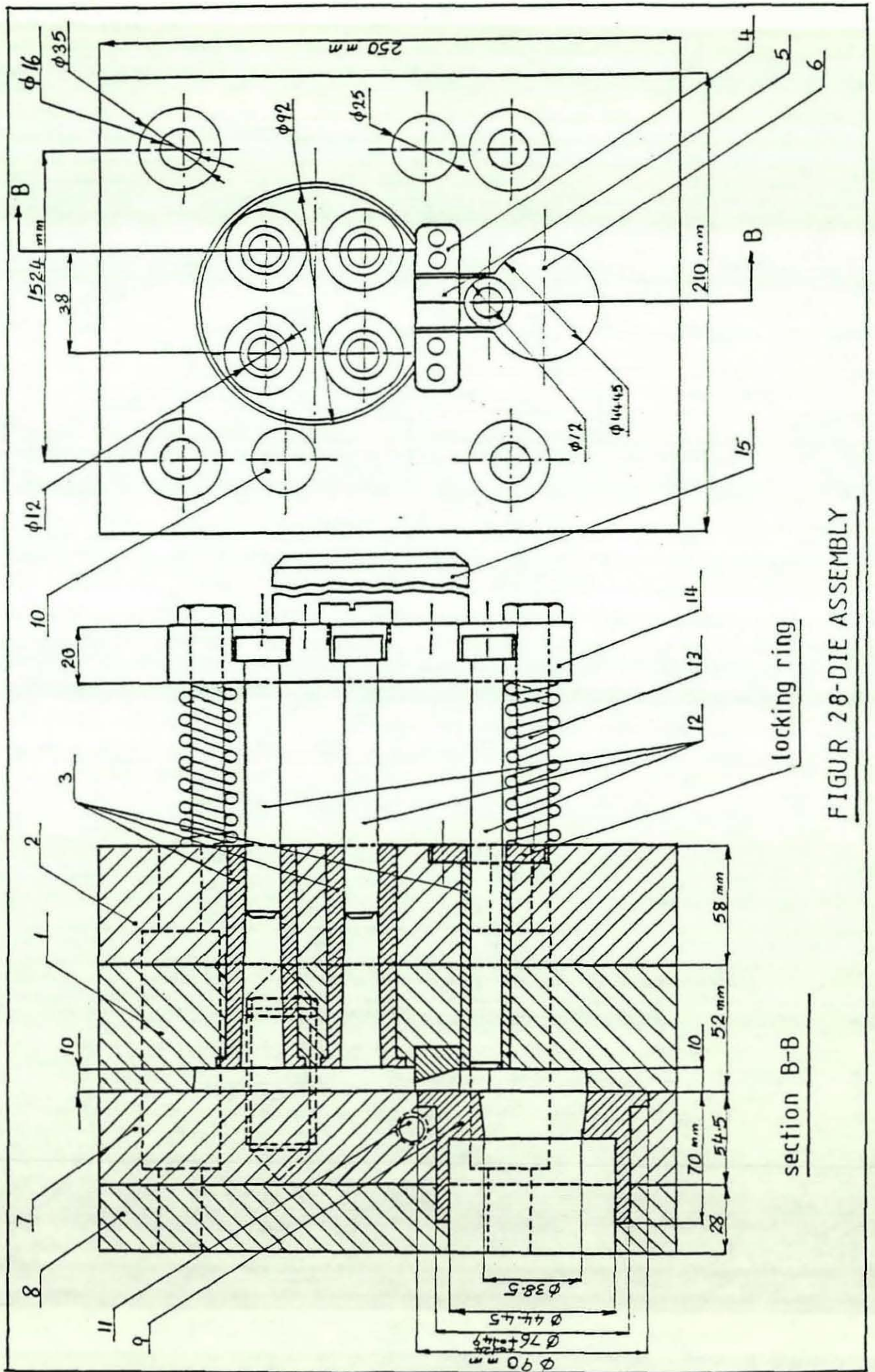
DESCRIPTION: fig.26-heating element , fig. 27- COPPER die

The die shown in Fig .22 and schematically in Fig.28 was used for the production of the castings to evaluate the compocasting process. The die consists of two halves and a simple die cavity was designed to provide the necessary specimens. The die cavity consists of four pins, of 12mm diameter and 70mm length with 1.5° taper, to provide the pin on disc wear specimens and the tensile specimens. The disc is 92mm in diameter and 10mm thick provided with 1.5° taper for ease of extraction, and it was designed to provide the necessary hardness test specimens. The die design also permits different gate dimensions to be used. Five gates were produced to the following dimensions:

Gate No 1	20mm x 1mm
Gate No 2	20mm x 2mm
Gate No 3	20mm x 3mm
Gate No 4	20mm x 4mm
Gate No 5	20mm x 5mm

It was found that gate No.4, with moderate injection speed for the given volume fraction solid, produced castings with minimum internal porosity and good surface finish. The die was also provided with an automatic ejector see Fig.28, so that when the moving platen retracted, the ejection plate holding the five ejector pins hit the ejection plate fixed to the machine and released the casting. The die was preheated to 300° C prior to injection. Heating of the die could be achieved by using the gas heating facilities provided with the cold chamber pressure diecasting machine, but difficulties in controlling the die temperature were experienced. Therefore, the system was replaced by seven compact cartridge heaters of 500 watt each, manufactured by Cole Equipment Ltd., in conjunction with a Newtronic temperature controller and chromel-alumel thermocouple. This allowed accurate control of die temperature in the range between the ambient temperature and 999° C.

The pressure die casting die was manufactured from H13 hot working die tool steel, hardened, tempered and ground in accordance with the manufacturer's instructions.



FIGUR 28-DIE ASSEMBLY

section B-B

Detail No	Description
1	Moving die member
2	Bolster
3	Ejector pin bushes
4	Gate
5	Runner
6	Sprue
7	Fixed die member
8	Bolster
9	Shot sleeve guide bush
10	Die guide pins
11	Cooling system
12	Ejector pins
13	Ejector guide pins
14	Ejector plate
15	Stop

Fig. 28A-- General Arrangement - Parts List

### 3.2.3 The Launder

A launder of 200mm length and 120mm width was designed to direct the composite slurry from the crucible of the compocasting unit to the shot chamber of the pressure die casting machine. The launder was first made of refractory material, since it is easy to form such material to the shape required. However, cracking, chipping and the necessity to preheat the launder to a temperature close to that of the composite slurry, to prevent heat exchange between the composite slurry and the cold launder, necessitated the use of a metal launder. This launder was made of cast iron using the refractory launder as a pattern, see Fig.21, and was provided with two thermostatically-controlled cartridge heaters of 750 watt each incorporated in the body of the launder to provide the required temperature. A Eurotherm temperature controller was used, in conjunction with a chromel-alumel thermocouple, to enable accurate measurement of the launder temperature to be obtained. The launder was fixed to the bottom of the compocasting unit and preheated to 400°C prior to the ejection of the composite slurry from the crucible of the compocasting unit.

## CHAPTER FOUR

### MATERIALS AND EXPERIMENTAL PROCEDURES

#### 4.1 Materials Used

(a) Alloy used for testing the compocasting unit as a slurry producer:

An alloy of 8wt% silicon (remainder aluminium) was used to evaluate the compocasting unit as a composite slurry producer. The alloy was made up from a master alloy of 50% silicon and 50% aluminium and LMO (99.6% purity), available from L.U.T. stock.

(b) Alloy used for the production of composite castings :  
BS 1490, 1970 LM30 Hypereutectic aluminium silicon alloy with a nominal composition of:

16 - 18%	silicon
4 - 5%	copper
0.4 - 0.7%	magnesium
1.1 max.%	iron
0.3 max.%	manganese
balance	aluminium

The alloy was supplied by "Tevacast Limited", Wolverhampton, as foundry ingots of 8lb (4kg) weight each. The analysis certificate provided with the alloy stated the following composition:

16.7%	silicon
4.55%	copper
0.61%	magnesium
1.08%	iron
0.17%	manganese
balance	aluminium

#### (c) Graphite

Multigrade synthetic graphite with particle sizes ranging from 44 mesh (353 $\mu$ m) down to dust and having a true density of 1.9 g/cm<sup>3</sup>, supplied by "James Durrans & Sons Ltd.", Barnsley, Sheffield was used. The graphite was sieved into different grades, using the mechanical sieve available. The graphite was subjected to vigorous shaking for at least 2 hours to ensure

that the graphite was separated properly. The literature made a reference for graphite grades ranging from 40 to 400 $\mu$ m and graphite addition levels up to 20wt% (16,32,41,44,46,83,95,109). To enable the results obtained from this investigation to be comparable with those obtained in previous investigations, the following graphite grades and graphite addition levels were chosen:

coarse graphite -44 +72 mesh (353-211 $\mu$ m)  
medium fine graphite -100 +150 mesh (150-105 $\mu$ m)  
fine graphite -200 +240 mesh (75 - 50 $\mu$ m)  
and the graphite addition levels were:

3%, 4½%, 6%, 7½% by weight

(d) Refractory coating.

Holcote 110, supplied by "Foundry Services Ltd.", Tamworth, Staffs, was used for coating the rotor to prevent the molten aluminium from sticking to it.

(e) Cement for sealing the plug and fixing the thermocouples. Triton Kaowool Cement, supplied by "Morgan Ceramics Ltd.", Merseyside, was used. The cement could withstand temperatures up to 1300°C.

(f) Aluminium foil.

Kitchen foil of 0.025mm thickness was used to keep the graphite inside the rotor until graphite injection took place.

(g) Nitrogen degassing.

Nitrogen degassing has been reported to release absorbed hydrogen and force the suspended inclusions to float on the surface of the molten aluminium so they can be removed by skimming the melt surface. White spot (oxygen free) nitrogen was used for degassing the melt. Silica gel was used for drying the nitrogen and the melt was degassed for ten minutes. For LM30 alloy it was found that degassing the melt for ten minutes typically reduced the level of hydrogen dissolved in the melt from 1.09 to 0.39CC/100g. Additional degassing for more than ten minutes, achieved no further reduction in hydrogen content. The alloy was tested using the technique called

"Quantitative Reduced Pressure Test" (QRPT) with equipment supplied by the Light Metal Founders' Association.

(h) Die lubricant

Acheson DAG 2582 graphite and water base mixture, supplied by "Acheson Colloids Company", Plymouth, was used as a die lubricant and release agent. The manufacturer's recommendation was to spray the die at 100°C to allow the water to evaporate, leaving a continuous thin layer of graphite on the die cavity surface. A pneumatic spray provided with the die casting machine was used to lubricate the die and the shot chamber of the diecasting machine.

4.2 Alloys preparation.

(I) Aluminium-8% silicon alloy.

The alloy of 8% silicon (remainder aluminium) was made up from the master alloys available from L.U.T. stock. The alloy was produced by melting together the required quantities of pure aluminium and the 50% silicon, 50% aluminium alloy in a salamander crucible using a gas furnace. The melt temperature was maintained at 800°C to allow the 50% silicon, 50% aluminium alloy to be fully dissolved. The melt was then degassed for ten minutes, skimmed and poured into steel ingot moulds which produced ingots of ~ 1lb (0.5kg) each. The alloy was produced only for evaluation of the compocasting unit as a slurry producer.

(II) Batches of 30lb (13.5kg) each of LM30 alloy were melted in a salamander crucible. The melt temperature was maintained at 750°C in order to prevent the precipitation of the primary silicon<sup>(86)</sup>. Other preparation procedures were identical to those mentioned in (I). The alloy was used for the production of test castings.

4.3 Composite alloy production.

4.3.1 Evaluation of the compocasting unit as slurry producer.

The compocasting unit shown in Fig.20 was evaluated as a slurry producer by using an 8wt% silicon-aluminium alloy. As this hypoeutectic alloy solidifies dendritically it is an excellent material for establishing whether or not the equipment, as designed, would provide an effective shearing action.

Four of the 1lb (0.5kg) ingots were remelted (using an electric

resistance furnace) to above the liquidus temperature, degassed, skimmed and poured into the crucible of the compocasting unit. When the alloy temperature reached the equilibrium value, the rotor was activated and a shear rate of  $343 \text{ sec}^{-1}$  was introduced and maintained until the slurry temperature in the semi-solid zone reached  $595^\circ\text{C}$ . The alloy was then discharged from the rheocasting unit and processed by the pressure diecasting route. For this temperature the volume fraction solid was calculated using the "Scheil equation" (see Appendix 3) and it was found to be 0.16 and the alloy was subjected to a cooling rate of  $1.5^\circ\text{C}/\text{min}$ . (constant by design).

The microstructure of the castings produced, shown in Fig.29, was examined to investigate the effect of process variables on the microstructure, in comparison with that of the same alloy processed by sand casting, see Fig.30. Further castings were made to assess the performance of the compocasting unit as a slurry producer, and to evaluate the method for incorporating graphite into the alloy slurry. The performance of the graphite injection system was first evaluated by using a similar method to that mentioned above except that graphite was injected when the temperature in the semi-solid zone reached  $610^\circ\text{C}$ . This was achieved by operation of the graphite injection screw. After graphite injection the alloy was stirred for at least five minutes before ejection to ensure good graphite distribution. An addition of 3wt% of -120 mesh, uncoated graphite was introduced successfully with even distribution, see Fig.31.

#### 4.3.2 Production of the Graphitic Hypereutectic alloy.

Having established that the compocasting unit performed satisfactorily with the hypoeutectic alloy the next stage was to utilise LM30 (the subject of this research) for making castings with different graphite addition levels and particle size distribution. This would permit the study of these two parameters on the mechanical properties and wear characteristics of the alloy processed by pressure diecasting.

In effect the production of a graphitic hypereutectic alloy requires the successful combination of three separate stages, each of which has it's own associated process variables.

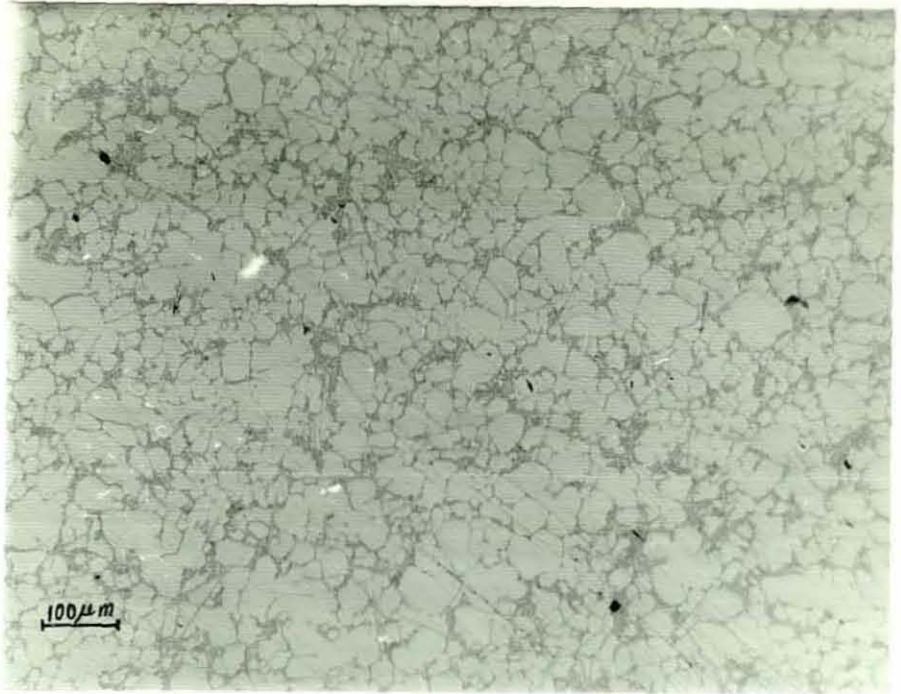


Fig. 29 - Aluminium - 8% silicon alloy rheocast,  
pressure diecast.

$$\dot{\gamma}_{\text{ave}} = 343 \text{sec}^{-1}, g_s = 0.18, \dot{\mathcal{E}}_{\text{ave}} = 1.5^\circ \text{C/min}$$



Fig. 30 - Aluminium - 8% silicon alloy  
processed by sand casting.

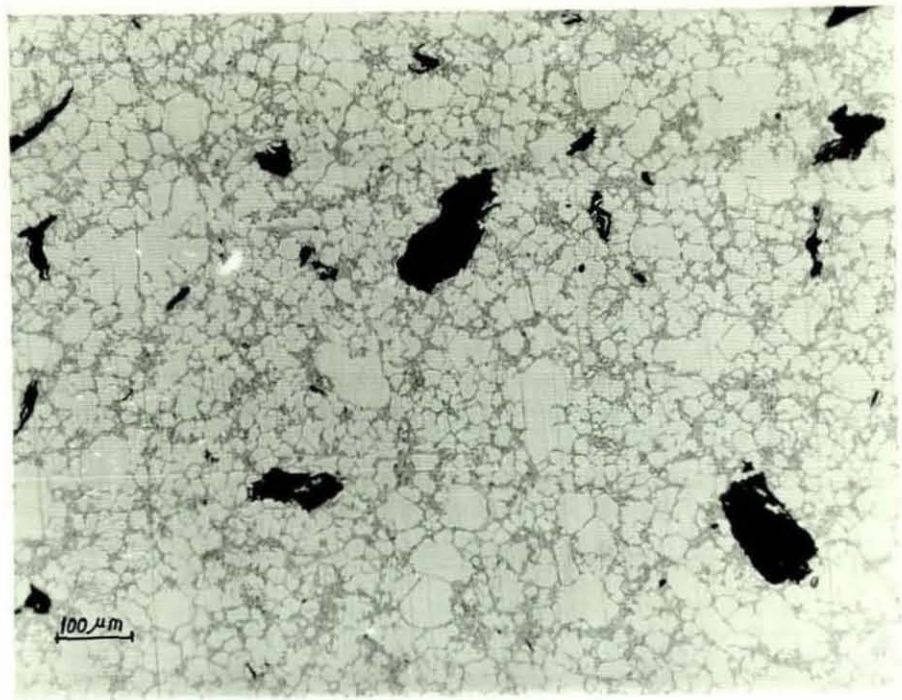


Fig. 31 - Aluminium - 8% silicon alloy compocast,  
pressure diecast, 3wt% graphite addition.  
 $\dot{\gamma}_{ave} = 550 \text{sec}^{-1}$ ,  $g_s = 0.18$ ,  $\dot{\epsilon}_{ave} = 1.5^\circ \text{C/min}$

### Rheocasting parameters

It has been shown that the important process variables in a continuous rheocaster (51) are:

- Average Shear Rate
- Average Cooling Rate
- Volume Fraction Solid

and the significance of these variables has been defined. It was not the intention in the current research to conduct a comprehensive evaluation of the influence of these variables on the structure and properties of the hypereutectic LM30 alloy. However, it was expected that these variables would have an important influence on the ability to produce an alloy containing different graphite addition levels. Consequently it was necessary to consider the effects of some of these variables. The first constraint in this respect was the construction of the equipment which was not provided with water cooling coils because this facility is usually only associated with a continuous rheocasting unit in which the average cooling rate has a significant influence on the throughput of the equipment. As the compocasting unit was to be used in a batch mode, water cooling coils were not provided, and therefore, average cooling rate was a constant.

In order to maintain a specific cooling rate, the compocasting unit was preheated to a specific temperature and the molten metal was poured into the compocasting unit at 725°C. Work by other researchers (51,53) showed that changes in the average shear rate, at a given volume fraction solid and average cooling rate, were not found to significantly affect the size of primary solid particles. However, increasing the shear rate was found to affect particle geometry and reduce viscosity. These effects were established using alloys which solidify dendritically whereas in alloy LM30 the primary silicon-rich  $\beta$  phase precipitates in the form of polyhedra. From the practical viewpoint it was necessary to establish the range of variables which would produce an alloy slurry that could be shaped into a casting. The viscosity or fluidity of the alloy slurry was therefore an important criterion.

### Viscosity measurement

In principle it should be possible to measure the power consumed during shearing when using a 3-phase induction motor

by using the two Watt meter method described by Hughes<sup>(37)</sup>. From the power consumed, torque and apparent viscosity may be determined using the following formulae:

$$\text{torque} = \frac{\text{power consumed}}{\text{angular velocity of rotor}}$$

$$\text{apparent viscosity} = \text{constant} \times \frac{\text{torque}}{\text{rotational speed}}$$

However, a major problem arose because the power consumed, under free load conditions and at constant speed of rotation, was found to decrease with time. To reach the steady state power it was necessary to run the electric motor continuously for 60 minutes. However, once the motor was switched off and on again the power value recorded by the two Watt meters changed to an unpredictable value above the steady state value. This was due to two reasons:

(I) The effective increase in oil temperature of the hydraulic variable speed drive coupled to the electric motor results in a reduction in its viscosity. This in turn reduces the frictional losses resulting in a reduction in the power consumed.

(II) The increase in temperature of the electric motor winding results in an increase in its resistance and hence a reduction in the amount of current passing through which resulted in less power consumption.

For these reasons, the power consumed after 60 minutes of continuous rotation was found to be about 50% less than that at the beginning of the test, see Table 1.

For the reasons mentioned above the method was considered unsuitable for use in the experimental work and it was necessary to exercise a subjective assessment based on the observed ability of the slurry to flow.

#### Shear rate

Shear rate can be varied simply by increasing the speed of rotation of the shearing rotor. The maximum speed of the motor arrangement employed was 2650 rpm but in practice a speed of 1500 rpm could not be exceeded without severe and unacceptable vibration. It was evident from the literature that increasing the shear rate reduces the slurry viscosity and this provides

Table 1: Relationship between power consumed and time for three phase induction motor on free load.

time (minutes)	power consumed by 1 <sup>st</sup> watt meter (Watt)	power consumed by 2 <sup>nd</sup> watt meter (Watt)	total power (Watt)
0	305	80	385
5	243	22	265
10	227	12	239
15	218	6	224
20	213	0	213
25	210	-1	209
30	207	-4	203
35	206	-5	201
40	204	-6	198
45	202	-7	195
50	202	-8	194
55	202	-8	194
60	202	-8	194

the incentive to maximise shear rate in order to maximise fluidity. However, before selecting a rotor speed of 1500 rpm it was necessary to establish if variations in shear rate would influence the primary silicon particle size and distribution. Rheocast melts were therefore produced using rotor speed of 750, 1000 and 1500 rpm (evident shear rates of 297, 396 and  $550 \text{ sec}^{-1}$ ) at a constant average cooling rate ( $1.5^\circ\text{C}/\text{min.}$ ) and volume fraction solid (0.075). Examination of the microstructure of each of these slurries did not reveal any significant difference in silicon polyhedra shape or size but it did affect their distribution in the melt, see Figs. 31A-31C. Under these circumstances there was no reason why the maximum attainable shear rate should not be used.

#### Volume fraction solid

With the average cooling rate a constant by design and the shear rate a constant by selection, the only variable which could be manipulated was volume fraction solid which would be affected directly by the temperature selected for the slurry zone in the rheocasting unit. Thermal analysis established the liquidus and solidus temperatures for the experimental alloy to be  $650^\circ\text{C}$  and  $505^\circ\text{C}$  respectively. At any temperature between these limits the volume fraction solid could be estimated from the relationship published by the SAE (88). The actual temperatures used in experimentation together with the estimated volume fraction solid values and observations on alloy fluidity are shown in Table 1A. The experimental procedure was as follows:

- (I) Liquid zone temperature controller set at  $670^\circ\text{C}$  ( $20^\circ\text{C}$  above the liquidus).
- (II) Slurry zone temperature controller set at a predetermined temperature.
- (III) Molten alloy transferred by crucible from the electric resistance furnace and poured into the rheocaster when its temperature reached the predetermined temperature.
- (IV) When the alloy temperature reached an equilibrium value the rotor was activated and its speed set and checked using a tachometer.
- (V) When the slurry temperature matched the pre-set temperature, established with an independent measuring system, the slurry was discharged.

(VI) To shape the discharged slurry it was necessary to establish initial values for the pressure die casting process variables. These were chosen arbitrarily to be: die temperature 250°C; gate dimensions 20x4mm; injection speed fast and launder temperature 300°C. The discharged slurry was allowed to run down via the preheated launder to the shot chamber and injected immediately.

(VII) The casting was then allowed to solidify completely before ejection from the die.

(VIII) After solidification, the microstructures of castings produced with different volume fraction solid values were observed.

### Observations

The microstructure observation for castings made from the hypoeutectic alloy revealed the effect of shear rate on the size and geometry of the primary  $\alpha$  particles at a given volume fraction solid and average cooling rate in comparison with the same alloy cast from above its liquidus temperature, see Figs.29-31.

Investigation of the microstructures for castings made of the hypereutectic alloy produced by different shear rates for given volume fraction solid and average cooling rate values revealed no significant difference in terms of size and geometry of silicon polyhedra produced. However, slurries produced with the lower shear rate exhibited lower fluidity and agglomerations of primary silicon in some areas, see Figs.31A-31C.

It was established that 557°C was the lowest temperature at which a fluid slurry, with a volume fraction of 0.15 and sheared at a rate of 550 sec<sup>-1</sup>, could be processed. Below this temperature the slurry solidified on the launder.

For hypoeutectic and hypereutectic alloys it was observed that in order to ensure good graphite distribution, shear rates in excess of 396 sec<sup>-1</sup> should be used and the alloy should be stirred for at least five minutes after graphite injection into the melt.

The procedure for calculating the rheocasting process variables is shown in Appendix 3.

Table 1A: Relationship between rheocasting process variables and viscosity observations.

Shear rate ( $\text{sec}^{-1}$ )	Ejection temperature ( $^{\circ}\text{C}$ )	Volume fraction solid	Viscosity observations
550 $\text{sec}^{-1}$ rotor speed 1500 rpm	640	0.0075	very fluid
	632	0.02	very fluid
	625	0.025	very fluid
	620	0.0275	low viscosity
	608	0.03	low viscosity
	589	0.04	low viscosity
	573	0.075	low enough for making castings
	565	0.10	low enough for making castings but part of the slurry solidified on the launder.
	557	0.15	just sufficient for making castings. slurry hardly filled the shot chamber of the diecasting machine

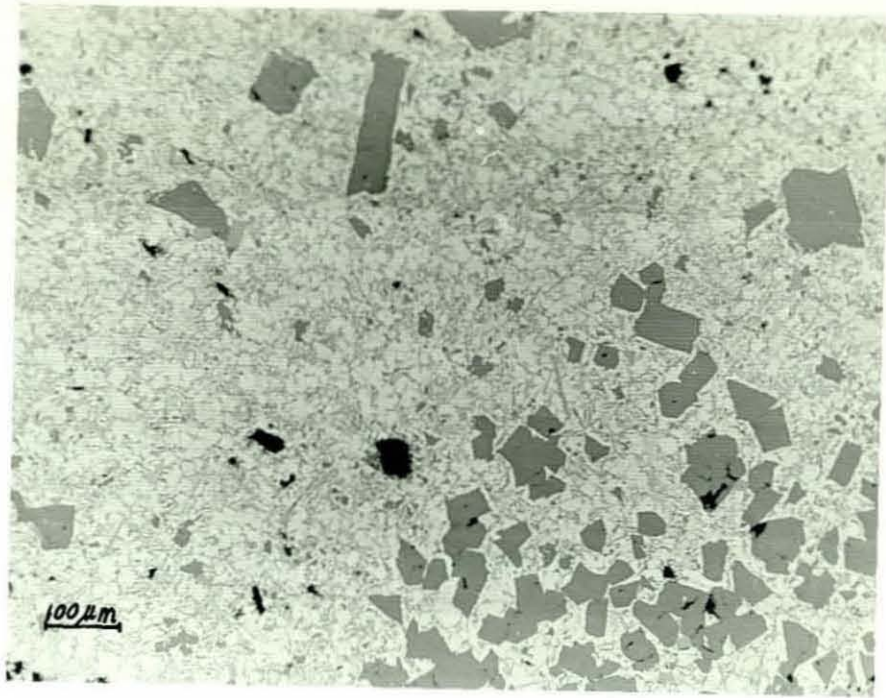


Fig.31A - LM30 alloy Rheocast, Pressure Diecast.  
 $\dot{\gamma}_{ave} = 297 \text{ sec}^{-1}$ ,  $g_s = 0.075$ ,  $\dot{C}_{ave} = 1.5^\circ \text{C/min.}$

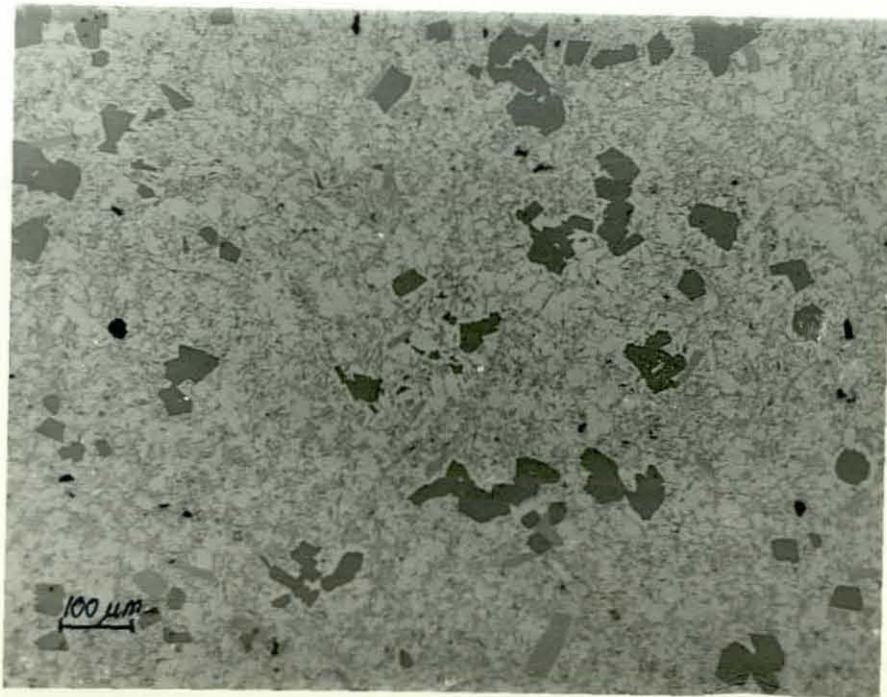


Fig.31B - LM30 Alloy Rheocast, Pressure Diecast.  
 $\dot{\gamma}_{ave} = 396 \text{ sec}^{-1}$ ,  $g_s = 0.075$ ,  $\dot{C}_{ave} = 1.5^\circ \text{C/min.}$

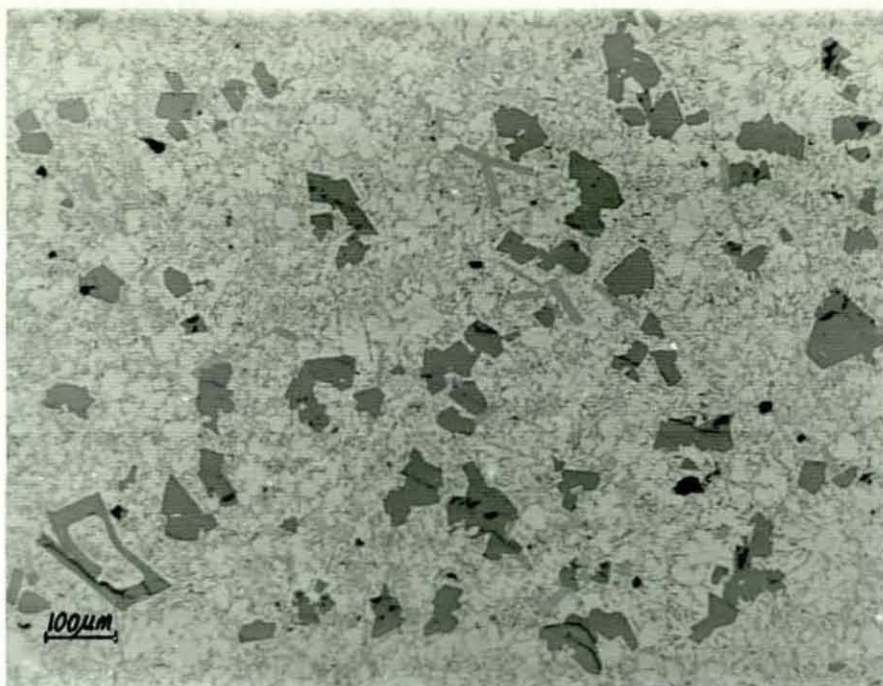


Fig.31C - LM30 Alloy Rheocast, Pressure Diecast.

$$\dot{\gamma}_{ave} = 550 \text{ sec}^{-1}, g_s = 0.075, \epsilon_{ave} = 1.5^\circ \text{C/min.}$$

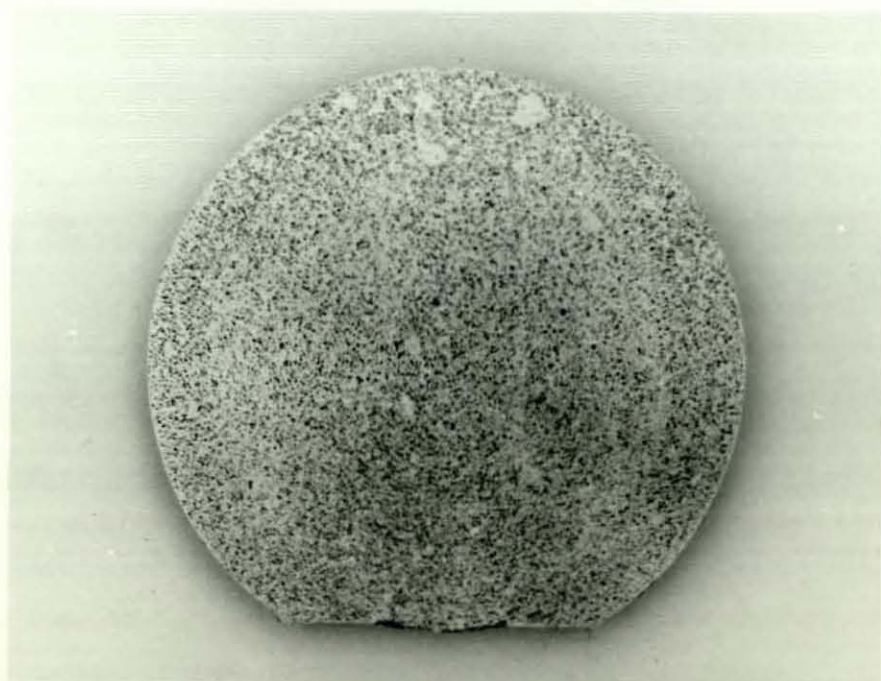


Fig.31D - LM30 Alloy Graphite distribution,  $7\frac{1}{2}$ wt% graphite.

$$\text{Shear Rate} = 297 \text{ sec}^{-1},$$

Scale 1/1.

### Compcasting parameters

The essential difference between rheocasting and compocasting is the presence of the graphite particles. As these graphite particles are stored within the rotor at a temperature in equilibrium with that of the alloy slurry, addition of the particles to the slurry should not change the temperature conditions. However, the addition of graphite particles will change the volume fraction solid and therefore the slurry's viscosity even if all other variables remained constant. Without the ability to accurately measure viscosity there was little point in experimentation requiring the production of a slurry at each of the nine volume fraction solid contents together with each of the twelve graphite addition levels (four weight additions of three different gradings).

With the objective being to produce slurries containing up to 7½wt% graphite the most difficult slurries to produce and process would be those containing the maximum amount of graphite.

Providing that the conditions for processing this alloy could be determined it was anticipated that slurries containing less than 7½wt% graphite would present little difficulty. Two approaches could be considered:

- (1) Maintain a constant initial volume fraction solid for all graphite addition levels.
- (2) Maintain a constant final volume fraction solid by adjusting the initial volume fraction to accomodate the graphite addition level.

In either case the objective would still be to obtain a final viscosity which would enable a fully shaped casting to be produced. Of these two approaches the former is the more attractive because it enables the three principal rheocasting variables to be maintained as constants. Then, by concentrating activity on the production of the most difficult alloy, the initial volume fraction solid would be established by determining the minimum temperature at which a slurry containing 7½wt% graphite could be processed. Using this approach would provide the advantage of improved fluidity as the graphite content was reduced, whilst maintaining standard processing conditions.

As three different grades of graphite were to be used and the particle size might be expected to exert an influence on viscosity this factor was also taken into account. However, instead of

considering each graphite grade at each predetermined temperature, the conditions for processing an alloy containing 7½wt% of the medium fine graphite were determined. These conditions were then used for slurries containing 7½wt% of the coarser and finer graphite grades respectively, and found to be acceptable.

The experimental procedure for establishing the compocasting parameters was essentially similar to that for establishing the rheocasting parameters, with the difference being that graphite particles were introduced at stage (V). The experimental conditions and observations are reported in Table 1B.

A final concern was that the graphite addition should be evenly distributed throughout the resultant castings. This was established by micro- and macro-structural evaluation of the castings produced. In addition, although a decision had already been made regarding shear rate, the effect of shear rate on graphite distribution was considered. Graphitic alloy slurries were processed using shear rates of 297, 396 and 550 sec<sup>-1</sup>. Whilst an acceptable graphite distribution was obtained with the two higher shear rates, the lowest shear rate produced a casting containing agglomerates of graphite particles and graphite free areas. This was observed even with coarse graphite additions, see Fig.31D.

Graphite was injected into the melt when the temperature in the semi-solid zone reached the required temperature. This was achieved by operation of the graphite injection screw.

To establish the relationship between shear rate, volume fraction solid and graphite addition level, the shear rate and temperature values used previously were used again to study the effect of slurry temperature on graphite dispersion and retention.

Observations were made about the effect of graphite addition on the volume fraction solid of the alloy slurry and hence its viscosity. It was found that in order to maintain a viscosity which would permit the slurry to fill the shot chamber of the pressure diecasting machine, the slurry should be ejected from the compocasting unit at a temperature of 573°C (i.e. at an initial volume fraction solid of 0.075+7½wt% graphite addition).

For slurry temperature below 573°C i.e. for volume fraction solid in excess of 0.075+graphite, the slurry either solidified on the launder or did not eject from the crucible of the compocasting unit. It was also observed that the fine grade of graphite slightly reduced the fluidity of the composite slurry in comparison with medium fine and coarse graphite for the same addition level.

However, the fluidity of the composite slurry was still sufficient for making castings.

Having established the optimum conditions for graphite dispersion and retention, the next stage was to establish the relationship between the pressure diecasting variables in order produce sound castings.

Table 1B: Relationship between the Compoasting Parameters and Viscosity Observations.

Shear rate ( $\text{sec}^{-1}$ )	Ejection temperature ( $^{\circ}\text{C}$ )	Volume fraction solid	Observations	
			Graphite	Viscosity
550 $\text{sec}^{-1}$ rotor speed 1500 rpm	640	0.0075	totally rejected	very fluid
	632	0.02	totally rejected	very fluid
	625	0.025	partially accepted	very fluid
	620	0.0275	partially accepted	low viscosity
	608	0.03	partially rejected	low viscosity
	589	0.04	totally accepted	low enough for making castings.
	573	0.075	totally accepted	just sufficient for making castings
	565	0.10	totally accepted	not sufficient for making castings

The above experiments were carried out using  $7\frac{1}{2}\text{wt}\%$  medium fine graphite addition level.

### Pressure Diecasting Parameters

In considering the pressure diecasting parameters it was assumed that the starting point was a graphitic alloy slurry with sufficient fluidity to enable a shaped casting to be produced. However, as already indicated, the slurries containing different amounts of graphite would in practice have different viscosities. Once more the number of experiments necessary to establish the optimum diecasting conditions for each graphite grade and addition level would be unacceptably large. For this reason the decision was again taken to concentrate on the most difficult case of a slurry containing 7½wt% graphite.

As the injection piston pressure was a machine constant the important processing variables were considered to be:

- die temperature
- injection speed
- gate dimensions

Variation of the injection speed was restricted to the three speeds provided by the manufacturer and specified non-numerically as: slow, moderate and fast.

From previous work on the squeeze casting of graphitic aluminium-silicon alloys <sup>(83)</sup> it was known that the die temperature should exceed 200°C to ensure conformity of the slurry to the die cavity and this temperature, together with 250°C and 300°C, was selected for the investigation. Whilst it might be anticipated that the gate dimensions for a slurry should be larger than those necessary for a superheated liquid, the gate plays an important role in providing a shearing action to counteract the reduction in viscosity caused as a slurry cools in the injection system. Whilst provisions had been made to incorporate five different gates in the die only three of these, the two extreme sizes and the mid-range size, were used in the experiments. Even with this modest selection of variables it was necessary to produce 27 castings to assess the diecasting parameters. Evaluation consisted of a subjective assessment of the conformity of the casting to the die cavity and an objective assessment of porosity by radiography, see Figs. 32 and 33. For comparison the castings were considered in three groups with the die temperature held constant whilst the other two parameters were varied. The conditions and results of these experiments are shown in Table 1C. The cold chamber EMB No.10 pressure diecasting machine available

in the department was used for the investigation. The machine consists of a split die, a locking mechanism, plunger and shot sleeve assembly and was provided with an accumulator tank and control. The machine also provides the following features:

Weight per shot (including slug)	0.94 lb (0.426 kg)
Diameter of injection plunger	1½ ins. (38.1 mm)
Total force on injection plunger (150 psi. air pressure)	11.775 lbs. (5,341 kg)
Maximum pressure on metal	6650 lb/in <sup>2</sup> (468 kg/cm <sup>2</sup> )
Full stroke of plunger	8 in. (203.2 mm)
Rate of injection	600 in <sup>3</sup> /sec (9832 cm <sup>3</sup> /sec.)
Die locking force	75 Tons (British)
Projected casting area	38 in <sup>2</sup> (245 cm <sup>2</sup> )
Minimum dry cycling time	4 seconds
Maximum compressed air used per shot	15 cu.ft. free air at 150 psi.
Recommended die temperature for aluminium silicon alloys	200°C

The pressure values on the diecasting machine were set to provide the maximum possible pressure since the compressed air supplied to the machine has a pressure value less than that recommended for the reasons mentioned before.

In order to investigate the relationship between the process variables, the following compocasting process parameters were held constant:

- shear rate 550 sec<sup>-1</sup>.
- cooling rate 1.5°C/min.
- volume fraction solid 0.075 + graphite

The die temperatures were set on the Newtronic temperature controller and monitored by a chromel-alumel thermocouple fixed in a hole made as close as possible to the die cavity in order to obtain accurate measurements of die temperature and the die was dressed with liquid graphite lubricant before each casting. The castings produced were evaluated according to the methods mentioned above and observations were made regarding the optimum combination of pressure diecasting variables for 7½wt% medium fine graphite composite slurry, these were found to be:

- die temperature 300°C
- gate dimensions 20x5 mm
- injection speed moderate

This was decided according to Table 1C and the radiographic examination which was carried out only for castings which exhibited very good conformity to the die cavity. Castings produced for the above parameters exhibited much reduced internal porosity in comparison with castings produced for the same parameters except the injection speed was fast. Four more castings were produced (two for each injection speed) to assess the above finding.

TO investigate the validity of the above parameters for shaping slurries with different graphite addition levels, three castings were made with medium fine graphite additions of 3%, 4½% and 6% by weight. Castings were evaluated in a similar manner and a conclusion was made about the optimum pressure diecasting parameters which were suitable for shaping the graphitic aluminium silicon alloy.

As mentioned before the injection speeds were specified non-numerically by the manufacturer of the pressure die casting machine. However, experimental work was carried out to establish the actual values of the injection speeds used in the investigation and they were found to be:

slow injection speed = 46 ft/sec. ( 14 ) m/sec.

moderate injection speed = 121 ft/sec. ( 37 ) m/sec.

fast injection speed = 161 ft/sec. ( 49 ) m/sec.

Table 1C: Relationship between pressure diecasting parameters and casting integrity

	Die temperature (°C)	Injection speed	Gate size (mm)	Observations on conformity to die cavity
Group one	200	slow	20x1	bad die filling obtained
		slow	20x3	bad die filling obtained
		slow	20x5	bad die filling obtained
		moderate	20x1	bad die filling obtained
		moderate	20x3	bad die filling obtained
		moderate	20x5	poor conformity to die cavity
		fast	20x1	poor conformity to die cavity
		fast	20x3	poor conformity to die cavity
		fast	20x5	poor conformity to die cavity
Group two	250	slow	20x1	poor conformity to die cavity
		slow	20x3	poor conformity to die cavity
		slow	20x5	poor conformity to die cavity
		moderate	20x1	poor conformity to die cavity
		moderate	20x3	poor conformity to die cavity
		moderate	20x5	poor conformity to die cavity
		fast	20x1	poor conformity to die cavity
		fast	20x3	poor conformity to die cavity
		fast	20x5	good conformity to die cavity
Group three	300	slow	20x1	poor conformity to die cavity
		slow	20x3	poor conformity to die cavity
		slow	20x5	good conformity to die cavity
		moderate	20x1	poor conformity to die cavity
		moderate	20x3	good conformity to die cavity
		moderate	20x5	very good conformity to die cavity
		fast	20x1	good conformity to die cavity
		fast	20x3	very good conformity to die cavity
		fast	20x5	very good conformity to die cavity

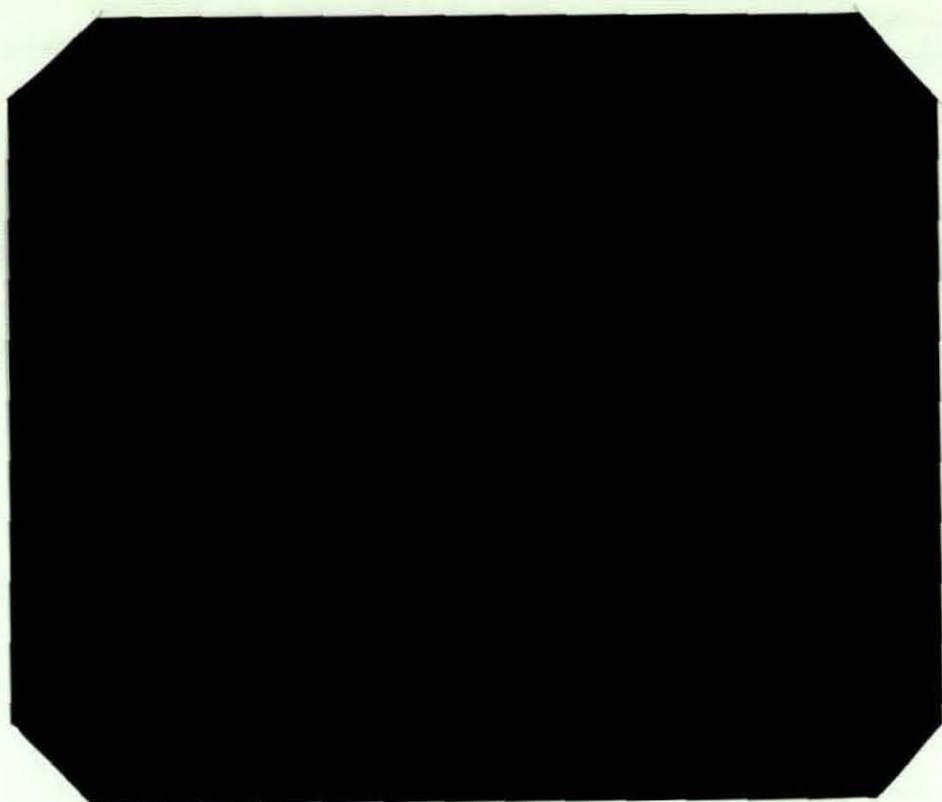


Fig. 32 - Determination of Pins Soundness According to the Quality Image Indicator. X-ray Sensitivity = 0.04

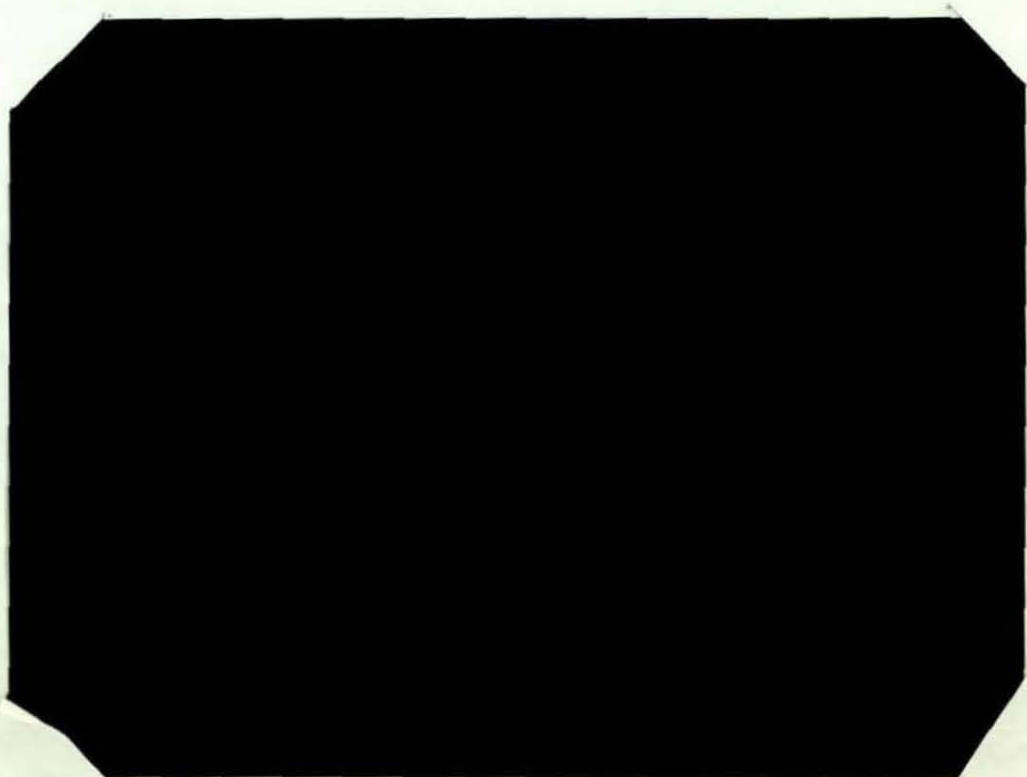


Fig. 33 - Determination of Sprues Soundness According to the Quality Image Indicator. X-ray Sensitivity = 0.011

variables to assess repeatability.

#### 4.3.4. The Production of Pressure Die Castings

Castings were produced with different graphite contents and different graphite particle sizes from which samples could be taken for the investigation of the mechanical and tribological properties.

The following parameters were held constant during the production of these castings:

- shear rate  $550\text{sec}^{-1}$
- volume fraction solid  $0.075 + \text{graphite}$
- cooling rate  $1.5^\circ\text{C}/\text{min.}$
- die temperature  $300^\circ\text{C}$
- gate dimension  $20 \times 4\text{mm}$
- injection speed Moderate
- launder temperature  $400^\circ\text{C}$

The castings (36 in total) were produced by the method previously outlined. The macrostructure of selected castings was examined to check graphite distribution. Specimens for pin on disc wear tests, tensile and hardness tests were prepared from each casting.

#### 4.3.5 The Production of Control Castings

Control castings were produced to obtain data which could be used as a basis for comparison with the compocast graphitic alloys. Control castings were made from the same alloy (LM30) but without graphite additions and were produced by four different routes:

- control castings produced by gravity die casting.
- control castings produced by conventional pressure die casting.
- control castings produced by rheocasting and pressure die casting.
- control castings produced by sand casting.

For gravity die casting, the alloy was superheated to  $750^\circ\text{C}$  and poured into the copper die preheated to  $130^\circ\text{C}$ .

For conventional pressure die casting, the alloy was superheated to the same temperature, poured into the shot chamber of the pressure die casting machine and injected immediately. The die was lubricated using liquid graphite and the process variables were similar to those used with the composite slurry and described in (4.3.4). For rheocasting, the alloy was processed following the procedures outlined for compocasting, but without the graphite addition.

For sand casting, the alloy was superheated to 750°C and poured into a green sand mould produced from sand having a moisture content of 5%. Two control castings were produced by each of the four routes. Specimens were prepared from each control casting for the previously specified tests.

#### 4.3.6 Introduction of Graphite Under Protective Gas Shielding

During the production of the graphitic aluminium-silicon alloy by the compocasting route a problem arose whereby hard spots were observed in the castings. Kay and Street<sup>(89)</sup> have classified the inclusions that appear in pressure die castings in three groups, these are:

- (1) aluminium oxide, either as a skin of oxide formed on the molten metal during transport, or oxide particles produced during melting and holding.
- (2) Intermetallic compounds formed firstly by the metal composition creating the right conditions and secondly by allowing them to segregate through inefficient temperature control or by neglecting to stir the metal in the crucible.
- (3) Non-metallic particles accumulated in the metal from ladles, crucibles or tools.
- (4) Small particles which have formed during the injection of the die-cast metal and have solidified separately.

The authors also stated that the molten metal forms oxide at a rate which increases with temperature and this is the major cause of hard spots.

The compocasting unit, shown in Fig.20, was designed to avoid any disturbance of the top layer of the molten metal, however,

in practice, the vortex formation was inevitable. The disruption of the oxide film on the surface of the molten aluminium from the turbulence created by the stirring rotor will lead to a continuous build up of further oxide formation. Therefore it was decided that an inert gas shield should be used to prevent oxygen being in contact with the molten aluminium.

Dry nitrogen (white spot-oxygen free) with a flow rate of 8l/min. was used to protect the melt surface during the preparation of the alloy in the compocasting unit. The use of a nitrogen shroud resulted in total graphite rejection from the melt, although the process parameters were exactly the same as when the graphite was totally accepted (without inert gas shielding). Different graphite grades were tried together with different flow rates of nitrogen, but total rejection of graphite still occurred. The replacement of nitrogen with argon and the use of a higher volume fraction solid (up to 0.15) resulted in similar findings. However, the use of nickel coated graphite particles resulted in total dispersion of graphite in the melt. Therefore it was assumed that the presence of oxygen has an effect on the dispersion of graphite in the alloy. During the course of the investigation, analysis has been carried out on specimens from the castings which rejected graphite (the use of inert gas shielding) and specimens which accepted graphite (without inert gas shielding). The analysis method and the results are considered in the discussion chapter under the heading "investigation of graphite rejection".

4.4

#### METHODS AND EQUIPMENT USED FOR THE EVALUATION OF THE COMPOSITE ALLOY

The evaluation was carried out on the castings produced by compocasting and the control castings. The evaluation consisted of the following:

- (1) macrostructure and microstructure observation
- (2) tensile properties determination
- (3) Brinell hardness measurement
- (4) pin on disc wear test evaluation

#### 4.4.1 Macrostructure and Microstructure Observation

(I) The macrostructure was examined with the naked eye or photographed and enlarged using the standard photographic equipment available. The samples were first ground and polished using the following equipment:

- (a) Buehler hand grinder with four grades of silicon carbide paper; P240, P360, P480 and P600.
- (b) Metaserv polisher with nylon cloth and 6 $\mu$ m diamond paste for rough polishing and Metron cloth with 1 $\mu$ m diamond paste for finishing.

Macrostructures were produced by cutting vertical and horizontal sections from castings, from which dispersion and distribution of graphite particles could be observed.

Microstructures were prepared by grinding with successive grades of wet silicon carbide paper from P360 down to P600. The samples were then rough polished with nylon cloth and 6 $\mu$ m diamond paste and fine polished with 1 $\mu$ m diamond paste and a Metron cloth.

Some difficulties were experienced during polishing of the graphitic alloy specimens due to the graphite becoming smeared on the surface of the matrix. However, the problem was solved by reducing the load on the specimen to the minimum during the last minute of the final polish. The LM30 alloy exhibited a very clear structure with the polishing procedures and etching was found to be unnecessary.

(II) Primary silicon particle counts.

To compare the effect of the cooling rate on the number of silicon particles present in the microstructure, a primary silicon particle count was carried out for specimens taken from graphitic and graphite free castings. The specimens were first prepared as in (I) and then subjected to visual examination using an optical microscope with T.V. screen. Ten counts were made on independent areas along a length of the specimen. A magnification of x100 was used and the particle counts relate to square areas of 0.5mm side length. Table 2 presents a direct comparison of the average silicon particle counts.

Table 2: Primary Silicon Particle Counts.

Casting Process	Primary Silicon Particle Counts										Average Si.Count
	1	2	3	4	5	6	7	8	9	10	
Gravity Die Cast	50	57	70	95	75	90	89	70	50	70	72
Conventional Pressure Die Cast	62	55	56	80	66	40	48	75	60	40	59
Rheocast	38	31	35	30	27	26	24	34	27	36	31
Sand Cast	27	34	34	44	36	31	36	34	32	24	33
Compocast 3wt% Gr.	11	9	6	11	8	6	4	3	7	5	7
Compocast 4½wt% Gr.	6	8	11	9	8	9	12	9	4	8	8
Compocast 6wt% Gr.	6	9	4	7	3	7	4	5	3	8	6
Compocast 7½wt% Gr.	12	9	7	6	2	10	6	7	5	7	7

Particle Counts Relate to Square Area of 0.5mm Side Length.

#### 4.4.2 Tensile Testing

The tensile test was carried out to generate fundamental data on the samples tested and for comparison purposes between different specimens. Therefore a higher degree of accuracy and reliability of results was required. For that reason it was necessary to control the strain rate in the tensile tests. This was achieved by using a Mayes ESH250 tensile testing machine and a strain rate of 0.6mm/min. was maintained for all tests. A load vs. extension graph was obtained from which the maximum load could be determined. A load range of 0-5kN. was employed and the magnification on the extension axis was 25.4 times (10in. on the chart paper = 10mm real extension).

Values obtained for ultimate tensile stress, % reduction in area and % elongation were the average of the values obtained from five specimens. The ultimate tensile stress (U.T.S.) was calculated from the following:

$$\text{U.T.S.} = \frac{\text{Ultimate Load}}{\text{Cross Section Area}} \text{ (MN/m}^2\text{)}$$

Hounsfield No13 tensile specimens were used.

Ultimate tensile stress calculations are shown in Appendix 4.

#### 4.4.3 Hardness Testing

Hardness testing was carried out on a Brinell hardness testing machine with 10mm ball diameter and 750kg load. The Brinell hardness test was considered appropriate for the composite alloy because the ball would cover a larger area than a point indenter. As this area would include all the constituents of the composite, the test was likely to provide a more accurate hardness value. In the Brinell hardness test the ball is pressed into the specimen for a 30 sec. period at the specified load. The diameter of the impression formed is proportional to the Brinell hardness number and the load applied is a

function of the ball diameter ie.:

$$\frac{P}{D^2} = \text{constant}$$

where: P = the load applied (kg)  
D = the ball diameter (mm)

For aluminium alloys, the constant is between 5 and 10.

The Brinell hardness number was calculated from the formula:

$$H = \frac{P}{\frac{\pi D}{2} (D - \sqrt{D^2 - d^2})}$$

where: H = the Brinell hardness number  
P = load applied (kg)  
D = ball diameter (mm)  
d = diameter of impression (mm)

The Brinell hardness calculations are shown in Appendix 4.

#### 4.4.4 Wear Testing

##### Pin on Disc Wear Testing

###### (I) Programme One: Dry Friction

The pin on disc wear test fulfills the requirement for accelerated combinations of adhesive wear, fatigue, fretting, delamination and abrasion. A hardened steel disc was used, so the requirement for data to be established which related to tribological properties of the composites when mated with ferrous components could be satisfied. This was important because the applications suggested in the literature for graphitic aluminium-silicon alloys usually involved mating with ferrous components, such as the piston ring in the automobile engine.

The wear test machine shown in Fig.34 and 35 provided the

following features:

- (a) a counting device to count revolutions of the disc. The device could be set to the required number of revolutions for a particular test, which when reached, triggered an electrical signal to cut the power from the motor.
- (b) An inductive position transducer which measured the deflection of the pin under test in a direction tangential to the disc. This enabled data suitable for the determination of tangential force to be obtained for calculation of the coefficient of friction. The transducer was placed in the pin holder.
- (c) An inductive position transducer placed in the load plate to measure the change in pin length during the test.
- (d) A chromel-alumel thermocouple was attached to the wear pin at a distance of 3mm from the pin-disc interface, to allow changes in pin temperature to be recorded.
- (e) A chromel-alumel thermocouple was placed in the wear testing environment to allow the ambient test temperature to be monitored.

The outputs from items b - e were fed into a four channel Linseis millivolt chart recorder which allowed coefficient of friction, change in length of wear pin, pin temperature and ambient temperature to be recorded continuously.

The general arrangement for the wear test machine is shown in Fig.35 and the parts list in Fig.35A. The machine also has a facility for conducting the reciprocating diamond scratch test.

In addition to the above requirement; a chemical balance accurate to 0.0001gm. was used to weigh test pins before and after the test. The test pin and its arrangements are shown in Fig.36 and the test pin in Fig.37. Surface texture measurements were carried out on a Rank Taylor Hobson Talysurf 4 with datum attachment and Talydata computer for computing roughness average (Ra) and bearing ratio (tp).

The following parameters were used:

- average wear interface linear velocity: 1 m/sec.
- Axial load: 12.6kg.
- Pin diameter at wear interface: 6.35mm
- Disc material: plain carbon steel with carbon content of 1% hardened to Rc 57. Five discs were made.
- Test duration: 30 minutes
- Pin and disc surface finish: 2 $\mu$ mRa and 0.2 $\mu$ mRa respectively.
- Environment:

Programme one: unlubricated system, enclosed environment with temperature and humidity monitored.

Programme two: lubricated system, enclosed environment with temperature and humidity monitored.

The results obtained from the wear test were:

- (I) Pin weight loss.
- (II) Change in pin length.
- (III) Pin temperature rise.
- (IV) Coefficient of friction.
- (V) Surface texture of pin and disc after test.

The tribological properties calculations are shown in Appendix 5.

#### Pin Weight Loss

The pins were cleaned and weighed before and after each test so that weight loss could be determined. Monitoring of weight loss was necessary in addition to monitoring change in pin length because it was possible for a situation to arise where the pin deformed plastically without loss of debris. This condition could be detected only by the change in length measurements. Ambient temperature and relative humidity were monitored to ensure that there were no significant changes in the ambient conditions during the period of test.

#### Change in Pin Length

This was measured by the position transducer in the load plate [8] see Fig.35. The system was calibrated by placing a feeler gauge of known thickness between the transducer probe and the disc and noting the millivolt reading on the chart

recorder. The change in length of pin during a wear test was recorded from a millivolt output from the transducer and converted to a linear distance (in mm) using the calibration data on completion of the test.

### (III) Pin Temperature Rise

A chromel-alumel thermocouple was wired to the pin at a distance of 3mm from the wear interface, which was proved by Razavizadeh and Davies<sup>(62)</sup> to be very close to the actual temperature at the wear interface. The millivolt output was recorded by the Linseis recorder which provided a continuous record. A mercury thermometer was used for calibration and the millivolt readings were converted to absolute temperature in °C.

### (IV) Coefficient of Friction

The position transducer [23] see Fig.36 was installed to measure the deflection of the pin resulting from rotation of the disc. The output from the transducer was fed into the millivolt recorder where the reading indicated was proportional to the pin deflection. To calibrate the system for coefficient of friction, the axial load was applied to the pin in contact with the stationary disc. The force required to cause a similar deflection to that caused by the rotating disc was then determined by attaching a spring balance to the base of the pin and applying a load to deflect the pin. A graph was then drawn for deflection force vs. the millivolt reading, which enabled the system to be calibrated.

When the disc was rotating with the loaded pin in contact, the millivolt reading could therefore be equated directly to the force required to cause a certain deflection of the pin.

In a friction system, when two surfaces come into contact with each other, the harder material sinks into the softer material until the real area of contact is sufficient to support the load under stationary conditions, this entails "cold welding" of the mating asperities. Bowden and Tabor<sup>(90)</sup> maintained that the force required to shear these welded junctions is directly related to the static frictional

force  $F_{stat}$ . They also claimed that the junctions still weld together when the surfaces slide over one another under the normal conditions of sliding contact between specimens. The force required to maintain a constant sliding speed whilst making and breaking the welded asperity contact is the kinetic frictional force  $F_{kin}$ , and the resultant coefficient of friction called the kinetic coefficient of friction  $\mu_{kin}$  (91):

$$\mu_{kin} = \frac{F_{kin}}{W}$$

where  $W$  = the load applied.

The millivolt recorder allowed  $F_{kin}$  to be recorded continuously throughout the pin on disc wear tests enabling a record to be obtained for any changes during the test.

#### (V) Surface Textures of Pin and Disc

Before all tests, surface texture was prepared on both pins and discs to be better than:  $2\mu mRa$  for pins and  $0.2\mu mRa$  for discs.

Measurements were taken perpendicular to the direction of lay in all cases. The disc surfaces were prepared by grinding while pins were finished by face turning.

The main parameters used were "roughness average"  $Ra$ , and "bearing ratio"  $tp$ .  $Ra$  alone gives little information about the actual shape of a bearing surface because it is simply a measure of areas above and below a centre line, while  $tp$  gives an indication of the actual proportion of the surface which would be in direct contact with the flat disc surface.  $Ra$  and  $tp$  together give useful information about the worn surface.

#### (II) Programme Two: Lubricated Friction

During the pin on disc wear test (dry friction), it was observed that the graphite in the test specimens was prevented from building up a continuous layer at the wear interface due to the continuous rubbing action between the two mated surfaces. It was considered that the presence of a wet media,

such as oil, could act as a graphite binder and allow a graphite rich layer to build and prevent direct contact between the two mated surfaces. On the other hand it was considered that the presence of oil in a large quantity, such as immersing the system in an oil bath, might cause the graphite to be washed out from the wear interface. It was decided therefore to run the system under very poor lubrication conditions. The procedures and the data obtained were exactly the same as in (I), except that the system was run under poor lubrication conditions. See (5.2.4)

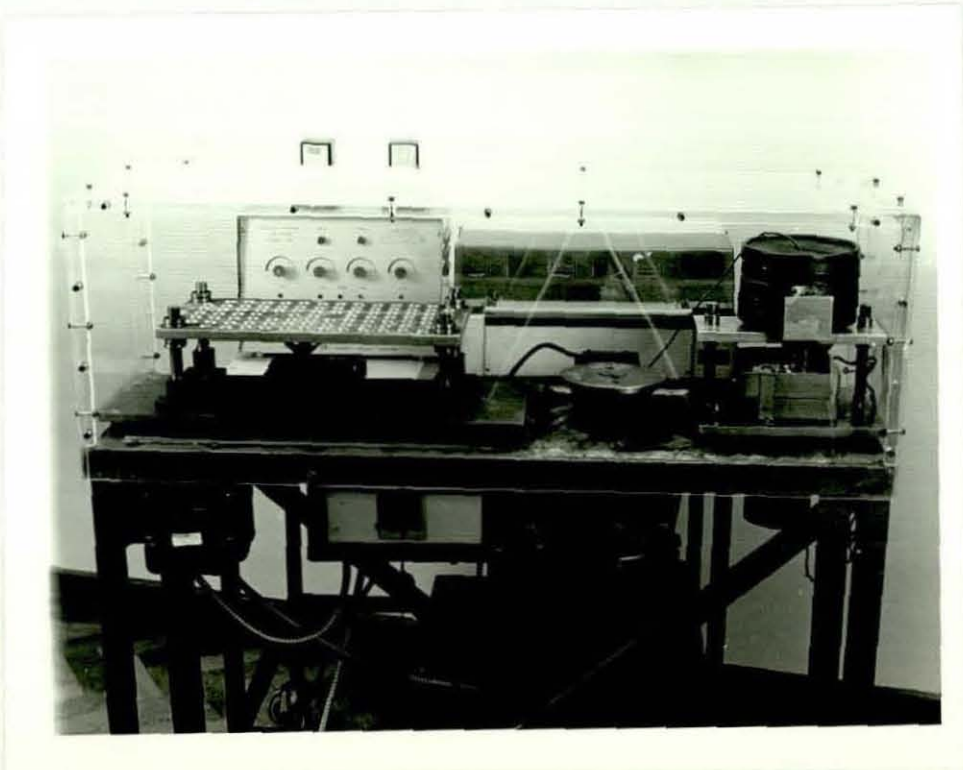
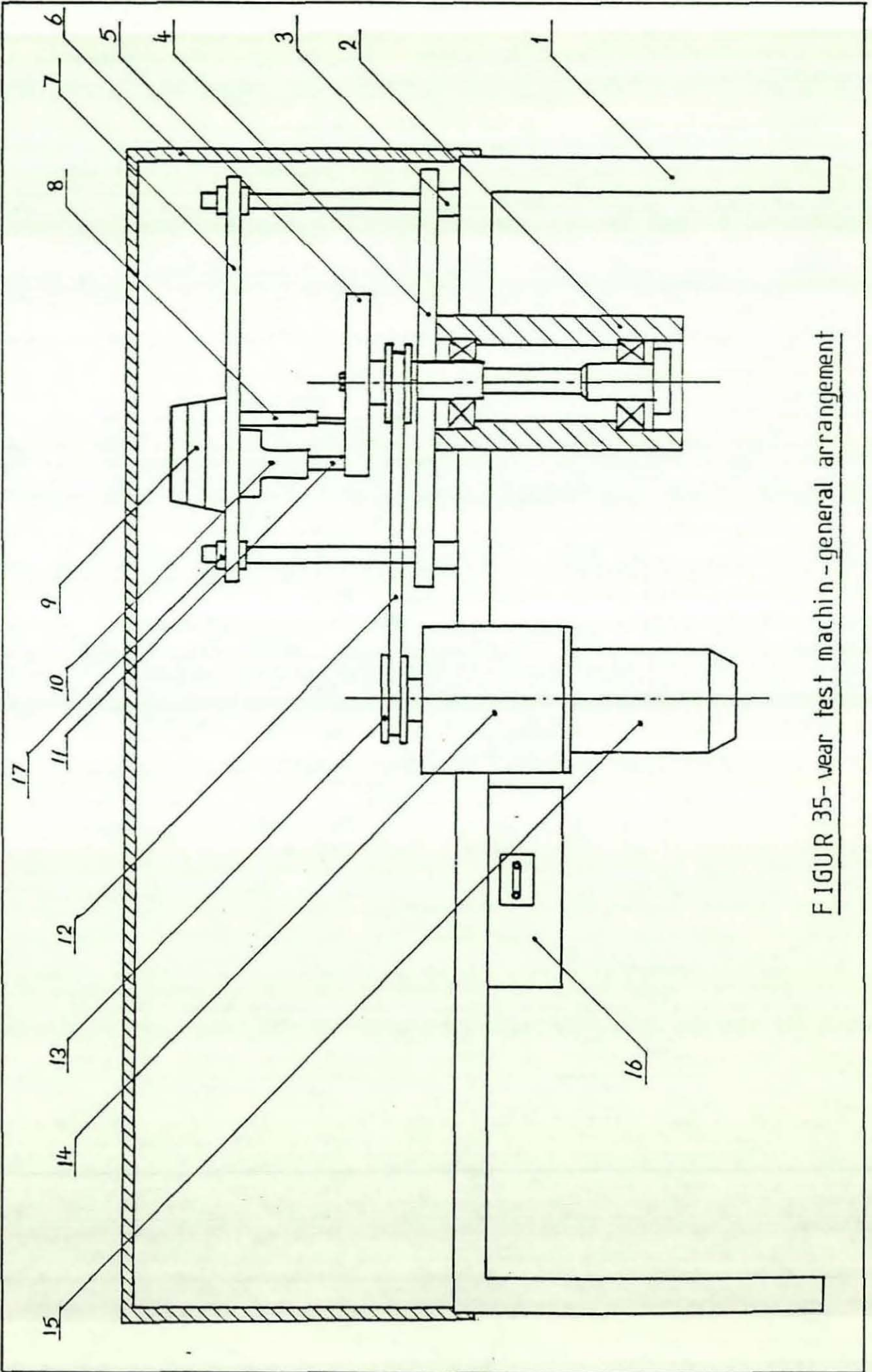


Fig. 34 - The Wear Test Machine



FIGUR 35-year test machine-general arrangement

Detail No.	Description
1	Framework
2	Bearing housing and shaft assembly
3	Resilient mounting
4	Base plate
5	Disc
6	Perspex cover
7	Load plate
8	Position transducer (to record change in pin length)
9	Weights (load)
10	Pin holder
11	Specimen
12	Timing belt
13	Pulley
14	Variable speed drive
15	Motor
16	Counter and automatic test-stop device
17	Ball bushes and ground pillars
	Items not shown
18	Position transducer (to record deflection force)
19	Thermocouples
20	Recorder (millivolt)
21	Transducer power supply

Fig.35A Parts List



## CHAPTER FIVE

### RESULTS AND OBSERVATIONS

#### 5.1 Results of Composite Alloy Production

##### Microstructures

- Fig.38 - Sand cast control specimen LM30 alloy.  
Fig.39 - Gravity die cast control specimen LM30 alloy.  
Fig.40 - Conventional pressure die cast control specimen LM30 alloy.  
Fig.41 - Pressure diecast, rheocast LM30 alloy, no graphite, shear rate  $550\text{sec}^{-1}$ , 0.075 volume fraction solid,  $1.5^\circ\text{C}/\text{min}$ . cooling rate.  
Fig.42 - Shear rate  $550\text{sec}^{-1}$ , 0.075 volume fraction solid,  $1.5^\circ\text{C}/\text{min}$ . cooling rate, LM30 alloy + 3wt% coarse graphite.  
Fig.43 - Shear rate  $550\text{sec}^{-1}$ , 0.075 volume fraction solid,  $1.5^\circ\text{C}/\text{min}$ . cooling rate, LM30 alloy +  $4\frac{1}{2}\text{wt}\%$  medium fine graphite.  
Fig.44 - Shear rate  $550\text{sec}^{-1}$ , 0.075 volume fraction solid,  $1.5^\circ\text{C}/\text{min}$ . cooling rate, LM30 alloy +  $7\frac{1}{2}\text{wt}\%$  fine graphite.  
Fig.45 - Fractured silicon particle.

The number of primary silicon polyhedra counted for graphitic and graphite free (control casting) specimens are listed in Table 2.

##### Macrostructure

- Fig.46 - Shear rate  $550\text{sec}^{-1}$ , 0.075 volume fraction solid,  $1.5^\circ\text{C}/\text{min}$  cooling rate, LM30 alloy +  $7\frac{1}{2}\text{wt}\%$  coarse graphite.

#### 5.2 RESULTS OF COMPOSITE ALLOY EVALUATION

##### 5.2.1 Tensile Testing

Tests were conducted to assess the effect of graphite addition level on the U.T.S., % elongation and % reduction in area.

Specimens : Hounsfield No.13  
Testing machine : Mayes ESH 250  
Strain rate 0.6mm/min  
Load range 0-5 kN

The % elongation and % reduction in area were determined using Hounsfield gauges.

The tensile testing results for control castings and graphitic castings are shown in Tables 3 and 4 respectively.

A graph showing the variation in U.T.S. with different graphite additions is shown in Fig.47. The tensile testing calculations are shown in Appendix 4.

#### 5.2.2 Hardness Testing

The Brinell hardness test was conducted to assess the effect of graphite additions on the hardness number of the alloys.

Load Used = 750kg  
Ball diameter = 10mm

The Brinell hardness testing results for control castings and graphitic castings are shown in Tables 5 and 6 respectively.

The Brinell hardness calculations are shown in Appendix 4.

A graph showing the variation in Brinell hardness number with various graphite contents is shown in Fig.48, and in Fig.49 there is a graph showing the correlation between hardness number and tensile strength for graphitic and graphite free specimens. The relationship between silicon particle counts, Brinell hardness number and tensile strength for control casting specimens is shown in Fig.50.

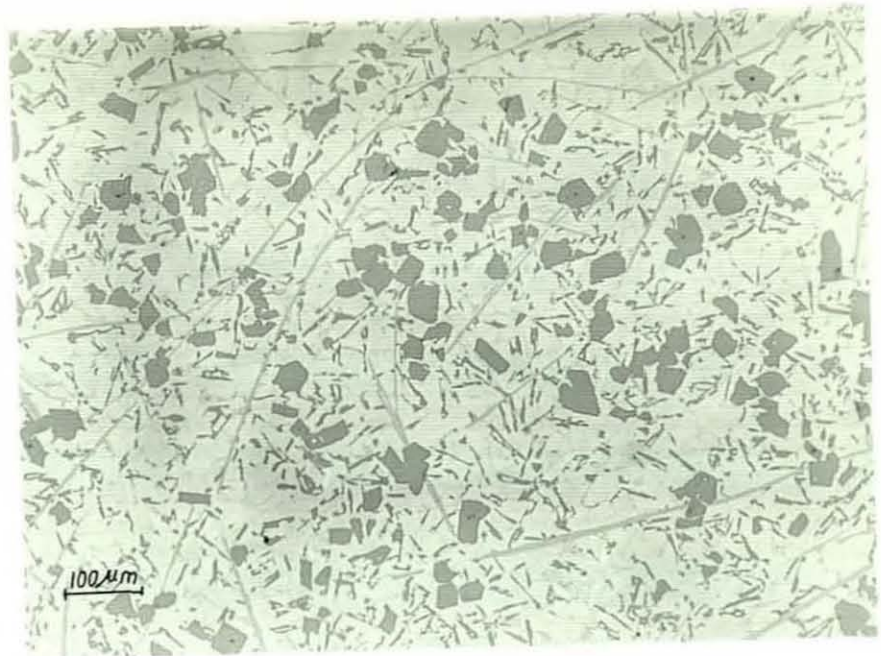


Fig.38 - LM30 - Sand Cast Structure



Fig.39 - LM30 - Gravity Diecast Structure

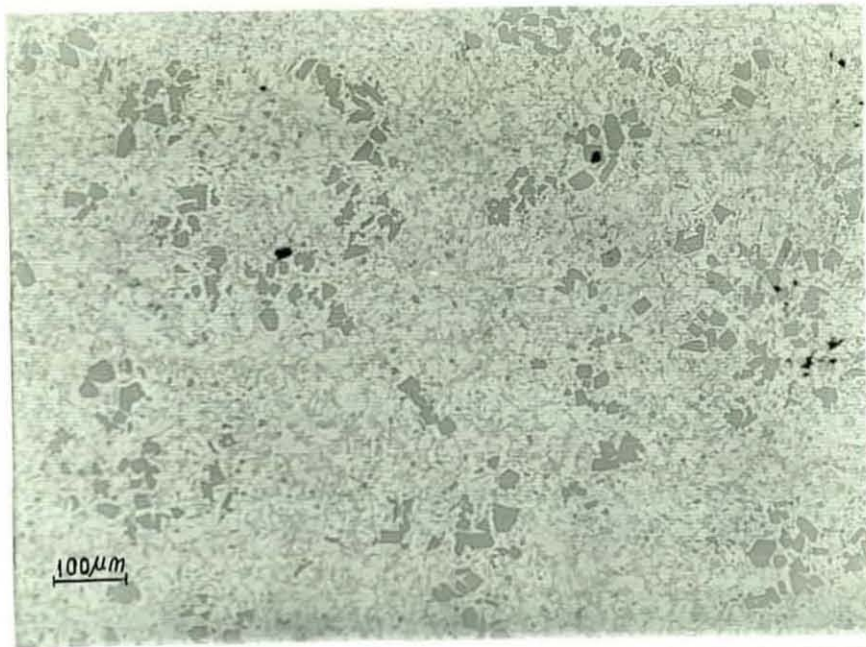


Fig.40 - LM30 - Conventional Pressure Diecast

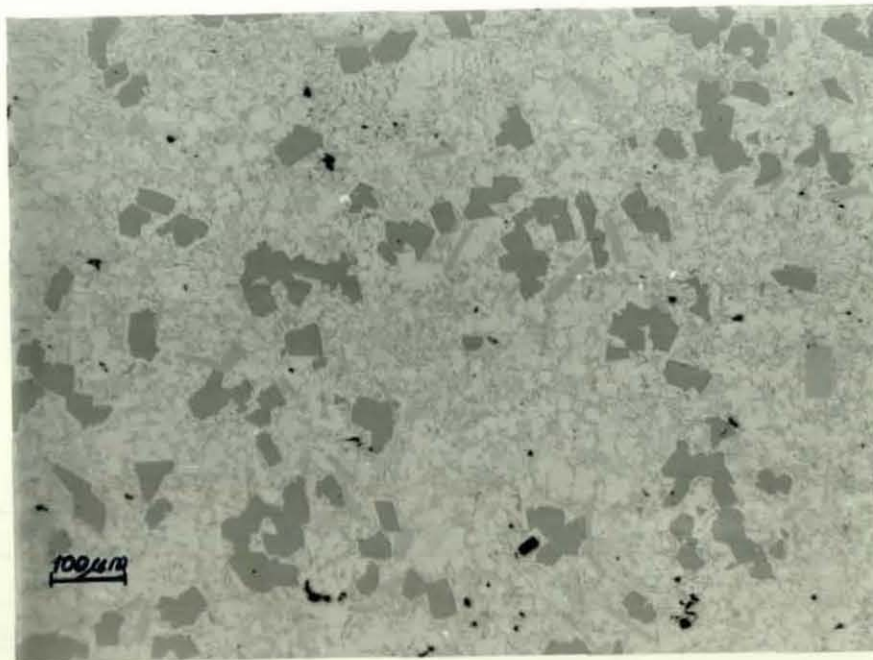


Fig.41 - LM30 - Pressure Diecast, Rheocast No Graphite Addition

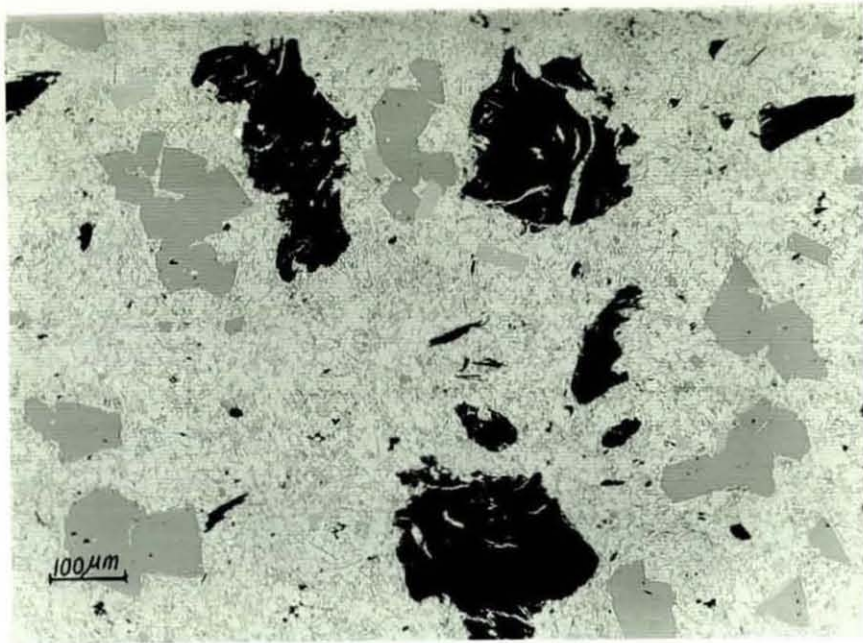


Fig.42 - LM30 Alloy Compcast, Pressure Diecast  $\dot{\gamma}_{ave} = 550\text{sec}^{-1}$ ,  
 $G_s = 0.05$ ,  $\dot{\epsilon}_{ave} = 1.5^\circ\text{C/min}$ . 3wt% Coarse Graphite.

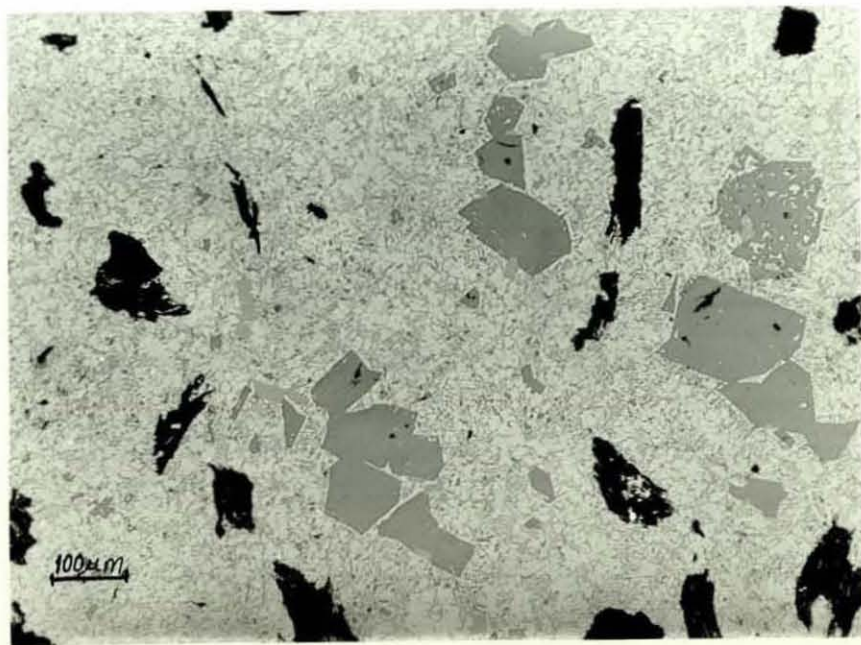


Fig.43 - LM30 Alloy, Compcast, Pressure Diecast  $\dot{\gamma}_{ave} = 550\text{sec}^{-1}$ ,  
 $G_s = 0.05$ ,  $\dot{\epsilon}_{ave} = 1.5^\circ\text{C/min}$ . 4½wt% Medium Fine Graphite

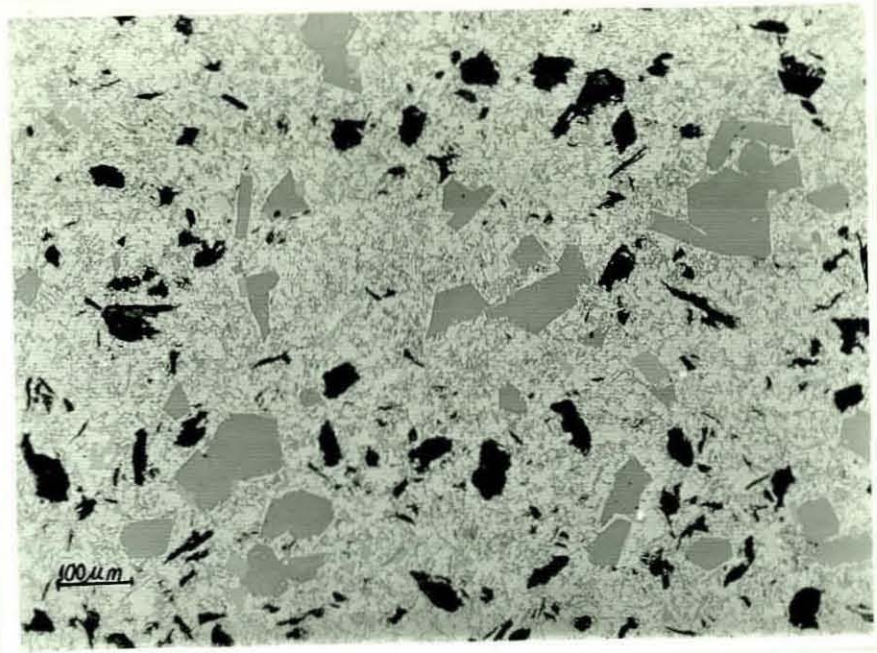


Fig.44 - LM30 Alloy Compcast, Pressure Diecast  $\dot{\gamma}_{ave} = 550\text{sec}^{-1}$ ,  
 $Q_s = 0.05$ ,  $\dot{\epsilon}_{ave} = 1.5^\circ\text{C}/\text{min}$ . 7½wt% Fine Graphite.

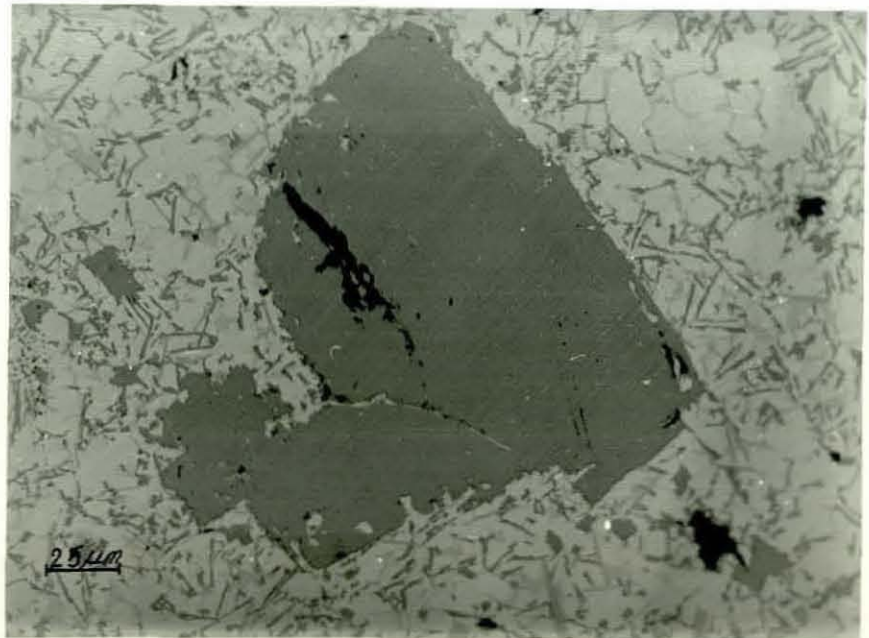


Fig.45 - Fractured Silicon Particle.

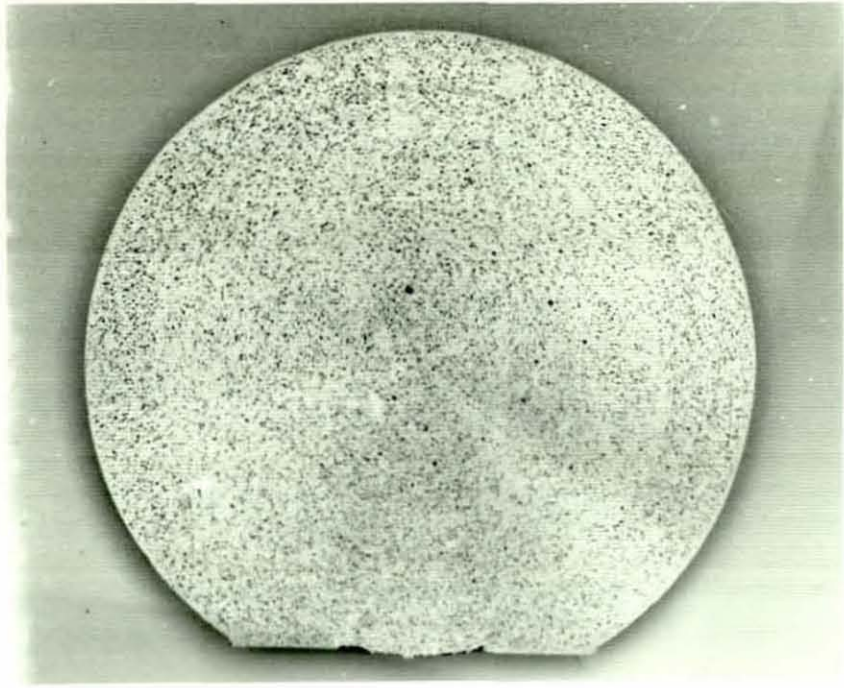


Fig. 46 - Graphite Distribution LM30 Alloy - 7½wt% Coarse Graphite. Scale : 1/1

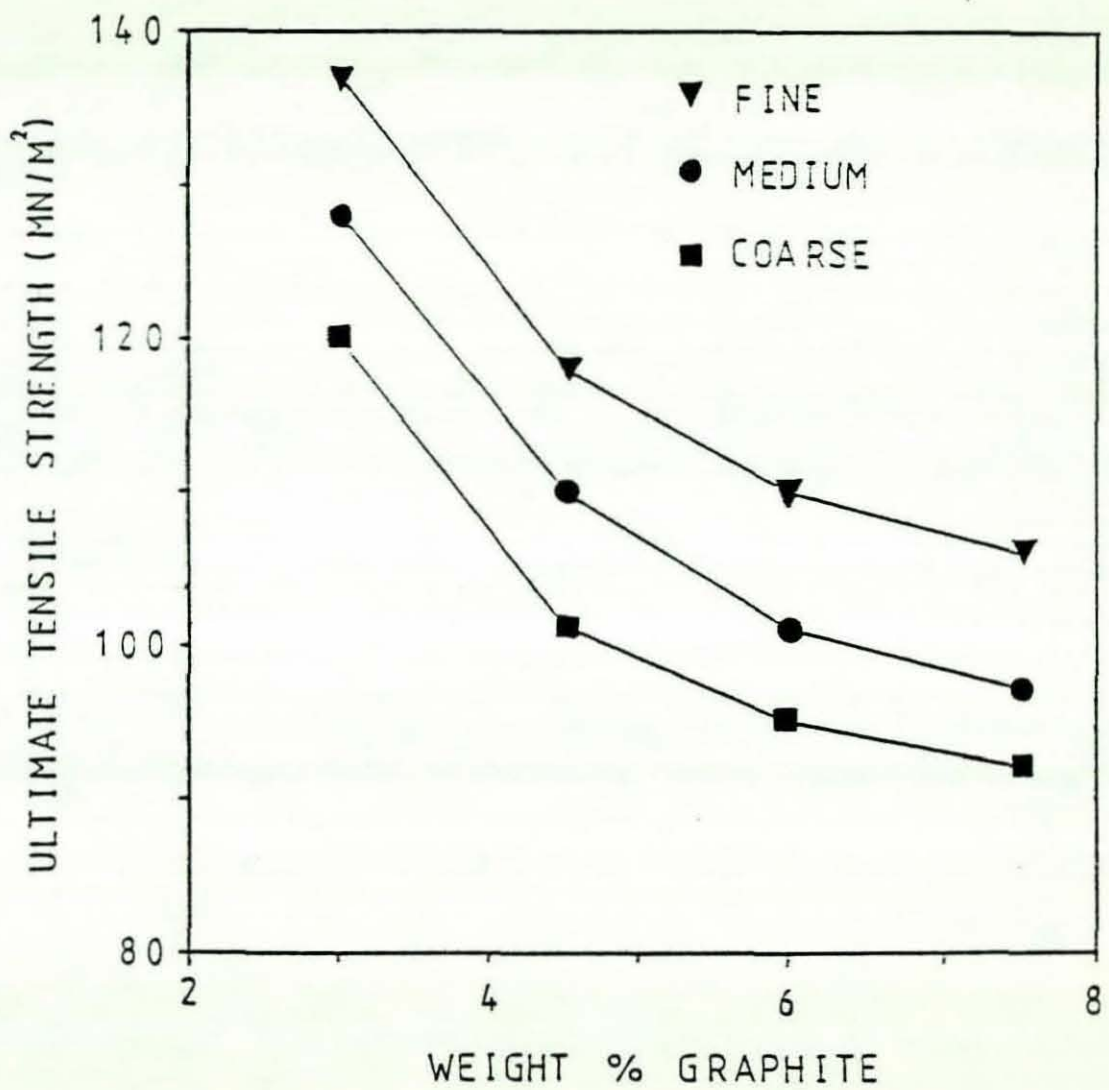


Fig.47 - The Effect of Graphite Content on Ultimate Tensile Strength.

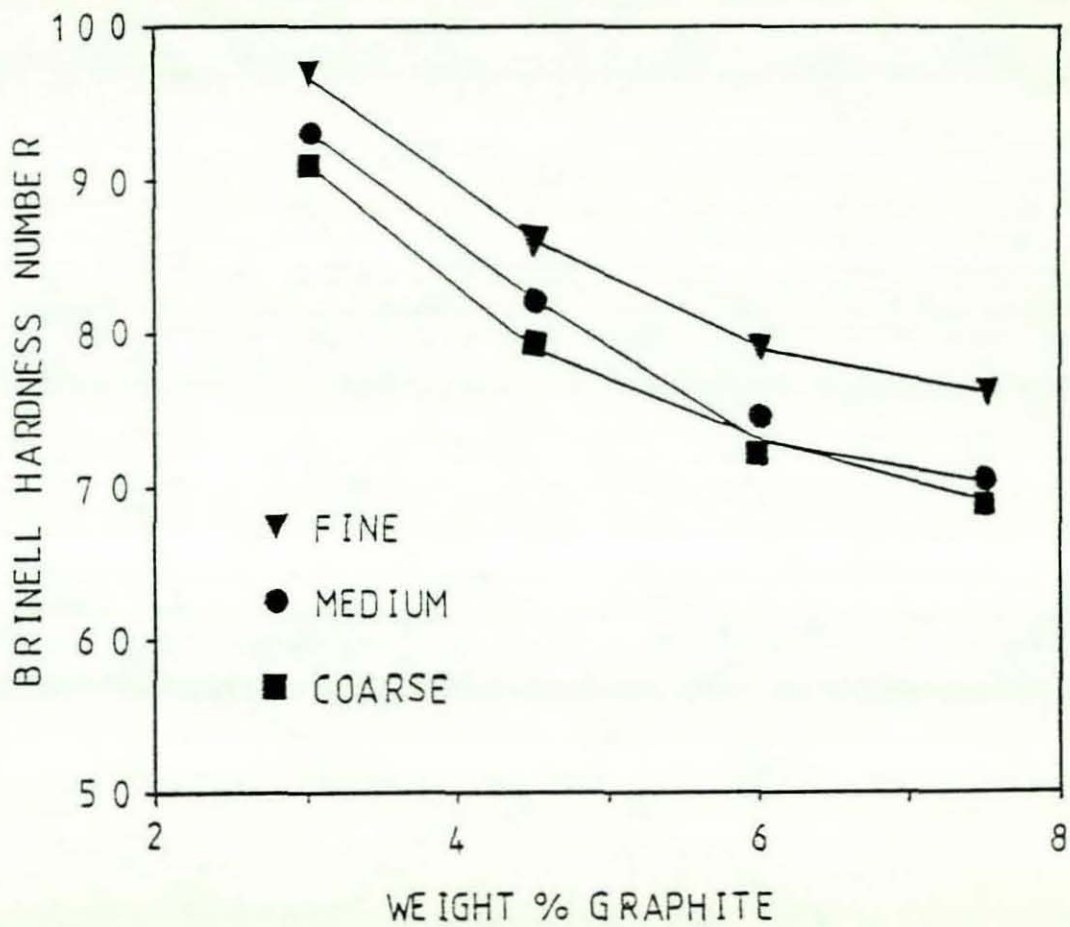


Fig.48 - The Effect of Graphite Content on Brinell Hardness Number.

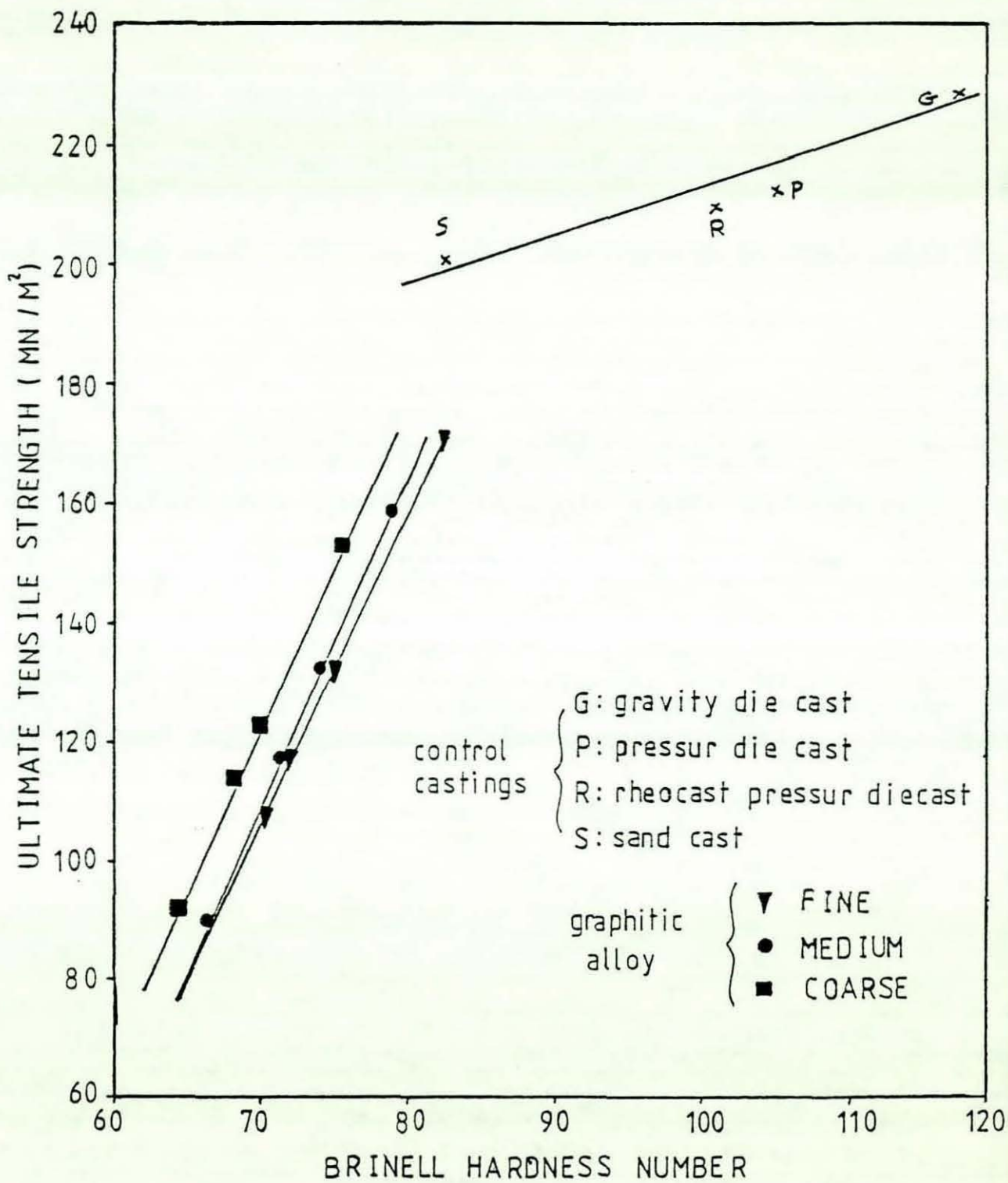


Fig.49 - Correlation Between Brinell Hardness Number and Tensile Strength

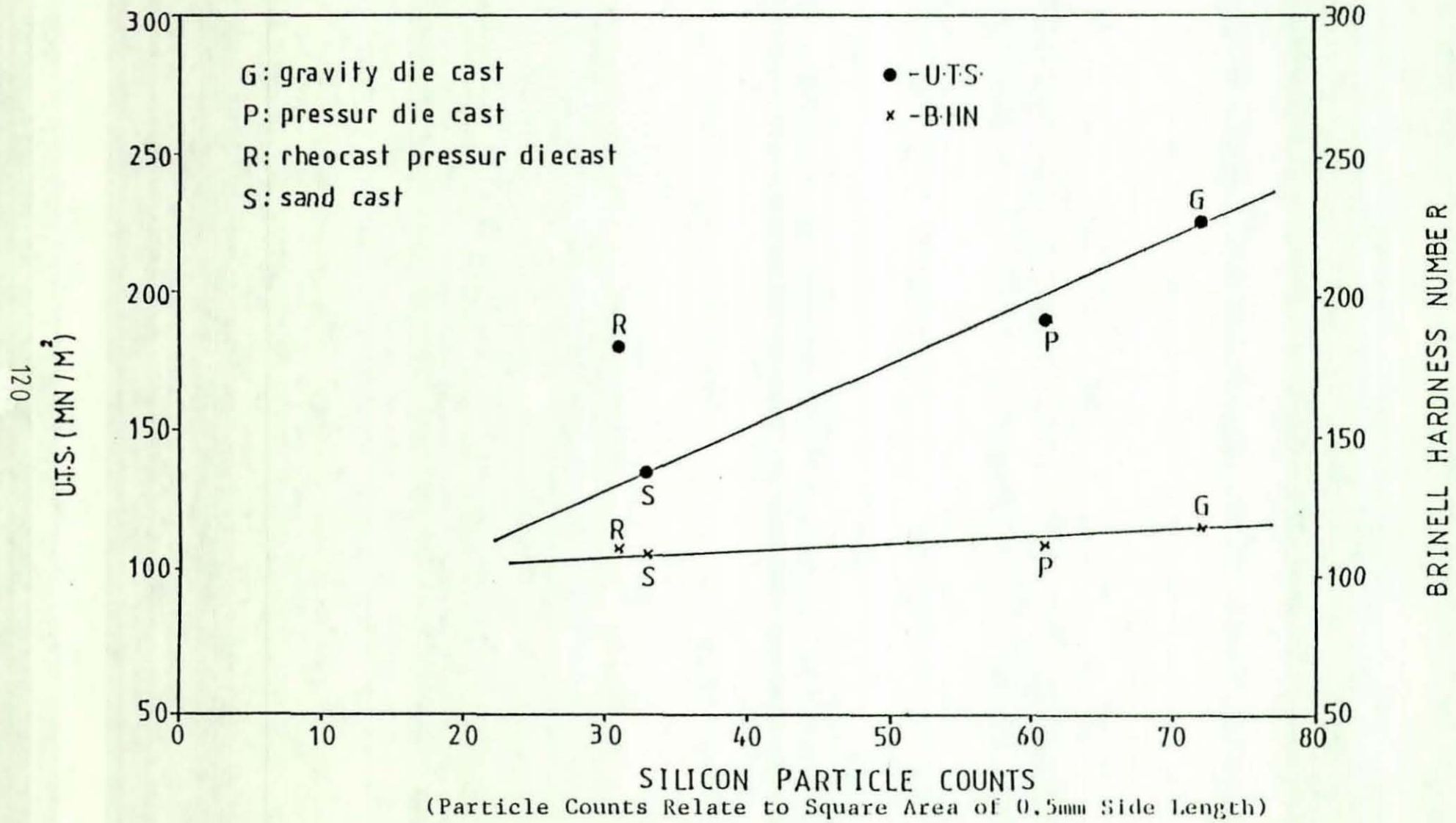


Fig.50 - The Effect of Primary Silicon Particle Number on the Mechanical Properties.

### 5.2.3 Wear Testing (Pin On Disc)

#### (I) Programme One: Dry Friction.

Parameters used:

Interface velocity: 1m/sec

Pin diameter: 6.35mm

Discs: Plain carbon steel with 1% carbon hardened to RC 57 and ground on both sides. Each side was used for one test only

Test duration: 30 minutes

Load: 12.6kg (281b)

Environment: unlubricated system, enclosed in perspex cover.

Data obtained for control castings and graphitic castings are shown in Tables 7 and 8 respectively.

Graphical representation:

Fig.51 - shows variation in length of pin lost vs. sliding distance.

Fig.52 - shows the correlation between hardness No. and volume loss of pin.

Fig.53 - shows the weight of pin loss vs. graphite content.

Fig.54 - shows pin temperature rise vs. graphite content.

Fig.55 - shows the relation between length of pin lost and weight of pin lost.

Fig.56 - shows pin temperature rise vs. sliding distance.

Fig.57 - shows the coefficient of friction vs. graphite content.

Fig.58 - shows the wear rate vs. graphite content.

The wear charts produced for specimens containing 3wt% graphite, 7½wt% graphite and specimens processed by a combination of rheocasting and pressure die casting are shown in Figs.61-63. The disc surface after a wear test is shown in Fig.64.

Surface textures of pins and discs before and after the test are shown in Figs.65-76.

\* Figs 66 - 76 are shown in Appendix 7.

(II) Programme Two: Lubricated Friction

Lubricated wear testing has been carried out to investigate the behaviour of graphitic and non graphitic specimens under very poor lubrication conditions.

The parameters used were exactly the same as in programme one except:

Environment: Lubricated system, enclosed in perspex cover.

Oil used: Castrol SAE 20W/50 multigrade oil.

Lubrication range: One drop of size  $0.5 \times 10^{-2}$  mL.

Provided at the beginning of the test.

Data obtained are shown in Tables 9 and 10. Graphical representation of the results are shown in Figs.49, 52, 53, 55 - 57.

Wear charts for control specimens and graphitic specimens with graphite content of 3wt%, 6wt% and  $7\frac{1}{2}$ wt% are shown in Figs.77 - 80.

Surface texture for pins and discs after the test are shown in Fig.81 - 90.

The tribological property calculations are shown in Appendix 5.

\* Figs.81 - 90 are shown in Appendix 7.

### 5.3 QUANTITATIVE ANALYSIS OF GRAPHITE CONTENT

Graphite distribution was visually determined on cut sections after wet grinding using number 80 grit silicon carbide paper. A Cambridge quantimet type 800 was used with an optical microscope and T.V. facility. The equipment is able to differentiate between separate phases from the colour of light reflected from them. The result was given in terms of the percentage of area which the graphite particles occupy in a given cross section. This enables quantitative metallographic techniques to be used to determine the quantities in volume or weight. The results are shown in Table 11.

The weight % graphite was calculated by multiplying the area% by the density ratio of graphite to LM30 aluminium-silicon alloy. The calculation procedures are shown in Appendix 6.

Graphs were plotted for tensile strength and wear rate versus the analysed values of graphite in the specimens and they are shown in Figs.59 and 60 respectively.

Fig.38 shows the microstructure obtained by the slow cooling of LM30 alloy in a sand mould. Fig.39 shows the structure obtained when the same alloy was cast in a copper die preheated to  $130^{\circ}\text{C}$ . The microstructure of the alloy produced by conventional pressure die casting (in a steel die preheated to  $300^{\circ}\text{C}$ ) is shown in Fig.40. The structures of both gravity die cast and conventional pressure die castings exhibited refinement of the primary silicon polyhedra and modification of the eutectic structure due to the faster cooling rate employed during solidification. The structure of the alloy which had been processed by a combination of rheocasting and pressure die casting revealed primary silicon polyhedra of coarser nature and fewer in number (due to the slower cooling rate which applied during the processing of the alloy in the compocasting unit) see Fig.41. The effect of cooling rate on the size of primary silicon polyhedra is demonstrated in Table 2. Figs.42-44 and Fig.46 show a uniform graphite distribution with no evidence of areas of high or low graphite concentration and they also show good contact between graphite particles and the alloy matrices. During production of the composites, viscosity was observed to vary according to graphite content ie. increasing the graphite addition level increased the viscosity at a given shear rate and volume fraction solid. It was found that in order to maintain a viscosity low enough for casting with a graphite content up to a nominal content of  $7\frac{1}{2}\text{wt}\%$ , a shear rate of  $550\text{sec}^{-1}$  must be employed.

Graphite rejection was observed when a shroud of inert gas was used. Graphite rejection occurred at volume fraction solid contents of up to 0.15 and with shear rates up to  $550\text{sec}^{-1}$ .

Two forms of graphite particle rejection were observed:

- (I) Flotation on the surface of the melt.
- (II) Segregation and agglomeration in the bottom of the crucible.

The former usually occurred with fine graphite particle size

and the rejection took place immediately after the graphite was injected into the melt, whilst the latter could not be observed before the slurry was allowed to run down from the crucible. At this time the graphite separated and agglomerated on the launder.

Fracture of the silicon polyhedra was observed, see Fig.43, but on a very minor scale. This fracture may have resulted from the shear action applied by the stirring rotor during the alloy preparation.

## 5.5 OBSERVATIONS ON RESULTS - COMPOSITE ALLOY EVALUATION

### 5.5.1 Observations on the Mechanical Properties

The tensile test results shown in Table 3 showed variations in the tensile strength of the alloy processed by different casting methods. Processing the LM30, hypereutectic aluminium-silicon alloy by gravity die casting resulted in the highest tensile strength achieved by any of the casting processes. Comparison between the results for the four casting processes, see Table 3, showed that the coarsest structures were associated with the lower tensile properties (as in sand casting) and fine structures with the better tensile properties (as in gravity die casting). Table 3 shows that the LM30 alloy has a very low ductility. This has been demonstrated by the very low elongation values obtained by the tensile testing. The results shown in Table 4, and graphically in Fig.47, show a reduction in tensile strength and ductility resulting from the addition of graphite. The addition of 3% graphite to the LM30 hypereutectic aluminium-silicon alloy resulted in a 30% reduction in ultimate tensile strength. This was accompanied by lower elongation and reduction in area values which indicate a further reduction in ductility as a result of the graphite addition. Table 4 also shows that graphite particle size has an apparent influence on the tensile strength. Coarse graphite particles resulted in lower tensile strength values than those for the medium and fine graphite particle sizes. The use of coarse graphite, of 355 $\mu$ m particle size, resulted in a 12-14% reduction in the tensile strength over that of fine graphite of 50 $\mu$ m particle size, for the same graphite addition level.

The hardness results in Tables 5 and 6 showed similar trends to the tensile properties in Tables 3 and 4. Coarse structures resulted in poor hardness properties and the addition of graphite particles to the aluminium-silicon alloy reduced its hardness. The reduction in hardness is almost proportional to the quantity of graphite added, see Fig.48. Graphitic and graphite free specimens showed a correlation between hardness and tensile strength, see Fig.49. For control specimens, the higher hardness was associated with significantly higher tensile properties, whilst for graphitic specimens correlation, whilst it existed, was less pronounced. Fig.50 shows the effect of primary silicon particle size on the mechanical properties of LM30 alloy. The presence of primary silicon polyhedra in great number resulted in higher tensile strength, whilst the effect on the hardness number was not significant.

#### 5.5.2 Observations On The Tribological Properties

In the pin on disc wear test (dry friction) the castings containing 3wt% exhibited a mild steady wear, whilst castings containing graphite in excess of 3wt% and control castings showed a steady wear of a more severe nature, see Figs.51 and 59-60.

In the lubricated wear test, the control specimens showed a very mild wear during the first ten minutes of the test, after that a transition to more severe wear occurred. The graphitic alloy specimens maintained a mild steady wear which did not change during the course of the test. In both lubricated and unlubricated tests the specimens containing 3wt% graphite showed the lowest wear rates observed in this investigation, see Table 10 and Figs.53 and 58. From Fig.52 it can be seen that graphitic and graphite free specimens show some correlation between Brinell hardness number and volume loss of the test pins. At lower hardness values there was a higher volume loss of the tested pins. Both the weight of pin lost and wear rate showed minimum values with a 3wt% graphite addition, an increase in graphite addition beyond that value resulted in a sharp increase in wear rate and weight of pin lost. For the lubricated wear test, at 7½wt% graphite addition,

the wear rate was about 60% of the wear rate of graphite-free specimens, whilst in dry friction the wear rate is almost similar to that of the control casting specimens or even higher see Figs.53 and 58.

The results in Table 8 and Fig.57 show that the coefficient of dry friction between the pin and the disc is lower for alloys which contain graphite particles and that the coefficient of friction decreases with an increase in graphite content. In the lubricated wear tests, specimens containing graphite below 7½wt% maintained a very low value for coefficient of friction during the test period, see Figs.78 and 79. The control specimens, see Fig.77, maintained a low value for coefficient of friction until the middle of the test, after that the coefficient of friction increased dramatically to a value which is comparable with those for control castings obtained with dry friction. Specimens containing 7½wt% graphite, see Fig.80, showed different trends. The coefficient of friction increased gradually during the test. However, the maximum value recorded was well below the value obtained with control specimens.

In the unlubricated wear test the pin temperature rise showed trends comparable with the coefficient of friction results. The presence of graphite particles resulted in reduced steady state temperatures. In the lubricated tests, specimens containing less than 7½wt% graphite showed very low and steady temperatures, Figs.78 and 79, whilst specimens containing 7½wt% graphite showed an increase in temperature during the test period which corresponds with the changes in coefficient of friction for the same specimens. However, the maximum temperature rise obtained with such graphite additions is still well below that exhibited by the control casting specimens. The surface texture of the pins and discs after wear tests are shown in Tables 7 and 8 for dry wear tests and 9 and 10 for the lubricated ones.

For dry friction, the surface roughness (Ra value) of the pins and discs was lower for specimens which contained graphite particles than for similar pins and discs of the matrix alloy.

The surface profile graphs of the specimens, Figs.65-76, show smoother surfaces on the pins containing graphite which was reflected in smoother surfaces on the mated discs. Graphitic alloy specimens exhibited more peaks and valleys for a given length of surface of both pins and discs than did the graphite free specimens. This was accompanied with a slight deterioration in bearing ratio, in comparison with specimens of the control castings. For lubricated friction, the higher graphite contents resulted in higher surface roughness values for both pins and discs. However, with the exception of the 7½wt% graphite specimens, the values obtained for (Ra) were far below those obtained from control casting specimens, see Figs.81-90. The number of peaks and valleys for tested pins and disc were found to decrease with the increase in graphite content. This was accompanied by a slight deterioration in bearing ratio. The effect of graphite particle size on the wear behaviour of LM30 alloy is demonstrated in Table 8 and Figs.51-58. The presence of coarse graphite particles resulted in a lower pin temperature rise and a lower coefficient of friction in comparison with those values obtained with medium fine and fine graphite particle sizes at the same graphite addition level. However, the specimens containing coarse graphite particles exhibited some deterioration in the surface roughness values (Ra) and bearing ratios when compared with the specimens containing medium fine and fine graphite particle size.

The results, in Table 8, for pin weight loss were plotted against the change in pin length values, see Fig.55. Although there was some scatter, within a narrow band, the straight-line relationship indicates that significant plastic deformation without loss of debris did not occur. The quantitative analysis of graphite in the castings, see Table 11, shows some variations in graphite content within the castings. However, the analysis showed that the average graphite content within the casting is very close to the assumed quantity for both coarse and medium size graphite particles. For the fine graphite particle size the amount of graphite recovered was between 87-99% of the assumed quantity. The graphs plotted for the analysed quantities, Figs.59 and 60, did not show a

significant difference in comparison with graphs plotted for the assumed quantities Figs.47 and 53.

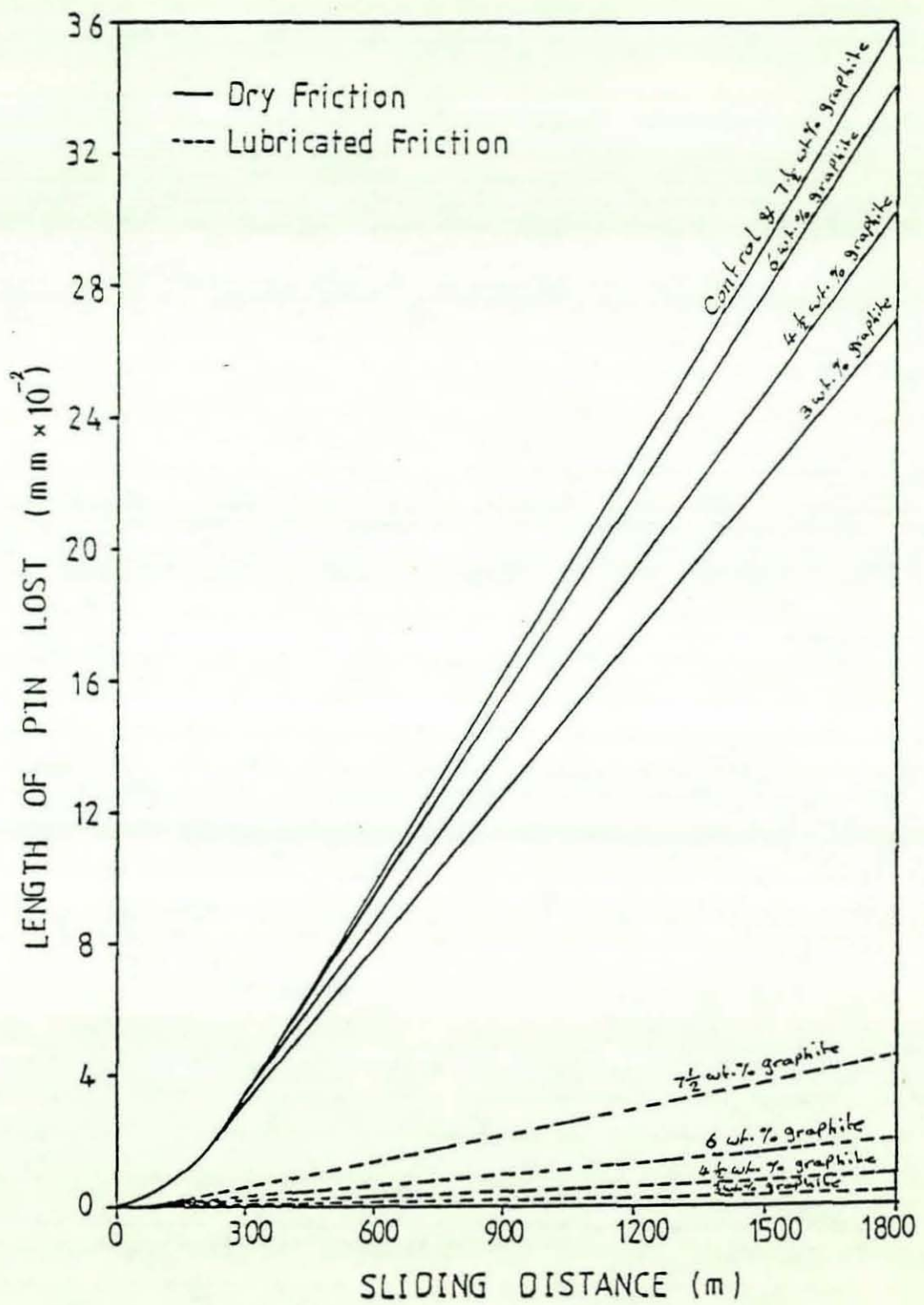


Fig.51 - Variation in Length of Pin Lost With Sliding Distance

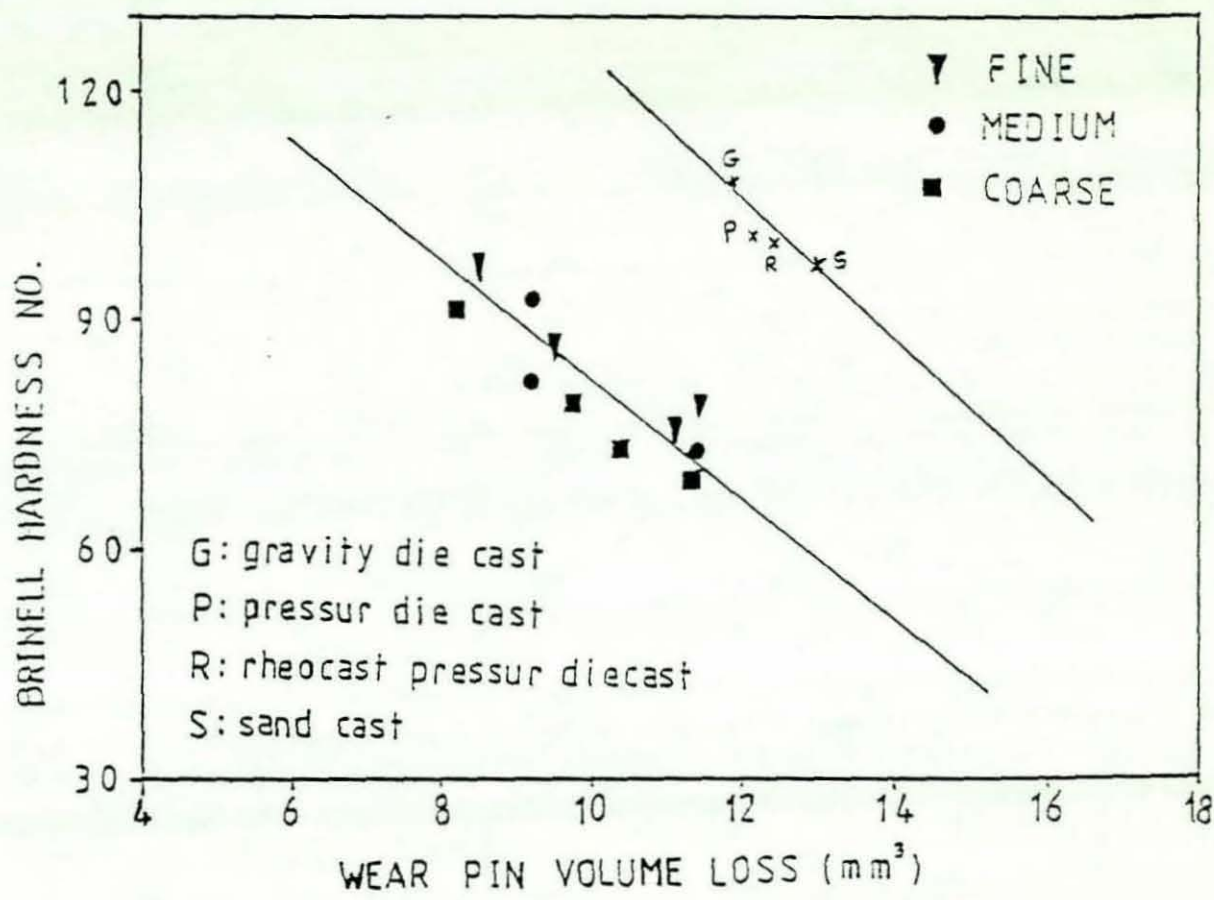


Fig.52 - Correlation Between Brinell Hardness Number and Wear Pin Volume Loss.

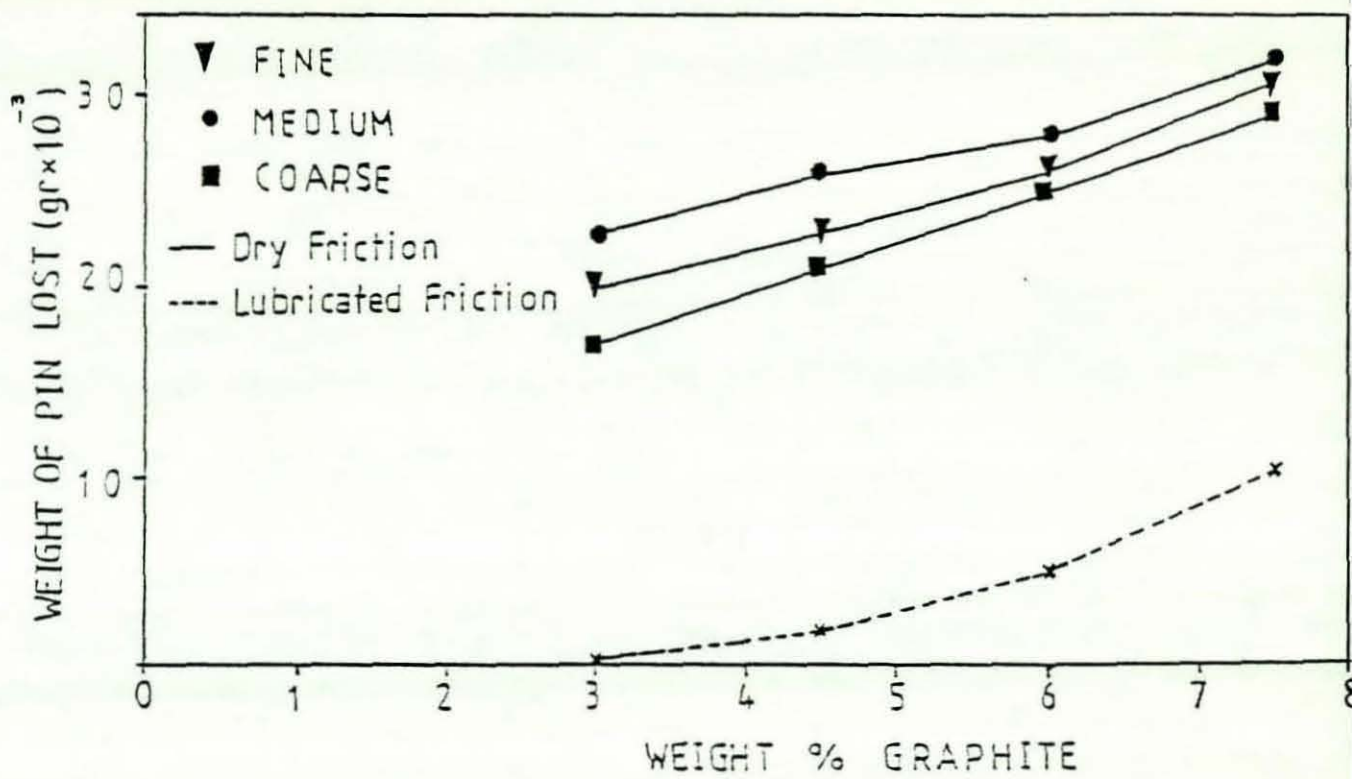


Fig.53 - The Effect of Graphite Content on Weight of Pin Lost.

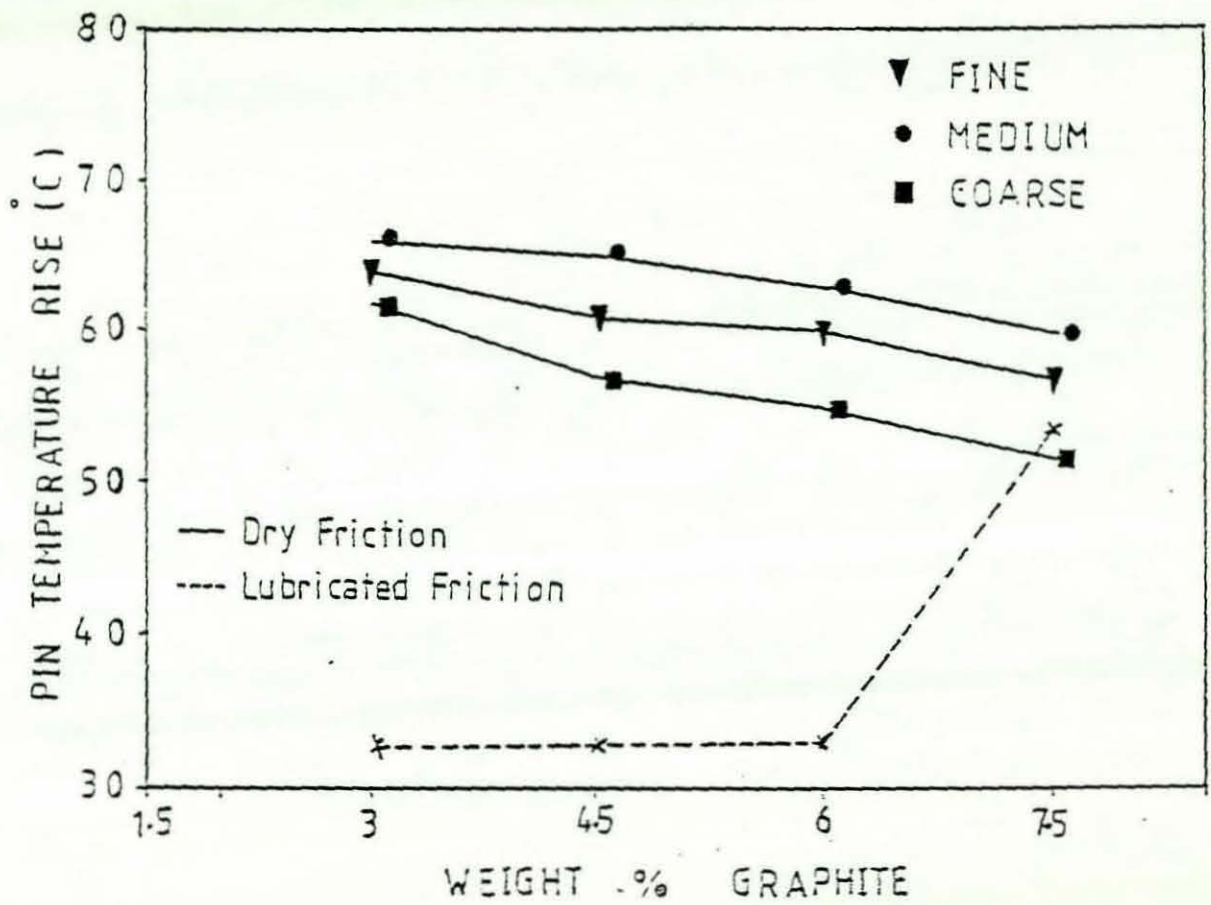


Fig. 54 - The Effect of Graphite Addition Level on Pin Temperature Rise.

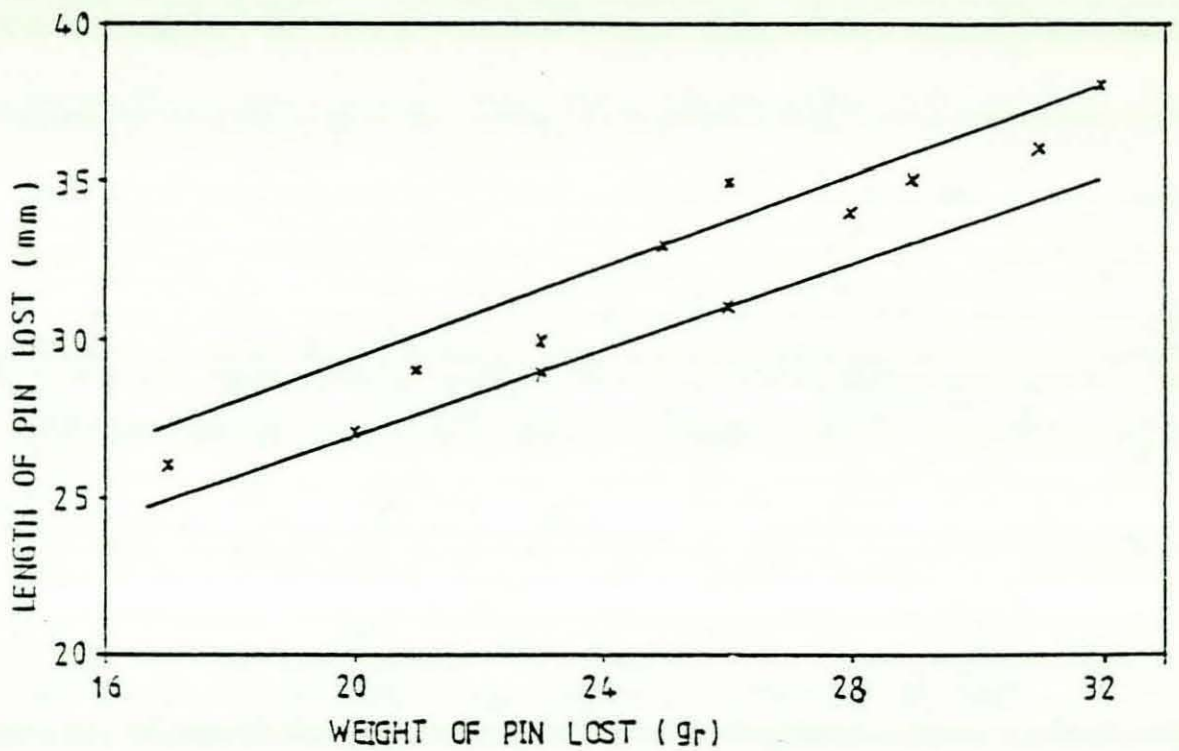


Fig.55 - Length of Pin Lost vs. Weight of Pin Lost.

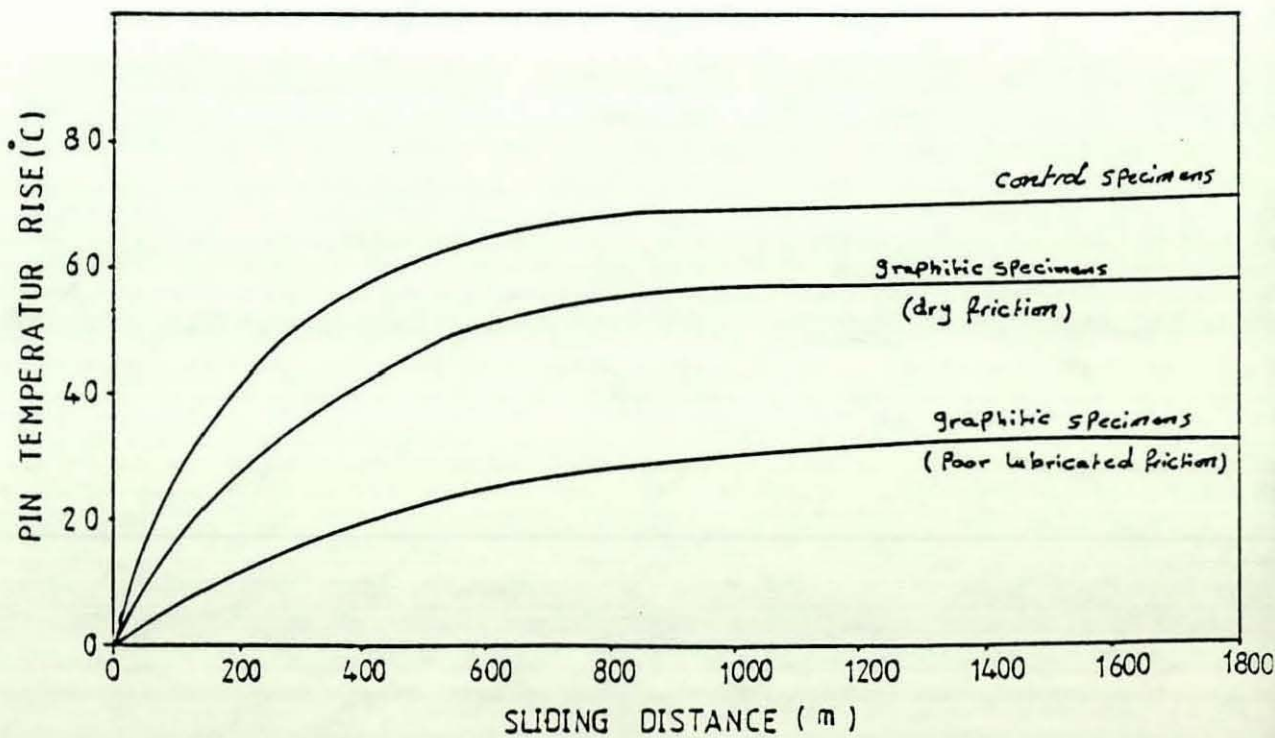


Fig.56 - Pin Temperature Rise vs. Sliding Distance.

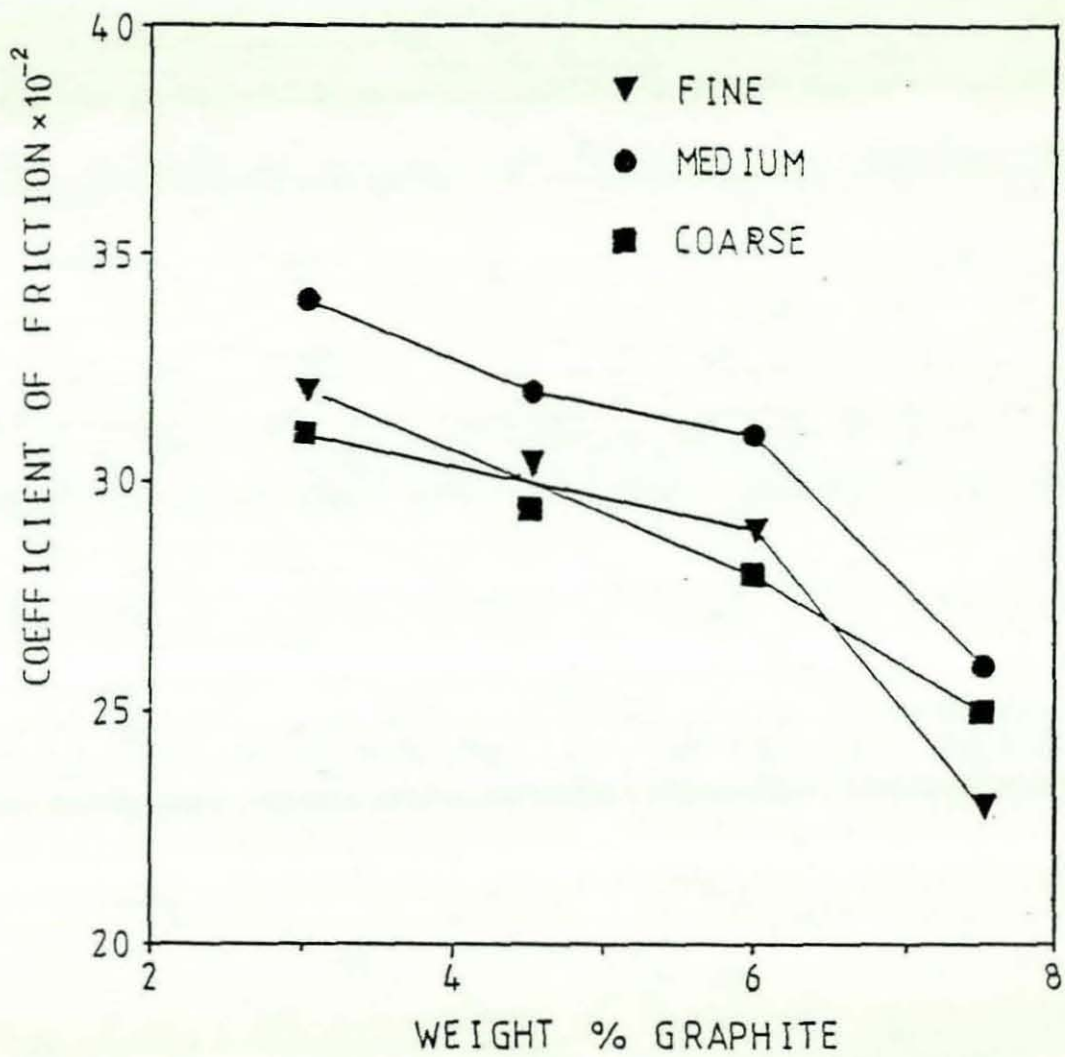


Fig.57 - The Effect of Graphite Content on Coefficient of Friction

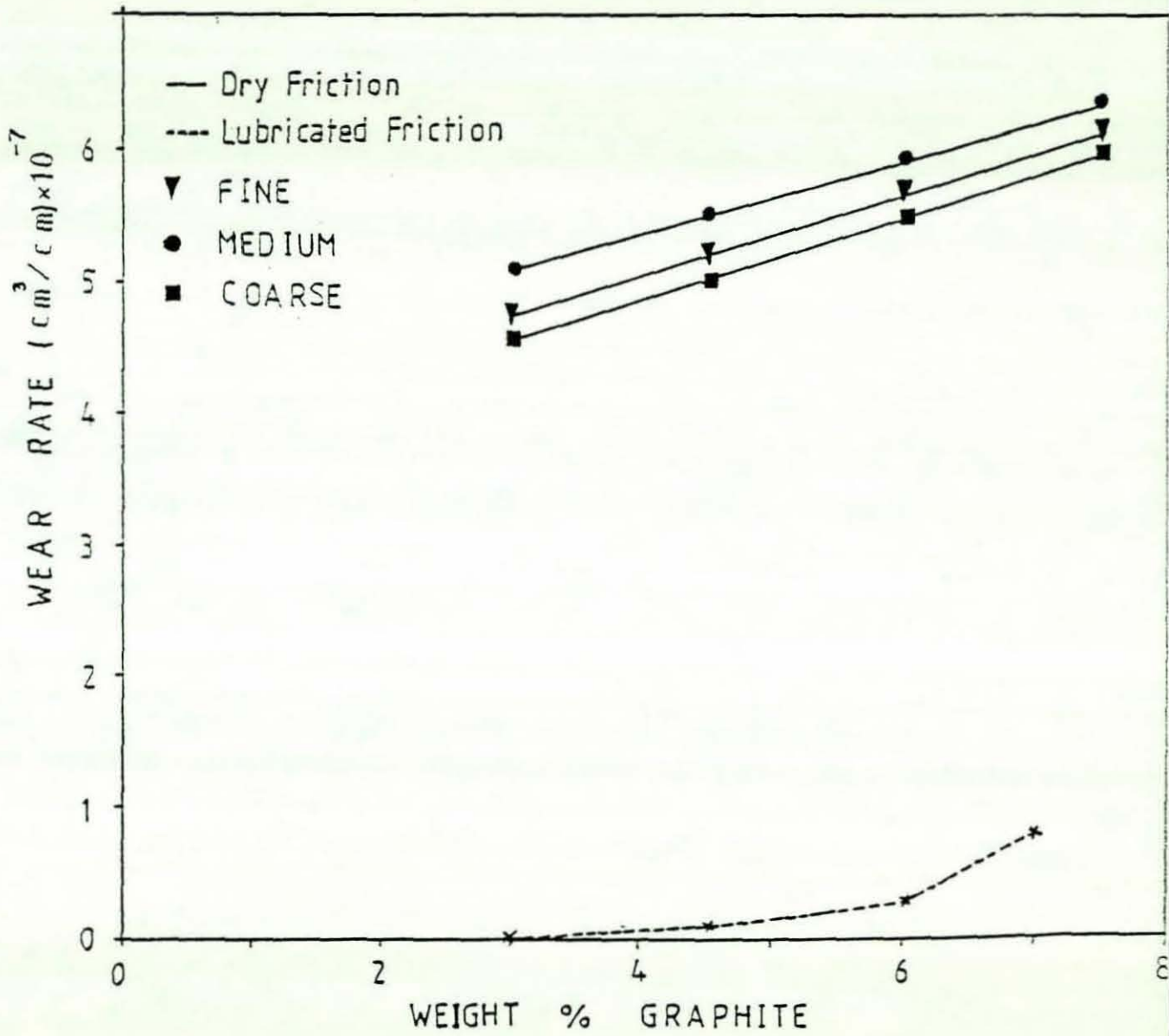


Fig.58 - The Effect of Graphite Content on Wear Rate.

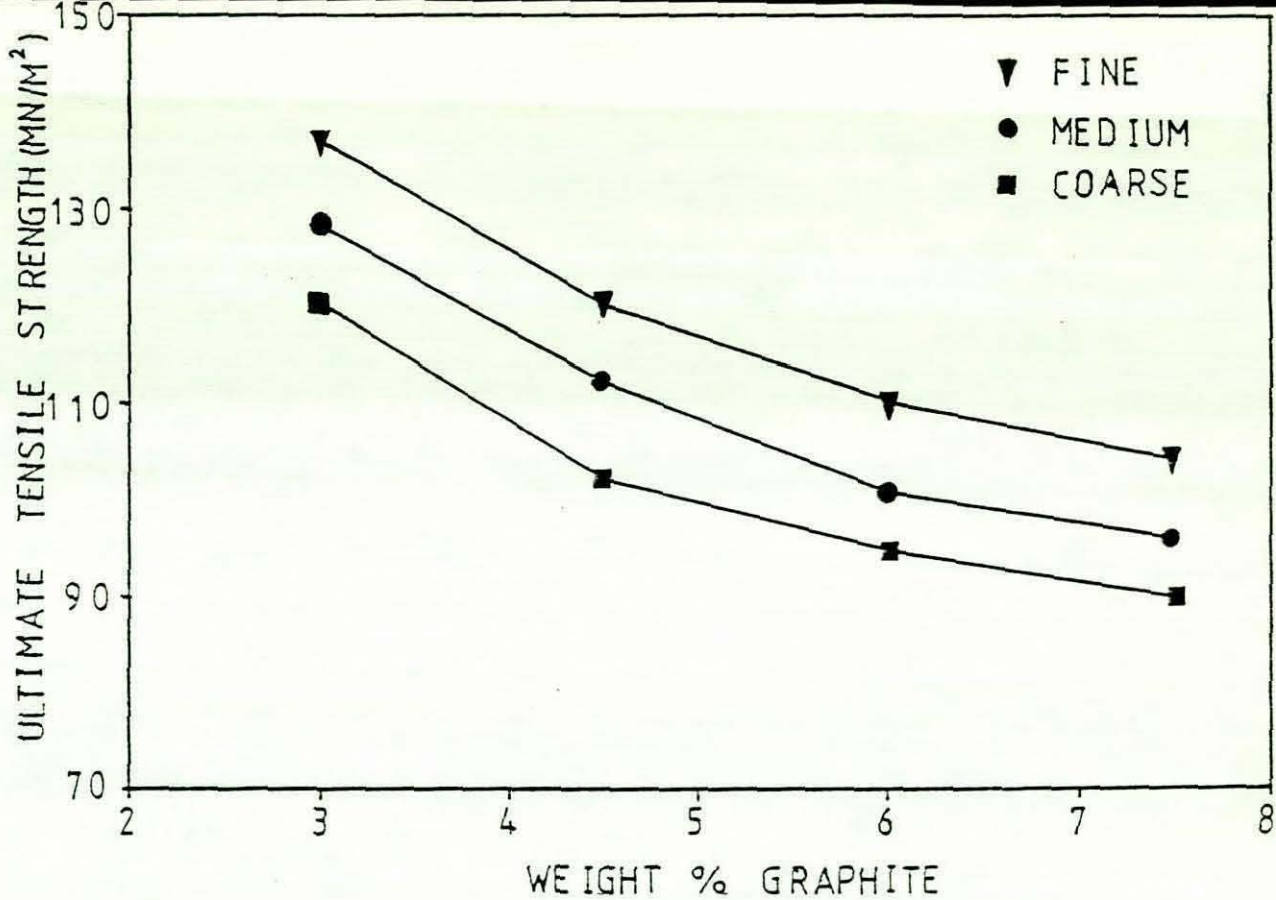


Fig.59 - Ultimate Tensile Strength vs. % Graphite  
(For Analysed Graphite Quantities)

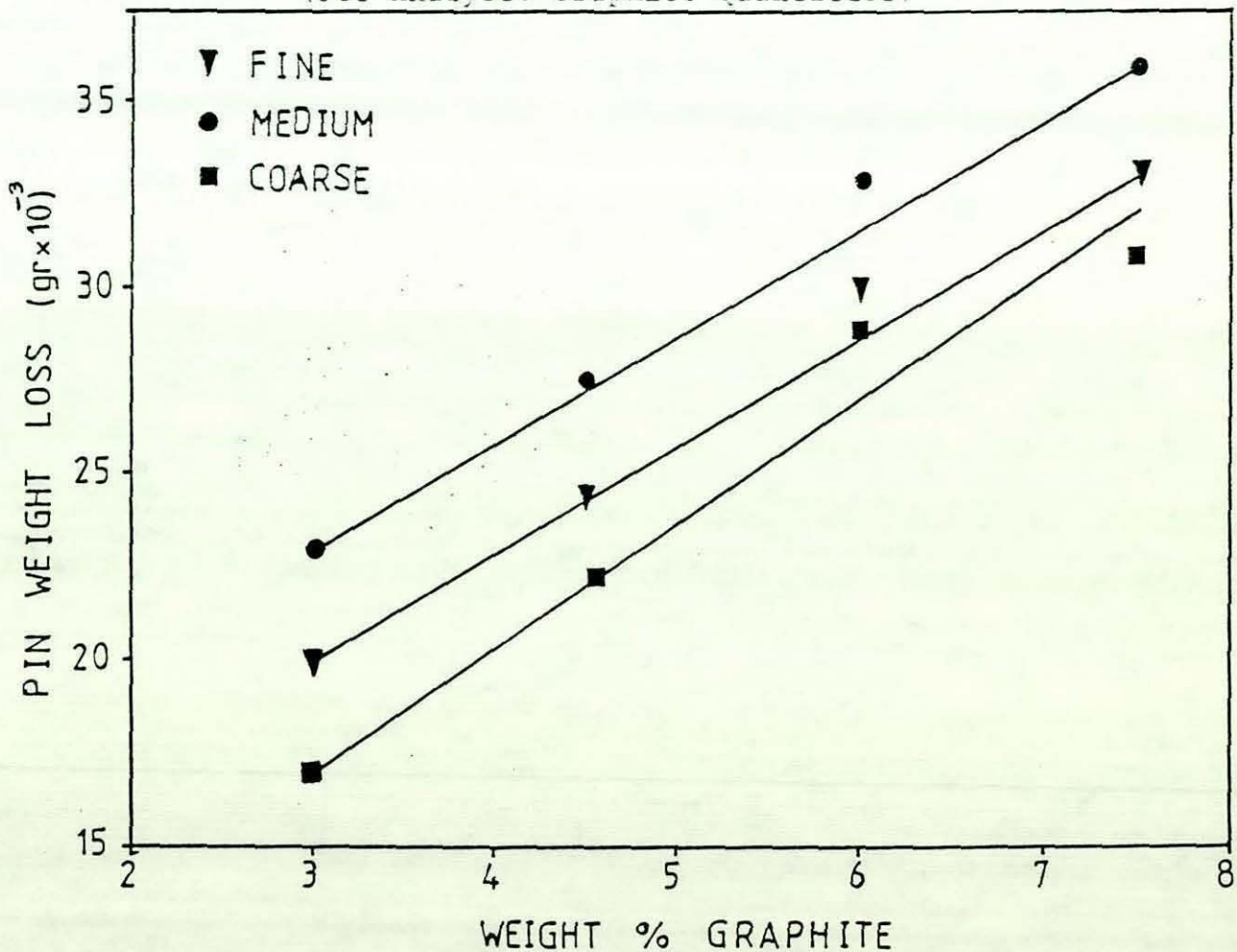


Fig.60 - Weight Loss vs. % Graphite (For Analysed Graphite Quantities)

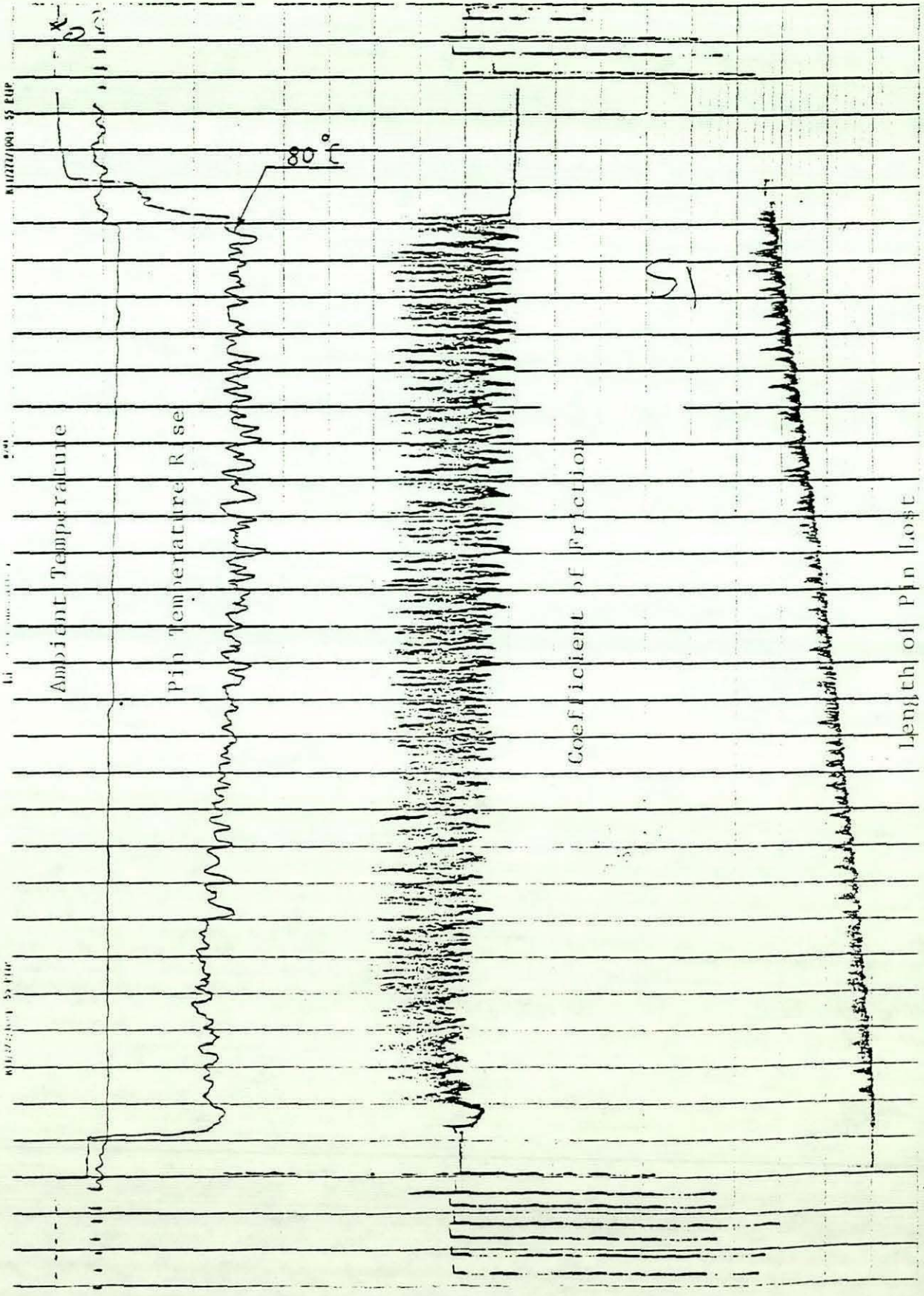


Fig.61 - Wear Chart for Control Casting Specimen Processed by Rheocasting and Pressure Die Casting (Dry Friction)

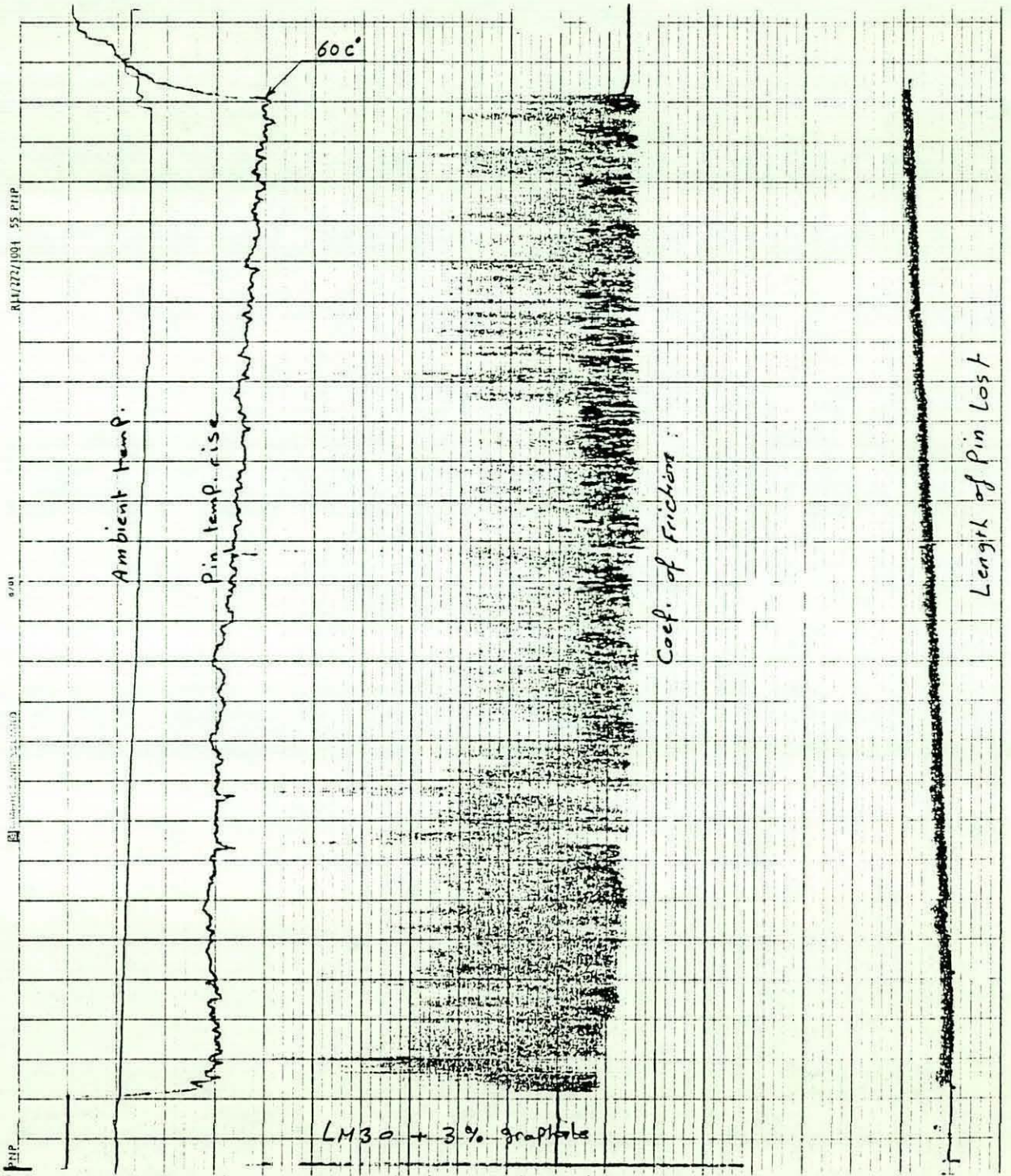


Fig.62 - Wear Chart for LM30 Alloy + 3wt% Graphite (Dry Friction)

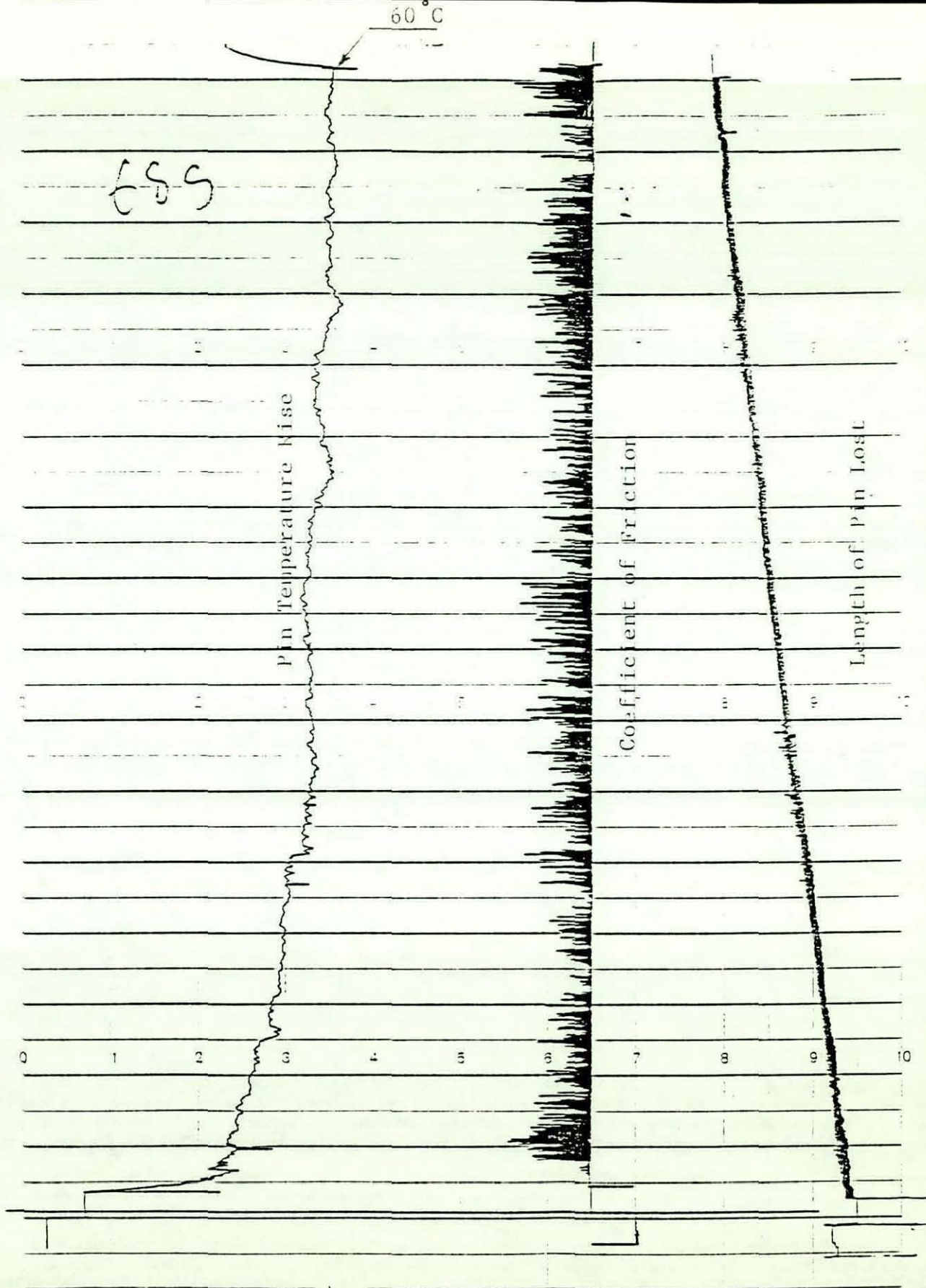


Fig.63 - Wear Chart for LM30 - 7½wt% Graphite  
(Dry Friction)

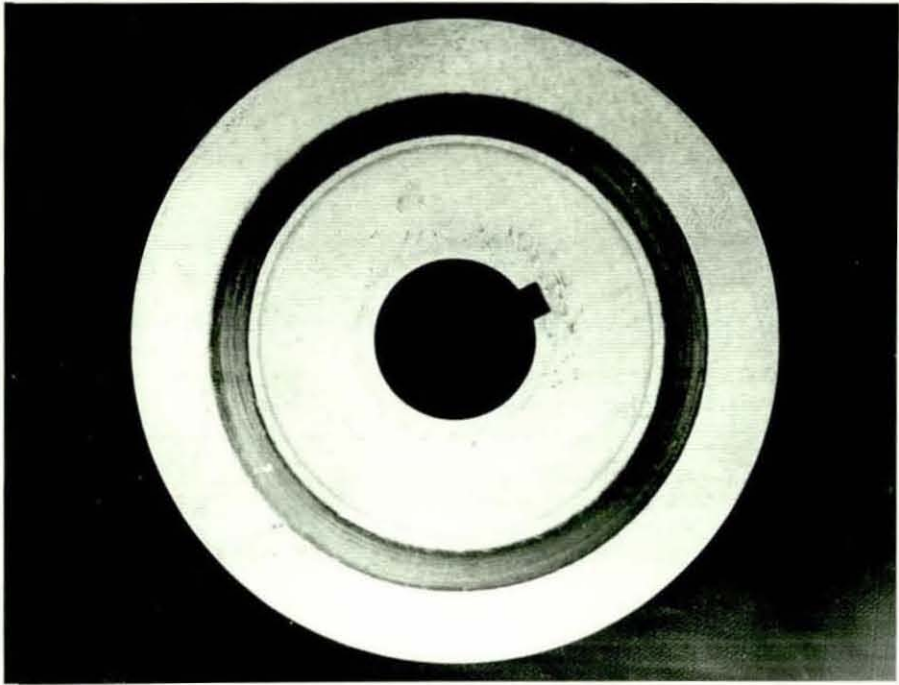
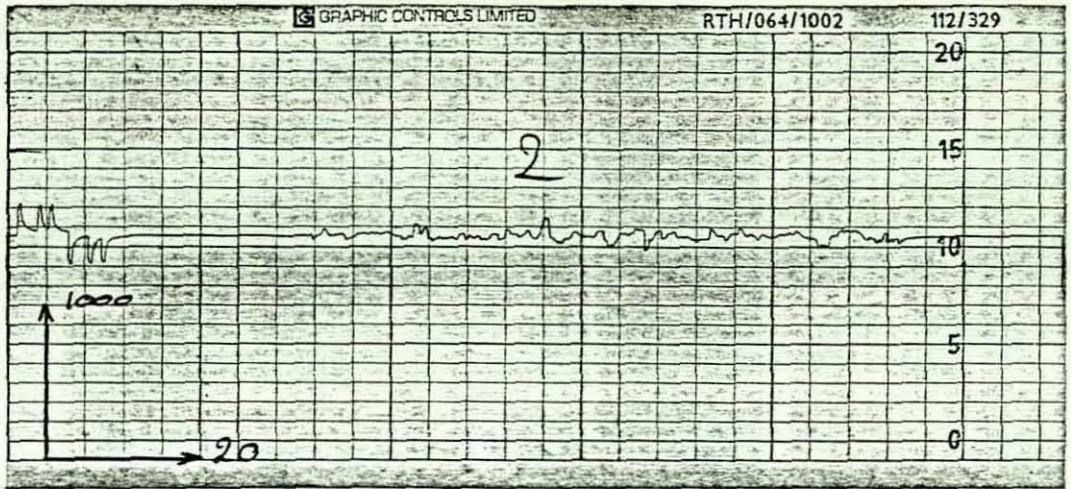
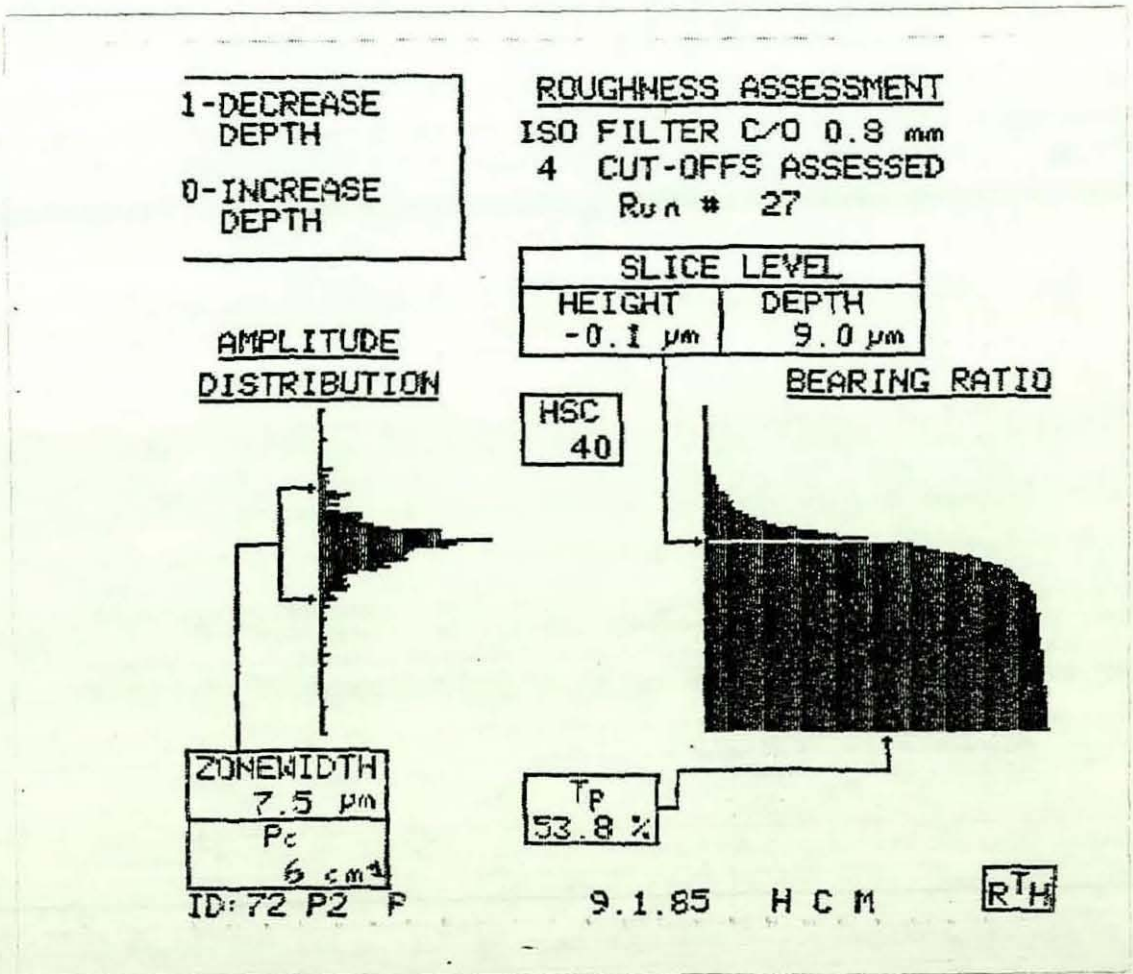


Fig.64 - Disc Surface After Wear Test.



(a)

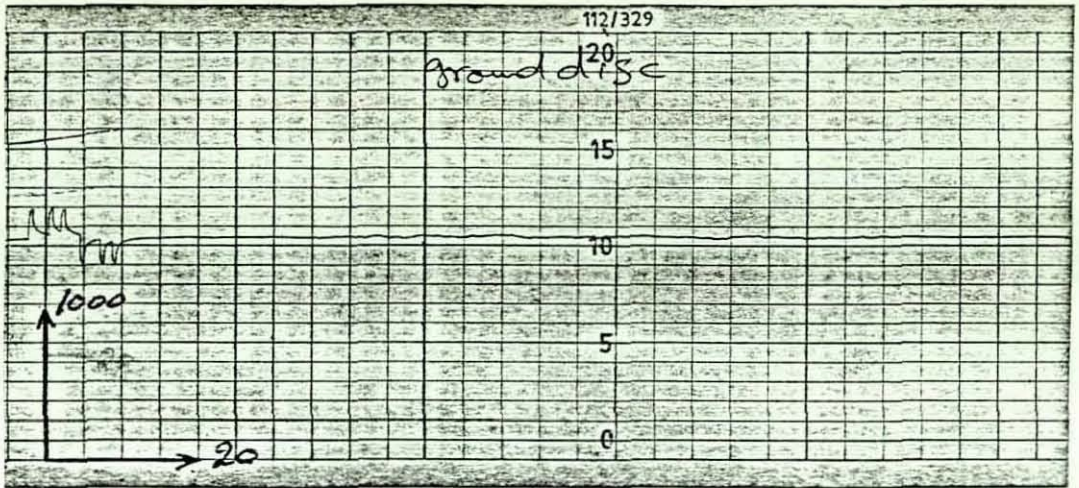
$R_a = 1.47 \mu\text{m}$



(b)

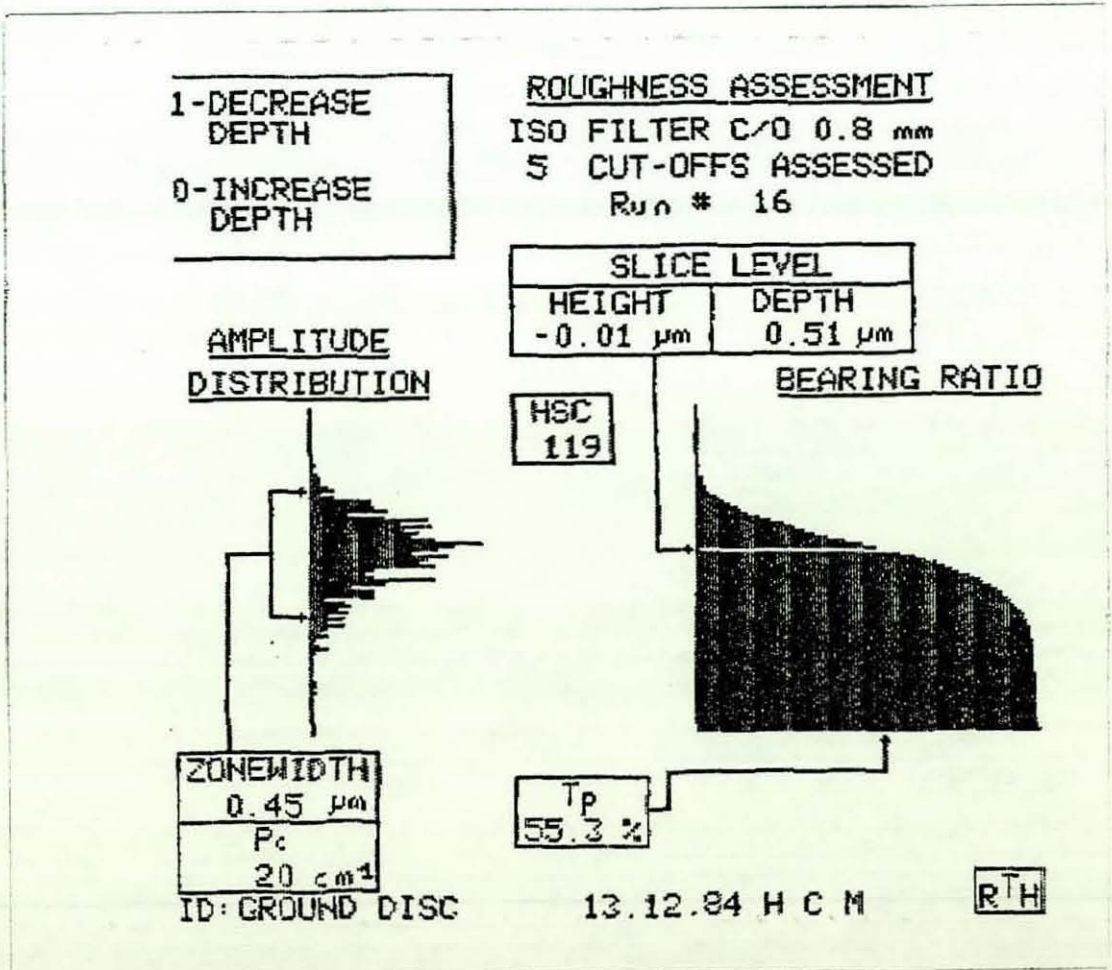
Fig.65 - Pin Surface Texture Before Test (typical)

(a) Surface Profile. (b) Bearing Area Analysis



(a)

$R_a = 0.07 \mu\text{m}$



(b)

Fig.71 - Disc Surface Texture Before Test (typical)

(a) Surface Profile. (b) Bearing Area Analysis.

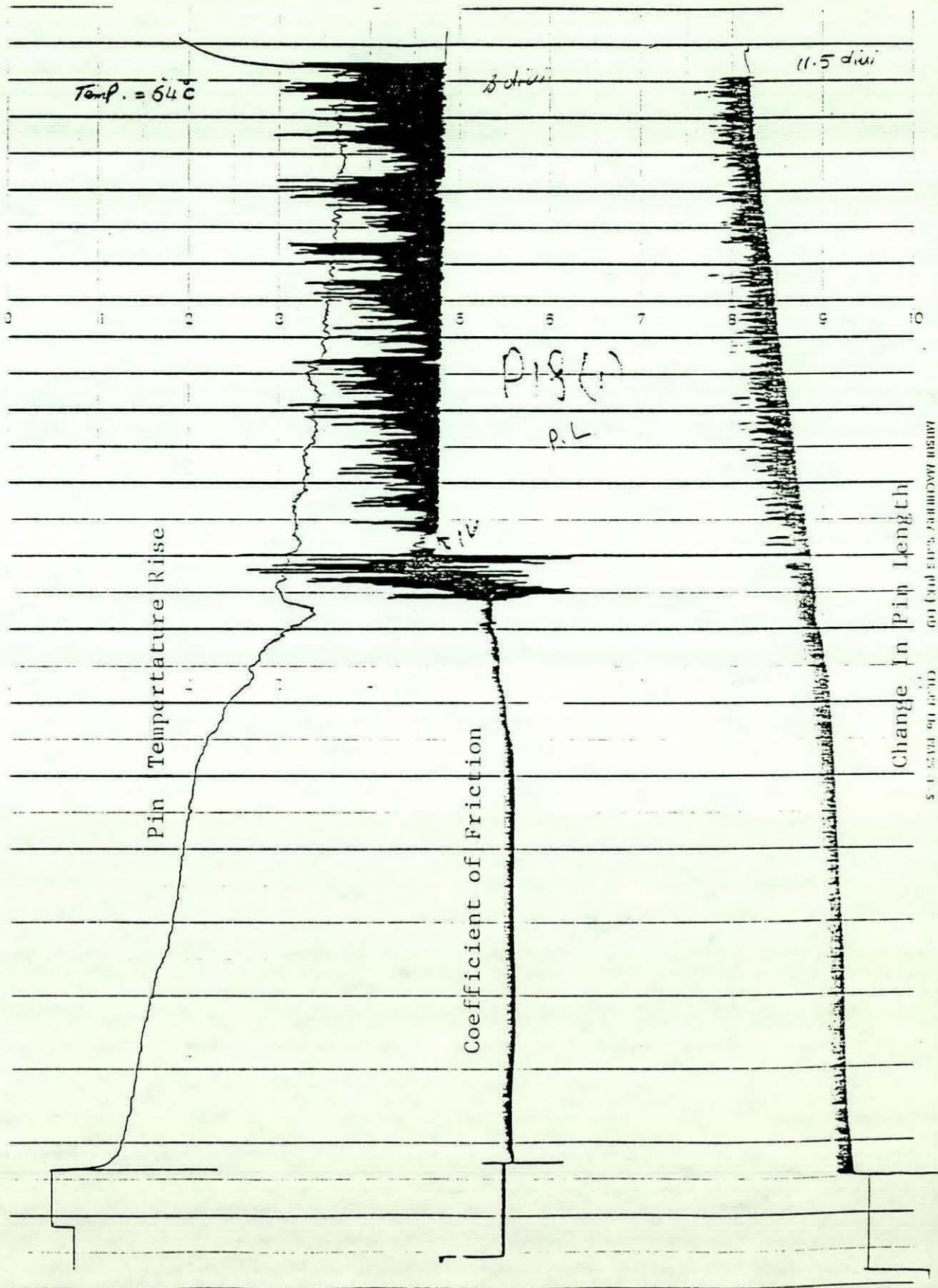


Fig.77 - Wear Chart For Control Casting Specimens Produced By Rheocasting And Pressure Die Casting (Lubricated Friction)

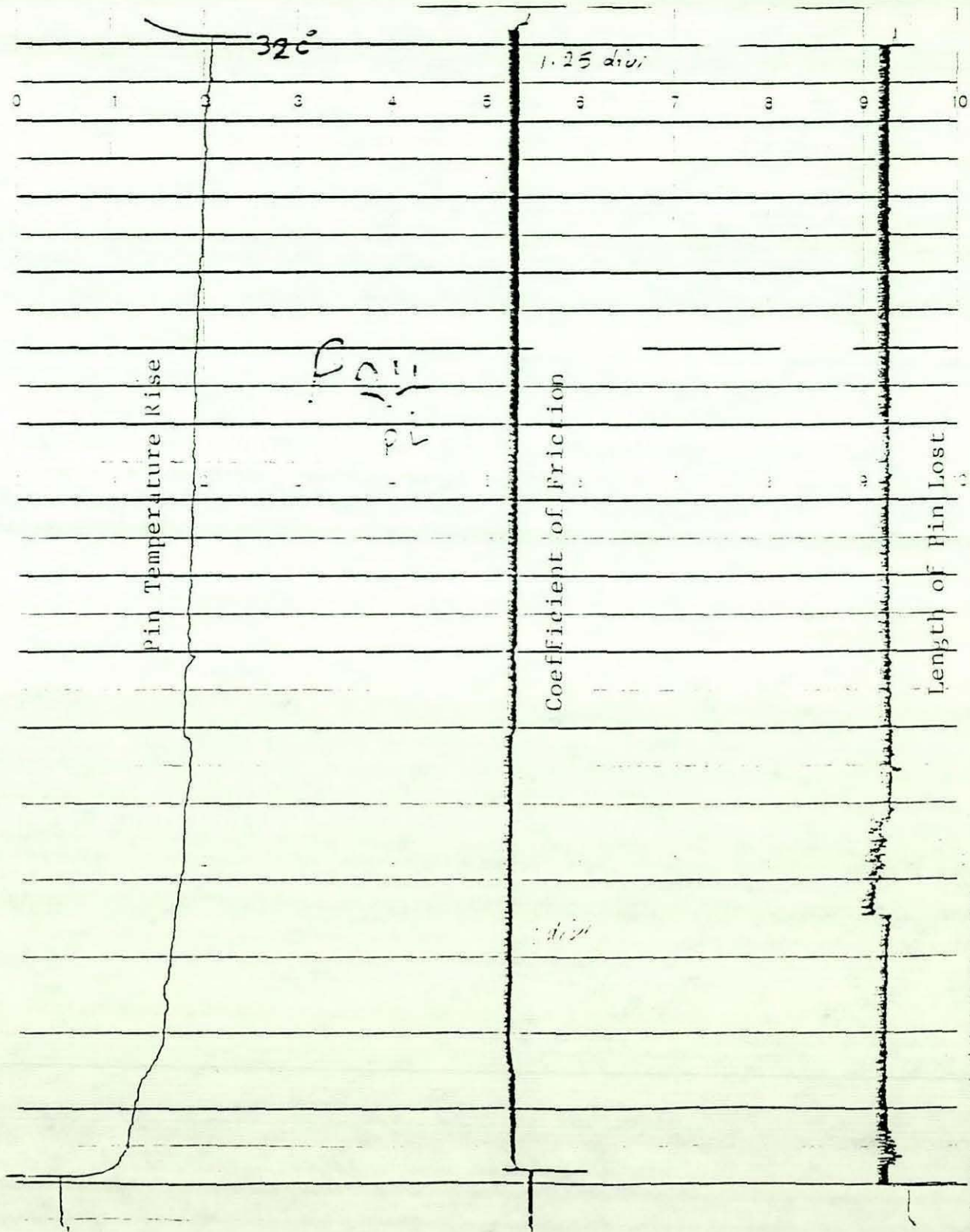


Fig.78 - Wear chart for LM30 - 3wt% Graphite Specimen  
(Lubricated Test)

AMERICAN SOCIETY OF MECHANICAL ENGINEERS

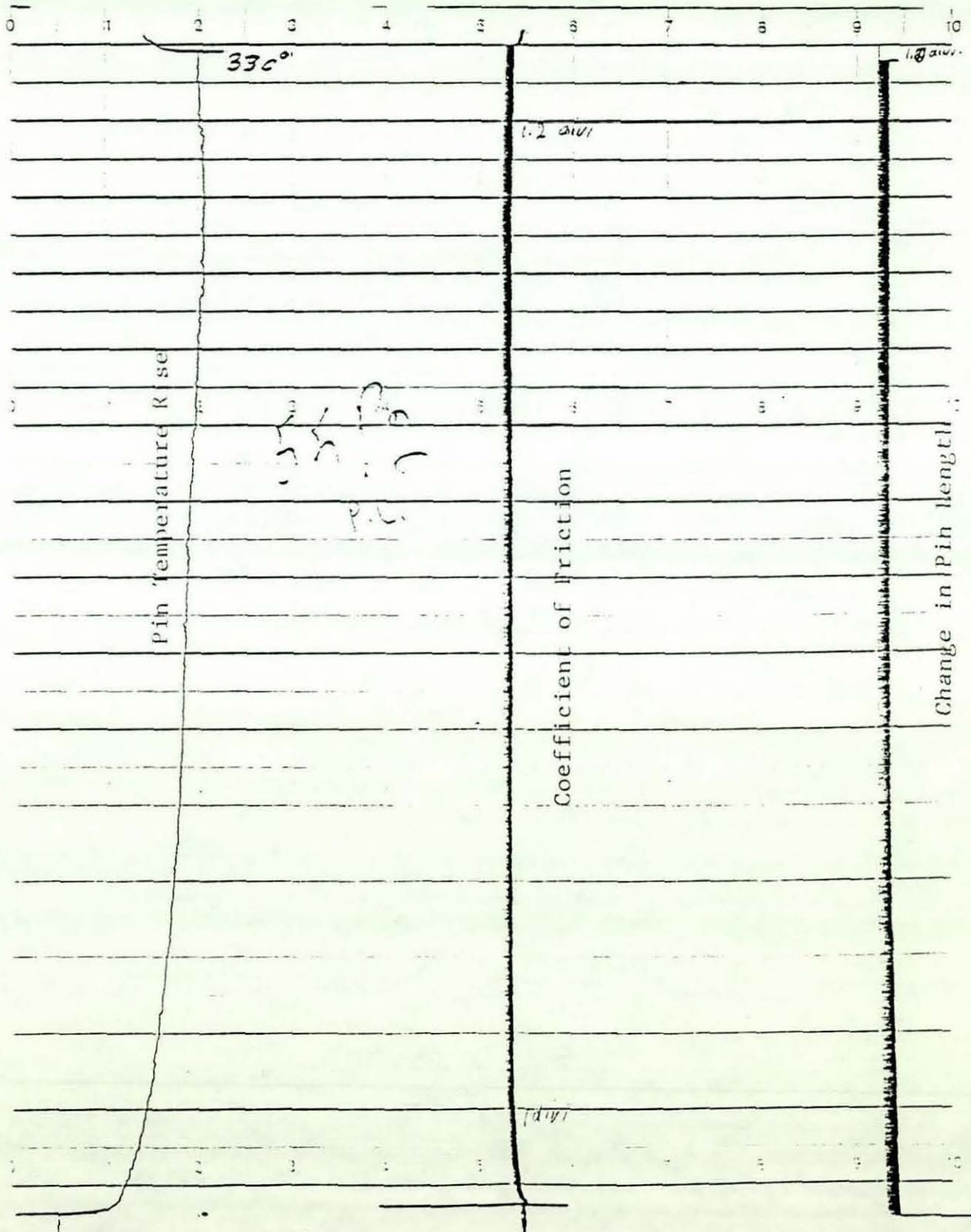


Fig.79 - Wear Chart of LM30 - 6wt% Graphite Specimen  
(Lubricated test)

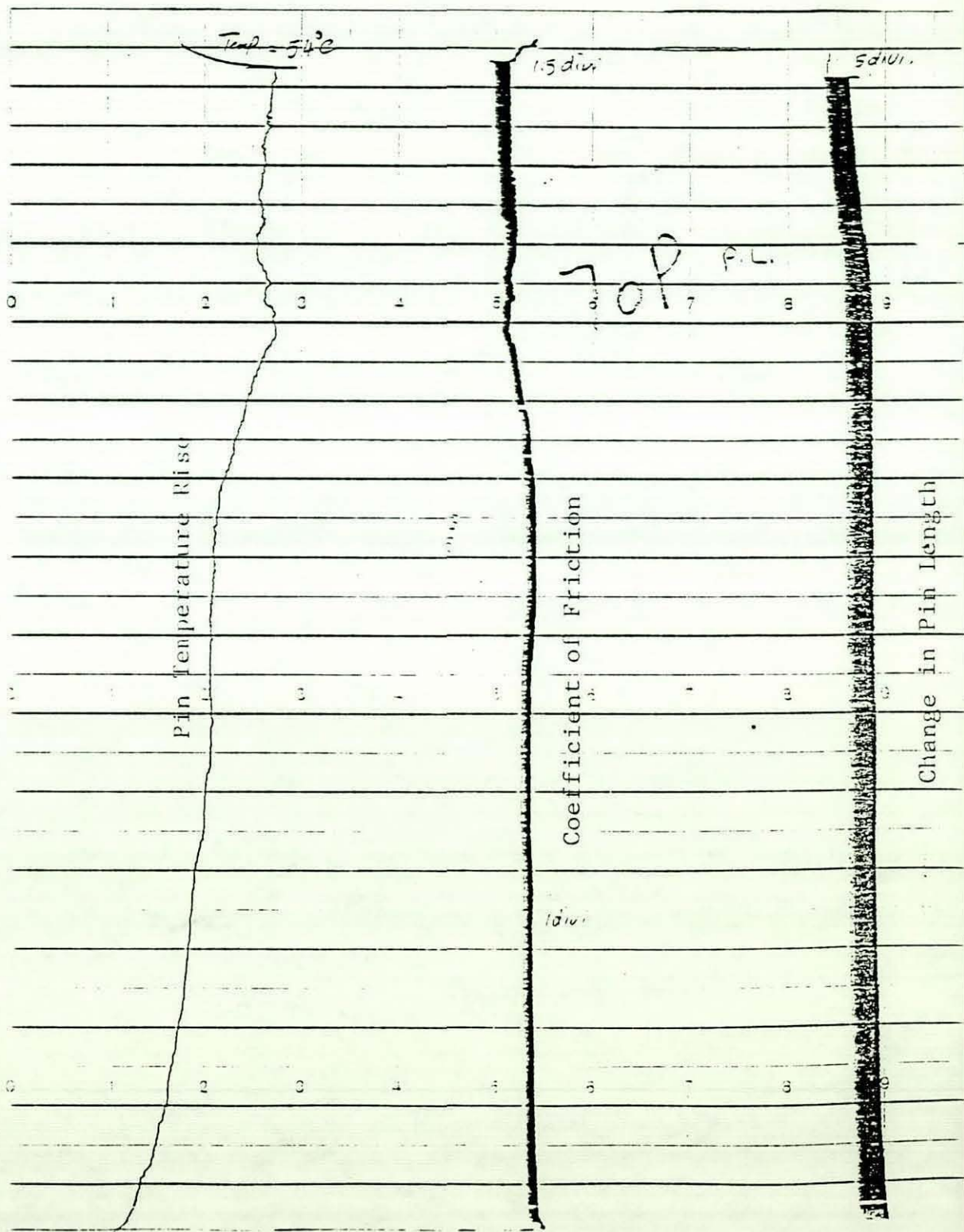


Fig.80 - Wear Chart for LM30 - 7½wt% Graphite Specimen (Lubricated Test)

Table 3: Tensile Test Results For Control Castings

Casting Process	Max. Load kN	U.T.S. MN/m <sup>2</sup>	% Elongation	% Reduction In Area
Gravity Die Casting	3.63	225	2	1
Conventional Pressure Die Casting	3.1	192	1.5	1
Rheocast Followed By Pressure Die Casting	2.96	183	1.5	1
Sand Casting	2.21	137	1	0.5

(Values were the average of four specimens)

Table 4: Tensile Test Results For The Composite Alloy Castings

Properties		Max.Load	U.T.S.	%	% Reduction
Graphite		kN	MN/m <sup>2</sup>	Elongation	In Area
3%	Coarse	1.94	120	1	0.75
	Med.Fine	2.06	128	1	0.75
	Fine	2.21	137	1	0.75
4½%	Coarse	1.63	101	0.75	0.75
	Med.Fine	1.78	110	0.75	0.75
	Fine	1.90	118	0.75	0.75
6%	Coarse	1.53	95	0.75	0.5
	Med.Fine	1.63	101	0.75	0.5
	Fine	1.78	110	0.75	0.5
7½%	Coarse	1.48	92	-	-
	Med.Fine	1.56	97	-	-
	Fine	1.71	106	-	-

(Values were the average of four specimens)

Table 5 : Hardness Test Results For Control Castings

Properties Casting Process	Diameter Of Impression (mm)	Average Diameter (mm)	Brinell Hardness No.
Gravity Die Casting	2.8 2.75 2.9 2.85 2.85 2.75 2.9 2.8 2.8 2.8 2.85 2.8	2.82	118
Conventional Pressure Die Casting	2.85 2.95 2.90 2.95 2.95 2.90 2.85 2.85 2.95 2.90 2.85 2.90	2.9	111
Rheocast Followed By Pressure Die Casting	2.85 2.9 2.85 2.85 2.9 2.85 2.95 3.0 2.9	2.91	110
Sand Casting	2.95 3.0 2.9 2.95 2.95 2.95 2.95 2.95 2.9 3.0 3.0 2.9	2.95	107

Table 6: Hardness Test Results For Composite Alloy Specimens

Graphite		Properties	Diameter Of Impression (mm)			Average Diameter (mm)	Brinell Hardness No.
3%	Coarse		3.2	3.2	3.2	3.2	91
	Med.Fine		2.18	3.15	3.15	3.2	93
	Fine		3.05	3.12	3.14	3.1	97
4½%	Coarse		3.42	3.43	3.42	3.42	79
	Med.Fine		3.38	3.36	3.40	3.38	82
	Fine		3.28	3.26	3.28	3.27	86
6%	Coarse		3.6	3.58	3.55	3.56	73
	Med.Fine		3.57	3.56	3.59	3.57	73
	Fine		3.44	3.4	3.44	3.43	79
7½%	Coarse		3.65	3.66	3.64	3.65	69
	Med.Fine		3.65	3.61	3.6	3.62	70
	Fine		3.5	3.5	3.5	3.5	76

Table 7: Pin On Disc Wear Test Results For Control Castings (dry friction)

Criteria Casting Process	Pin Weight Loss(gr)	Length Of Pin Lost (mm)	Coefficient Of Friction	Pin Temperature Rise °C	Pins		Discs	
					Surface Finish µm Ra	Bearing Ratio tp %	Surface Finish µm Ra	Bearing Ratio tp %
Gravity Die Casting	0.027	0.34	0.39	68	4.54	51.8	1.1	51.2
Conventional Pressure Die Casting	0.028	0.35	0.41	66	3.69	55.9	0.87	49.4
Rheocast Followed By Pressure Die Casting	0.029	0.36	0.35	67	4.62	56.4	0.89	50.3
Sand Casting	0.031	0.38	0.40	70	5.39	49.6	0.80	47.3

Table 8: Pin On Disc Wear Test Results For Composites (dry friction)

Criteria Graphite		Pin Weight Loss (gr)	Length Of Pin Lost (mm)	Coefficient Of Friction	Pin Temperature Rise °C	Pins		Discs	
						Surface Finish µm Ra	Bearing Ratio tp %	Surface Finish µm Ra	Bearing Ratio tp %
3%	Coarse	0.017	0.26	0.31	62	4.20	52.4	0.56	44.5
	Med.Fine	0.023	0.29	0.34	66	4.8	53.6	0.71	49.8
	Fine	0.020	0.27	0.32	64	3.55	54.7	0.65	48.3
4½%	Coarse	0.021	0.29	0.30	57	3.51	54.5	0.59	48.7
	Med.Fine	0.026	0.31	0.32	65	3.91	51.1	0.64	49.4
	Fine	0.023	0.30	0.30	61	2.2	54.8	0.63	47.7
6%	Coarse	0.025	0.33	0.28	56	3.2	56.0	0.53	46.8
	Med.Fine	0.028	0.34	0.31	63	3.3	51.3	0.62	46.9
	Fine	0.026	0.35	0.29	60	3.1	52.7	0.66	46.5
7½%	Coarse	0.029	0.35	0.25	52	3.37	52.9	0.54	48.0
	Med.Fine	0.032	0.38	0.26	60	2.65	52.6	0.57	47.5
	Fine	0.031	0.36	0.23	58	2.29	53.5	0.62	45.8

Table 9: Pin On Disc Wear Test Results For Control Castings (Lubricated Friction)

Criteria Casting Process	Pin Weight Loss (gr)	Length of Pin Lost (mm)	Coefficient Of Friction	Pin Temperature Rise °C	Pins		Discs	
					Surface Finish $\mu\text{m Ra}$	Bearing Ratio tp %	Surface Finish $\mu\text{m Ra}$	Bearing Ratio tp %
Rheocast Followed By Pressure Die Casting	0.0196	0.21	0.35 0.05	64	3.34	56.0	0.74	53.2

Results were the average of two values.

Table 10: Pin On Disc Wear Test Results for Graphitic Castings (Lubricated Friction)

LM30 - 3wt% Gr.	0.0005	0.005	0.05	32	0.44	45.8	0.28	44.8
LM30 - 4½wt% Gr.	0.0021	0.010	0.05	30	0.49	52.9	0.59	48.9
LM30 - 6wt% Gr.	0.0050	0.019	0.05	32	0.72	48.5	0.72	50.2
LM30 - 7½wt% Gr.	0.0102	0.047	0.1 0.05	54	1.60	56.1	0.82	50.8

Results were the average of two values.

Table 11: Quantitative Analysis of Graphite Content

Sample	Assumed Quantity of Graphite	Analysed Quantity % Area of Graphite				Ave.	Equiv. %wtGr.
LM30+3%Gr.	3% Coarse Gr.	4.14	3.24	6.46	4.26	4.53	3.17
	3%Med.Fine Gr.	3.94	4.92	5.96	2.92	4.45	3.11
	3% Fine Gr.	1.86	3.24	4.90	3.72	3.68	2.6
LM30+4½%Gr.	4½% Coarse Gr.	8.44	4.35	3.62	9.26	6.42	4.49
	4½%Med.Fine Gr.	3.9	8.74	6.26	8.96	6.97	4.87
	4½% Fine Gr.	3.9	3.56	11.54	6.40	6.35	4.45
LM30+6%Gr.	6% Coarse Gr.	13.16	7.98	7.22	5.9	8.57	6.0
	6%Med.Fine Gr.	8.14	6.32	4.68	9.02	7.0	4.93
	6% Fine Gr.	10.24	9.26	3.94	6.46	7.48	5.23
LM30+7½%Gr.	7½% Coarse Gr.	16.0	6.90	8.90	12.2	11.0	7.7
	7½%Med.Fine Gr.	10.58	11.54	10.82	8.90	10.46	7.32
	7½% Fine Gr.	9.02	13.33	8.14	10.95	10.36	7.25

DISCUSSION6.1 Composite Alloy Production

The microstructures in Figs.38-40 were produced by casting fully liquid LM30 alloy to provide control microstructures which could be compared with microstructures produced from the partially solid alloy. Fig.39 presents an alloy produced by gravity die casting, Fig.40 presents the same alloy solidified by conventional pressure die casting and Fig.38 presents the same alloy when sand cast. The difference in structure between these three figures reflects the effect of cooling rate on the microstructure of the casting alloy. Sand casting produces a very slow cooling rate in comparison with die casting. This resulted in coarse primary silicon polyhedra (dark grey cuboids), coarse needles of  $\alpha$ -(Fe Si Al), light grey faceted  $\text{Cu Al}_2$ , and dark grey eutectic silicon. The silicon polyhedra are large in size and fewer in quantity, see Figs.38-40 and Table 2, because slow solidification encouraged few nucleation sites. In comparison, the more rapid cooling inherent in gravity and pressure die casting encouraged many more nucleation sites resulting in finer structures so that the silicon polyhedra are smaller in size and greater in number. The microstructure in Fig.41 represents the same alloy processed by the rheocasting route followed by pressure die casting. The rheocast structure exhibited coarse primary silicon polyhedra which are comparable in size and quantity to those in the sand cast structure, see Table 2. This is due to the very slow cooling rate employed in the rheocast process. Although a high shear rate was employed ( $550 \text{ sec}^{-1}$ ) in the preparation of the rheocast slurry it appears that the shear rate has no influence on the size of primary silicon polyhedra in the hypereutectic aluminium-silicon alloys. The alloy processed by rheocasting and followed by pressure die casting exhibited a fine eutectic matrix which is comparable to that produced by conventional pressure die casting. The modification of the eutectic matrix and the absence of  $\alpha$  complex is most likely due to the fast cooling rate which resulted from the rapid rate of heat extraction in the die during the processing of the alloy by the pressure die casting route. This is because the eutectic matrix

is similar to that produced by conventional pressure die casting, and the rheocast alloy was discharged from the rheocasting unit at about the eutectic temperature which is 574 °C. So the formation of the eutectic phase occurred during the processing of the alloy by pressure die casting.

In the aluminium-silicon binary system, the influence of rheocasting on structure is most readily demonstrated in the hypoeutectic alloys. In sand casting, the primary  $\alpha$  phase solidifies dendritically, as shown in Fig.30. However, when the alloy is processed through the rheocaster the dendrites are broken by the shearing action of the rotor, as shown in Fig.29 and 31. Consequently the rheocast structure contains round particles of primary phase and the size of these particles is a function of the shearing and cooling rates employed.

In the hypereutectic alloys the  $\beta$  phase nucleates first and consists of silicon-rich polyhedra. Under the shearing action these polyhedra, unlike the  $\alpha$  phase dendrites, do not break down (there is evidence that break down occurred with some of these particles, as shown in Fig.45, but on a very minor scale). As a result the structure of LM30 alloy processed in the rheocaster and pressure die cast is that shown in Fig.41. When compared with the structure in Fig.40 it can be seen that the polyhedra are appreciably larger in size and fewer in number. However, the eutectic matrix is equally fine in both cases. Comparison between sand cast and rheocast structures shows that the size and the number of silicon polyhedra are similar in both structures. This is because of the slow cooling associated with sand casting and the slow cooling rate whilst the alloy is resident in the rheocasting unit. Chemical treatments to modify the eutectic or refine the primary-silicon polyhedra, have not been used. The coarse silicon polyhedra obtained from processing the alloy by the rheocasting route could be refined by the addition of phosphor-copper. This practice is used commercially to improve the mechanical properties of hypereutectic aluminium-silicon alloys.

The microstructures of LM30 alloy processed by the compocasting route, with different graphite addition levels, exhibited

coarser silicon polyhedra in comparison with the microstructure of the same alloy processed by the rheocasting route. This could be explained by the fact that the addition of hot graphite to the semi-solid alloy slurry delayed the discharge of the alloy from the crucible i.e. giving the silicon polyhedra more time to grow in size, see Figs.41-44 and Table 2. The microstructures of graphitic specimens show an intimate contact between the graphite particle and the matrix, see Fig.91, where the graphite particle is surrounded by the matrix alloy. Even at a higher magnification, Fig.92, voids do not appear to be present between the graphite particle and the matrix. The viscosity of the agitated slurry has been observed to be at a minimum when there is the greatest proportion of liquid phase in the semi-solid alloy i.e. when less volume fraction solid is present. Therefore lower viscosities were obtained in alloys which discharged from the compocasting unit at higher temperatures. The reduction in the temperature of the alloy slurry resulted in an increase in the slurry's viscosity due to the increase in volume fraction solid. It has also been observed that any slight reduction in slurry temperature below 570°C resulted in a sharp increase in the viscosity of the semi-solid slurry of the LM30 alloy. This could be the result of the aluminium-silicon-copper phase beginning to form at this temperature<sup>(88)</sup> causing an increase in the volume fraction solid. Porosity and shrinkage holes have been observed in the test castings processed by the compocasting route followed by pressure die casting. The porosity and shrinkage holes appear to be concentrated in the disc, especially at the junction between the pins and disc. This can be seen in the X-ray photograph Fig.31. This might be attributed to two reasons; 1) the lack of pressure provided to the casting for the reasons outlined before and 2) the design of the test casting itself. The long freezing range in the hypereutectic alloy accentuates the problem of shrinkage porosity in castings. Double thick sections take about twice as long to solidify, so it is extremely important that consistent section thickness be maintained. The disc in the test casting see Fig.18 is relatively thick and provides the largest volume in the test casting so, for the reason mentioned above, this part will solidify last and act as a feeder for the rest of the test casting which consists of

the four pins. The problem might be overcome by reducing the thickness of the disc. Specimens for mechanical and tribological tests were chosen from the sound parts of the casting (this was decided by radiographic examination) which are the sprue and the section of the pin remote from the disc see Figs.32 and 33. The microstructure investigation and the mechanical and tribological properties evaluation showed no difference between pin and sprue specimens for the same casting.

#### 6.1.1 Investigation of Graphite Rejection With Inert Gas Shielding

It has been considered that one of the advantages of compocasting by utilizing semi-solid slurry, is the possibility of dispersing uncoated and untreated graphite particles in aluminium-silicon alloys without rejection or agglomeration. The literature describes the following different mechanisms for graphite dispersion and retention in these alloys:

- (I) some sources<sup>(17,92)</sup> reported that non-wetted particles are mechanically entrapped and prevented from agglomeration by the high effective viscosity of the semi-solid slurry due to the presence of primary solid particles, although none of these sources stated the minimum viscosity or volume fraction solid required to cause such entrapment.
- (II) Badia<sup>(37)</sup> and Krishnan<sup>(32)</sup> reported that graphitic aluminium-silicon alloys can be remelted twice without significant loss of graphite particles.
- (III) Some researchers<sup>(43,46,93)</sup> reported the inclusion of uncoated, but pretreated graphite in fully liquid aluminium-silicon alloys. The aim of the treatment was to release the adsorbed gases and contamination from the graphite surface. Krishnan<sup>(43)</sup> added that the presence of alloying elements such as magnesium, silicon, copper.. etc. is essential for successful graphite dispersion.
- (IV) Kahan<sup>(94)</sup> reported chemical reaction between graphite and aluminium at the graphite aluminium interface. This reaction begins at 500°C and is time and temperature dependant, and the reaction product is aluminium carbide ( $Al_4C_3$ ).

(V) In this research programme the introduction of graphite under inert gas shielding resulted in total rejection of graphite particles from the melt even though the volume fraction of primary solid particles was higher than when processing in air. The incorporation of graphite with air contact resulted in total acceptance. Molten aluminium alloys oxidise when in contact with air and the oxide layer build-up on the melt surface is time and temperature dependent. The problem increases when the alloy is subjected to a stirring action. This increases the amount of aluminium oxide in the melt (as inclusions) which results in inferior mechanical and tribological properties of the alloy. For this reason it might be expected that an inert gas cover would be beneficial. However, none of the researchers reported the use of a gas cover and, in this research, inert gas covers were shown not to be conducive to graphite retention. It is interesting to note that in the control casting results, the rheocast/pressure diecast material was 5% lower in strength than that produced by conventional pressure diecasting.

(VI) Guo and Liang<sup>(95)</sup> reported the inclusion of up to 20wt% of spectrally pure graphite in an aluminium-8% silicon alloy in the semi-solid state with volume fraction solid of 0.4-0.6. The graphite introduction was carried out under vacuum.

Metcalf<sup>(96)</sup> reported six possible types of bonding between graphite and aluminium matrix, these are:

- (1) Mechanical bond.
- (2) Dissolution and wetting bond.
- (3) Reaction bond
- (4) Exchange reaction bond.
- (5) Oxide bond.
- (6) Mixed bond.

In the aluminium-silicon-graphite system, a bond based upon pure mechanical bonding is unlikely to occur unless the volume fraction of primary solid particles is high enough (as in VI) to form a mesh which traps the graphite particles and prevents

them from flotation.

A dissolution and wetting bond is unlikely to occur because the contact angle between aluminium and graphite is significantly larger than  $90^\circ$  (36,97). However, some researchers, as in (III), found that molten aluminium-silicon alloys could wet graphite yarn or graphite particles if pretreatment was used which they considered removed contaminants from the graphite surface.

A reaction and exchange reaction bond may be present on a small scale resulting from the transfer of atoms from one or both constituents to the reaction site. Gorbunov<sup>(46)</sup> stated that this is the type of bond present between aluminium-silicon alloys and graphite, but offered no evidence to support his statement. Kahan (IV) reported the formation of aluminium carbide at the graphite-aluminium interface during the preparation of Al-graphite fibre by a solid-state diffusion method. Metcalfe mentioned in his book<sup>(98)</sup>, that Pepper et al. reported a similar finding.

Oxide bonds may be generated by wetting but could also include bonds where intermediate compounds form at the interface. Traces of oxygen may form an intermediate zone within a bond between matrix and particle. Metcalfe<sup>(99)</sup> has shown that bonding can be assumed to be between natural aluminium oxide films and oxide films on the other constituents of the composite by solution or reaction.

Quigley et al.<sup>(97)</sup> stated that, in Al-Mg-fibre composites alloy, interactions between the  $Al_2O_3$  fibres and the matrix resulted in the formation of a Mg-rich region around the fibres. He added that electron diffraction and X-ray diffractometry indicated that the interaction zone consisted of  $MgAl_2O_4$ , MgO and fine polycrystalline  $\alpha-Al_2O_3$ . The formation of  $MgAl_2O_4$  spinel was the result of the reaction between Mg which was in solution, and both  $Al_2O_3$  fibre and fine  $\alpha-Al_2O_3$ , which resulted from oxidation of the melt. However, the oxide bonds mainly occur in composites containing oxide as a reinforcement<sup>(100)</sup>. The X-ray microprobe analysis carried out for specimens of the castings which accepted graphite (no

gas shielding was used) showed a concentration of magnesium and oxygen at the boundary of the graphite particle, see Fig.93. This has been observed with every graphite particle analysed. The analysis also showed that the peak in the magnesium concentration was always accompanied by a peak of oxygen concentration, which might indicate the presence of magnesium oxide or other compounds containing magnesium and oxygen similar to those described by Quigley et al.

For specimens which rejected graphite (when inert gas shielding was used), the height of the concentration peaks was much less and there did not appear to be an association, as shown in Fig. 94. However, graphite dispersion obtained without gas shielding could result from the formation of aluminium oxide films which wrap around the graphite particles. The interaction between the  $Al_2O_3$  and the matrix could result in the formation of a magnesium rich region around the graphite particle<sup>(97)</sup> which could act as a wetting agent between the graphite and its matrix. This is more likely and could be supported by the X-ray microprobe analysis results which showed magnesium concentration on the boundary of the graphite particles and by the findings of Krishnan and Badia(II) who stated that the graphitic aluminium-silicon alloys could be remelted twice before significant loss in graphite occurred. This suggests that the bond is not only based on mechanical entrapment and/or mechanical interaction.

The exchange reaction reported by Kahan<sup>(94)</sup> is unlikely to occur because the time for graphite to be in contact with aluminium in the comocasting method is not sufficient to allow such a reaction to occur.

Fractured surfaces examined using scanning Electron Microscopy (SEM) showed that fracture occurred in the graphite particles, see Fig.95, with no evidence of graphite particles having vacated the fractured surface. This might indicate the presence of bonding between the graphite particles and the matrix which could be related to a mechanical bond based on entrapment of the graphite particles in the matrix and interaction between the graphite particles and the matrix due to the irregularity in the graphite particle shape, see Fig.91.

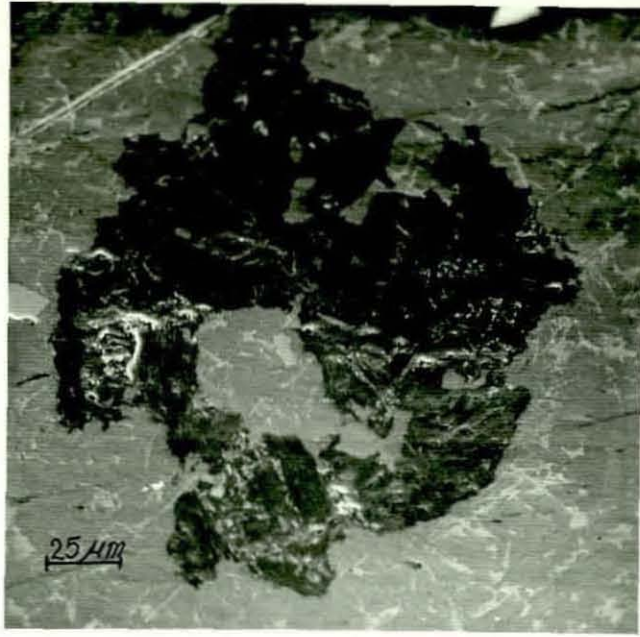


Fig.91 - Graphite Particle



Fig.92 - Graphite Particle At High Magnification

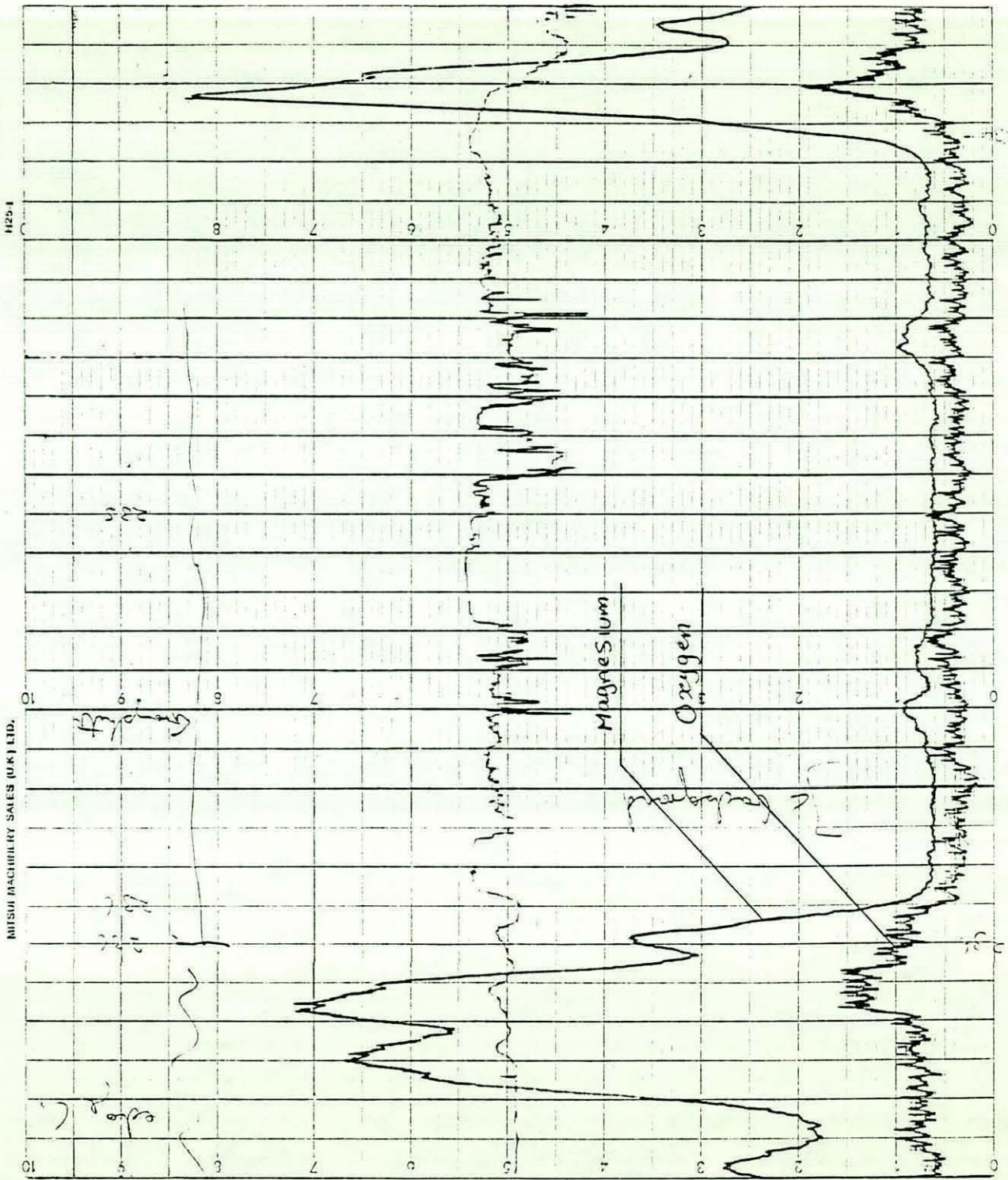


Fig. 93 - SMPA Trace  
Magnesium  
And Oxygen

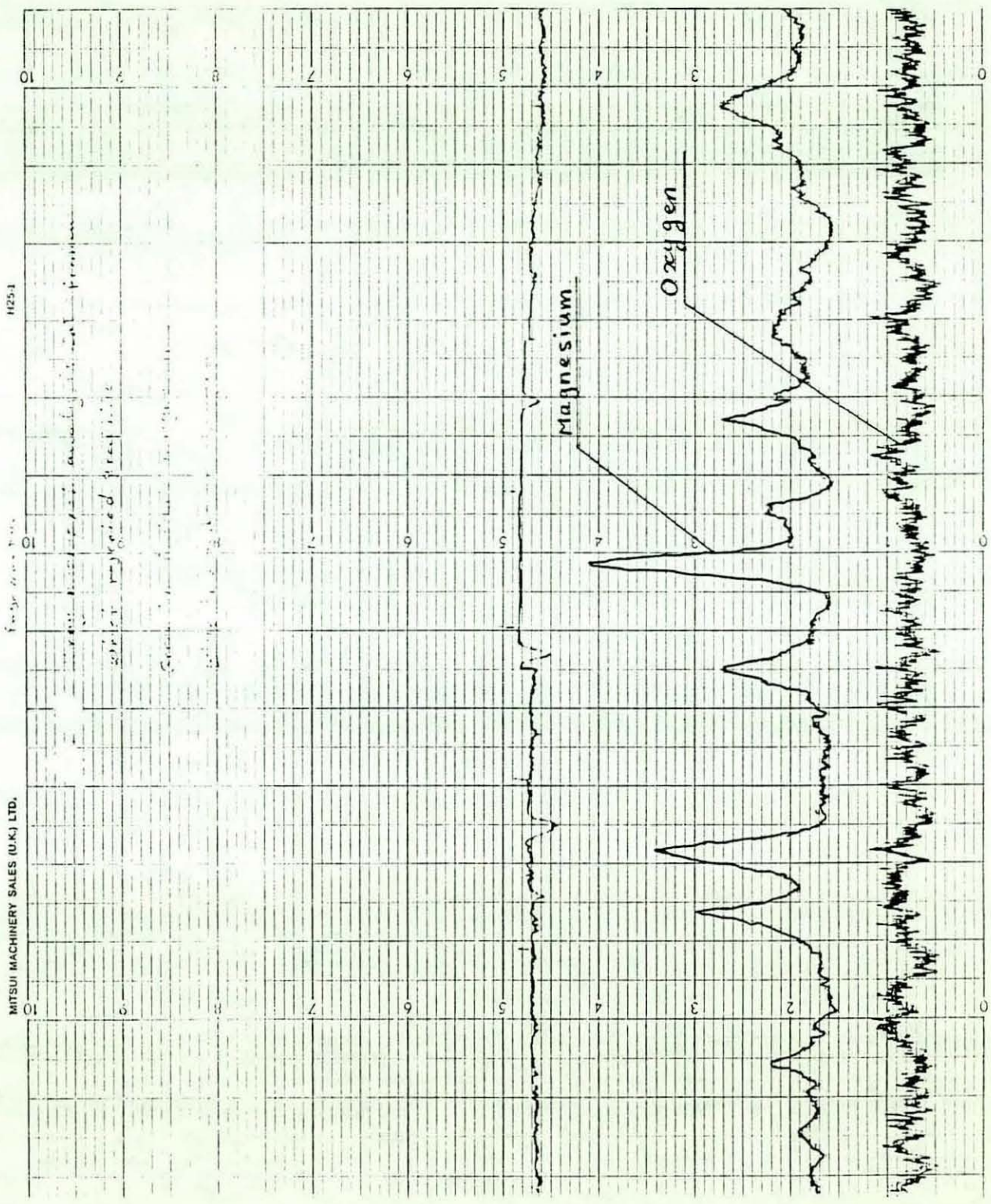


Fig. 94 - SMPA Trace  
 Magnesium  
 And Oxygen

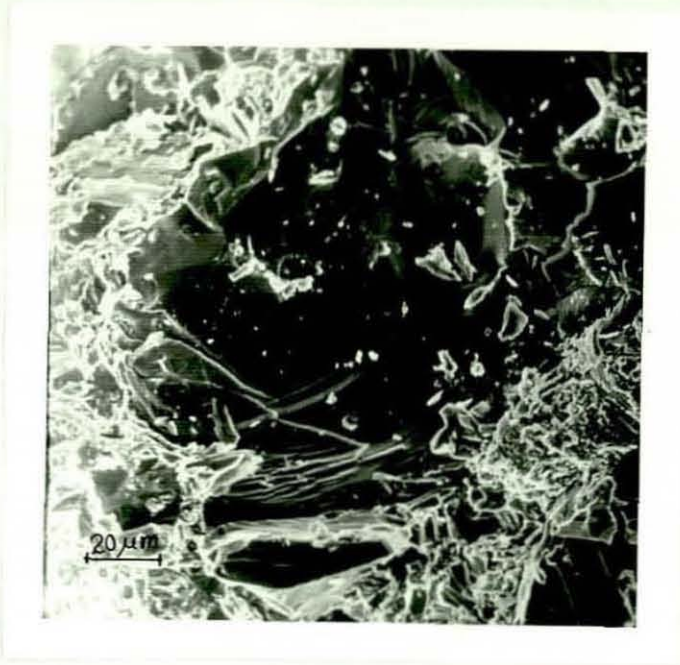


Fig.95-S.E.M. Micrograph For Fractured  
Graphite Particle.

However, mechanical bonds based only on the entrapment of the particles in the matrix (not interaction) are considered to be less desirable than bonds involving interaction or a significant chemical contribution because their strength is inferior<sup>(96)</sup>.

Graphite rejection in Table 1B could be explained by the fact that at high slurry temperatures the amount of primary solid particles is not sufficient to cause graphite entrapment. In addition the time given to the alloy in the comocasting unit to be in contact with air was not enough to form a sufficient amount of oxide to wrap around the graphite particles and prevent their rejection from the melt.

Although the comocasting unit was designed and produced carefully to keep the top layer of the molten metal undisturbed, to minimise the oxidation process, it was found in practice that vortex formation was inevitable due to the agitation provided by the stirring rotor. The stirring action was necessary to ensure uniformity in the graphite distribution. The castings produced exhibited a very uniform graphite distribution throughout the casting, see Fig.46. The inclusion of graphite particles results in an increase in the viscosity of the alloy slurry. This is due to the effective increase in the volume fraction solid in the alloy slurry. To maintain a viscosity suitable for casting the volume fraction solid must be reduced, or alternatively, the shear rate must be increased.

## 6.2 COMPOSITE ALLOY EVALUATION

### 6.2.1 Mechanical Properties

In the plane of the microsection eutectic silicon particles appear as elongated plates or lamellae apparently disconnected from one another. Deep etching and scanning photomicrography reveals that these silicon particles are interconnected into a single, coral-like silicon mesh, the sections of which appear in the plane of the photomicrograph<sup>(25)</sup>. Therefore the state of silicon in the microstructure is dependant upon the number of silicon "corals" and the degree of branching of

such corals. Fine branching results in better mechanical properties. This explains the superiority in mechanical and tribological properties of rheocast specimens compared with those for sand cast specimens.

Although the structures of pressure diecast specimens exhibited very fine silicon polyhedra and fine eutectic silicon, comparable with those in the gravity die cast structures, the reduction in tensile properties was obvious, see Table 3. The reduction in tensile properties is a consequence of the internal porosity inherent in the pressure die casting process when fully liquid alloys are used. In the rheocast structures the silicon polyhedra are coarser in size and about 50% less in number (see Table 2) than in the conventionally pressure die cast structures but the mechanical properties are almost the same. The stirring action may have introduced oxide inclusions which would be expected to adversely affect the mechanical properties. However, this may have been compensated to an extent by the reduced turbulence and splashing when semi-solid alloy slurry is injected into the die cavity, which results in less internal porosity and hence better mechanical and tribological properties. The lowest mechanical properties were obtained when the alloy was sand cast. This is due to the formation of a very coarse structure. The SEM micrographs for fractured surfaces of graphitic and graphite free specimens, Figs.96-115, showed a brittle cleavage fracture. The effect of the size, number and distribution of primary silicon polyhedra on the fracture behaviour of LM30 is demonstrated in the diecast control specimens, Figs.96-99. The large number of fine and well distributed primary silicon polyhedra resulted in fine cleavage cracks, whilst the coarse structures Figs.102-115 indicated brittleness. Although the rheocast structure exhibited primary silicon particles which are comparable in size and in number to those obtained with sand casting (see Figs.38,41 and Table 2), the fractured surface for the alloy produced by the rheocasting route exhibited fine cleavage fracture comparable to that obtained in pressure die cast specimens. This is probably due to the refinement of the eutectic matrix as a result of the rapid rate of heat extraction in the die. Castings which had the highest tensile properties (gravity die

\* Figs.96 - 115 are shown in Appendix 7.

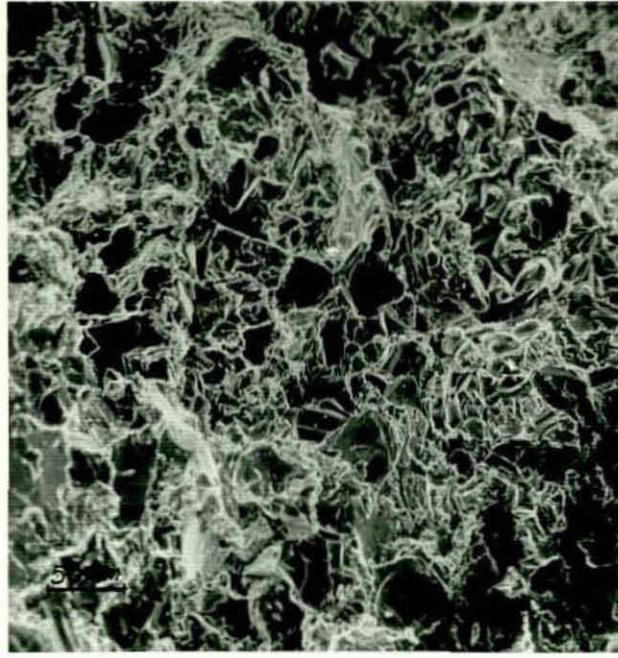


Fig.96 - SEM Micrograph for Gravity  
Die Cast Fractured Surface

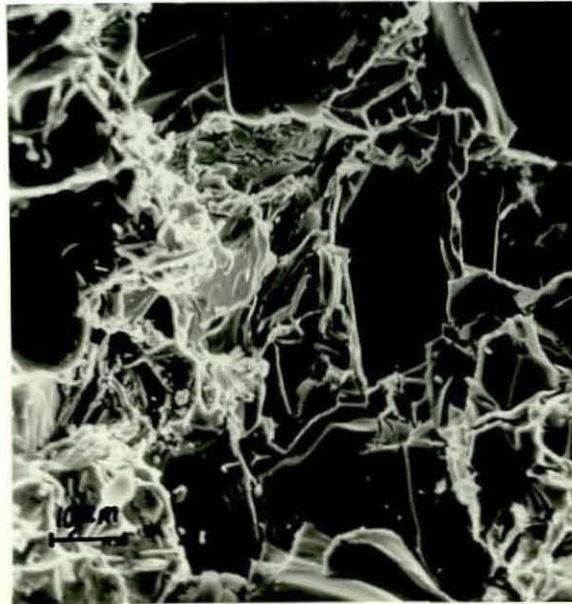


Fig.97 - SEM Micrograph for Gravity  
Die Cast Fractured Surface

cast specimens) demonstrated fine cleavage fractures. This appears to suggest that the presence of a large number of fine silicon polyhedra arrests crack propagation. Castings containing graphite particles showed a deterioration in tensile properties in comparison with castings made under the same conditions without graphite addition. This is due to the fact that graphite is softer and lower in strength<sup>(101)</sup> than the matrix and so its inclusion has the effect of introducing casting defects or voids, which reduce the effective load bearing cross-sectional area. An increase in graphite content effectively increases the number of voids and creates discontinuities in the cast structure which will inevitably result in a deterioration in the tensile properties. In addition graphite particles create cavities of irregular shape with small corner radii which become highly stressed and act as stress raisers<sup>(102)</sup> which encourage crack formation. The coarse graphite particles produce large voids which facilitate and accelerate crack propagation and so the tensile properties obtained with coarse graphite particles were lower than those for medium fine and fine graphite particle sizes, see Table 4 and Fig.47. Whilst it is true that graphite additions caused a deterioration in the tensile properties of the matrix alloy, a close look at Tables 2-4 and Fig.50 will reveal that there are other factors contributing to the deterioration in the tensile properties. It is interesting to note that while a 3wt% addition of graphite to the base alloy reduced the tensile strength by 30%, doubling the graphite content only reduced the strength by a further 14%. From these figures it could be concluded that the addition of 3wt% graphite reduced the tensile strength by 14% only. A contributing factor may be the size of the silicon polyhedra. From Table 3 the rheocast, pressure diecast specimens showed a reduction in tensile strength by 19% in comparison with the gravity diecast specimens: This is most likely due to the increase in the primary silicon particle size. So the reduction in tensile strength found in the alloys containing graphite may be due to the combined effects of graphite and large silicon polyhedra. The SEM studies of fracture surfaces of specimens which contained graphite particles showed coarse cleavage cracks Figs.104-115. The fractured surface for these specimens showed

close similarity with sand cast fracture surfaces, Figs.102-103, which exhibited brittle cleavage fractures. Fractured surfaces for graphitic specimens appear to show that cleavage cracks have been initiated from the graphite particles. For cleavage fractures it is known that crack growth along certain crystallographic planes leads to a brittle cleavage fracture. This is indicated by smooth areas separated by cleavage steps and feathers, river markings and cleavage tongues which are a result of crack path disturbances by phase boundaries and inclusions<sup>(103)</sup>. Observations indicate evidence of this type of fracture, see Figs.96-115. The boundary of a primary silicon polyhedra presents a strong barrier against the propagation of cleavage cracks<sup>(104)</sup>. Hence, the greater the number of silicon polyhedra the greater the number of barriers against crack propagation and fracture. This results in the higher tensile properties found in gravity diecast specimens.

Conversely, the lower the number of silicon polyhedra the less are the barriers against crack propagation and fracture which results in the lower mechanical properties for the rheocast specimens. For graphitic specimens when the strain is applied the voids containing graphite particles are unable to deform without fracturing the matrix, and so cracks tend to be initiated from small (highly stressed) radii within the voids. The crack grows in the eutectic phase and is unlikely to be terminated unless a primary particle or inclusion is encountered. The different graphite particle sizes did not show any significant effect on the fracture behaviour of specimens, see Figs.110-115. In general, the SEM examination showed largely brittle (cleavage) fracture for LM30 alloy (graphite and non graphitic) which might be due to the presence of a large quantity of silicon in the alloy.

The difference in hardness values observed in control specimens could be attributed to the same factors which caused the difference in tensile strength values.

The reduction in hardness with different graphite addition levels and different graphite grades showed trends similar to those for tensile strength, see Fig.48. This is due to the

inclusion of soft material (graphite) in the aluminium-silicon matrix. The coarse graphite particle size produces large soft spots in the matrix which results in a greater indented area in the Brinell hardness test and hence lower hardness number. The reduction in mechanical properties with increasing graphite content is reported by several independent sources<sup>(43,36,105)</sup>.

The loss in hardness is usually accompanied by a loss in tensile strength and can be explained by their being proportions of a comparatively soft, low strength material (graphite) in the alloy see Fig.49.

## 6.2.2 Tribological Properties

### 6.2.2.1 Programme One: Pin On Disc Dry Wear Test

The hypereutectic aluminium-silicon alloy LM30 exhibited two forms of wear under dry sliding conditions, these are oxidative and metallic wear. Oxidative wear, which occurred in the graphitic specimens, can be recognised from the appearance of the worn surface which exhibited a dark, smooth and non-metallic appearance and also from the shape and the size of the debris generated from the rubbing action between the pin and the steel disc. Whilst metallic wear demonstrated by the control specimens, can be recognised by the deformation of the surface which occurred on a fairly massive scale, because the yield strength has been exceeded, and also from the size, shape and appearance of the debris generated during the test. Shivanath et al.<sup>(106)</sup> stated that the two wear regimes can be recognised by their distinctive wear rates:

Oxidative wear rate:  $10^8$  to  $10^7$  cm<sup>3</sup>/cm

Metallic wear rate:  $10^5$  to  $10^4$  cm<sup>3</sup>/cm

In the pin on disc dry wear test used in this research, the graphitic and graphite free specimens exhibited the following wear features:

Specimens with 3wt% graphite addition: oxidative wear  
rate:  $4.8 \times 10^7$  cm<sup>3</sup>/cm

Specimens with 4½wt% graphite addition: oxidative wear  
rate:  $5.3 \times 10^7$  cm<sup>3</sup>/cm

Specimens with 6wt% graphite addition: oxidative wear  
rate:  $6 \times 10^7 \text{ cm}^3/\text{cm}$

Specimens with 7½wt% graphite addition: oxidative wear  
rate:  $6.3 \times 10^7 \text{ cm}^3/\text{cm}$

Control specimens (no graphite added): metallic wear  
rate:  $6.3 \times 10^7 \text{ cm}^3/\text{cm}$

From the figures mentioned above it can be seen that specimens containing 3wt% graphite exhibited an oxidative wear of mild nature, whilst non-graphitic specimens and specimens containing graphite additions in excess of 4½wt% exhibited wear rate of a more severe nature.

The SEM examination of the worn surfaces of graphite-free specimens (control castings), Figs.116-123, showed that large patches of plastic flow accompanied by cracking and spalling of the surface of the wear pin had occurred to form metallic debris. The wear debris generated from these specimens was large in size and had a metallic appearance, see Figs.124 and 125. Whilst the debris generated from graphitic specimens was smaller in size and darker in colour (non-metallic appearance) which indicated an oxidative wear regime, see Figs.126 and 127.

SEM micrographs for graphitic specimens, Figs.128-139, showed worn surfaces of a different nature. The worn surface which appears in the micrograph has been covered with dark, smooth areas. Cracks and plastic flow patches were much reduced in comparison with control specimens. Specimens containing 3wt% graphite exhibited less scoring marks and fine grooves in comparison with specimens containing graphite in excess of 3wt%. This might indicate that 3wt% graphite provides the required amount of lubrication with a minimum impairment of alloy strength. Specimens with graphite addition in excess of 3wt% showed scoring marks and grooves of a more severe nature, see Figs.130-139. This could occur because the increased graphite content reduces the effective cross sectional area and hence there is an increase in the bearing pressure applied resulting in a faster break down and replenishment of the oxide layer formed on the wear pin asperities, followed by fracture and compaction into valleys on the wear pin test

\* Figs.118 - 123 and 128 - 139 are shown in Appendix 7.

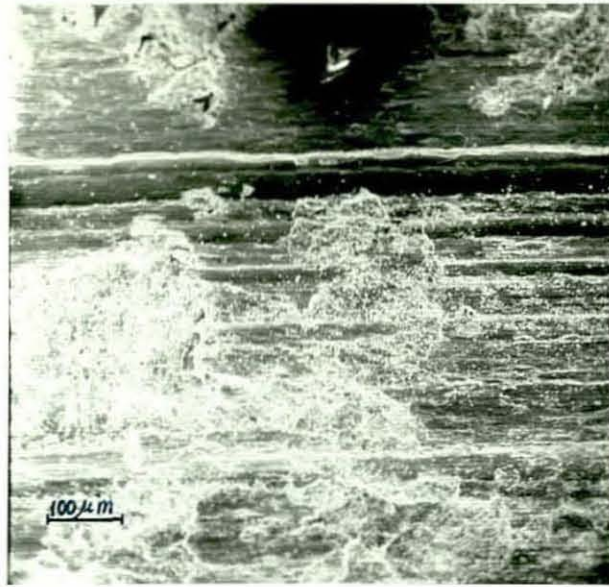


Fig.116 - SEM Micrograph for Gravity Die Cast Worn Surface (Dry Friction)



Fig.117 - SEM Micrograph for Gravity Die Cast Worn Surface (Dry Friction)



Fig.124 - Debris of the Base Alloy (No Graphite Addition)  
is Shown to be Mainly Laminates  
(Dry Friction) x50



Fig.125 - Same Debris at Higher Magnification  
(Dry Friction) x500



Fig.126 - Debris of the Composite Material, Which  
Appear as Agglomerates (Dry Friction) x50

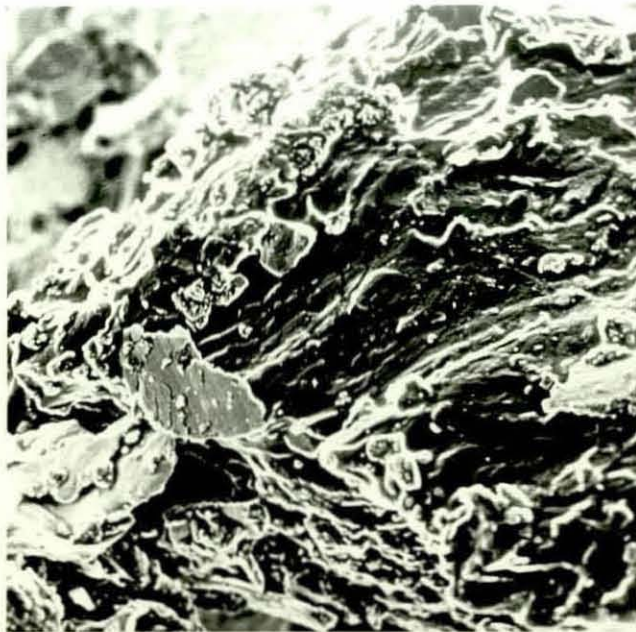


Fig.127 - Same Debris at Higher Magnification  
(Dry Friction) x500

surface. In contrast with the 3wt% graphite specimens, the oxide layer increases in thickness and becomes smoother so that the wear rate remains relatively low<sup>(106)</sup>. This situation may exist with the 3wt% graphite addition which resulted in a substantial reduction in the pin weight loss, see Table 8 and Fig.53. It is likely that there is an extension of oxidative wear, aided by lubrication from simultaneous compaction and smearing of graphite particles over the wear surfaces.

There is evidence of graphite particles being pulled out from the matrix by the rubbing action. This was observed in specimens containing high graphite addition levels (6wt% and 7½wt%), see Figs.132 and 134. This might suggest that with high levels of graphite addition, the matrix is no longer capable of holding the graphite particles and/or no longer capable of supporting the load.

From the quantitative analysis of graphite content (procedure 5 . 3), the effect of graphite addition level on the reduction in matrix area of the wear pin surface in the pin on disc wear test is demonstrated in Table 12.

Table 12 shows that the graphite addition effectively reduced the cross sectional area of the matrix resulting in a significant increase in the load applied and hence the bearing pressure. Although the addition of 3wt% graphite resulted in a 5% increase in the load applied, specimens containing such a graphite addition level maintained a low wear rate. This appears to suggest that the 3wt% graphite provided the necessary lubrication without impairing the alloy strength. Whilst the higher graphite addition levels reduced the load carrying capacity by reducing the effective cross sectional area which resulted in a significant increase (7 - 12%) in the load applied.

It has been observed that the hypereutectic aluminium-silicon alloy (LM30) behaved in a relatively ductile manner during the pin on disc wear test, unlike its behaviour under tensile condition. This can be demonstrated by the plastic flow patches

and ploughed tracks which were observed in graphitic and graphite free specimens.

The mild, steady and uniform wear rates obtained with graphitic and control castings specimens suggests that the load of 12.6kg (126N), which produced a bearing pressure of  $0.4\text{kg/mm}^2$  ( $4\text{ N/mm}^2$ ), and even the higher loads resulting from the reduction in the effective cross section area (due to the graphite addition), are below the transition load for the LM30 alloy which contains 16-18% silicon. Shivanath et al.<sup>(23)</sup> stated that the transition load (the load at which the alloy shows a transition from a mild wear regime to a severe one) for alloys containing 16-18% silicon is 18kg (180N). Oxidative wear has been reported to be associated with mild wear<sup>(106-108)</sup>. These observations suggest that there is an optimum graphite addition to maximise load carrying capacity whilst maintaining a mild wear characteristic. However, the presence of graphite particles of different addition levels allows the material to exhibit a reduced coefficient of friction when mated with a hardened carbon-steel disc, see Fig.57. This is due to the lubrication effect provided by the solid graphite particles at the wear interface. However, with graphite contents in excess of 3wt%, although the coefficient of friction remained low, the composites exhibited a transition to a severe rate of wear. SEM microphotographs, Figs.116-139, of worn pin surfaces show that the mild wear rate is characterized by wear taking place on flattened asperities, which adds further evidence to the oxidative wear hypothesis. There are no indications of large fragments of material having been torn off by abrasive or adhesive wear mechanisms. At higher magnifications, there is no evidence of crack formations on the worn surfaces of graphitic specimens. This is attributed to a reduction in adhesive wear caused by the lubrication action of graphite particles in the wear interface. Also the presence of graphite particles has resulted in a considerable reduction in the size of the plastic flow patches. This is probably because graphite is inhibiting direct contact, and hence adhesion, between the pin and the disc.

SEM microphotographs indicate that there is little difference between the worn surfaces of alloys which contain graphite and

those that do not for the wear test conditions (procedure 5.2.3). This indicates that there is also little difference between wear mechanisms and that wear essentially takes place by a process of comparatively large scale fracture, although the shape and the size of debris are significantly different, see Figs.124 and 126. This is probably because, with graphitic specimens, material can be fractured easily and cracks can be developed from the voids in the material which accommodated graphite and so the debris generated is smaller. The relatively higher ductility of the material without graphite tends to inhibit fracture and so a higher stress is required to fracture plates of material which have become adhered to the disc. Therefore the friction force will tend to be higher. This might explain the higher values of coefficient of friction obtained from control specimens. In general, in pin on disc wear testing, the reduced coefficient of friction exhibited by the specimens with graphite is usually accompanied by a reduced steady state running temperature. This is a direct result of a reduced energy input being required to overcome friction force and so less energy is dissipated in the form of heat.

Surface texture measurements indicate that graphite inclusions result in reduced surface damage to both pins and discs. This could be a useful property in reducing scuffing problems on mating components run with aluminium-silicon bearing material. Under mild wear conditions, specimens containing graphite particles, this is probably due to an increase in the flattening of asperities resulting from smearing of graphite particles. Under severe wear conditions, non-graphitic specimens, this is due to more favourable shear and fracture conditions which results in a reduced depth of fracture. This has been confirmed by other researchers<sup>(108,109,110)</sup>, who reported that the improved tribological properties of aluminium-silicon alloys containing graphite are partly due to reduced sub-surface damage. The presence of graphite in a hypereutectic aluminium-silicon alloy (LM30) resulted in significant improvement in the tribological properties under dry wear conditions, at certain graphite addition levels, see Table 13.

However, it is also believed that the benefits of graphite as a solid lubricant in the hypereutectic aluminium-silicon alloy LM30 are not fully exploited for the following reasons:

- (1) It was observed that during the tests graphite was removed continuously from the wear interface by the rubbing action between the pin and the disc. This prevented the formation of a continuous graphite layer which would have prevented direct contact between the two mated surfaces and resulted in better tribological properties.
- (2) The lowest coefficient of friction value (0.23) obtained, see Table 8 is relatively high in comparison with the coefficient of dry friction for pure graphite which is reported to be 0.1 under heavy loading conditions <sup>(112)</sup>.

Barwell <sup>(113)</sup> reported that the adsorption of water or other molecules on to the surface of graphite is responsible for its lubrication action. Another source <sup>(114)</sup> reported that graphite's self-lubricating properties are influenced by water vapour and added that if the water vapour is not present, heavy wear results.

Indeed, the results obtained from the lubricated test (procedure 5.2.4) showed that the one drop of oil of size  $0.5 \times 10^2 \text{ ml}$ . provided to the pin-disc wear interface at the beginning of the test resulted in a massive change in the tribological properties of the graphitic specimens, see Table 10, and the improvements in tribological properties over those obtained with dry friction for the same graphite addition levels are listed in Table 14. This suggests that the presence of a wet media such as water vapour or oil acts as a graphite binder and allows the formation of a continuous graphite layer which prevented a direct contact between the mated surfaces and resulted in better tribological properties, even under very poor lubrication conditions. This will be a very useful property especially in the automobile engine when lubrication conditions are scarce or intermittent and at cold start. Under poor lubrication conditions, specimens containing 3wt% graphite showed superiority over those of higher graphite addition levels. This confirms that the 3wt% graphite addition provides the necessary lubrication and produces better tribological properties in both dry and poorly lubricated friction. Higher

graphite addition levels impaired the alloy strength and resulted in lower tribological properties.

Table 12: The Effect of Graphite Addition Level on the Increase in Load Applied

Graphite Content %	Graphite Area %	Effective Cross Section Area	Load Applied (N)	Bearing Pressure Applied ( $N/mm^2$ )
0	0	100%	126	4.0
3	4.3	95.7%	132	4.2
4½	6.4	93.5%	135	4.3
6	8.6	91.4%	138	4.4
7½	10.7	89.3%	141	4.5

Table 13: The Effect of Graphite Addition on the Tribological Properties of LM30 Alloy

Criteria Graphite Addition Level	% Improvement				
	Pin Weight Loss	Coefficient of Friction	Pin Temperature Rise	Pin Surface Finish	Disc Surface Finish
3wt%	31%	9%	5%	10%	28%
4½wt%	21%	11%	9%	31%	30%
6wt%	10%	17%	11%	31%	33%
7½wt%	No Improvement	29%	15%	40%	35%

Table 14: The Effect of Poor Lubrication Conditions on Tribological Properties

Criteria	% Improvement				
	Pin Weight Loss	Coefficient of Friction	Pin Temperature Rise	Pin Surface Finish	Disc Surface Finish
3wt%	98%	84%	50%	90%	56%
4½wt%	91%	84%	51%	85%	5%
6wt%	81%	83%	47%	78%	no improvement
7½wt%	67%	60%	5%	42%	no improvement

## CHAPTER SEVEN

### CONCLUSIONS

The following conclusions can be drawn from the present investigation:

1 . Processing variables.

- Rheocasting variables:

(i) For the levels of shear rate investigated, the shearing action of the rotor had no influence on the structure of either the primary silicon polyhedra or the eutectic matrix. However, increasing the shear rate reduced the slurry viscosity.

(ii) Viscosity can be altered either by changing the shear rate or the initial volume fraction solid. However, to obtain a slurry with a viscosity suitable for casting at the maximum attainable shear rate of  $550 \text{ sec}^{-1}$ , a volume fraction solid of 0.15 could not be exceeded.

- Compcasting variables:

(i) To ensure good graphite distribution throughout the casting a shear rate in excess of  $396 \text{ sec}^{-1}$  must be employed and the composite slurry should be agitated for at least five minutes.

(ii) For a constant initial volume fraction solid of 0.075, and a shear rate of  $550 \text{ sec}^{-1}$  it was possible to produce a castable slurry containing up to a maximum of  $7\frac{1}{2}\text{wt}\%$  ( $14\frac{1}{4}\text{vol}\%$ ) of graphite particles.

- Pressure diecasting variables.

In order to produce an acceptable casting using an alloy containing up to  $7\frac{1}{2}\text{wt}\%$  graphite it was necessary to use a die preheat temperature of  $300^\circ\text{C}$ , injection speed of  $121 \text{ ft/sec}$  ( $37 \text{ m/sec}$ ) and minimum gate dimensions of  $20 \times 5 \text{ mm}$ . These parameters, established by experimentation, produced castings which exhibited very good conformity to the die cavity in addition to reduced shrinkage porosity.

- Shrinkage.

Shrinkage was observed to be present in castings produced by: conventional pressure diecasting; rheocasting followed by pressure diecasting; and compcasting followed by pressure diecasting. Whereas claims are made in the literature that

processing by rheocasting reduces shrinkage significant reduction could not be expected in this research because the initial volume fraction solid did not exceed 0.075.

2 . The LM30 alloy should be degassed for at least 10 minutes to release dissolved hydrogen. Degassing the melt before graphite injection did not influence graphite acceptance. However, graphite rejection was found to occur if a nitrogen gas shield was employed during agitation and injection of the graphite. It would appear from observation and electron probe microanalysis results that the presence of oxide inclusions, formed by agitation of the melt in air, is necessary for successful retention of the graphite particles.

3 . Cooling rate has a significant effect on the structure and properties of the graphite-free LM30 alloy. Fast cooling rates, provided by gravity and pressure diecasting, refined the primary silicon and modified the eutectic thus providing improved mechanical properties in comparison with those obtained by sand casting.

Processing the graphite-free LM30 alloy by rheocasting followed by pressure diecasting produced a structure in which the silicon polyhedra were similar in size and number to those obtained by sand casting the alloy. However, the eutectic was modified to the same extent as the pressure diecast control specimens. The mechanical properties, hardness and tensile strength, of the rheocast material were not found to be significantly different to those obtained by conventional pressure diecasting.

4 . The addition of graphite to the LM30 alloy impaired the mechanical properties of the alloy as measured by hardness and tensile testing. It was observed that there was a significant reduction in the number of silicon polyhedra present in the specimens containing graphite, at all the graphite addition levels. However, it is the effect of increasing the graphite addition level which has the more significant effect on mechanical property impairment.

The addition of graphite at the 3wt% addition level was found, on average, to reduce the tensile strength of the alloy by approximately 30% compared with the rheocast and pressure diecast

control specimens. An addition of 7½wt% graphite was found, on average, to reduce the tensile strength of the alloy by approximately 47% compared with the control specimens.

The results also show that addition of the coarse grade of graphite particles have the greatest effect on the reduction in tensile strength. On average, the tensile strength was approximately 13% lower with coarse particle additions than for fine particle additions.

Whilst the hardness of the alloy decreased significantly with the increase in graphite addition level, the effect of particle grading was not found to be significant.

- 5 . At low addition levels (3wt%) graphite improved the wear resistance of the alloy, compared with the graphite-free control specimens produced by rheocasting followed by pressure die-casting. However, at higher addition levels (6wt% and 7½wt%) the wear resistance is no better than the graphite-free control specimens. Although the wear test results appear to show that the wear resistance is better with the coarse graphite grades the improvement in wear rate could not be claimed to be significant . As already noted the coarse graphite grade causes the greatest reduction in tensile strength.

Although the higher graphite addition levels might be expected to reduce friction and improve wear resistance these advantages are outweighed by their effect on the actual, as opposed to apparent, bearing pressure. The presence of graphite reduces the cross sectional area of the matrix bearing the load. For a 7½wt% addition of graphite the load bearing cross sectional area of the matrix is reduced by approximately 11%. The bearing pressure was effectively increased from 4.0 to 4.5 N/mm<sup>2</sup> with a consequent increase in the wear rate.

- 6 . Although comprehensive experiments were not conducted using lubricated wear tests, the small number of experiments conducted using marginal lubrication indicated that a significant improvement in tribological characteristics may be obtained by using lubrication with the specimens containing graphite.

## CHAPTER EIGHT

### SUGGESTIONS FOR FURTHER WORK

- The combination of comocasting to disperse untreated graphite particles and pressure die casting to produce components made from semi-solid slurries offers a number of areas for further development.
  
- A comocasting unit could be developed to provide a continuous supply of partially solid, composite alloy. A design similar to the continuous rheocasting unit<sup>(82)</sup> would provide a continuous supply of semi-solid slurry and minimize the possibility of oxide formation because the mixing action occurs in a closed tube, it would also eliminate the possibility of particle (eg. graphite) segregation associated with high speed stirring rotors due to the difference in density between the particles and the molten alloy. In addition, a high volume fraction solid, up to 0.80, can be obtained. This is achieved by replacing the stirring mechanism by a system of stationary baffles through which the semi-solid alloy is forced to pass by mechanical pressure. However, some modifications are necessary to enable such a device to be suitable for industrial production. The device could be developed to allow composite materials to be produced. This could be achieved by forcing non-metal particles into the alloy slurry through a hole in the body of the device. The output from this device could be used to form a continuous bar for thixocasting or a valve could be incorporated to allow the output to be controlled in a manner which would enable discontinuous material to be produced for immediate pressure die casting or other casting processes. The comocasting process variables such as shear rate, volume fraction solid and cooling rate could be controlled automatically with the use of a microprocessor. Automation of slurry handling after exit from the production unit could be achieved with a mechanical handling device to transfer composite slurry to the shot chamber of the pressure die casting machine.
  
- Electrodes for spark erosion machining are usually made of copper or graphite. Graphite electrodes are cheaper and used for fast cutting, whilst copper electrodes are expensive so

they are used for fine finishing<sup>(115)</sup>. Electrodes which could offer the advantages of both copper and graphite simultaneously are not available commercially. Graphitic aluminium-silicon alloy (LM30) containing 7½wt% graphite has been tried as an electrode material in spark erosion cutting tests and it was found that such a combination has very good potential. However, further investigation is required to ensure the possibility of using graphitic LM30 electrodes for spark erosion machining commercially.

- During the production of graphitic LM30 alloy, the rheocast structure exhibited very coarse primary silicon polyhedra which resulted in lower mechanical properties in comparison with gravity die casting which produced very fine silicon polyhedra (the eutectic matrix was fine in both cases). However, to obtain better mechanical properties, better surface finish and longer tool life, the primary silicon polyhedra must be refined. The refinement can be achieved in two ways:

- (1) By controlling the cooling rate during solidification which can be achieved by incorporating a water cooling system in the compocasting unit.
- (2) The use of refining agent such as phosphor-copper which is used commercially to treat the melts of hypereutectic aluminium-silicon alloys.

However, investigation is required to establish the relation between primary silicon particle size and mechanical properties for the compocast material.

- LM30 alloy is heat-treatable due to the presence of between 4 and 5% copper in the alloy. The tensile properties of the alloy may be increased significantly by solution and precipitation heat treatment, in which the deterioration in mechanical properties due to the presence of graphite in the alloy may be offset. However, it is interesting to note that BS1490:1970 specified the alloy only in the as-cast and stress relieved conditions.

-The incorporation of 3wt% graphite into LM30 showed improvement in the tribological properties and minimum deterioration in the mechanical properties however, at this stage it would become necessary to conduct an investigation into the economies of the production of components by this production route. A need may arise for compromise between the advantages and disadvantages of cost versus performance. Alternatively, there may be applications where the properties of composites offer a unique solution to problems such as the seizure in aluminium-silicon alloy engines at poor lubrication conditions and in the food industry where liquid lubricants are not desirable.

If suitable, commercial applications can be identified, prototypes of components made from the composite alloy could be produced and their performance evaluated in their working environments.

-In this research, graphite addition levels of 3, 4½, 6 and 7½wt% were incorporated in the LM30 alloy. Their mechanical and tribological properties were evaluated and it was found that the addition of 3wt% offered the best tribological properties with minimum deterioration in mechanical properties. However, there is still a gap between 0 and 3wt% which has not been investigated. For example, the addition of 2wt% graphite might offer improved tribological properties with better mechanical properties. However, graphite addition levels below 3wt% require investigations to optimise the mechanical and tribological properties of graphitic hypereutectic aluminium-silicon alloy LM30.

## REFERENCES

- 1 - Brook G.B.  
Improving The Quality Of Aluminium Die Castings  
By Novel Techniques.  
Materials & Design, 1982, 3, (10), 558.
- 2 - Jorstad J.L.  
Trends In Automotive Aluminium Castings.  
A.S.M. Metals Congress Conf. Paper No. 8305-046, 1983.
- 3 - Brook G.B.  
Semi-Solid Metal Injection Castings.  
Proceeding Of The Conference On Materials Engineering,  
Institution Of Metallurgists, 1984, 109.
- 4 - Dohler H.H.  
Die Casting  
(McGraw-Hill) 1951, 254.
- 5 - Smart R.F.  
Quality Improvements In Aluminium Castings.  
Aluminium Industry, 1984, 3, (4), 25.
- 6 - McGrath P.W.  
Potential For Aluminium Castings In The Automobile  
Industry.  
The British Foundryman, 1981, 74, (6), 133.
- 7 - McDonald J.W.  
What's New In Aluminium Casting.  
Die Casting Engineer 1976, 20, (5), 28.
- 8 - Jorstad J.L.  
Trends In Aluminium Castings  
(Part 1: Automotive Applications).  
Modern Casting, 1984, 74, (10), 26.
- 9 - Macklin H.M.  
Anatomy And Development Of An Aluminium Cylinder Block  
Automotive Industries, 1971, 144, (9), 42.

- 10 - Eyre T.S.  
Wear Characteristics Of Castings Used In Internal  
Combustion Engines.  
Metals Technology, 1984, 11, (3), 81.
- 11 - Heine H.J.  
Cast Aluminium 390 Alloy - A Growth Material.  
Foundry, 1982, 110, (7), 64.
- 12 - Slemen W.  
Aluminium Engine - Block Challenges Iron.  
Foundry Trade Journal, 1971, 130, (3), 153.
- 13 - Cuthbertson J.W. and Ellwood E.C.  
Improved Aluminium-Tin Bearing Alloys.  
Tin Research Institute, July 1954, 85, (5).
- 14 - Smith J.M.  
Aluminium Engines - Design For Modern Fabrication.  
S.A.E. Transaction, 1959, 67, 295.
- 15 - Pratt G.C.  
Graphite/Metal Composites For Dry And Sparsely  
Lubricated Bearing Applications.  
Tribology, 1973, 6, (6), 259.
- 16 - Badia I.A., MacDonald D.F. and Pearson J.R.  
Graphitic-Aluminium - A New Method Of Production  
And Some Foundry Characteristics.  
A.F.S. Trans., 1971, 79, 265.
- 17 - Mehrabian R., Riek-R.G. and Flemings M.C.  
Preparation And Casting Of Metal-Particulate  
Non-Metal Composites.  
Metallurgical Transactions, 1974, 5, (5), 1899.
- 18 - Badia F.A. and Rohatgi P.K.  
Gall Resistance Of Cast Graphitic-Aluminium Alloy.  
S.A.E. Trans., 1969, 78, 1200.

- 19 - Pai B.C. and Rohatgi P.K.  
Cast Graphitic-Aluminium - A Potential Bearing Alloy.  
Trans. Indian Inst. Of Metals, 1974, 27, (2), 97.
- 20 - Biswas S., Dwarakadasa E.S. and Biswas S.K.  
Bearing And Wear Properties Of Cast Graphitic  
Aluminium Composites.  
Proc. All India Seminar On Aluminium, New Delhi,  
October 1979.
- 21 - Baker R.G.  
Bearings In The Automobile - A Challenge For The  
Materials Engineer.  
Metals And Materials 1985, 1, (1), 45.
- 22 - MacCoon R.P. and Ernest R.P.  
The Thunder Aluminium 390 Alloy Aircraft Engine.  
S.A.E. Tech. Paper Series 830008. 1983.
- 23 - Shivanath R., Sengupta P.K. and Eyre T.S.  
Wear Of Aluminium-Silicon Alloys.  
British Foundryman, 1977, 70, (12), 349.
- 24 - Bruni I.L. and Iguera P.  
Silgraph - A New Silicon-Graphite Aluminium Alloy  
For Cylinder Liners.  
Automotive Engineer, 1978, 3, (1), 29.
- 25 - Boulton E.F. and Schofield F.A. (Editors)  
Typical Microstructures of Cast Metals.  
(The Institute Of British Foundrymen), 1983, 48.
- 26 - The Iron and Steel Institute  
The Solidification Of Metals.  
Conference, Brighton, 4-7 Dec. 1967, 224.
- 27 - Murphy A.J.  
Non-Ferrous Foundry Metallurgy.  
(Pergamon Press) 1954, 411.

- 28 - The Society of Automotive Engineers.  
Aluminium Engine Blocks: Casting Considerations.  
Automotive Engineering, March 1983, 91, (3), 31.
- 29 - Heine H.J. (Technical Editor  
Cast Aluminium 390 Alloy - A Growth Material.  
Foundry M & T, 1982, 110, (6), 64.
- 30 - Clegg A.J. and Das A.A.  
The Influence Of Structural Modification On The  
Wear Resistance Of A Hypereutectic Aluminium-Silicon  
Alloy.  
British Foundryman, 1977, 70, (11), 333.
- 31 - Kuzmicki L.  
Rootes 54 Cuin Light Alloy Engine.  
Trans. S.A.E., 1967, 670003.
- 32 - Krishnan B.P., Raman N., Narayanaswamy K., and Rohatgi P.K.  
Performance Of An Aluminium-Silicon Graphite  
Particle Composite Piston In A Diesel Engine  
Wear 1980, 60, 205.
- 33 - Kay A. and Street A.  
Die Casting Metallurgy.  
(Portcullis Press) 1982, 332.
- 34 - Jorstad J.L.  
"Acurad Casting Of Hypereutectic Aluminium Engine  
Block".  
Society Of Die Casting Engineers. 1970  
Congress: Paper No. 65.
- 35 - French R.D. and Hodi F.S. (Editors)  
Proceedings Of A Workshop On Rheocasting Held At  
Army Materials And Mechanics Research Centre.  
3 - 4 February 1977.  
Metals And Ceramics Information Centre, Columbus,  
Ohio.  
Report No. MCIC 78-35, 65.

36 - Imich G.

Methods Of Preparing Composite Products Containing  
Metallic And Non-Metallic Materials.  
U.S. Patent No. 2, 793, 949, (1957).

37 - Badia F.A. and Rohatgi P.K.

Dispersion Of Graphite Particles In Aluminium  
Castings Through Injection Of The Melt.  
Trans. A.F.S. 1969, 77, 402.

38 - Patton F.A.

Foundry Trials On Graphite Aluminium Alloys.  
J. Inst. Of Materials, 1972, 100, 197.

39 - Surappa M.K. and Rohatgi P.K.

Melting, Degassing And Casting Characteristics  
Of Al-11.8 Si. Alloys Containing Dispersion Of  
Copper Coated Graphite Particles.  
Metals Technology, 1980, 7, 378.

40 - Krishnan B.P., Shetty H.R. and Rohatgi P.K.

Centrifugally Cast Graphite Aluminium With  
Segregated Graphite Particles.  
Trans. A.F.S. 1976, 84, 73.

41 - Surappa M.K. and Rohatgi P.K.

Production Of Aluminium-Graphite Particle Composites  
Using Copper Coated Graphite Particles.  
Metals Technology, 1978, 5, 358.

42 - Pai B.C.

Copper Coating On Graphite Particles.  
Mat. Sci. And Engineering 1975, 21, 161.

43 - Krishnan B.P., Surappa M.K. and Rohatgi P.K.

The UPAL Process: A Direct Method Of Preparing Cast  
Aluminium Alloy-Graphite Particle Composites.  
J. Of Mat. Sci. 1981, 16, (5), 1209.

- 44 - Pai B.C. and Rohatgi P.K.  
Production Of Cast Aluminium-Graphite Using A Pellet Method.  
J. Of Mat. Sci. 1978, 13, (2), 329.
- 45 - Rossi R.C., Papper R.T., Upp J.W. and Riley W.C.  
Development Of Aluminium-Graphite Composites.  
American Ceramics Society Bulletin, 1971, 5, 485.
- 46 - Gorbunov V.G., Parshin V.D. and Panin V.V.  
Aluminium-Graphite Anti-Friction Alloys.  
Russian Castings Production, 1974, 348.
- 47 - Eppich R.E.  
Method Of Producing Graphitic Aluminium Castings.  
U.S. Patent No. 3, 758, 298, (1970).
- 48 - Teikoku Piston Ring Company Ltd.  
Lubricated Aluminium Alloy Production.  
Japanese Patent, No. 4800311, 1972.
- 49 - Singer A.R.E.  
A New Generation Of Engineering Materials Produced By Spray Forming.  
Materials & Design, Oct./Nov. 1983, 4, 892.
- 50 - Perrot R.  
Chemises De Moteur En Alliage D'alluminium Hypersilicie, Réalisées Par Métallurgie Des Pouders. (Communication From Aluminium Pechiney, With Summaries In English).
- 51 - French R.D. and Hodi F.S. (Editors)  
Proceedings Of A Workshop On Rheocasting Held At Army Materials And Mechanics Research Centre 3-4Feb. 1977.  
Metals And Ceramics Information Centre, Columbus, Ohio.  
Report No. MCIC 73-35, 3.

- 52 - Mehrabian R., Rick R.G. and Flemings M.C.  
Preparation And Casting Of Metal Particulate  
Non-Metal Composites.  
Met. Trans. 1974, 5, 1399.
- 53 - Joly P.A. and Mehrabian R.  
The Rheology OF A Partially Solid Alloy.  
J. Of Mat. Sci. 1976, 11, 1393.
- 54 - Mehrabian R. and Flemings M.C.  
Casting In The Liquid-Solid Region.  
A.S.M. Seminar - New Trends In Material  
Processing, 1974, 98.
- 55 - Metcalfe A.G. (Editor)  
Interfaces In Metal Matrix Composites.  
Composite Materials, 1974, 1, 98 (Academic Press).
- 56 - Chloride Technical Ltd.  
Report On Visit To Rheocast Corporation U.S.A. 1981.  
(Not Published).
- 57 - West G.H. and Seymour B.  
Casting With Metal Slurries.  
Production Engineer, 1979, 58, (11), 31.
- 58 - Eyre T.S.  
Wear Characteristics Of Metals.  
Tribology International, 1976, 9, (10), 203.
- 59 - O.E.C.D.  
Friction, Wear And Lubrication, Terms And Definitions.  
O.E.C.D., Delft, Netherland.
- 60 - Eyre T.S.  
Wear Mechanisms.  
Powder Metallurgy, 1981, 5, 57.
- 61 - Rabinowicz E.  
Friction And Wear Of Materials.  
(Wiley And Sons) 1966.

- 62 - Razavizadeh K., and Davies B.L.  
The Effect Of Steam Treatment On The Wear  
Resistance Of Sintered Iron And Fe-Cu Alloys.  
Wear, 1981, 69, 355.
- 63 - Welsh N.C.  
Dry Wear Of Steels.  
R. Soc. Philos. Trans. A., 1964, 257, 31.
- 64 - Pugh B.  
Friction And Wear.  
(Butterworth & Co.) 1973, 142.
- 65 - Lipson C. and Colwell L.V.  
Handbook Of Mechanical Wear.  
(The University Of Michigan Press), 1961, 449.
- 66 - Suh N.P.  
An Overview Of The Delamination Theory Of Wear.  
Wear, 1977, 44, 1.
- 67 - Nadal J., Eyre T.S.  
Cylinder Linear Wear In Low Speed Diesel Engines.  
Tribology International, 1978, 11, (5), 267.
- 68 - Summers-Smith D.  
An Introduction To Tribology In Industry.  
(The Machinery Publishing Co.) 1969, 101.
- 69 - Bayer R.G.  
Selection And Use Of A Wear Test For Metals.  
A.S.T.M., S.T.P.615, 1976, 102.
- 70 - Forrester P.G.  
Bearing Materials.  
Metall. Rev., 1960, 5, (20), 507.

- 71 - Habig K.G., Broszeit E. and DeGee A.W.J.  
Friction And Wear Tests On Metallic Bearing Materials.  
Wear, 1981, 69, 43.
- 72 - Pai B.C., Rohatgi P.K. and Venkatesh S.  
Wear Resistance Of Cast Graphite Aluminium Alloys.  
Wear, 1974, 30, 117.
- 73 - Bierlein J.C., Detlart A.O. and Rosenberg R.C.  
Performance Characteristics Of General Motors  
Aluminium Babbit Bearing Material.  
Trans. S.A.E. 1969, 690113.
- 74 - Neyman A.  
Comparative Tribological Evaluation Of Journal  
Bearings.  
Tribology International, 1979, 12, 112.
- 75 - Clark J. and Sarkar A.D.  
Topographical Features Observed In A Scanning  
Electron Microscope Study Of Aluminium Alloy  
Surfaces In Sliding Wear.  
Wear, 1981, 69, 1.
- 76 - Wilson W.H.  
A Test Machine For Assessing The Fatigue Properties  
Of Impulsively Loaded Plain Bearings.  
Symposium On Experimental Methods In Tribology.  
I. Mech. E. March 1968.
- 77 - Chandrashekar R. and Rohatgi P.K.  
Electrochemical Compatibility Of Aluminium-Graphite  
Particulate Composites For Use As Automobile Pistons.  
Trans. Indian Inst. Metals, 1978, 31, 456.
- 78 - Spencer D.B., Mehrabian R. and Flemings M.C.  
Rheological Behaviour Of Sn 15 Pct. Pb In The  
Crystallization Range.  
Met. Trans. 1972, 3, 1925.

- 79 - Campbell J.  
Rheocasting And Thixocasting - A Review Of Progress  
To Date.  
Foundry Trade Journal, 1975, 138, 291.
- 80 - Mehrabian R. and Flemings M.C.  
Casting Semi-Solid Aluminium Alloys.  
Aluminium, 1975, 51, (11), 710.
- 81 - French R.D. and Hodi F.S. (Editors)  
Proceeding Of A workshop On Rheocasting Held At  
Army Materials And Mechanics Information Centre,  
Columbus, Ohio.  
Report No. M.C.I.C. 78-35, 13.
- 82 - Manfre G., Mironi J. and Moschini R.  
Process For The Preparation Of A Mixture Comprising  
A Solid Phase And A Liquid Phase Of A Metal Alloy  
And Device For Its Performance.  
U.S. Patent, 4, 310, 352, 1982.
- 83 - Gibson P.R., Clegg A.J. and Das A.A.  
Compcast Graphitic Aluminium-Silicon Alloys.  
Foundry Trade Journal, 1982, 152, (3232), 253.
- 84 - The Foseco Foundryman's Handbook  
(Pergamon Press) 1975, 315.  
Eighth Revised And Enlarged Edition.
- 85 - Barton H.K. and Barton L.C.  
Die Casting Die Design.  
(The Machinery Publishing Co. Ltd.), 19-- , 30.
- 86 - The Properties and Characteristics of Aluminium Casting  
Alloys.  
The Association Of Light Alloy Refiners And  
Smelters (Publisher) 1971, 92.

- 87 - Hughes E.  
Electrical Technology.  
(Longmans) 1969, 375.
- 88 - The Society of Automotive Engineers.  
Aluminium Engine Blocks: Casting Consideration.  
1983, 91, (3), 31.
- 89 - Kay A. and Street A.  
Die Casting Metallurgy.  
(Butterworth & Co.) 1982, 71.
- 90 - Bowden F.P. and Tabor D.  
The Friction And Lubrication Of Solids.  
(Oxford University Press) 1964, Part II.
- 91 - Quinn T.F.J.  
The Application Of Modern Physical Techniques To  
Tribology.  
(Butterworth & Co.) 1971, 9.
- 92 - Flemings M.C., Riek R.G. and Young K.P.  
Rheocasting.  
Material Science And Engineering, 1976, 25, 103.
- 93 - Pepper R.T., Upp J.W., Rossi R.C. and Kendall E.G.  
The Tensile Properties Of A Graphite Fibre  
Reinforced Al-Si alloy.  
Met. Trans. 1971, 2, 117.
- 94 - Kahan I.H.  
The Effect Of Thermal Exposure On The Mechanical  
Properties Of Aluminium-Graphite Composites.  
Met. Trans. A., 1976, 7A, (9), 1281.
- 95 - Guo K and Liang L.  
Aluminium/Graphite Composite By the Rheocast Method.  
Dalian Gongx Ueyuan Xeubao 1982, 21, (1), 23.

- 96 - Metcalfe A.G.  
Interface In Metal Matrix Composites.  
Academic Press 1974, 1, 67.
- 97 - Quigley B.F., Abbaschian G.J., Wunderlin R. and Mehrabian.  
A Method For Fabrication Of Aluminium-Alumina  
Composites.  
Met. Trans. A., 1982, 13A, (1), 93.
- 98 - Metcalfe A.G.(Editor)  
Interface In Metal Matrix Composites.  
Academic Press 1974, 1, 83.
- 99 - Ibid. Page No. 73.
- 100 - Sutton W.H. and Chorne J.  
Potentials Of Oxide-Fibre Reinforced Metals.  
American Society For Metals, Oct. 1964.
- 101 - Lancaster J.K.  
Dry Bearings: A Survey Of Materials And Factors  
Affecting Their Performance.  
Tribology, 1973, 6, (12), 219.
- 102 - Benham P.P. and Warnock F.V.  
Mechanics Of Solids And Structures.  
(Pitman Publishing Co.), 1973, 399.
- 103 - Rollason E.C.  
Metallurgy For Engineers.  
(Edward Arnold Ltd.) 1973, 368.
- 104 - Kitajima K.  
Proceedings Of The International Conference On  
Mechanical Behaviour Of Materials.  
The Society Of Material, Kyoto, Aug. 15-25, 1971.

- 105 - Suwa M., Komuro K. and Soeno K.  
Mechanical Properties And Wear Resistance Of  
Graphite-Dispersed Al-Si Casting Alloys.  
J. Japan Institute Met. 1976, 40, (10), 1074.  
The Paper In Japanese Language  
(Abstract In English).
- 106 - Rigney D.A. and Glaeser W.A. (Editors)  
Source Book On Wear Control Technology.  
(American Society For Metals) 1978, 136.
- 107 - Razavizadeh K. and Eyre T.S.  
Oxidative Wear Of Aluminium - Alloys. Part I.  
Wear, 1982, 79, 325.
- 108 - Razavizadeh K. and Eyre T.S.  
Oxidative Wear Of Aluminium - Alloys. Part II.  
Wear, 1983, 87, 261.
- 109 - Biswas S. and Rohatgi P.K.  
Tribological Properties Of Cast Graphite Aluminium  
Composites.  
Tribology International, 1983, 16, 39.
- 110 - Pramila Bai B.N., Dwarakadasa E.S. and Biswas S.K.  
Sub-Surface Damage In Dry Wear Of Al-Si Alloys.  
Wear, 1981, 71, 381.
- 111 - Pramila Bai, B.N., Dwarakadasa E.S. and Biswas S.K.  
Scanning Electron Microscopy Studies Of Wear  
In LM13 And LM13-Graphite Particulate Composites.  
Wear, 1982, 76, 211.
- 112 - Summers-Smith D.  
An Introduction To Tribology In Industry.  
(The Machinery Publishing Co.) 1969, 48.

- 113 - Barwell F.T.  
Bearing Systems, Principles And Properties.  
(Oxford University Press) 1979, 131.
- 114 - M.P. Staff Report.  
Fight Against Wear Starts With Material Selection.  
Metal Progress, May, 1967, 91, (5), 69.
- 115 - Street A.  
The Die Casting Book.  
(Portcullis Press) 1977, 408.
- 116 - Bird R.B., Stewart W.E. and Lightfoot E.N.  
Transport Phenomena.  
(John Wiley And Sons), 1960, 82.
- 117 - Flemings M.C.  
Solidification Processing.  
(McGraw-Hill) 1974, 143.
- 118 - Ibid. Page 87.

DESIGN AND MANUFACTURE OF EQUIPMENT USED IN COMPOCASTING

(I) The Compocasting Unit (See Parts List Fig.20A)

(1) Frame Work:

This was made as a welded structure, mainly from 30mm x 30mm x 3mm angle iron. While the crucible holder frame was made of 20mm x 20mm x 3mm angle iron. The base of the compocasting unit was covered with mild steel sheet of 2mm thickness with a hole of 100mm diameter in the centre to allow the slurry to flow down to the launder. The structure dimensions are:

445 x 410 x 362mm.

(2) Variable Speed Drive:

Different rotor speeds were required to obtain different shear rates. A hydraulic variable speed drive coupled to an induction motor allowed speed variation from 0 to 1500rpm. in both clockwise and anti-clockwise directions. The hydraulic speed drive used was a Stone Platt Var-Spe type 11-12/000.

(3) Electric Motor:

The induction motor used with the hydraulic speed drive was a GEC, 3 phase, 415v, 0.75kw unit.

(4) Bearing Housing Assembly:

The bearing housing was manufactured from cast iron and was mounted on a dovetail slide to allow rotor height adjustment. The dovetail slide was made of mild steel. The bearing housing was designed to incorporate a hollow drive shaft [5], which allowed the push rod [8] to pass through, to force the graphite injector piston [7] down. Bearings were of the angular contact type installed in a back-to-back mode. The cavity around the drive shaft was filled with grease and sealed from both sides. The bearing housing assembly is shown in Fig.25.

- (5) The Rotor Drive Shaft:  
The rotor drive shaft was manufactured from mild steel.
- (6) The Rotor:  
The rotor was manufactured from a hollow mild steel bar for graphite storage and to accommodate the graphite injector screw, detail [ 9 ] .
- (7) Graphite Injector Piston:  
This was manufactured of mild steel and was designed to force graphite from within the rotor into the melt.
- (8) Push-Rod:  
This was manufactured of mild steel and was designed to make the graphite injection screw as short as possible.
- (9) Graphite Injection Screw:  
This was operated to apply force to the push-rod and graphite injector piston. A phosphor-bronze thrust bearing was incorporated where contact took place with the push-rod to allow smooth movement.
- (10) Crucible:  
This was manufactured by Refractory Moulding and Casting Ltd., Kegworth, Derby. The material from which the crucible was made was J/A Mullite. The crucible consisted of two zones with an overall maximum capacity of 2 kg. of aluminium.
- (11) The Fork Arrangement:  
The fork was manufactured of mild steel. The other end of the fork was provided with a 2lb (1kg) counterbalance to support the plug during the preparation of the composite slurry, see Fig. 24. The swivel joint shown on the same figure was designed to allow 360° fork rotation.
- (12) The Plug:  
The plug was manufactured of cast iron with 3° taper (Fig.23) to provide good locking. Cast iron has much less thermal expansion than steel so that when it expands it will not crack the crucible at the contact points.

(13) Semi-Solid Zone Heater:

Heating was by electrical resistance wire windings wound on a sillimanite tube. The resistance wire was Kanthal Nikrothal of diameter 0.70mm giving a resistance of 3.51 ohms/metre. The wire length required was calculated from Ohms Law:

$$I = V.R$$

where: V = the voltage used.

I = the current available from the main supply.

R = the resistance.

A 240 a.c. single phase mains supply was to be used with a maximum steady current of 10 amps to give a power of approximately 2.0KW which was estimated to be sufficient to melt the alloy from the solid state. From Ohms Law:

$$R = \frac{V}{I} = \frac{240}{10} = 24 \text{ ohms}$$

The wire is 3.51 ohms/m

Therefore the length of wire required =  $\frac{24}{3.51} = 6.90\text{m}$

For semi-solid zone heater [13] .

Tube diameter = 125mm

Tube length = 130mm

Tube circumference =  $\pi D = \pi \times 125 = 393\text{mm}$

Therefore the number of turns of wire =  $\frac{6.9}{0.393} = 18$

Pitch of turns =  $\frac{130}{18} = 7\text{mm}$

(14) For Liquid Zone Heater [14] , Calculations Were Similar Except:

Tube diameter = 172mm

Tube length = 165mm

Wire diameter = 1.0mm

Wire resistance = 1.72 ohms/m

Therefore the number of turns required is 26 and the pitch of turns is 6.4mm.

(15) Insulation:

Kaowool needle blanket manufactured by Morgan Ceramic Fibres Ltd., was specified. The thickness required was determined from the literature published by the company.

A thickness of 51mm of  $127\text{kg/m}^3$  density material from a hot face temperature of  $1100^\circ\text{C}$  allowed a cold face temperature of  $65^\circ\text{C}$ .

(16) Timing Belt and Pulleys:

The timing belt and the pulleys were manufactured by J. H. Fenner & Co. Ltd. A 345L timing belt with 318mm centre distance and 92 teeth was chosen. The driving pulley has 18 teeth and the driven pulley has 32 teeth. The pulleys provided a speed ratio of 1.78 and they were provided with taper-lock bushes.

(17) Fork Arrangement Swivel Joint:

The swivel joint was designed to allow the fork to be rotated through  $360^\circ$ . The joint was manufactured of mild steel and was fixed to the bottom of the compocasting unit, see Fig.24.

(18) Liquid Zone Temperature Controller:

A Newtronic analogue thyristor operated controller, with temperature range of  $0-800^\circ\text{C}$  was used. This temperature controller is accurate to  $\pm 3^\circ\text{C}$  with automatic cold junction compensation.

(19) Semi-Solid Zone Temperature Controller:

A Newtronic digital thyristor operated controller, with temperature range of  $0-999^\circ\text{C}$  was used. This temperature controller is accurate to  $\pm 1^\circ\text{C}$  with automatic cold junction compensation.

(20) Thermocouples:

Temperatures were in the range suitable for nickel/chromel-nickel/alumel thermocouples, which were manufactured from 30 s.w.g. wire. One thermocouple was required for each temperature controller and one was fixed to the crucible within the semi-solid zone in order to monitor the temperature in that region.

(21) Temperature Readout:

A digital voltmeter accurate to 0.01 mv was used to

measure voltage from the crucible thermocouple. The voltage was then converted to temperature in °C using B.S.1827.

(22) Tachometer:

A digital tachometer, manufactured by Graham and White Instruments, which functioned using a photoelectric counter to count reflected light pulses from a reflector attached to the rotor drive shaft, was used to adjust the speed of rotation of the rotor.

(II) The Launder

The launder [23] was made of cast iron produced in a sand mould, using the refractory launder as a pattern. Heating the launder was essential to prevent the slurry losing too much heat on its way to the shot chamber. Two thermostatically-controlled cartridge heaters, of 750 watt each were used to bring the launder temperature up to 400 °C.

A Eurotherm temperature controller with a range of 0-1300 °C, and Platinum-(13% Platinum-Rhodium) thermocouple were used to control the launder temperature. The launder, coated with liquid graphite to prevent the alloy slurry sticking on it, was fixed to the bottom of the compocasting unit, see Figs. 20 and 21.

## APPENDIX TWO

### (I) Design and Manufacture of the Pressure Die Casting Die

The die design involved a simple die cavity shape which consisted of four pins and a disc to provide the necessary specimens required for mechanical and tribological tests. The die was mainly manufactured of H13, hot working die tool steel supplied by "Uddeholm Limited" in Birmingham, and the die dimensions were designed in accordance with the die casting machine specifications. The die was provided with an automatic ejector, so that when the die was opened, the ejector automatically acts to eject the casting from the die cavity. The die was manufactured and assembled as shown in Figs. 22 and 23, and it was tried with a low melting temperature alloy "cirocast", which has a melting point of 200°C, and found to perform well. The die consisted of the following: see Parts List in Fig.28A.

#### (1) Moving Die Member:

The moving die member which contains most of the cavity, the gate, the runner and part of the sprue, was manufactured from H13 die tool steel. It was manufactured, hardened and ground in accordance with the manufacturer's instructions. Two holes were also made in this part of the die, to accommodate the die guide pins [8] .

#### (2) Bolster:

The bolster was designed to support the moving die member and also to accommodate part of the cavity and the ejector pins. The bolster was manufactured from H11 carbon steel which is relatively cheaper than H13. The bolster and the moving die member [1] were joined together with four 3/8in. Allen screws to form the moving die half. Four holes were made in the moving die half, to enable that part of the die to be mounted on the moving platen of the pressure die casting machine.

#### (3) Ejector Pins Guide Bushes:

Five bushes were designed to prevent the direct contact between the ejector pins and the moving die half in order

to protect the moving die member. The bushes were manufactured from H13 steel, hardened and ground. A tolerance of 0.05mm (0.002in.) on the diameter, was given to these bushes to provide the required venting to the die cavity, i.e. to allow the air entrapped in the cavity to escape through these vents. The bushes were also provided with 1.4° taper to provide easy ejection of the casting.

(4) Gating System:

The die was designed to permit different gate dimensions to be used. The gates [4] were manufactured of H13, hardened, ground and fixed to the moving die member with two 1/4in. Allen screws. Two threaded holes were made in the gate body to permit gate ejection. The gates were provided with 3° taper for easy extraction. The runner [5] and part of the sprue [6] were formed in the moving die member's body. The runner has a rectangular cross section of 20 x 10mm and is provided with 3° taper toward the fixed die member. The part of the sprue which was made in the body of the moving die member has 44.45mm diameter and 10mm thickness and is also provided with 3° taper.

(7) Fixed Die Member:

This was designed to incorporate the die guide pins [10], the shot sleeve guided bush [9] and the cooling system [11]. The fixed die member was manufactured of H13, hardened and ground in accordance with the manufacturer's specifications. The cooling system consisted of a hole drilled through the fixed member and was made as close as possible to the sprue, to provide efficient cooling

(8) The Bolster:

This was designed to accommodate part of the shot sleeve guide bush and the shot sleeve. The bolster was made of H11 carbon steel and attached to the fixed die member with four 3/8in. diameter Allen screws to form the fixed die half.

(9) Shot Sleeve Guide Bush:

This was designed to prevent any damage to the fixed die half caused by the movement of the plunger inside the die. The shot sleeve guide bush was manufactured of H13, hardened and ground and inserted into the fixed die half.

(10) Guide Pins:

Two guide pins were designed to provide the required alignment for the two die halves. The two guide pins were made from H13 die tool steel, hardened, ground and fastened into the fixed half of the die.

(II) The Ejector. see Parts List 28A

The ejector consisted of the following:

(12) Ejector Pins:

Five ejector pins were designed to provide simultaneous ejection of the casting. Four of these ejector pins were made identical, while the fifth one, which directed to the runner, was made longer. The ejector pins were manufactured from H13 die tool steel hardened, ground and fixed to the ejector plate by five lock screws.

(13) Ejector Guide Pins:

Four ejector guides were designed to provide the necessary alignment to the ejector pins. The ejector guides were manufactured from H13 die tool steel, hardened and ground and provided with four die springs to push back the ejector pins, after ejection had occurred.

(14) Ejector Plate:

This was designed to distribute the ejection force equally on the ejection pins. The ejector plate was manufactured of H13 die tool steel and it was hardened and ground in accordance with the manufacturer's specifications.

(15) Stops:

Two stops were designed to protect the ejector plate [4] by receiving the ejection force from the ejection plate fixed to the die casting machine and transmit it to the ejector plate on the die. The stops were manufactured

of mild steel and fixed to the ejector plate with four 3/8in. diameter Allen screws.

SEMI-SOLID ALLOY PROCESSING VARIABLES AND THEIR CALCULATIONS

The variables affecting the structure of an alloy processed by the rheocasting/compcasting process are:

- Average Shear Rate:

The average shear rate is a function of the stirring rotor geometry, the clearance between the rotor and the mixing chamber and the rotation speed. The average shear rate was calculated using the definition:

$$\dot{\gamma}_{ave} = \frac{d\theta}{dr} \cdot r$$

where  $\theta$  was the angular velocity at a distance  $r$  from the centre of the rotor calculated from the equations of motion (116) and equal to, in the case of a Newtonian fluid,

$$\dot{\gamma}_{ave} = \frac{2\Omega_o}{(1-K^2)} K \quad (1) \quad (51)$$

where:  $\dot{\gamma}_{ave}$  = the average shear rate  
 $\Omega_o$  = the angular velocity of the rotor  
 $K$  : is defined as:

$$K = \frac{\text{Perimeter of the Rotor}}{\text{Perimeter of the Mixing Chamber}}$$

- Average Cooling Rate:

The average cooling rate is a function of the thermal profile within the mixing chamber including the temperature and volume fraction of solid of the discharged slurry. The average cooling rate in the mixing chamber is defined by the following equation:

$$\epsilon_{ave} = \frac{\Delta T_s (G_s)}{t_f}$$

where:  $\Delta T_s (G_s)$  = the difference between the liquidus temperature and the temperature of the existing slurry at a given volume fraction solid.

$t_f$  = the residence time of the alloy in the mixing chamber while in the solidification range.

- Volume Fraction Solid:

The volume fraction of primary solid particles in the existing slurry is dependent on the rate of heat withdrawal in the mixing chamber, the rate of material flow through the chamber, and the physical properties of the alloy produced. For a binary alloy the volume fraction solid was calculated as a function of temperature from the "Scheil Equation"<sup>(117)</sup> and the lever rule. The former assumes no solid diffusion, equilibrium at the liquid-solid interface, complete diffusion in the liquid and constant partition coefficient  $K$ <sup>(117)</sup>. The latter assumes complete diffusion in the solid. For the reasons outlined above, the Scheil equation is likely to be most accurate. However, both equations were deduced from a mass balance and give fraction solid in weight. Differences between calculated weight fractions and volume fractions are claimed to be very small due to the small differences in density of the solid and liquid phases<sup>(53)</sup>. In published work, the Scheil equation has been used almost universally and fractions solid have been referred to as "volume". The equation used for calculating the volume fraction solid was:

$$g_s = 1 - \left[ \frac{T_m - T_l}{T_m - T} \right]^{1/1 - K} \quad (2)$$

where:  $g_s$  = volume fraction solid,  
 $T_m$  = melting temperature of the pure solvent,  
 $T_l$  = liquidus temperature of the alloy,  
 $T$  = actual temperature in the liquid solid range.

K is defined as "the equilibrium partition constant"<sup>(117)</sup>, and was obtained from the equation:

$$K = \frac{C_s^*}{C_l^*}$$

where:  $C_s^*$  : composition of the solid  
 $C_l^*$  : composition of the liquid

$C_s^*$  and  $C_l^*$  are obtained from the equilibrium diagram of the binary alloy.

For a more complex alloy (ternary alloy) system, the relationship between volume fraction solid and temperature can be established either by considering the ternary alloy as two binary alloys and calculating the volume fraction solid according to this assumption<sup>(118)</sup> or experimentally.

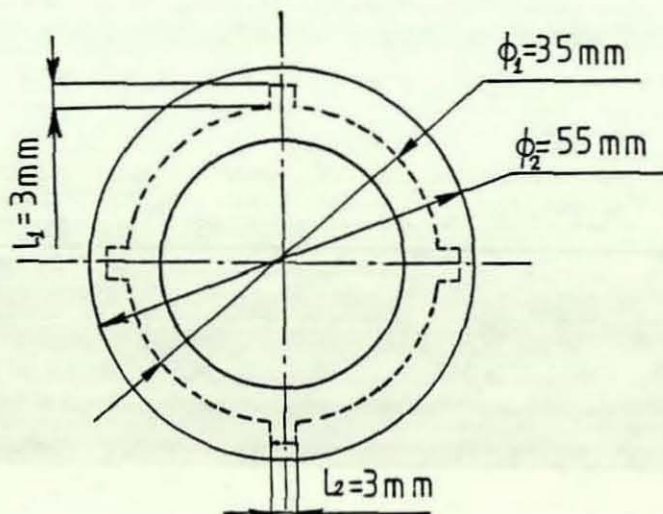
- Calculation of the Average Shear Rate

The average shear rate can be calculated from the following equation:

$$\dot{\gamma}_{ave} = \frac{2\Omega_0}{1-K^2} K$$

$$K = \frac{\text{Perimeter of the rotor}}{\text{Perimeter of the Crucible}}$$

The perimeter of the rotor is the one indicated with a dotted line.



$$\begin{aligned}\text{Perimeter of the rotor} &= 2\pi \times r_1 + 8 \times l_1 \\ &= 2\pi \times 17.5 + 8 \times 3 = 134 \text{ mm}\end{aligned}$$

$$\begin{aligned}\text{Perimeter of shearing chamber} &= 2\pi \times r_2 \\ &= 2\pi \times 27.5\end{aligned}$$

$$K = \frac{134}{173} = 0.77$$

For  $\Omega_0 = 1500$  r.p.m.

$$\dot{\gamma}_{\text{ave}} = \frac{2 \times \frac{1500 \times 2\pi}{60}}{1 - (0.77)^2} \times 0.77 = 550 \text{ sec}^{-1}$$

#### - Calculation of the average cooling rate

The molten alloy was poured into the compocasting unit at a temperature of  $725^\circ\text{C}$ . When the alloy temperature reached the equilibrium value ( $675^\circ\text{C}$ ) the residency time for the alloy in the compocasting unit was considered and the time required for the alloy to cool down to the predetermined temperature was measured. A digital multimeter was used to monitor the alloy temperature and the average cooling rate was calculated using the following formula:

$$\mathcal{E}_{\text{ave}} = \frac{\Delta T_s (\text{gs})}{t_f}$$

For slurry discharged at  $573^\circ\text{C}$  (volume fraction solid 0.075), the time required for the alloy to cool down from the equilibrium temperature to  $573^\circ\text{C}$  was found to be 67 minutes.

$$\Delta T_s (\text{gs}) = 675 - 573 = 102^\circ\text{C}$$

$$\mathcal{E}_{\text{ave}} = \frac{102}{67} = 1.5^\circ\text{C/min.}$$

## APPENDIX FOUR

### MECHANICAL PROPERTIES CALCULATIONS

#### (I) Ultimate Tensile Stress (U.T.S.)

The ultimate tensile stress can be obtained as follows:

$$\text{U.T.S.} = \frac{\text{Ultimate load}}{\text{Cross sectional area}} \quad (1)$$

For example:

The ultimate load for three specimens: 1.94 kN  
2.06 kN  
2.21 kN

$$\begin{aligned} \text{Average} &= \frac{1.94 + 2.06 + 2.21}{3} \\ &= 2.07 \text{ kN} \\ &= 2.07 \times 10^3 \text{ MN} \end{aligned}$$

diameter of specimen  $r = 4.53\text{mm}$

Therefore the cross-sectional area  $A = \pi r^2$

$$\begin{aligned} A &= \pi (4.53)^2 \\ A &= 16.12\text{mm}^2 \\ &= 16.12 \times 10^6 \text{ m}^2 \end{aligned}$$

From equation (1)

$$\text{U.T.S.} = \frac{2.07 \times 10^3}{16.12 \times 10^6} = 128 \text{ MN/m}^2$$

(II) Brinell Hardness Number Calculations

The Brinell hardness number can be calculated from the following formula:

$$\text{B.H.N.} = \frac{P}{\frac{\pi D}{2} (D - \sqrt{D^2 - d^2})} \quad (2)$$

where: P = load applied = 750kg.

D = ball diameter = 10mm.

d = diameter of impression measured.

Consider the first twelve specimens in Table 4.

The diameters of impression were: 2.8, 2.75, 2.9, 2.85, 2.85, 2.75, 2.9, 2.8, 2.8, 2.8, 2.85 and 2.8mm.

$$\begin{aligned} \text{The average} &= \frac{5 \times 2.8 + 2 \times 2.75 + 2 \times 2.9 + 3 \times 2.85}{12} \\ &= 2.82 \end{aligned}$$

$$\text{B.H.N.} = \frac{750}{\frac{2 \times 10}{2} (10 - \sqrt{(10)^2 - (2.82)^2})}$$

$$\text{B.H.N.} = 118$$

## APPENDIX FIVE

### TRIBOLOGICAL PROPERTIES CALCULATIONS

#### (I) Wear Volume:

The wear volume is the amount of material lost from the pin during the wear test and can be obtained by multiplying the cross-sectional area (A) of the test pin by the change in pin length(l).

Wear Volume = Cross-sectional area x change in pin length

The diameter of the wear test pin d= 6.35mm.

$$\begin{aligned}\text{The cross-sectional area} &= \pi \left(\frac{d}{2}\right)^2 \\ A &= \pi \left(\frac{6.35}{2}\right)^2 \\ A &= 31.7 \text{ mm.}^2 \\ A &= 0.317 \text{ cm.}^2\end{aligned}$$

For specimen which lost 0.3mm. (0.03cm.) of its length

$$\begin{aligned}\text{the wear volume} &= A \times l \\ &= 0.317 \times 0.03 = 9.51 \times 10^{-3} \text{ cm.}^3\end{aligned}$$

(II) The wear rate can be obtained by dividing the wear volume by the total running distance (L) of the pin over the disc. The running distance can be calculated from the speed of rotation of the disc and the track circumference.

$$\begin{aligned}\text{The pin was running at a distance of 30mm. from the disc centre, so the track circumference} &= 2 \pi \times 30 \\ &= 188.5 \text{ mm.} \\ &= 18.85 \text{ cm.}\end{aligned}$$

The disc rotates at 318 rpm. (1m./sec. linear velocity).

The test duration = 30 minutes and so the total running distance = track circumference x r.p.m. x test duration

$$= 18.85 \times 318 \times 30$$

$$= 179829 \text{ cm.}$$

$$= 1798.29 \text{ m.}$$

$$\text{Wear rate} = \frac{\text{Wear Volume}}{\text{Running distance}}$$

$$\text{Wear rate} = \frac{9.51 \times 10^3}{179829} = 5.29 \times 10^{-8} \text{ cm.}^3/\text{cm.}$$

(III) The coefficient of friction can be obtained from the formula:

$$\mu_{\text{kin}} = \frac{F_{\text{kin}}}{W}$$

where:  $F_{\text{kin}}$  = the friction force (the deflection force),  
 $W$  = the axial load applied on the pin = 12.6kg.(28lb.)

For deflection force = 3.78 kg<sub>f</sub>. (8.4lb.)

$$\mu_{\text{kin}} = \frac{3.78}{12.6} = 0.3$$

## APPENDIX SIX

### GRAPHITE CALCULATION

The graphite area (%) was calculated for each specimen from the following formula:

$$A = \frac{x}{y \cdot n} \times 100 \quad (1)$$

where: A = area of graphite (%)  
x = area of graphite measured  
y = field area =  $1.276 \times E6$   
n = number of fields measured (10fields)

The weight (%) was obtained by multiplying the area (%) by the density ratio of graphite to aluminium alloy.

$$\text{density ratio} = \frac{\text{density of graphite}}{\text{density of aluminium alloy}}$$

The density of graphite =  $1.9 \text{ gm/cm}^3$

The density of LM30 =  $2.73 \text{ gm/cm}^3$

$$\text{density ratio} = \frac{1.9}{2.73} = 0.7$$

#### Example:

The area of graphite measured for specimen no. S20 was  $5.65E^5$ .  
From equation (1).

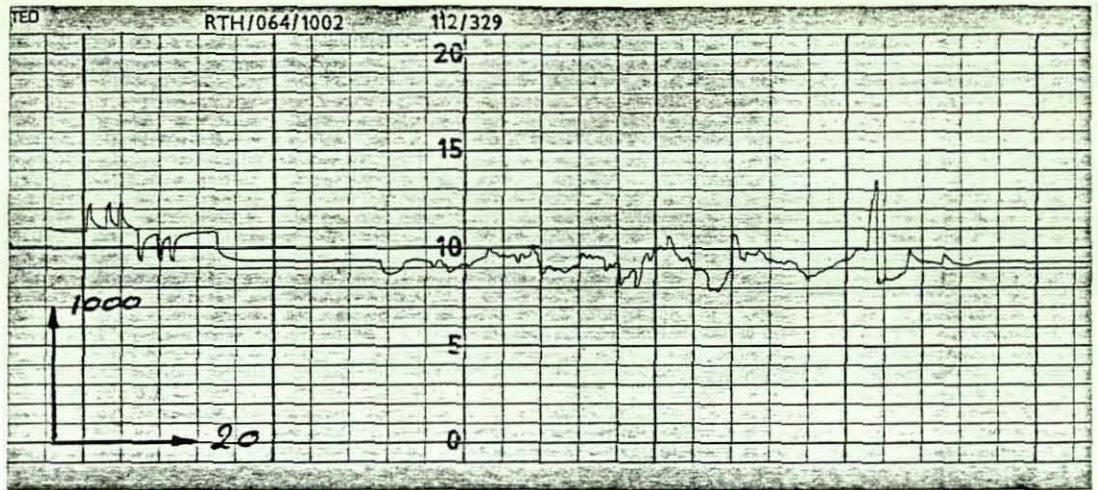
$$\begin{aligned} \text{The area \% } A &= \frac{5.65E^5}{1.276E^6 \times 10} \times 100 \\ A &= 4.43\% \end{aligned}$$

Graphite wt.% = A x density ratio

Graphite wt.% =  $4.43 \times 0.7 = 3.10\%$

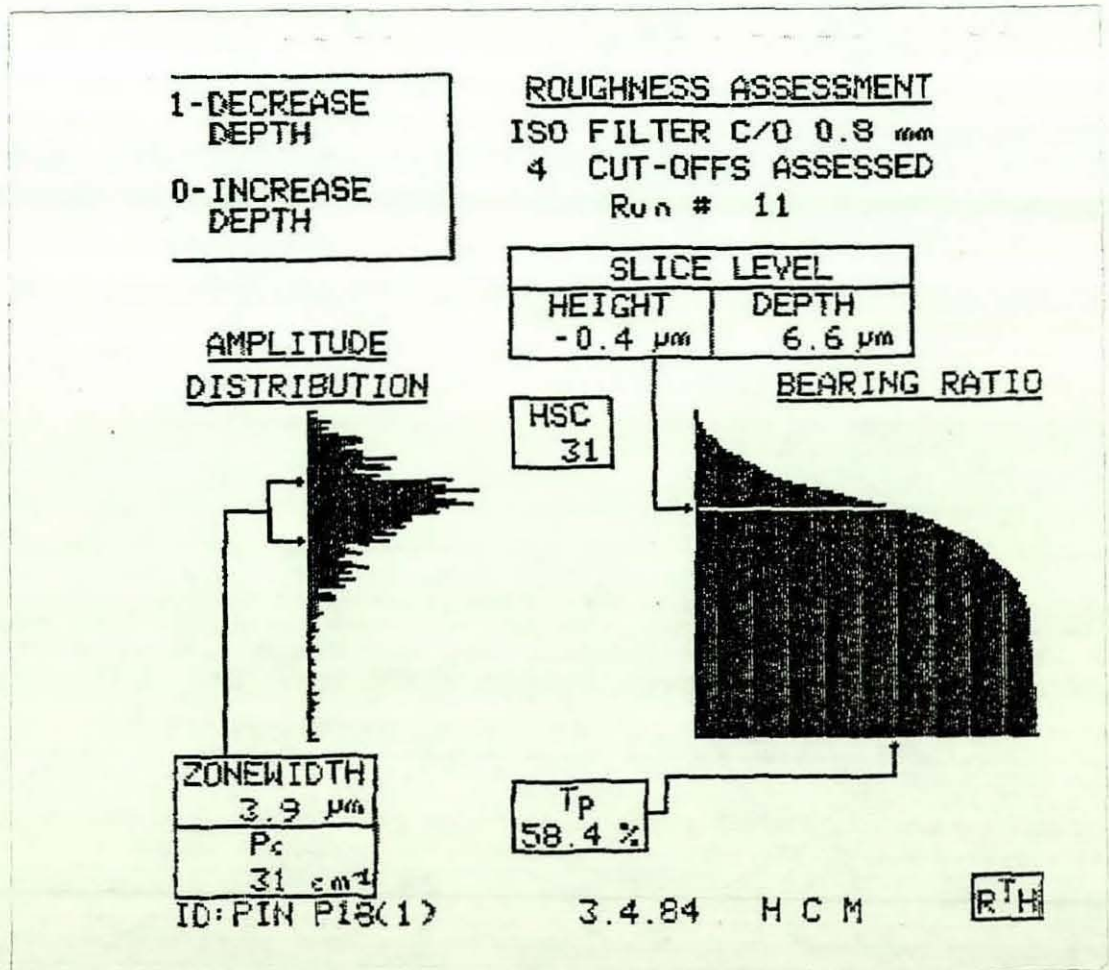
APPENDIX SEVEN

- Fig. 66                      Presents the surface texture for a graphite free specimen after the wear test (dry friction).
- Figs. 67 - 70                Present the surface texture for graphitic specimens after the wear test (dry friction).
- Fig. 72                      Presents the surface texture of a disc mated with graphite free specimen after the wear test (dry friction).
- Figs. 73-76                 Present the surface texture of discs mated with graphitic specimens after the wear test (dry friction).
- Fig. 81                      Presents the surface texture of a graphite free specimen after the wear test (lubricated friction).
- Figs. 82 - 85                Present the surface texture of graphitic specimens after the wear test (lubricated friction).
- Fig. 86                      Presents the surface texture of a disc mated with graphite free specimen after the wear test (lubricated friction).
- Figs. 87 - 90                Present the surface texture of discs mated with graphitic specimens after the wear test (lubricated friction).



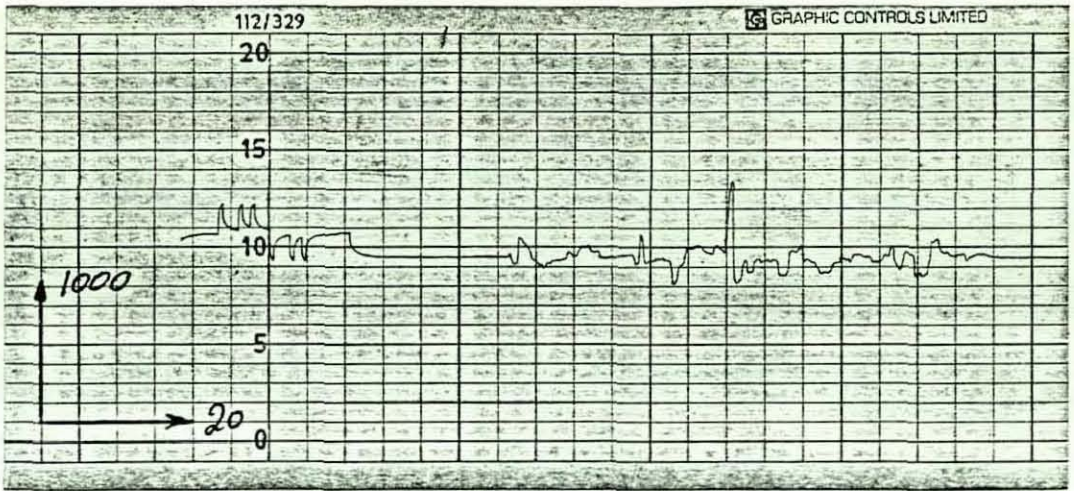
(a)

$R_a = 4.62\mu\text{m}$



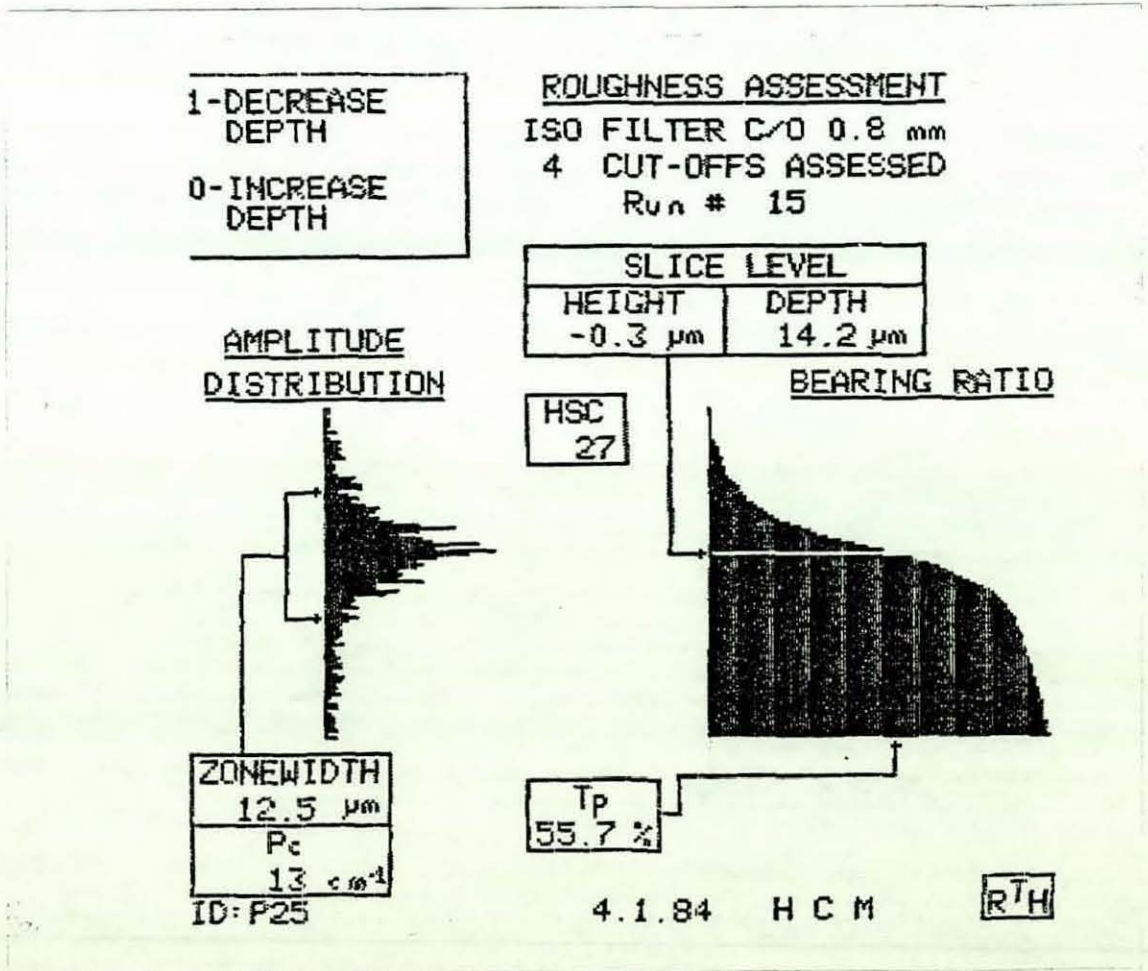
(b)

Fig.66 - Pin Surface Texture After Test. LM30 - Rheocasting  
(a) Surface Profile. (b) Bearing Area Analysis.



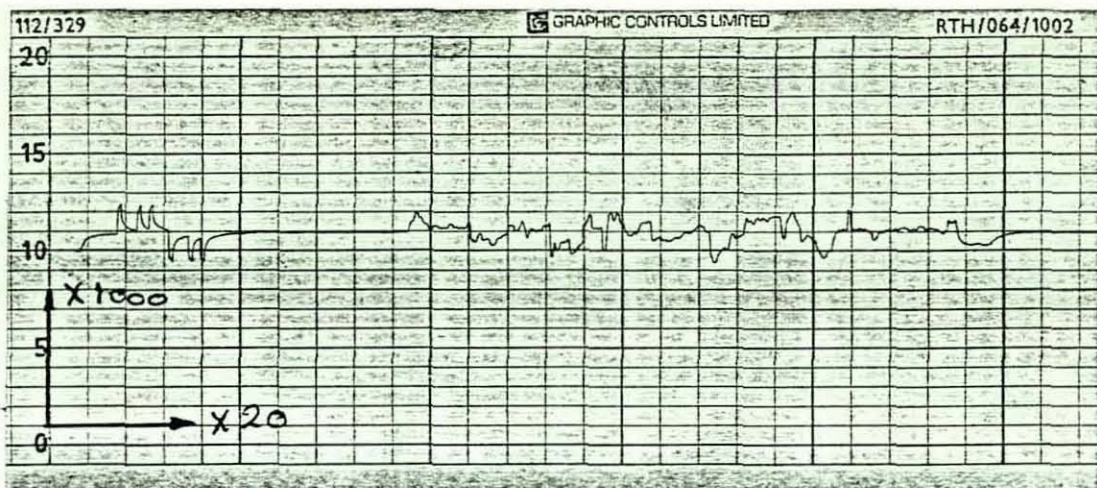
(a)

$R_a = 4.2 \mu\text{m}$



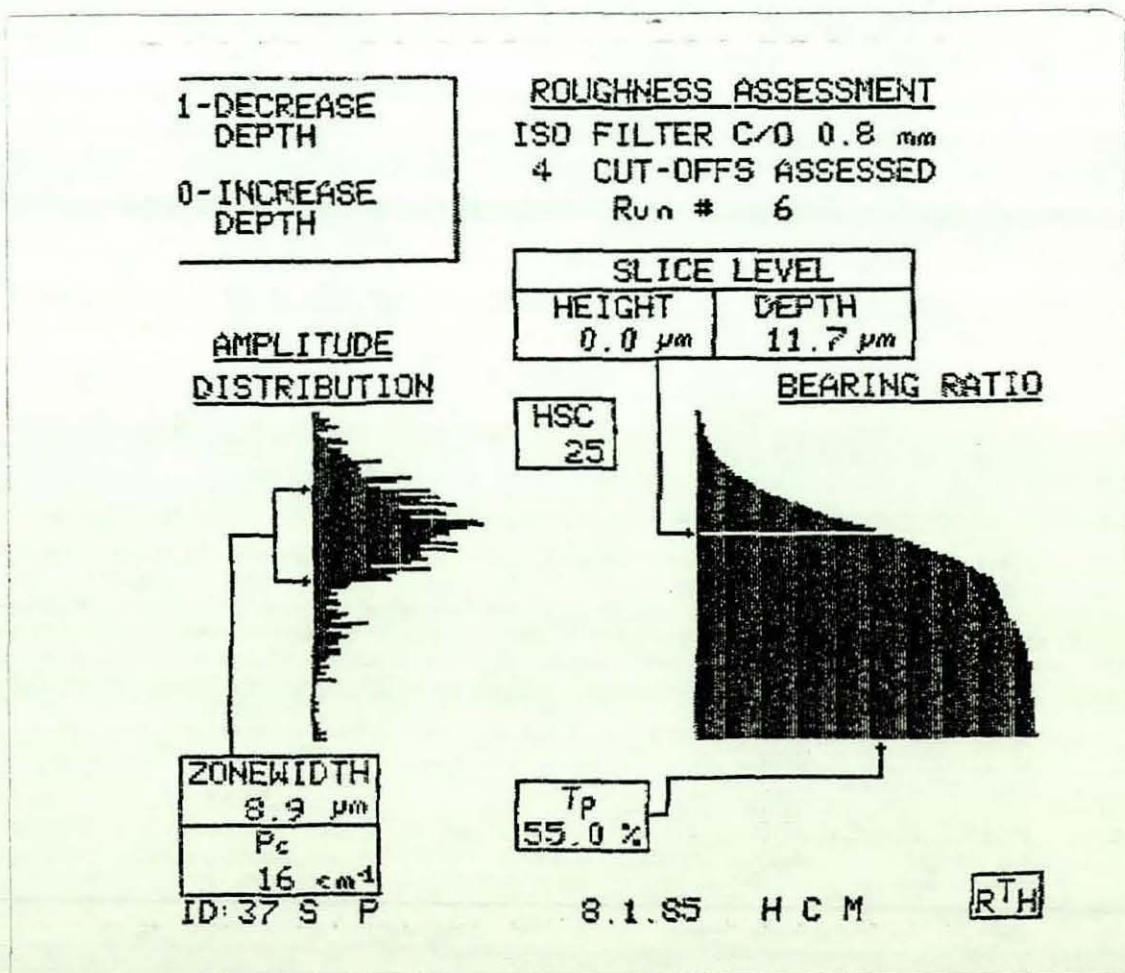
(b)

Fig.67 - Pin Surface Texture After Test. LM30 - 3wt% Graphite  
(a) Surface Profile. (b) Bearing Area Analysis.



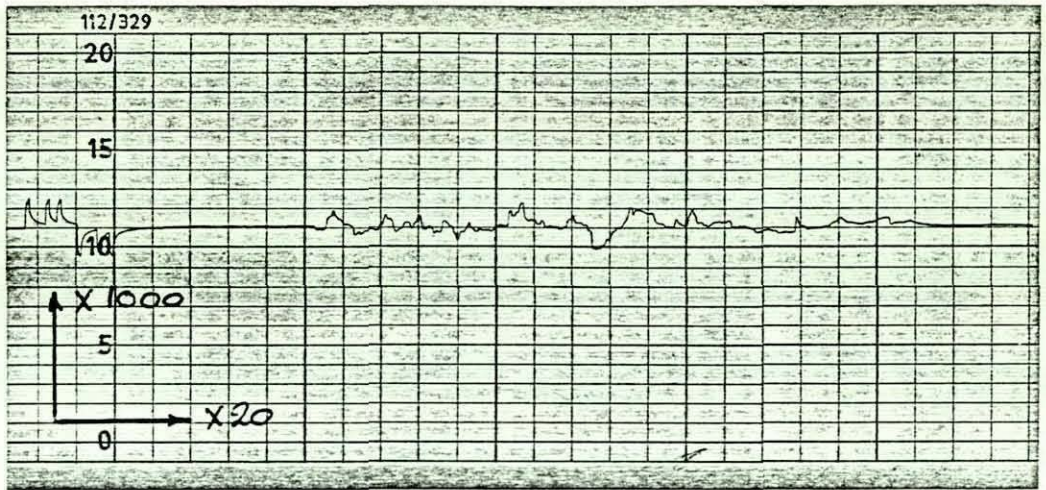
(a)

$R_a = 3.9 \mu\text{m}$



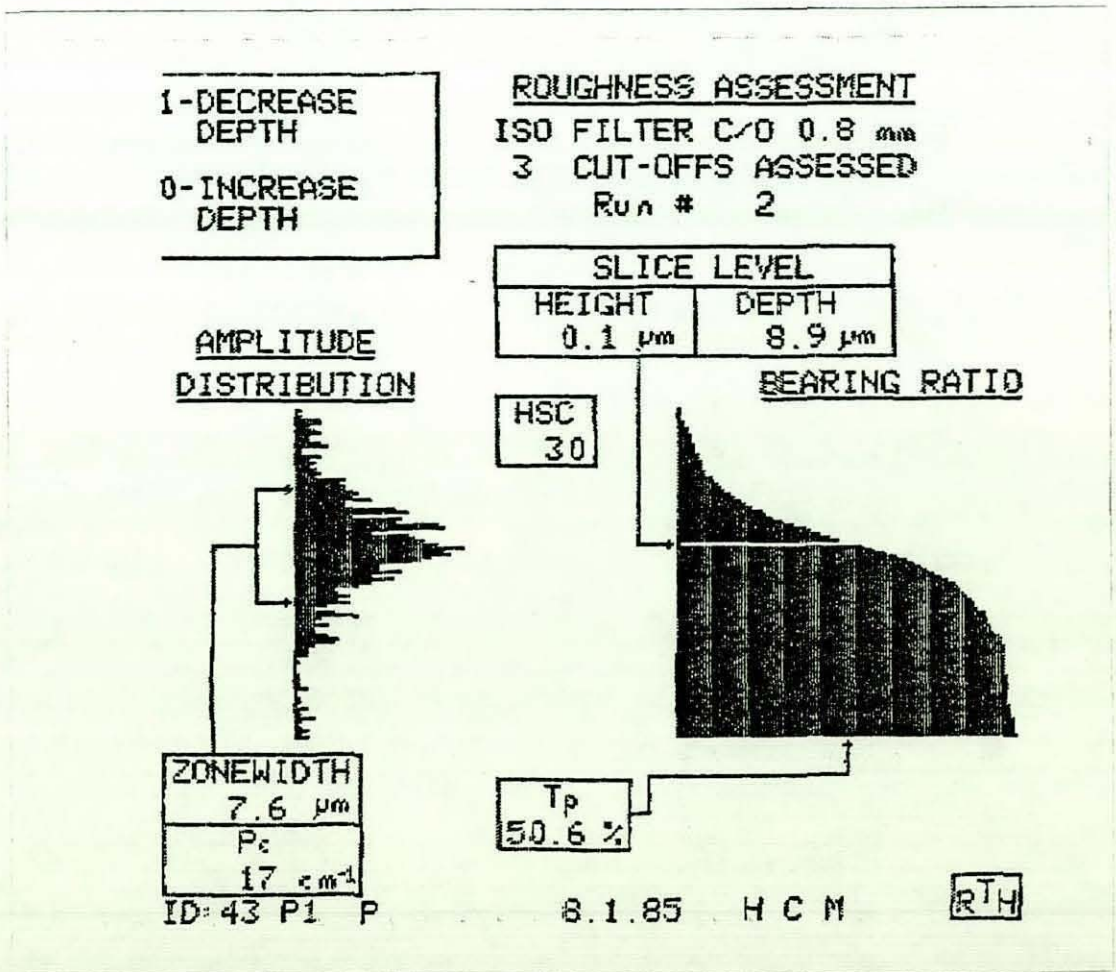
(b)

Fig.68 - Pin Surface Texture After Test. LM30 - 4½wt% Graphite  
(a) Surface Profile. (b) Bearing Area Analysis.



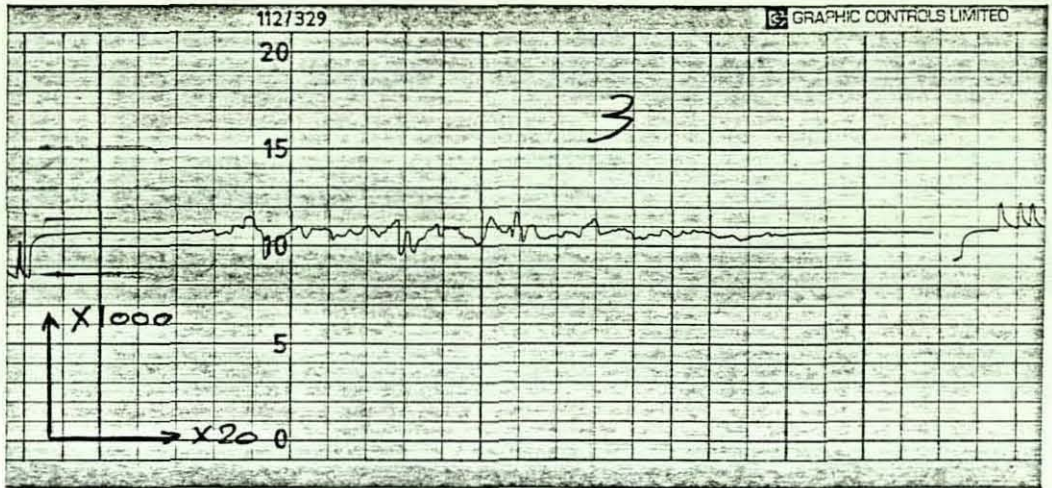
(a)

$R_a = 3.2\mu\text{m}$



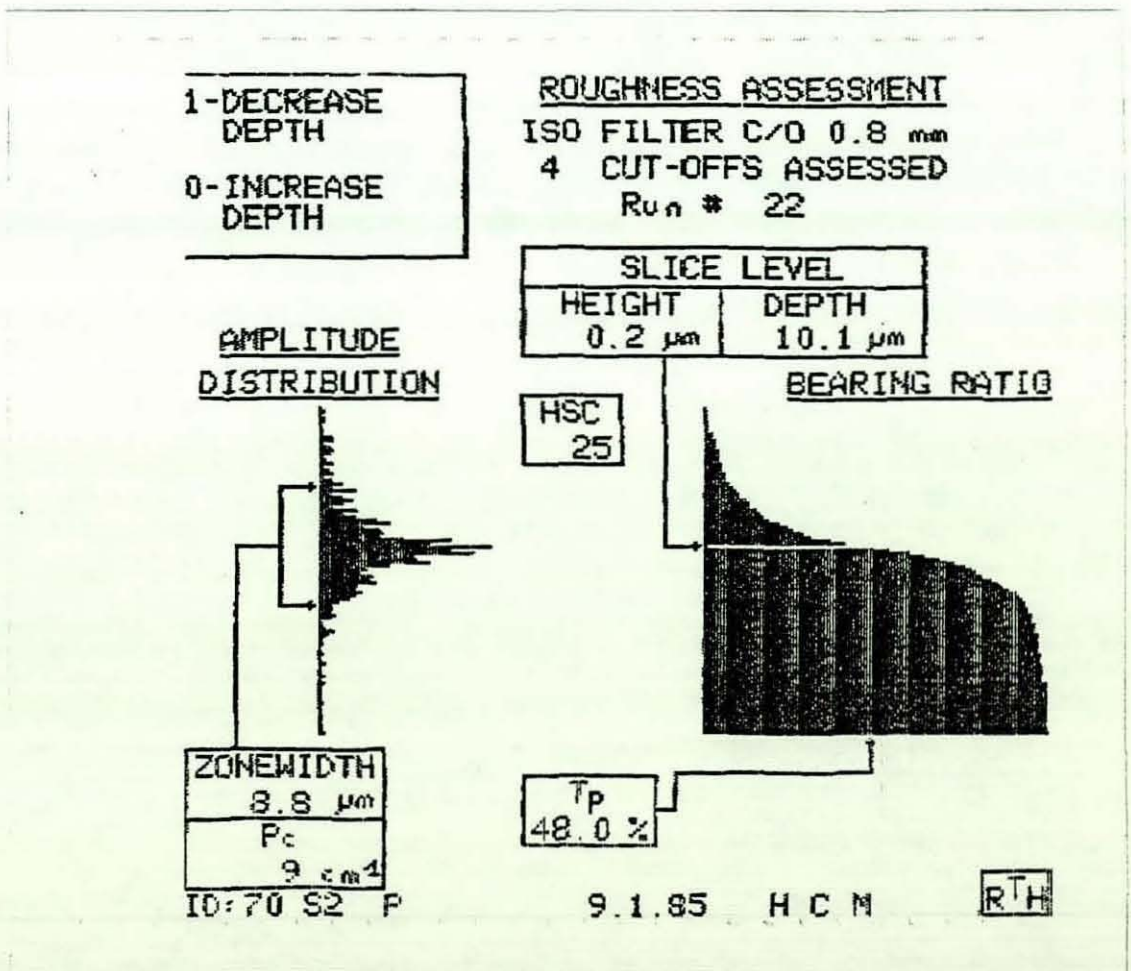
(b)

Fig.69 - Pin Surface Texture After Test. LM30 - 6wt% Graphite  
 (a) Surface Profile. (b) Bearing Area Analysis.



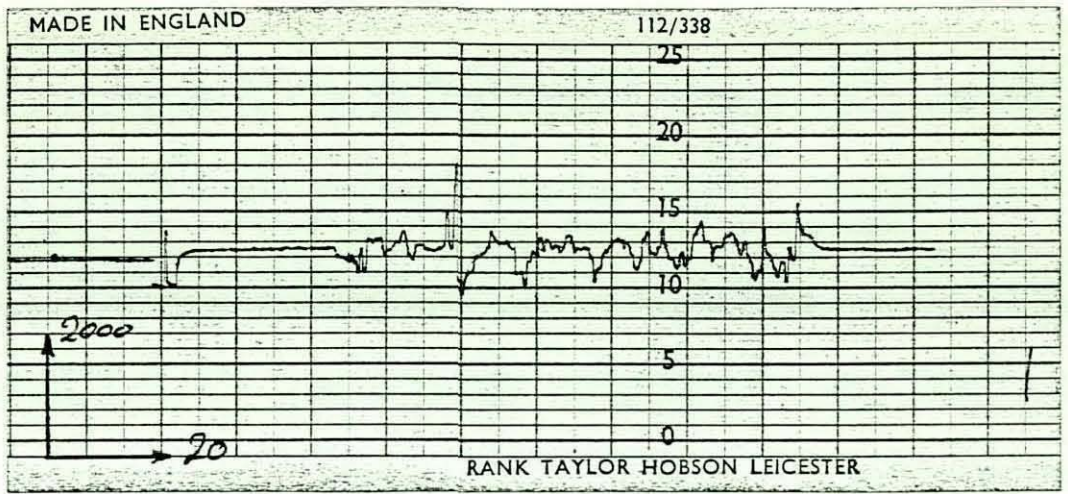
(a)

$R_a = 2.65\mu\text{m}$



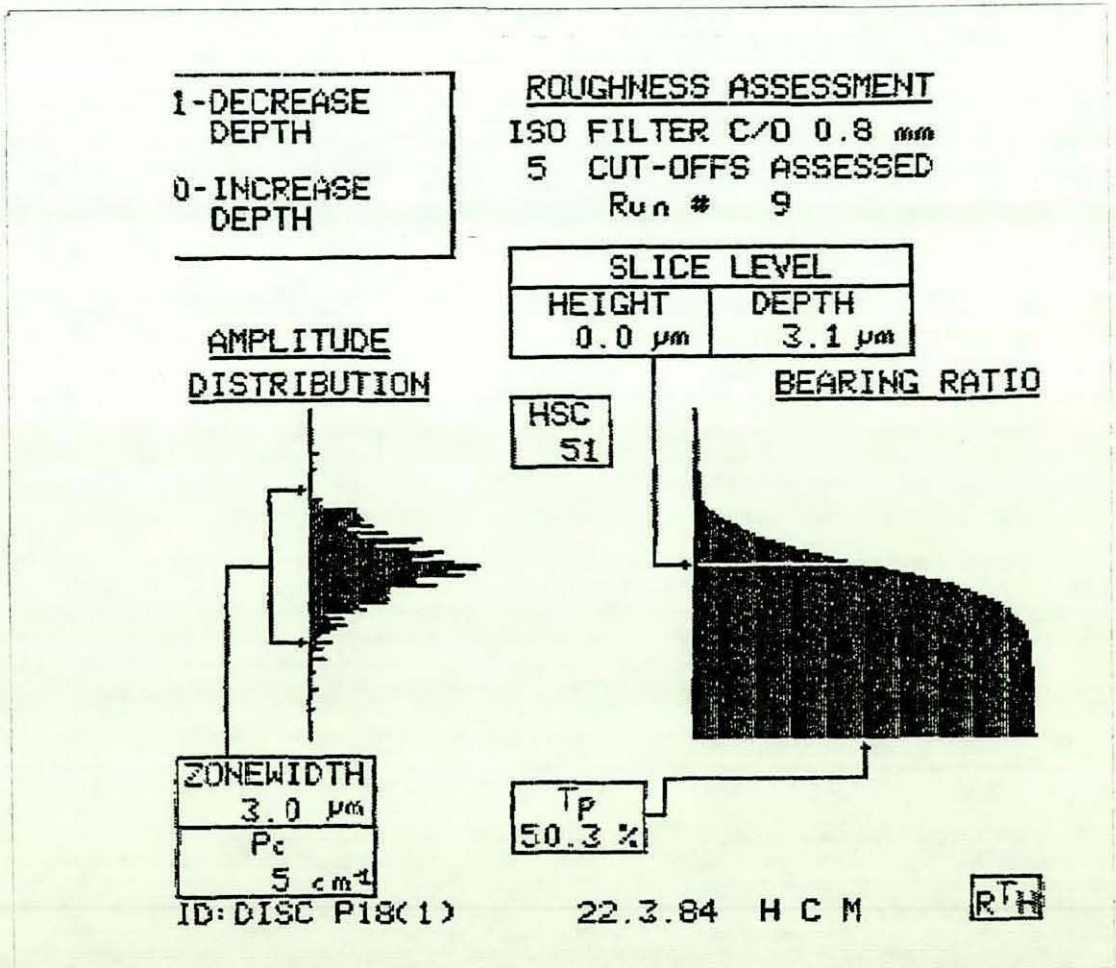
(b)

Fig.70 - Pin Surface Texture After Test. LM30 - 7½wt% Graphite  
(a) Surface Profile. (b) Bearing Area Analysis.



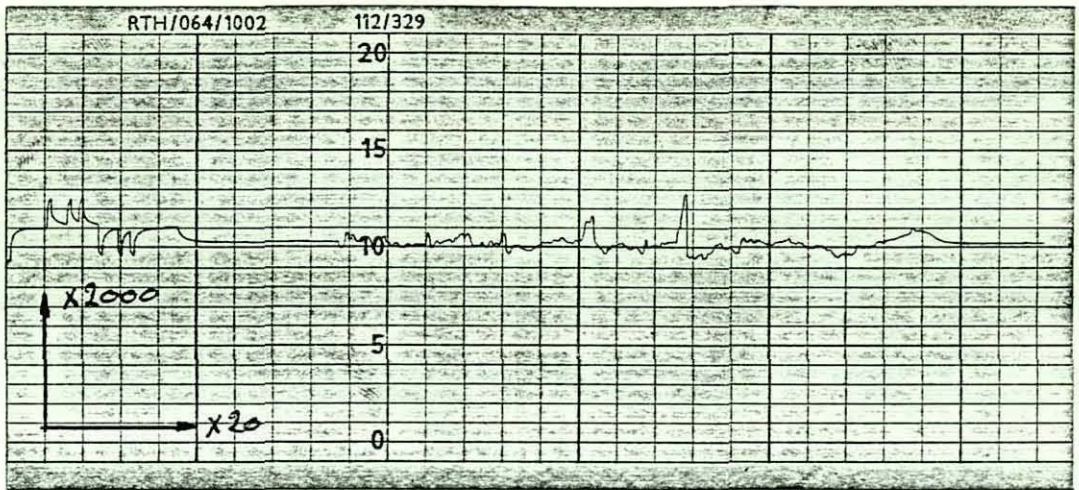
(a)

$R_a = 0.89\mu\text{m}$



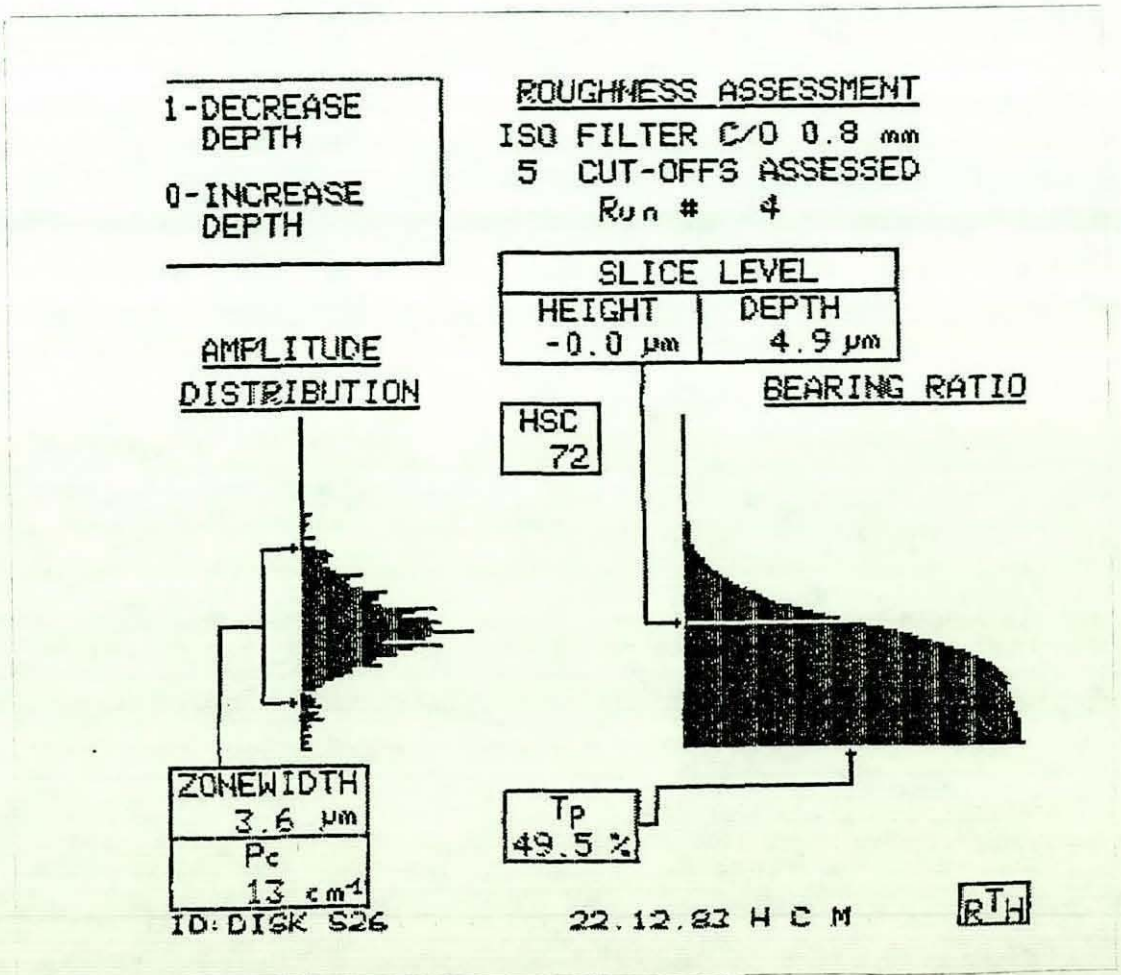
(b)

Fig.72 - Disc Surface Texture After Test. LM30 - Rheocasting  
(a) Surface Profile. (b) Bearing Area Analysis.



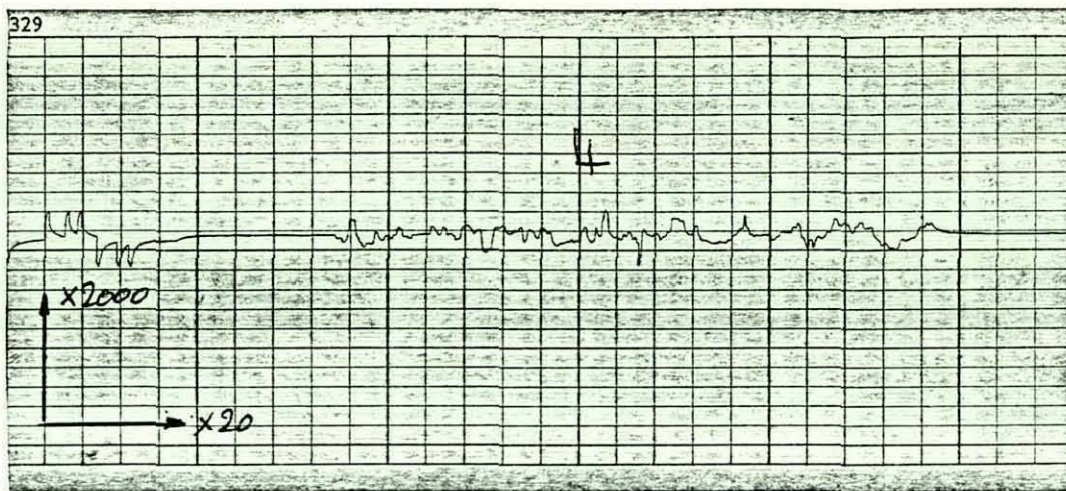
(a)

Ra = 0.65 $\mu$ m



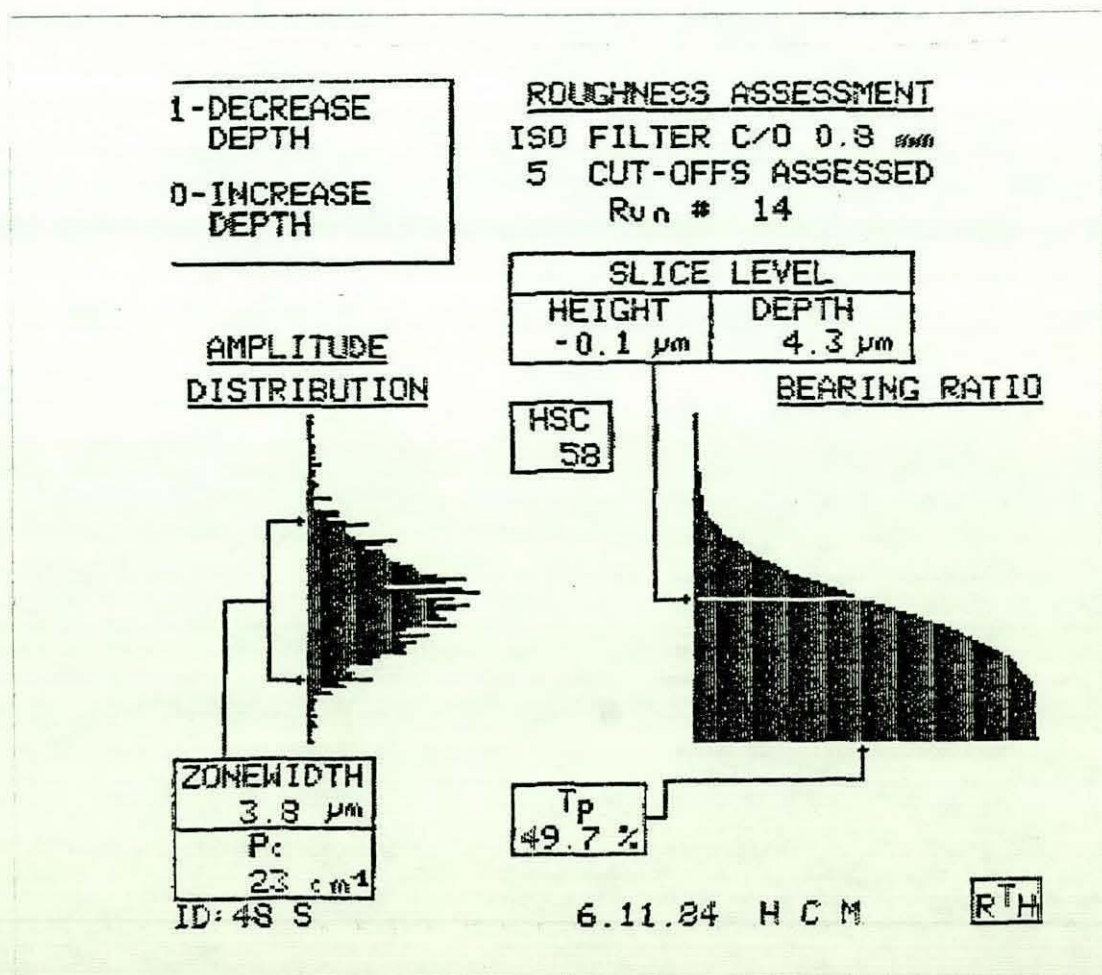
(b)

Fig.73 - Disc Surface Texture After Test. LM30 - 3wt% Graphite  
(a) Surface Profile. (b) Bearing Area Analysis.



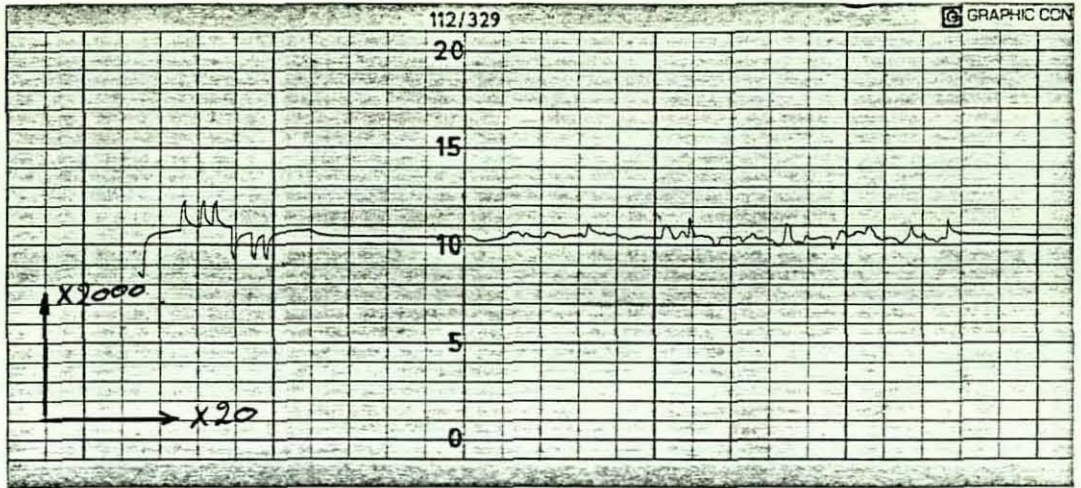
(a)

Ra = 0.63 $\mu$ m



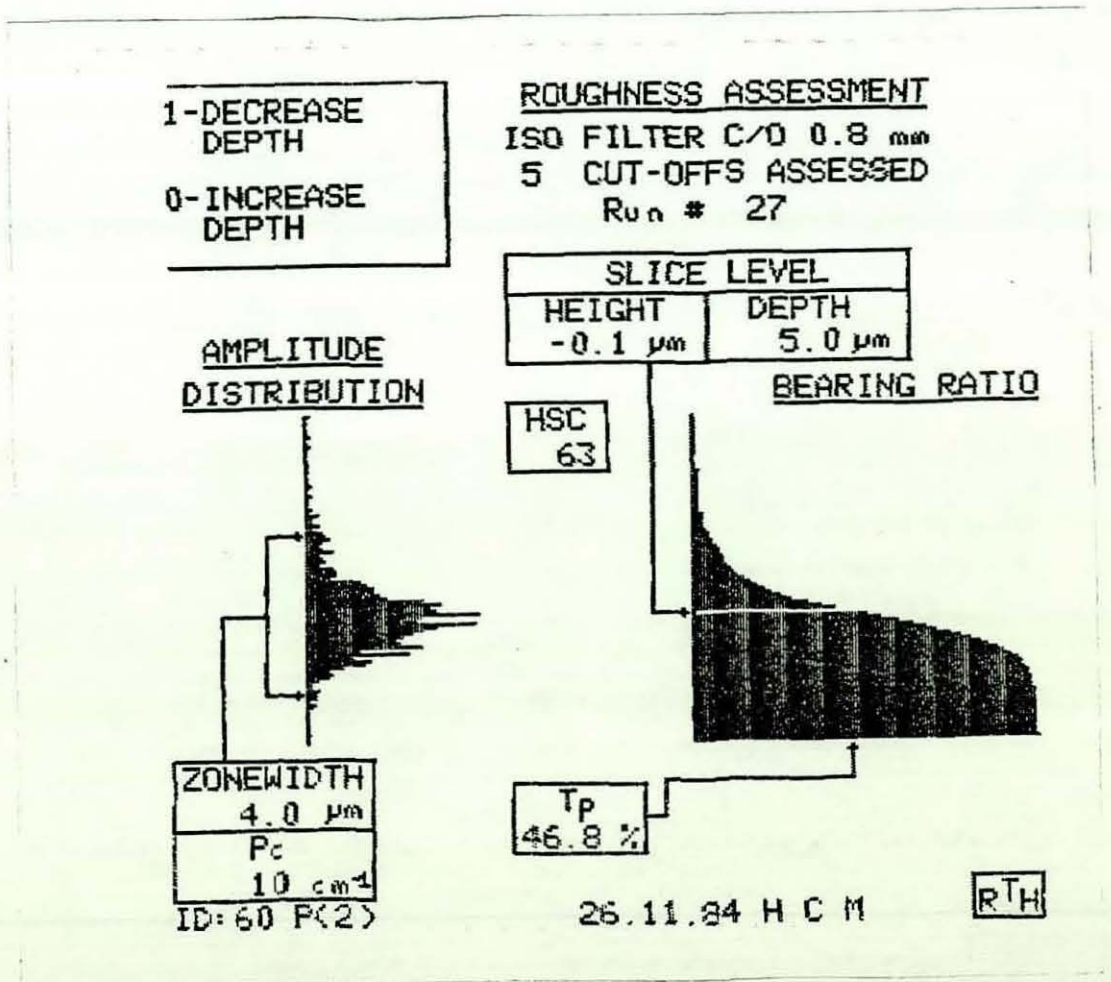
(b)

Fig.74 - Disc Surface Texture After Test. LM30 - 4½wt% Graphite  
(a) Surface Profile. (b) Bearing Area Analysis.



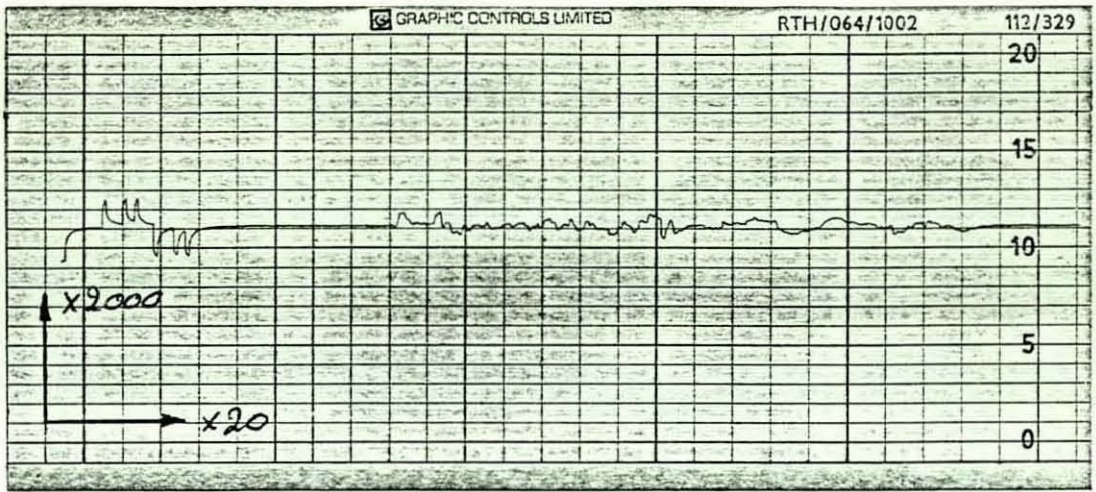
(a)

$R_a = 0.62 \mu\text{m}$



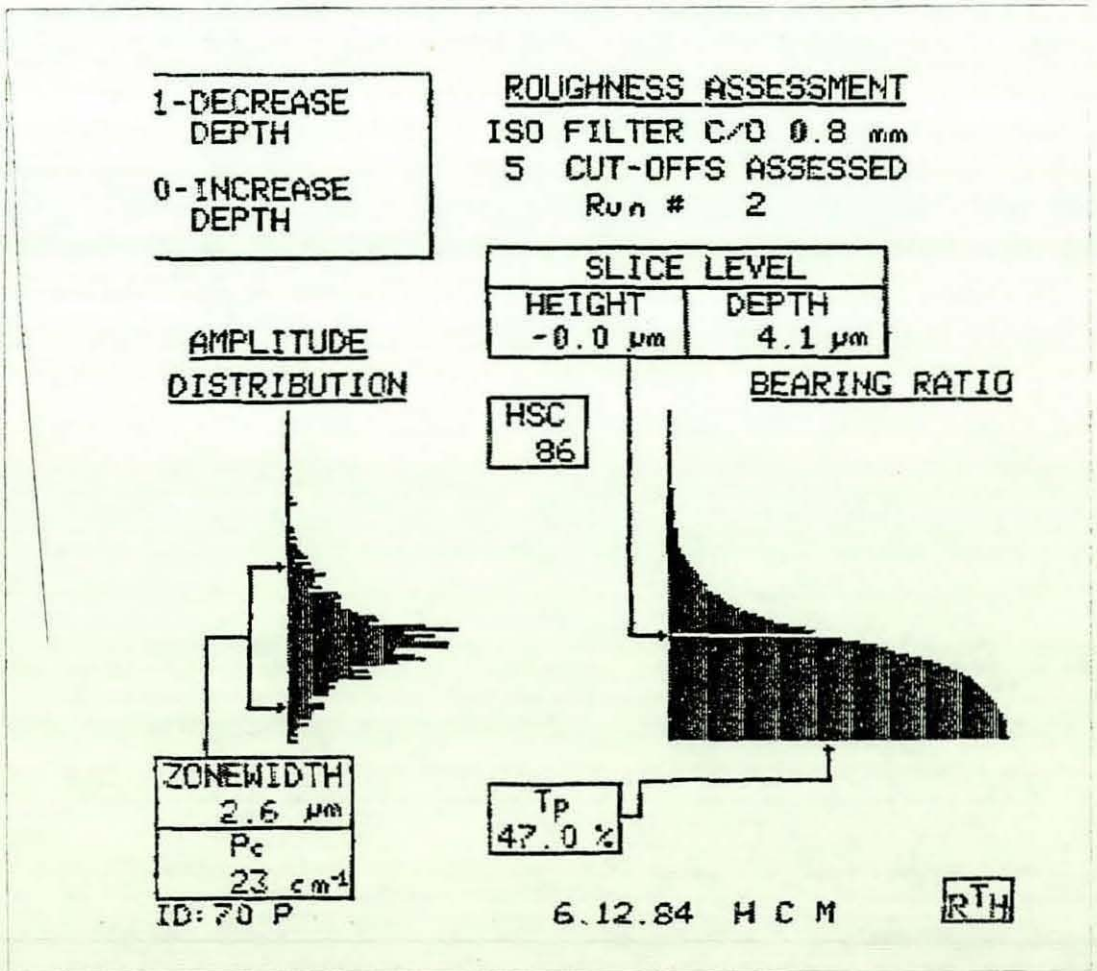
(b)

Fig.75 - Disc Surface Texture After Test. LM30 - 6wt% Graphite  
(a) Surface Profile. (b) Bearing Area Analysis.



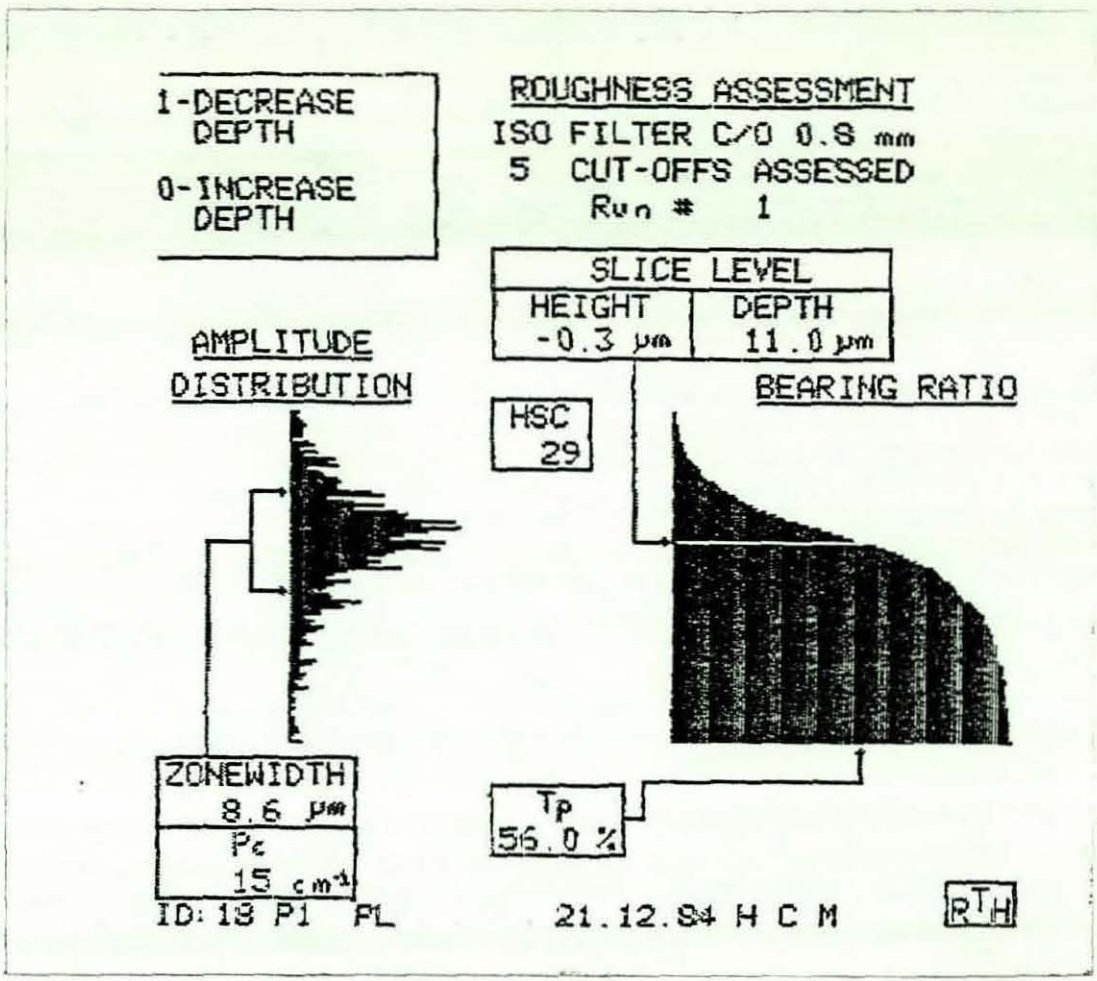
(a)

Ra = 0.57µm

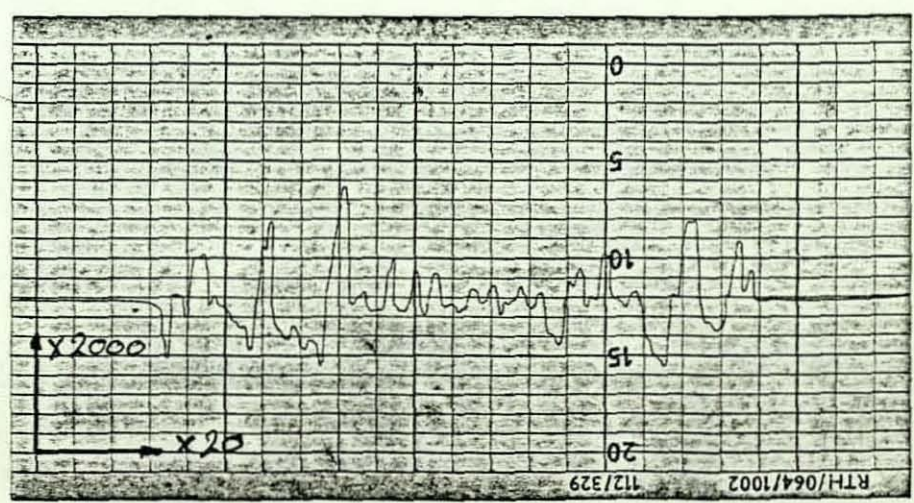


(b)

Fig.76 - Disc Surface Texture After Test. LM30 - 7½wt% Graphite  
(a) Surface Profile. (b) Bearing Area Analysis.



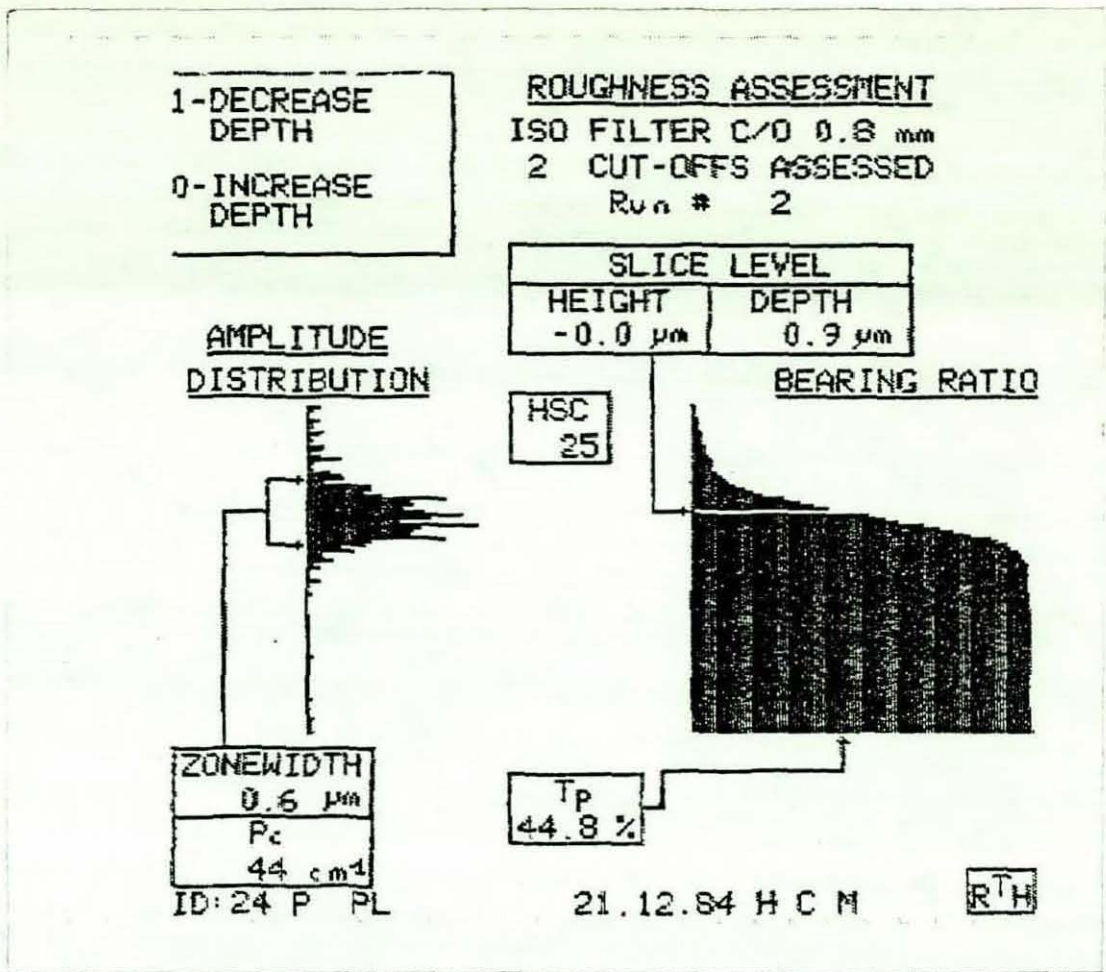
(a)



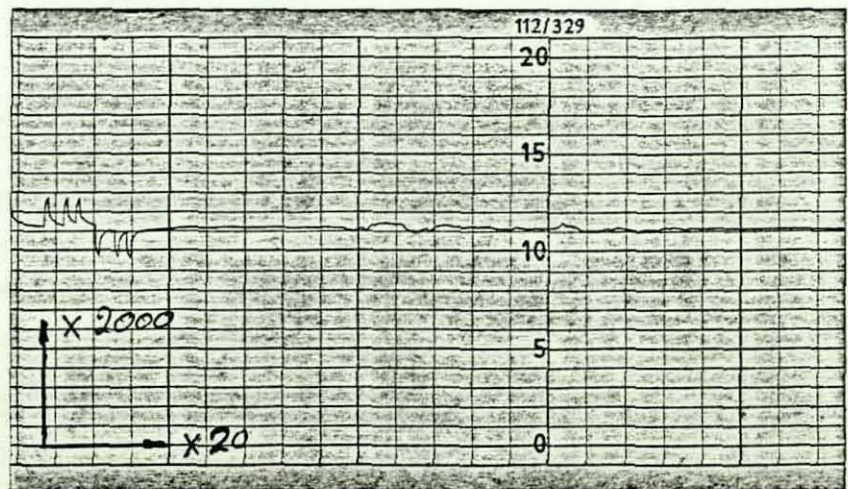
(b)

Ra = 3.34  $\mu\text{m}$

Fig.81 - Pin Surface Texture After Test (Lubricated Friction)  
 LM30 - Rheocast, Pressure Diecast.  
 (a) Bearing Area Analysis. (b) Surface Profile



(a)

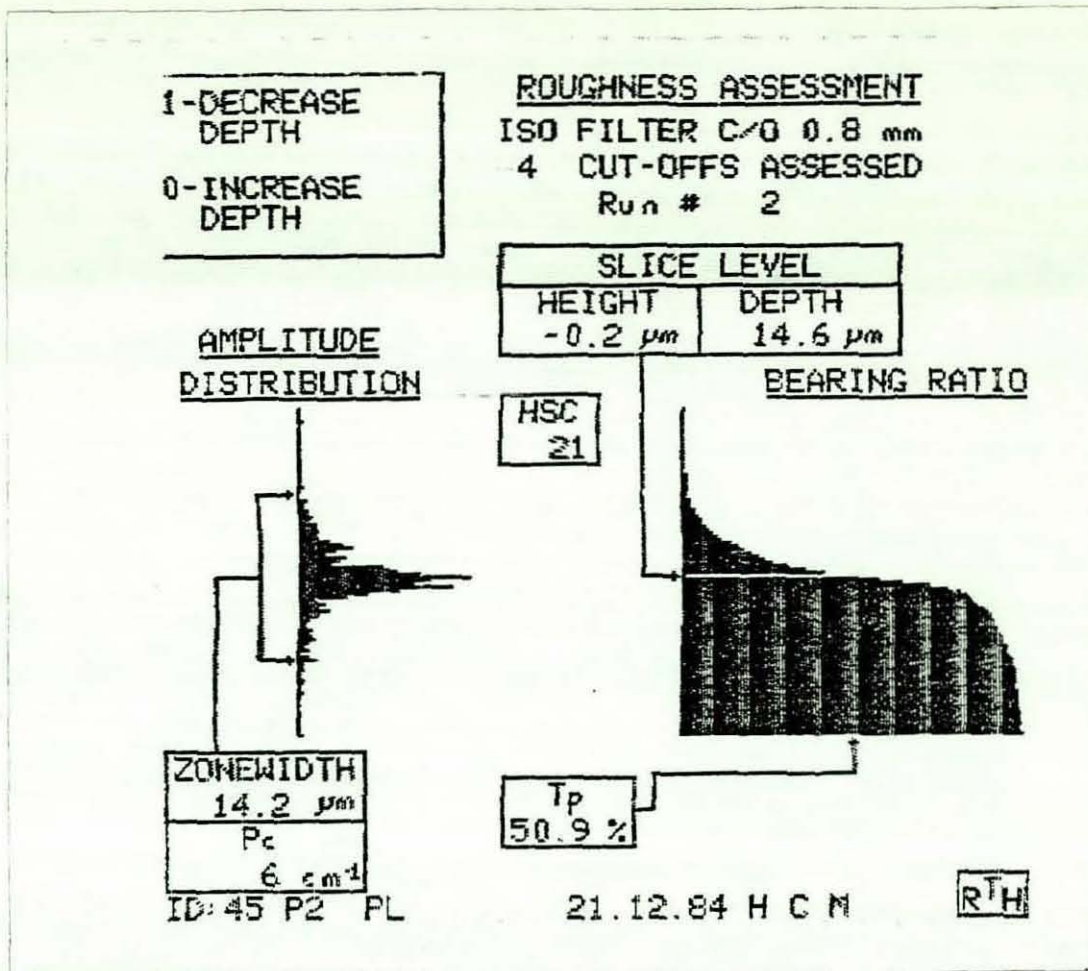


(b)

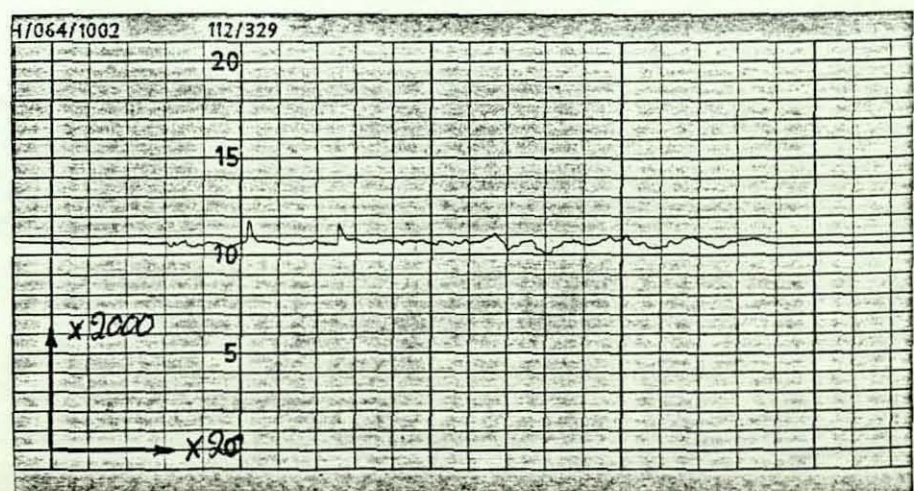
Ra = 0.44  $\mu\text{m}$

Fig.82 - Pin Surface Texture After Test (Lubricated Friction)  
LM30 - 3wt% Graphite.

(a) Bearing Area Analysis. (b) Surface Profile.



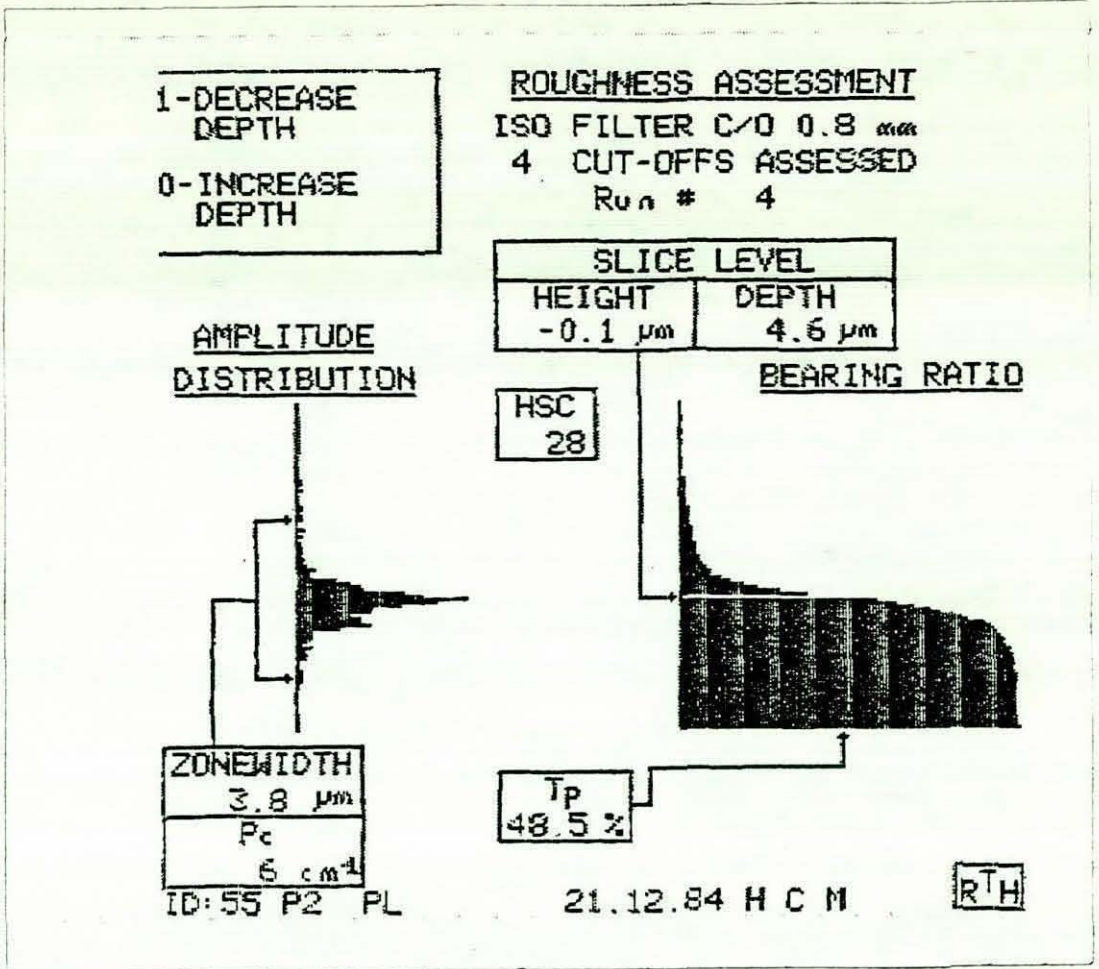
(a)



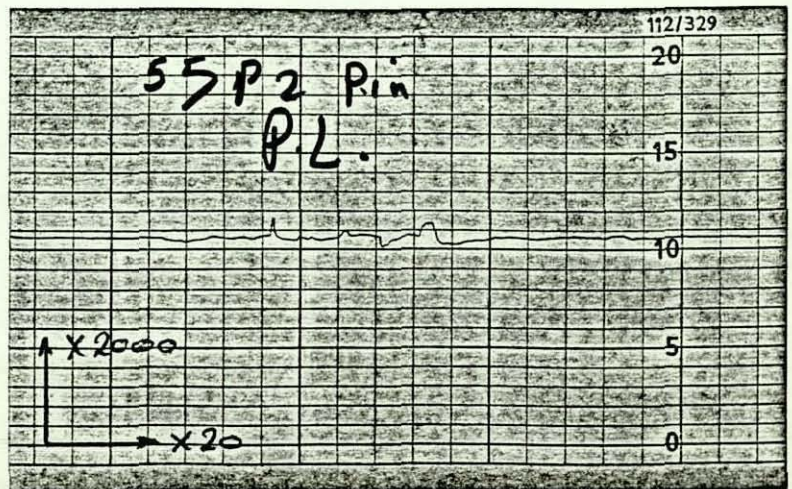
(b)

Ra = 0.49 $\mu\text{m}$

Fig.83 - Pin Surface Texture After Test (Lubricated Friction) LM30 - 4½wt% Graphite.  
 (a) Bearing Area Analysis. (b) Surface Profile.



(a)

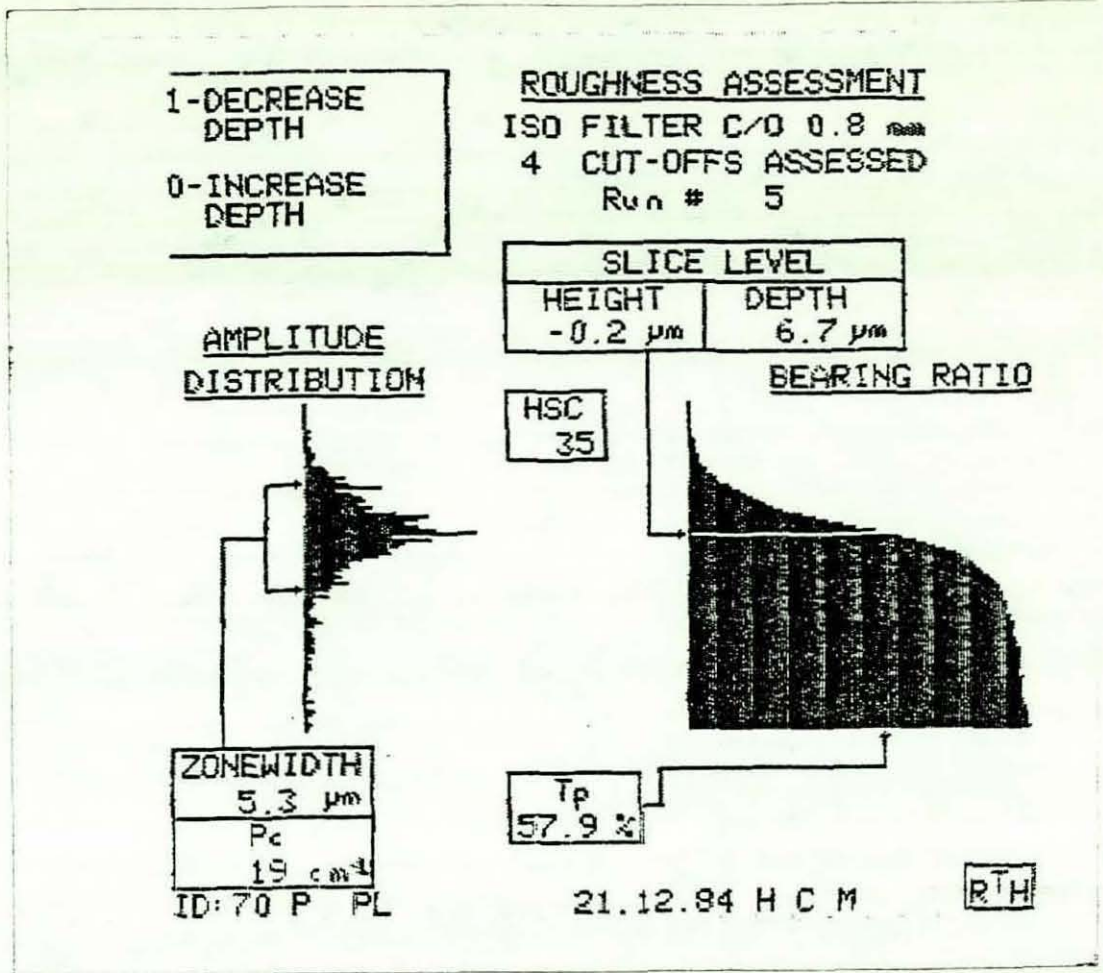


(b)

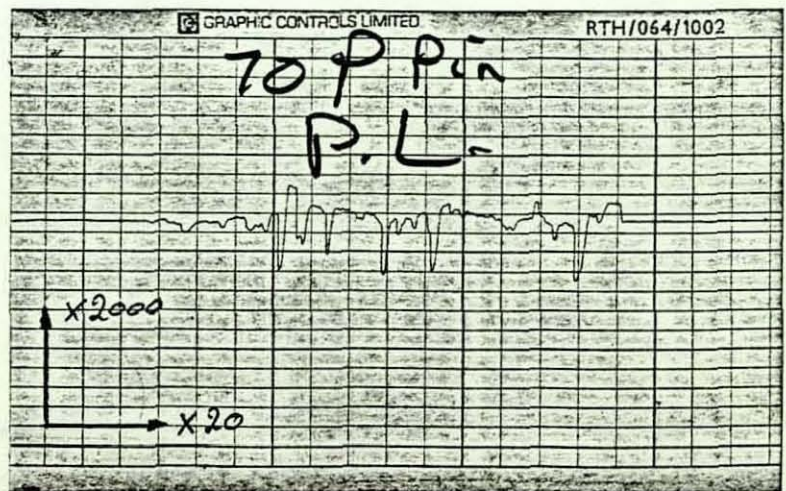
Ra = 0.72  $\mu\text{m}$

Fig.84 - Pin Surface Texture After Test (Lubricated Friction)  
LM30 - 6wt% Graphite.

(a) Bearing Area Analysis. (b) Surface Profile.



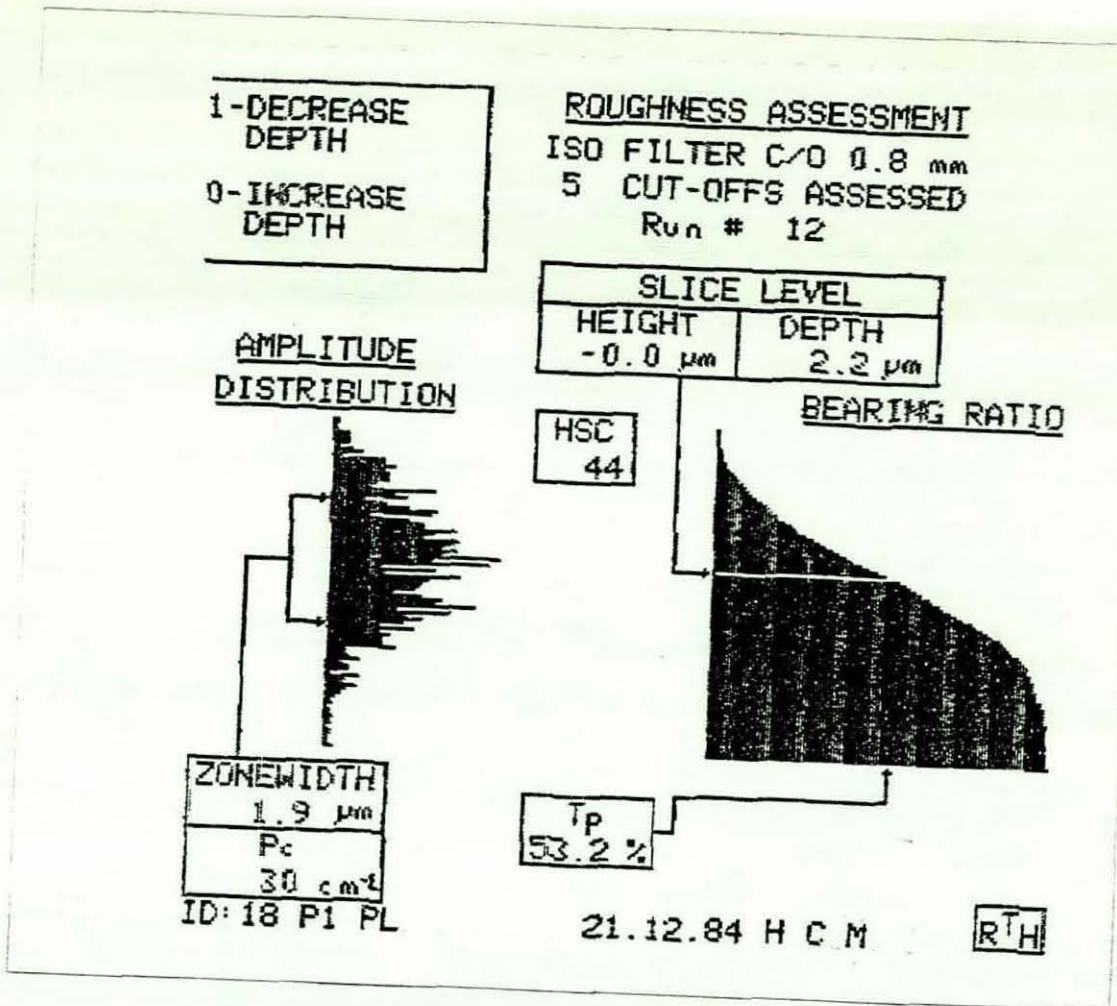
(a)



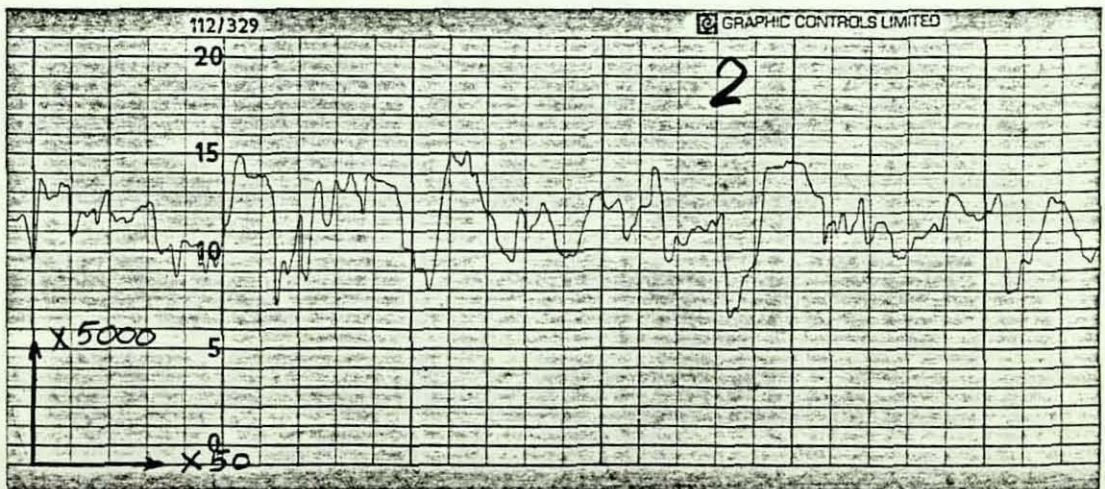
(b)

Ra = 1.60  $\mu\text{m}$

Fig.85 - Pin Surface Texture After Test (Lubricated Friction)  
 LM30 - 7½wt% Graphite.  
 (a) Bearing Area Analysis. (b) Surface Profile.



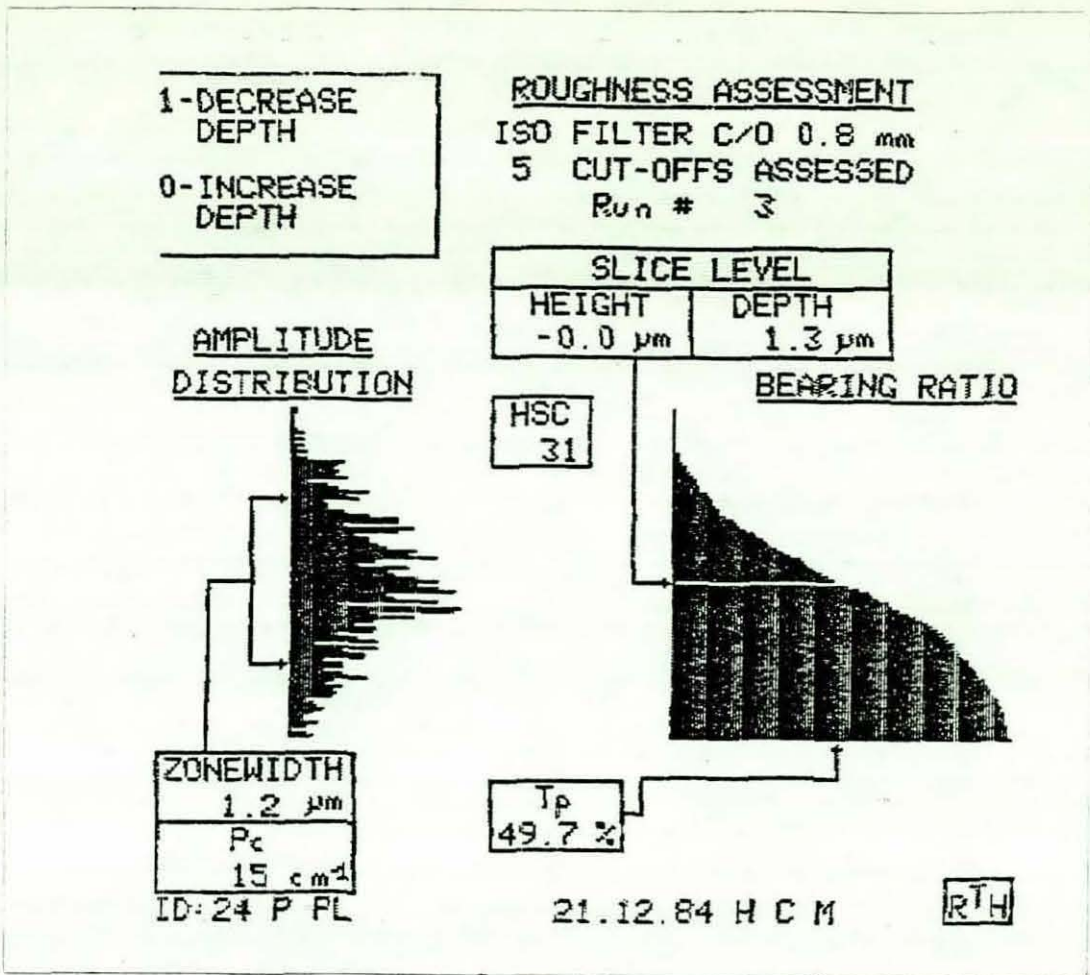
(a)



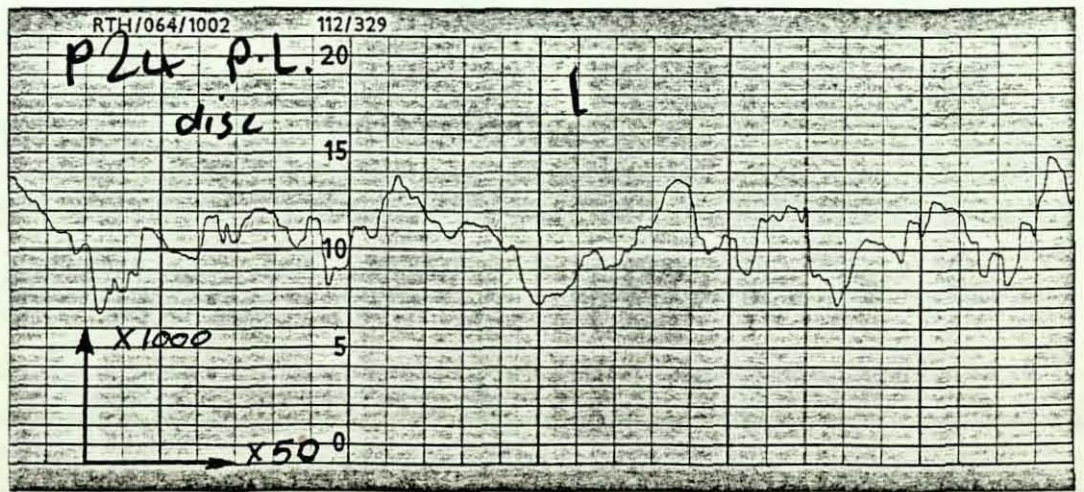
(b)

Ra = 0.74  $\mu\text{m}$

Fig.86 - Disc Surface Texture After Test (Lubricated Friction)  
 LM30 - Rheocast, Pressure Die Cast.  
 (a) Bearing Area Analysis. (b) Surface Profile.



(a)

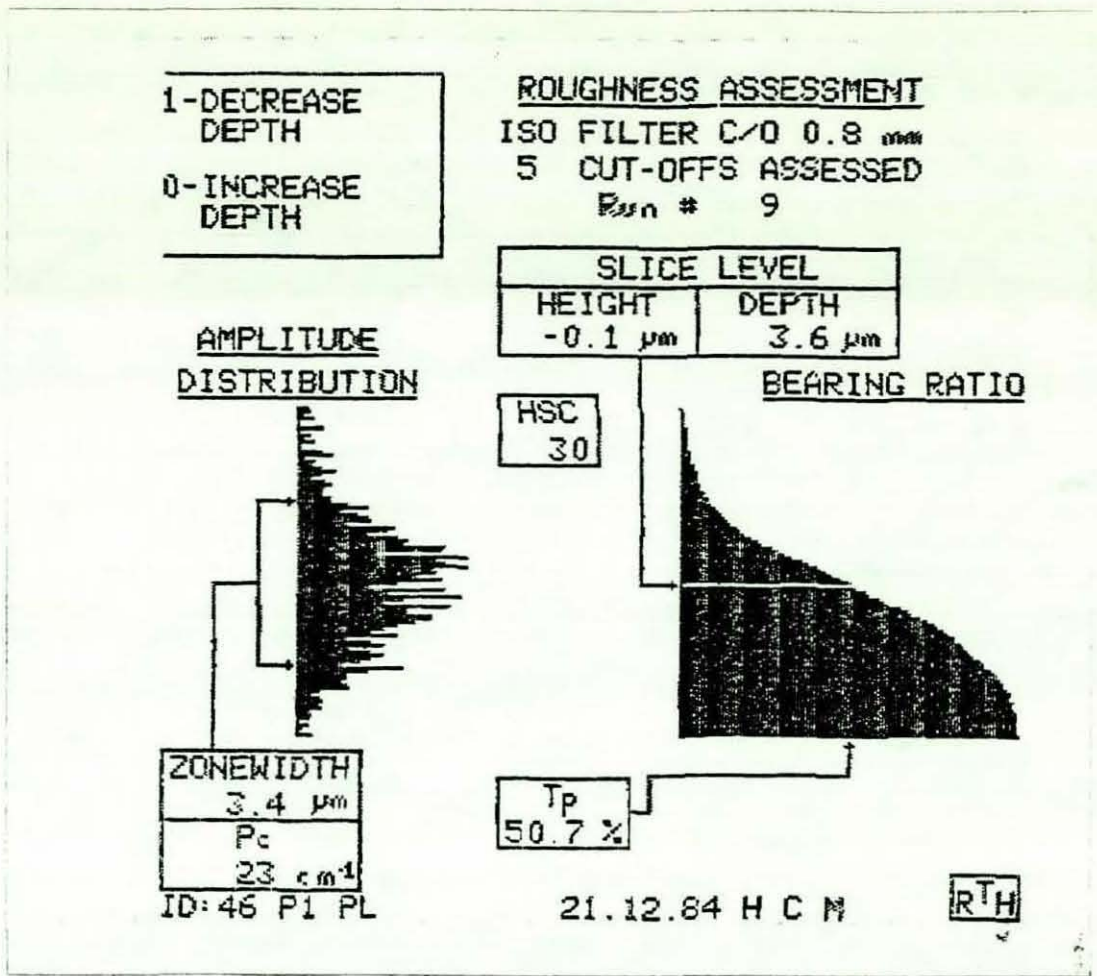


(b)

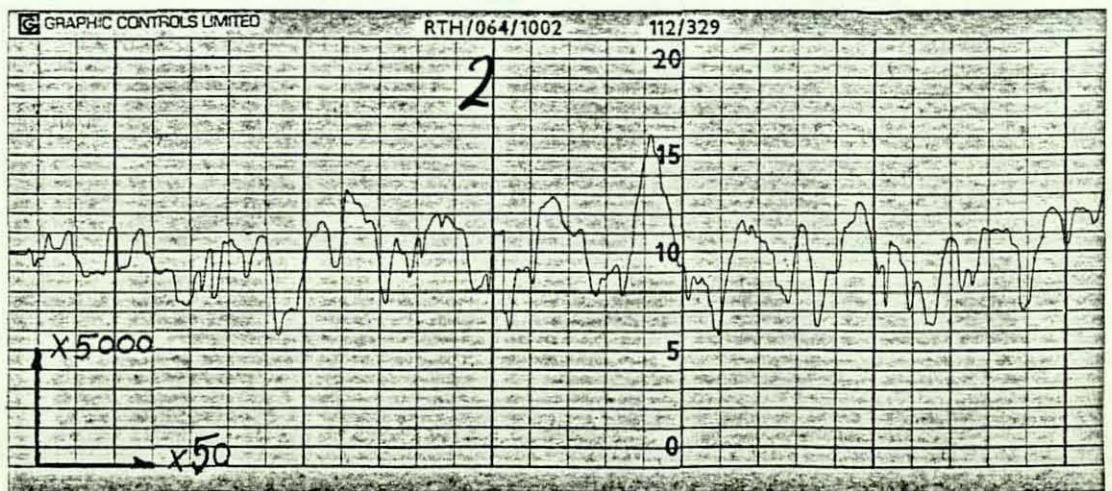
Ra = 0.28  $\mu\text{m}$

Fig.87 - Disc Surface Texture After Test (Lubricated Friction) LM30 - 3wt% Graphite.

(a) Bearing Area Analysis. (b) Surface Profile.



(a)

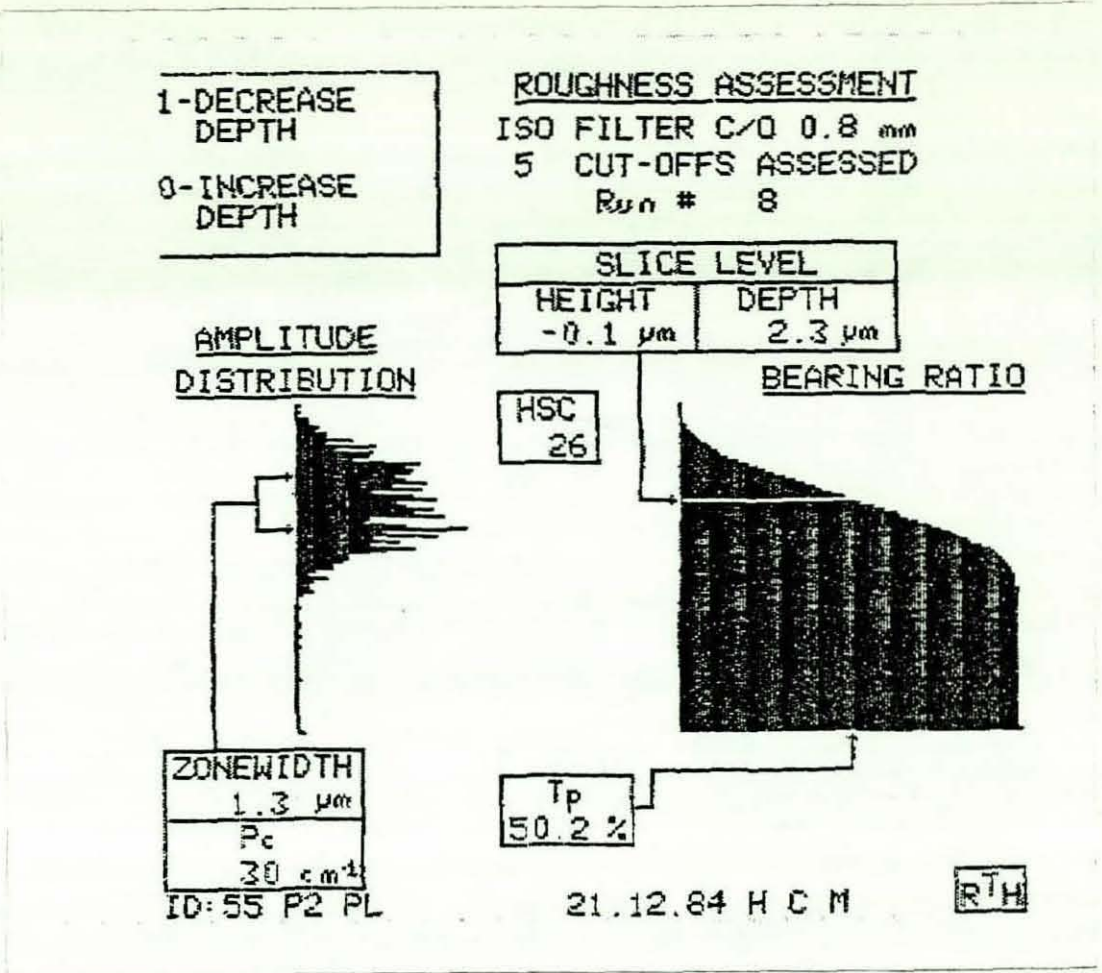


(b)

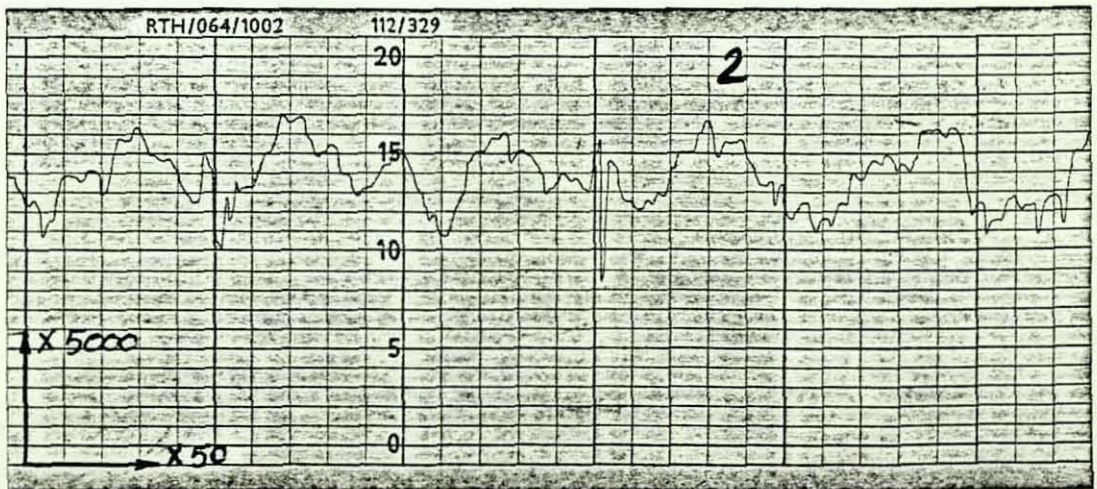
Ra = 0.59 μm

Fig.88 - Disc Surface Texture After Test (Lubricated Friction)  
LM30 - 4½wt% Graphite.

(a) Bearing Area Analysis. (b) Surface Profile.



(a)

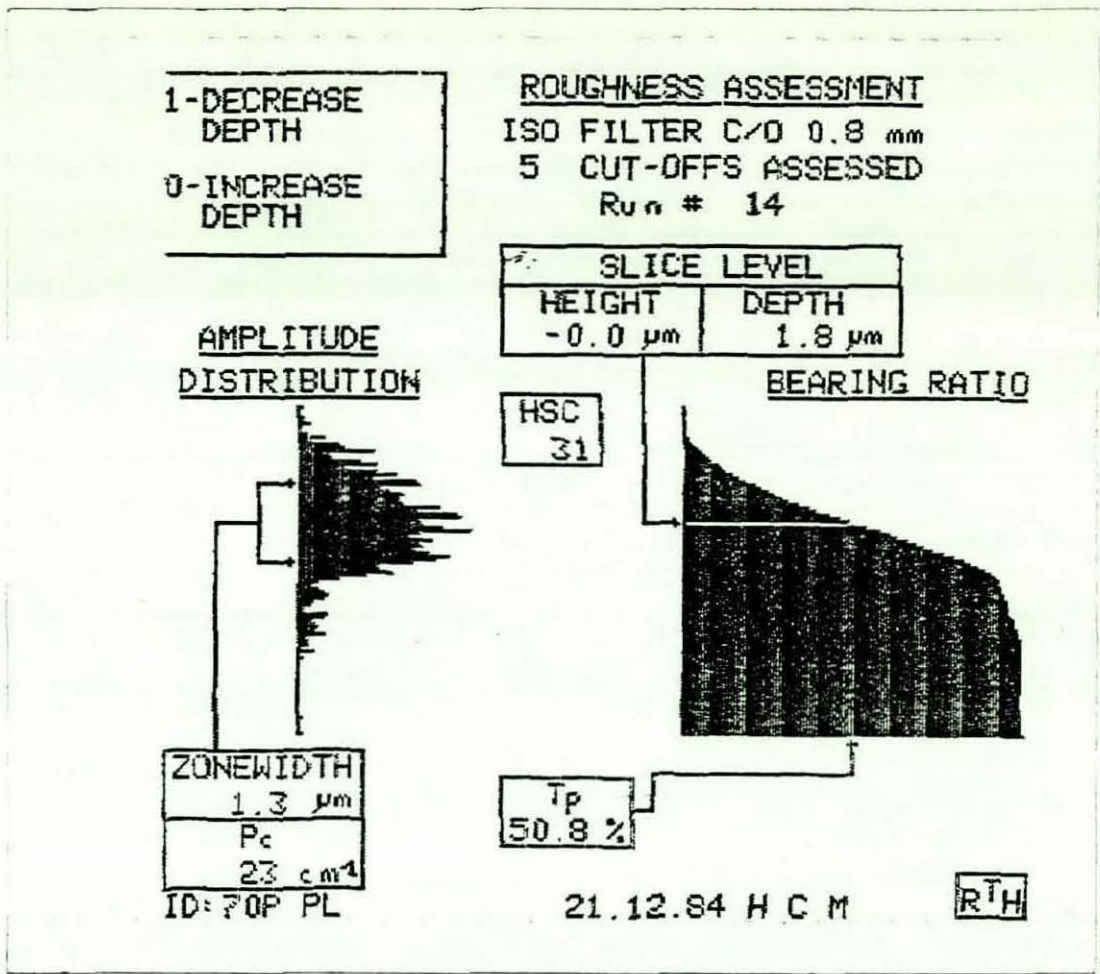


(b)

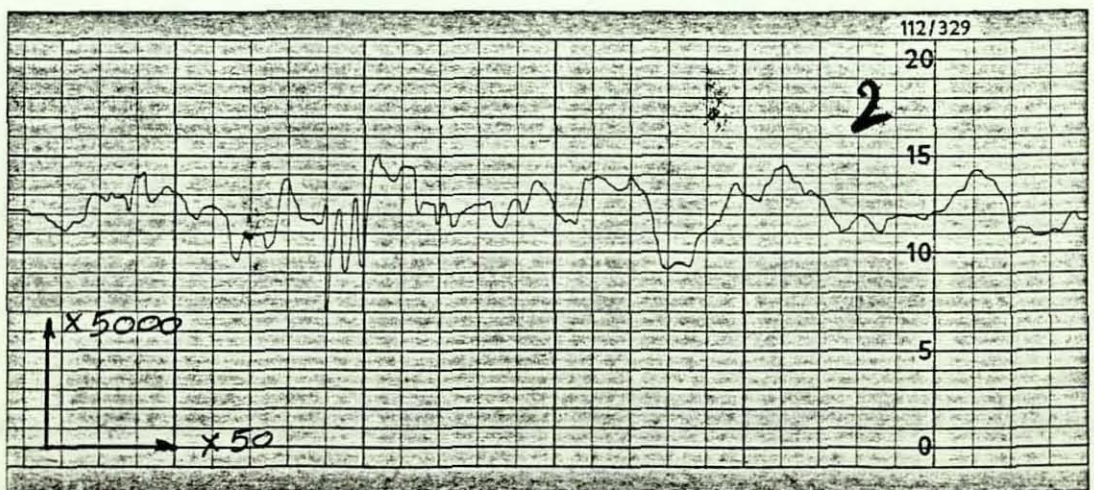
Ra = 0.72  $\mu\text{m}$

Fig.89 - Disc Surface Texture After Test (Lubricated Friction)  
LM30 - 6wt% Graphite.

(a) Bearing Area Analysis. (b) Surface Profile.



(a)



(b)

Ra = 0.82  $\mu\text{m}$

Fig.90 - Disc Surface Texture After Test (Lubricated Friction)  
LM30 - 7½wt% Graphite.

(a) Bearing Area Analysis. (b) Surface Profile.

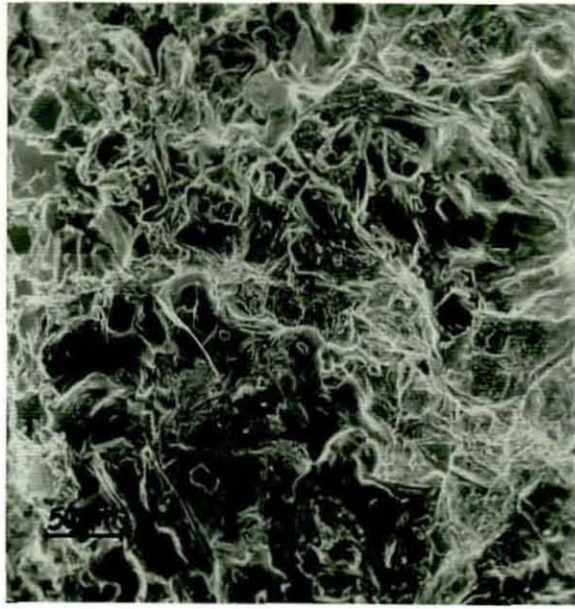


Fig.98 - SEM Micrograph for Pressure  
Die Cast Fractured Surface

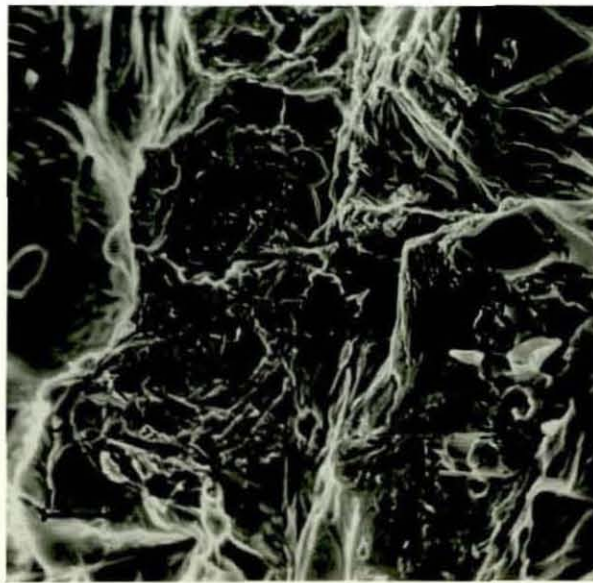


Fig.99 - SEM Micrograph for Pressure  
Die Cast Fractured Surface

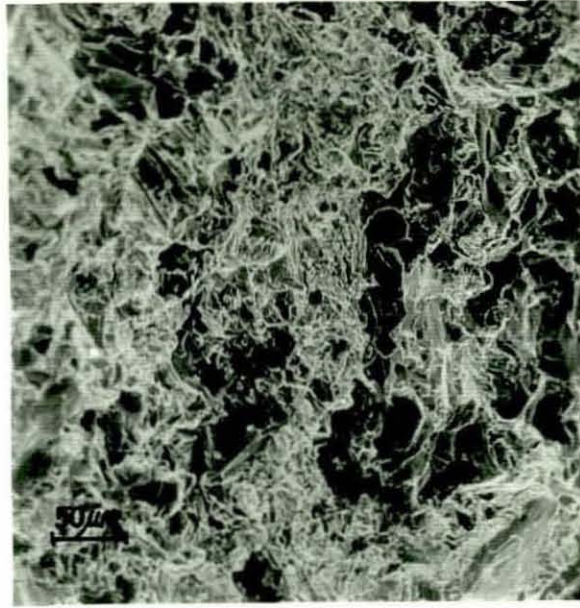


Fig.100 - SEM Micrograph for Rheocast  
Fractured Surface

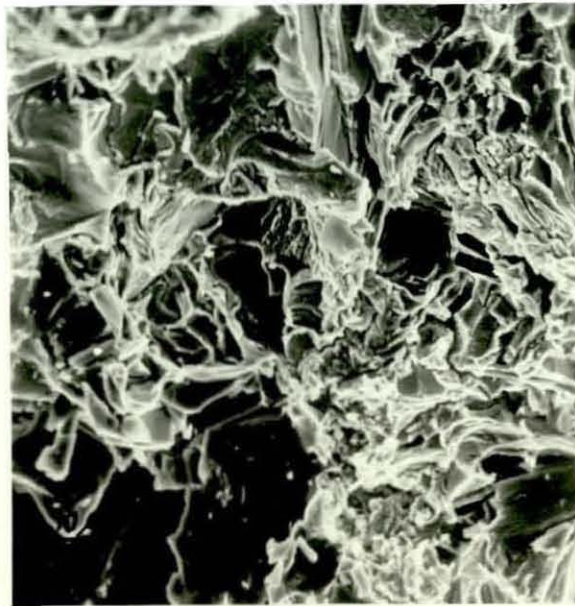


Fig.101 - SEM Micrograph for Rheocast  
Fractured Surface



Fig.102 - SEM Micrograph for Sand Cast  
Fractured Surface

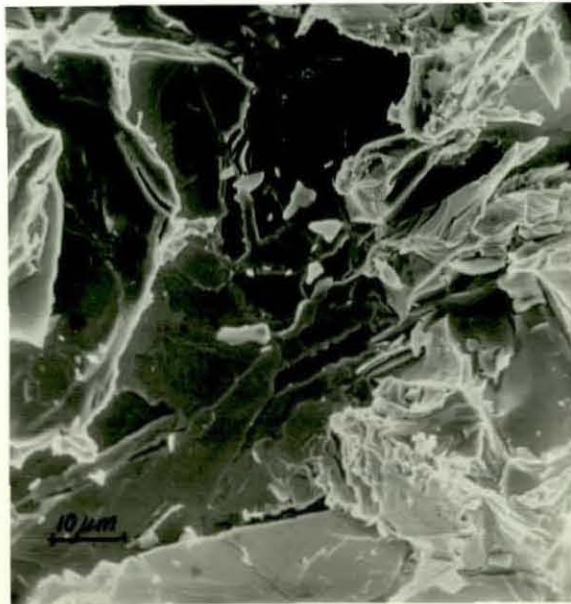


Fig.103 - SEM Micrograph for Sand Cast  
Fractured Surface

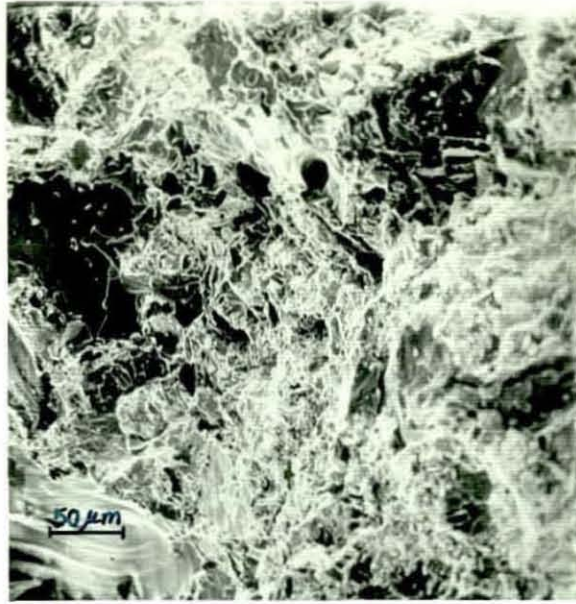


Fig.104 - SEM Micrograph for Compocast  
Fractured Surface With 3%wt  
Coarse Graphite

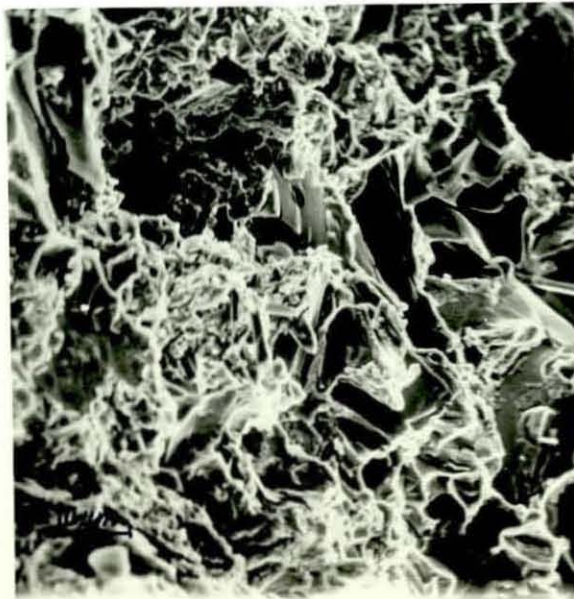


Fig.105 - SEM Micrograph for Compocast  
Fractured Surface With 3%wt  
Coarse Graphite

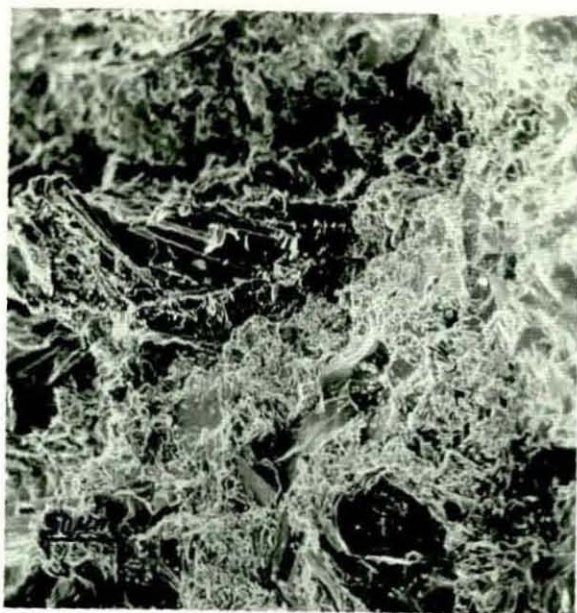


Fig.106 - SEM Micrograph for Compocast  
Fractured Surface With 4½wt  
Course Graphite

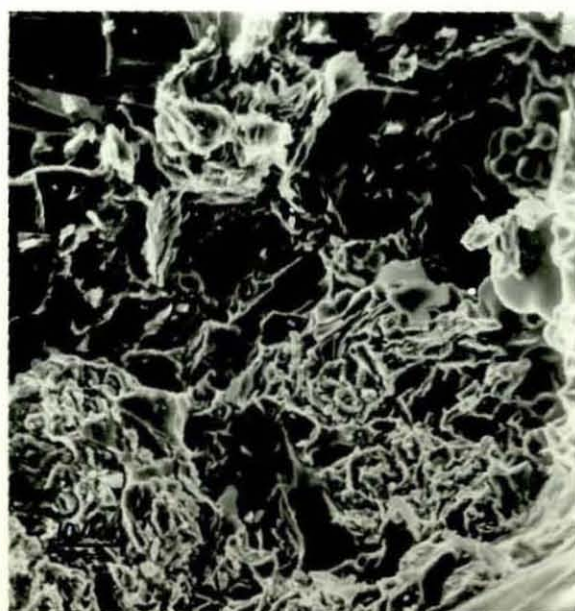


Fig.107 - SEM Micrograph for Compocast  
Fractured Surface with 4½wt  
Coarse Graphite

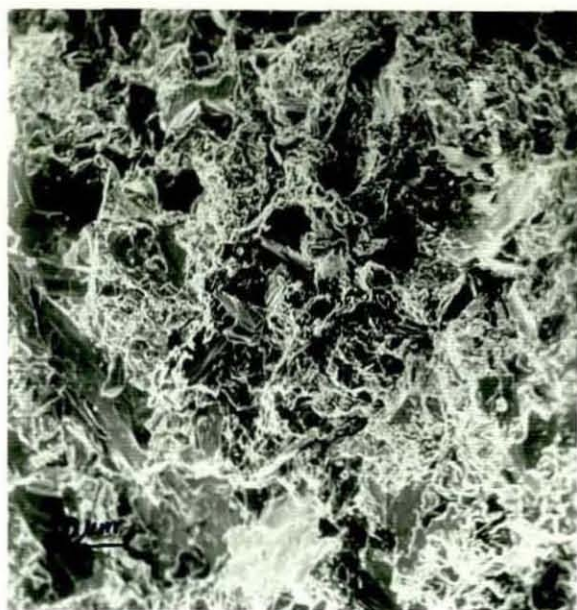


Fig.108 - SEM Micrograph for Compocast  
Fractured Surface with 6%wt  
Coarse Graphite

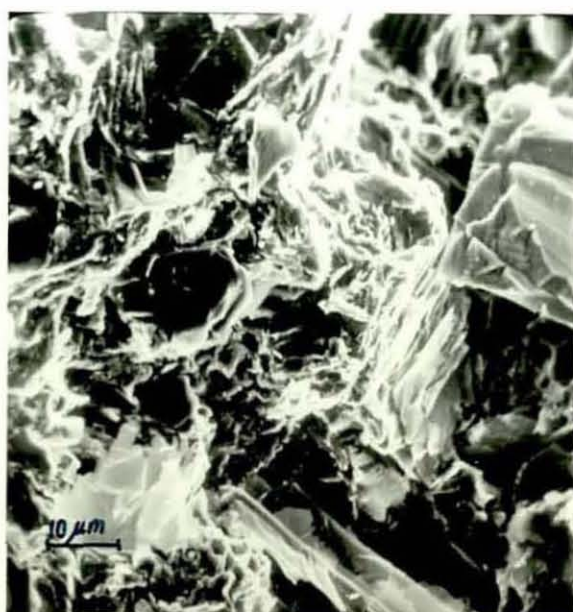


Fig.109 - SEM Micrograph for Compocast  
Fractured Surface with 6%wt  
Coarse Graphite

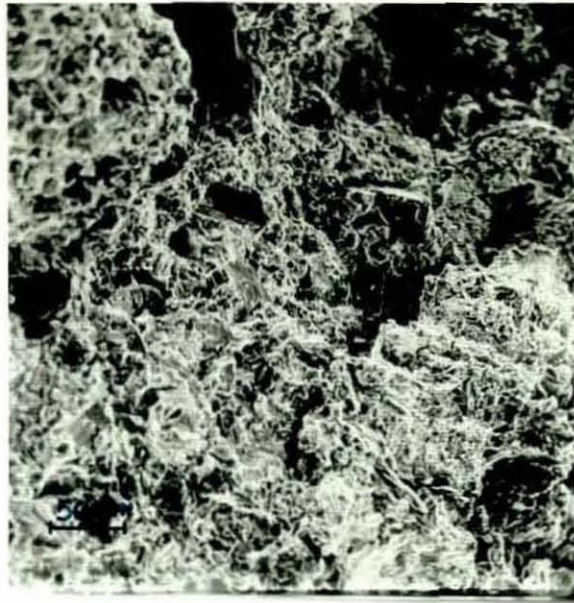


Fig.110 - SEM Micrograph for Compocast  
Fractured Surface With  $7\frac{1}{2}\%$ wt  
coarse Graphite

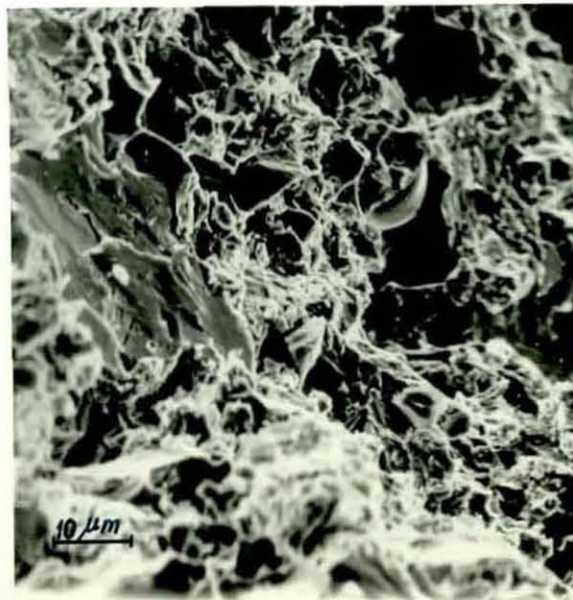


Fig.111 - SEM Micrograph for Compocast  
Fractured Surface With  $7\frac{1}{2}\%$ wt  
Coarse Graphite

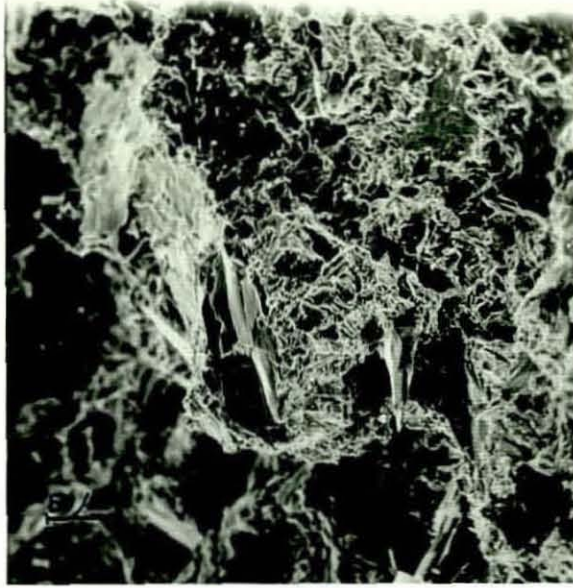


Fig.112 - SEM Micrograph for Compocast  
Fractured Surface With 7 $\frac{1}{2}$ wt  
Medium Fine Graphite

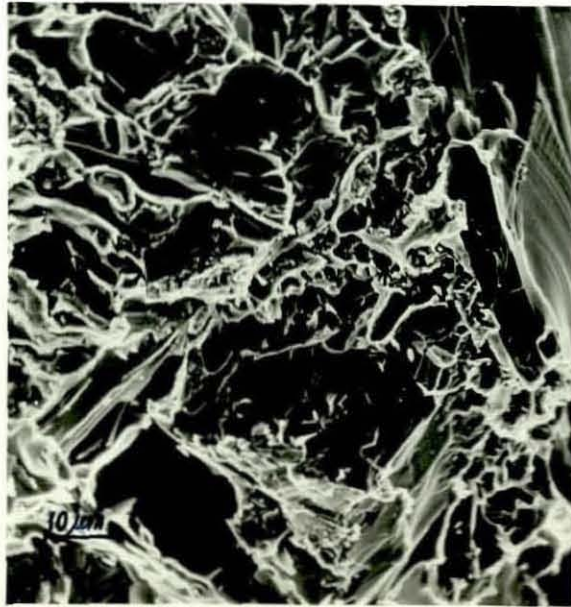


Fig.113 - SEM Micrograph for Compocast  
Fractured Surface With 7 $\frac{1}{2}$ wt  
Medium Fine Graphite

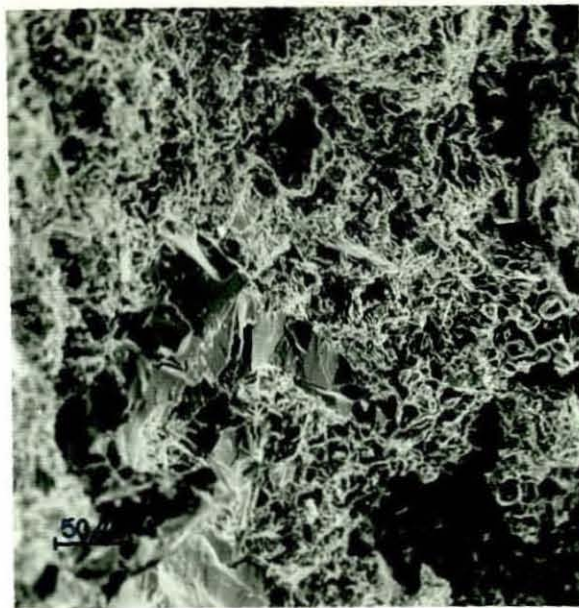


Fig.114 - SEM Micrograph for Compocast  
Fractured Surface With 7 $\frac{1}{2}$ % wt  
Fine Graphite



Fig.115 - SEM Micrograph for Compocast  
Fractured Surface With 7 $\frac{1}{2}$ %wt  
Fine Graphite



fig.118 - SEM Micrograph for Pressure  
Die Cast Worn Surface  
(Dry Friction)

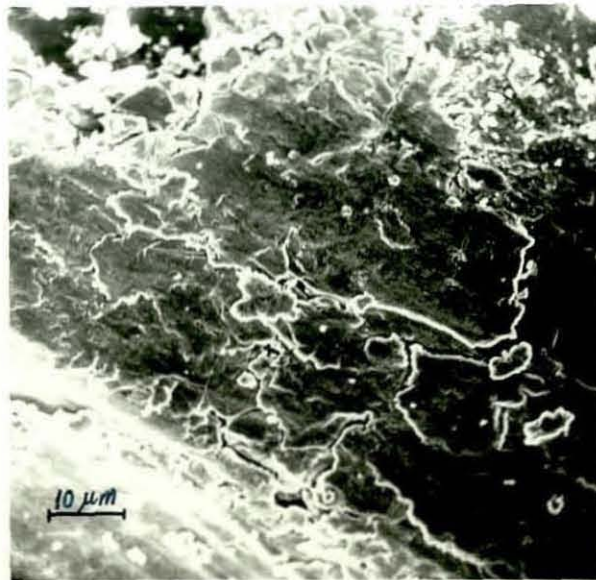


Fig.119 - SEM Micrograph for Pressure  
Die Cast Worn Surface  
(Dry Friction)



Fig.120 - SEM Micrograph for Reocast-Pressure  
Die Cast Worn Surface  
(Dry Friction)



Fig.121 - SEM Micrograph for Rheocast-Pressure  
Die Cast Worn Surface  
(Dry Friction)

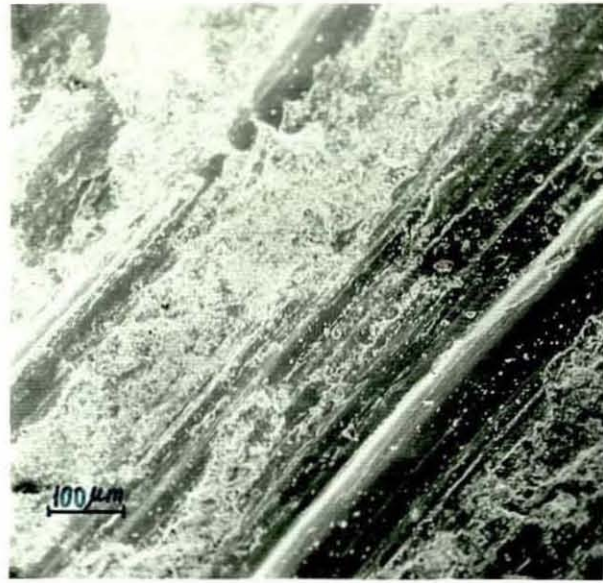


Fig.122 - SEM Micrograph for Sand Cast  
Worn Surface (Dry Friction)

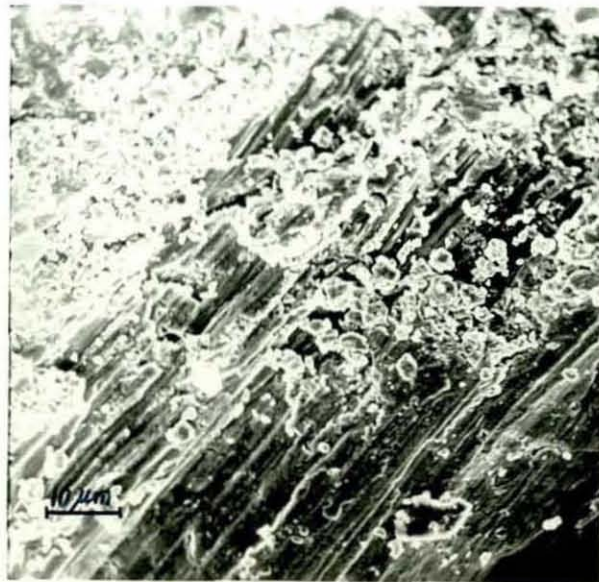


Fig.123 - SEM Micrograph for Sand Cast  
Worn Surface (Dry Friction)



Fig.128 - SEM Micrograph for Compocast Worn Surface  
With 3%wt Coarse Graphite.  
(Dry Friction)



Fig.129 - SEM Micrograph for Compocast Worn Surface  
With 3%wt Coarse Graphite.  
(Dry Friction)

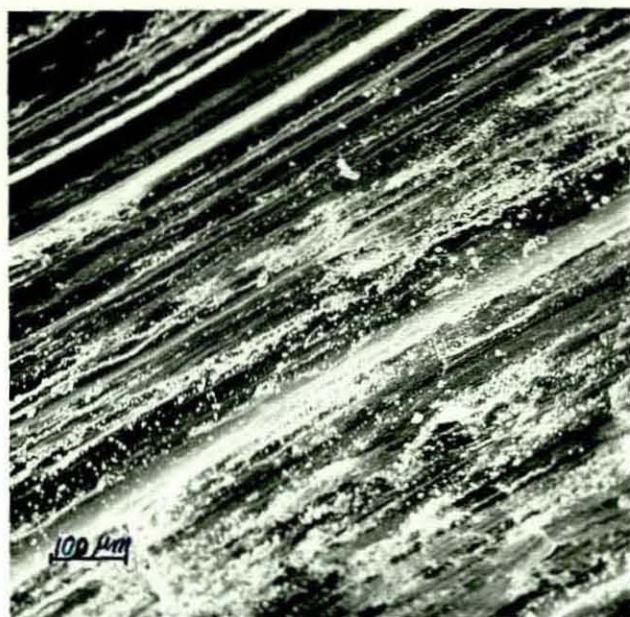


Fig.130 - SEM Micrograph for Compocast Worn Surface  
With 4½%wt Coarse Graphite.  
(Dry Friction)

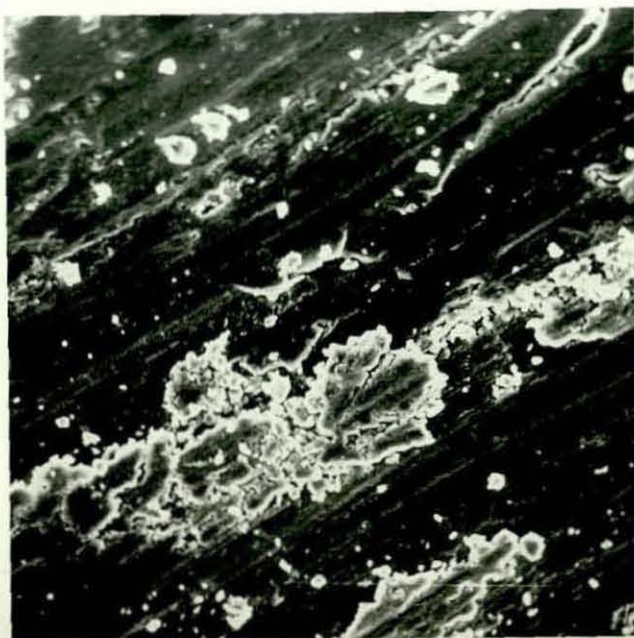


Fig.131 - SEM Micrograph for Compocast Worn Surface  
With 4½%wt Coarse Graphite.  
(Dry Friction)



Fig.132 - SEM Micrograph for Compocast Worn Surface  
With 6%wt Coarse Graphite.



Fig.133 - SEM Micrograph for Compocast Worn Surface  
With 6%wt Coarse Graphite.  
(Dry Friction)

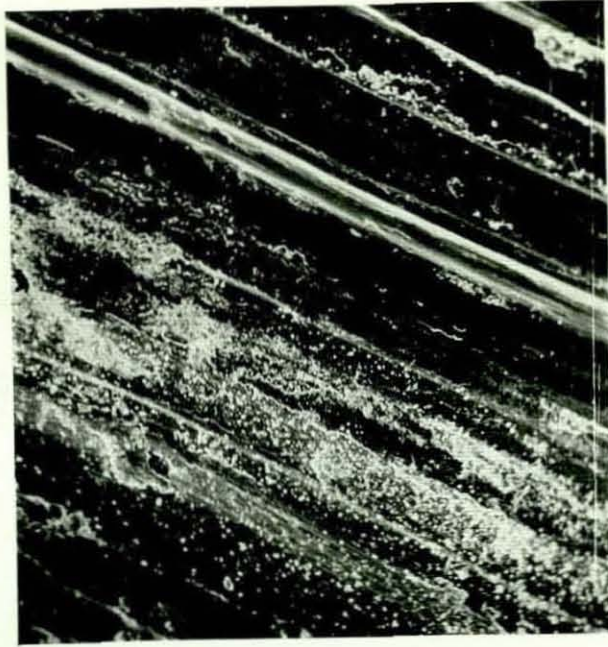


Fig.134 - SEM Micrograph for Compocast Worn Surface  
With 7½%wt Coarse Graphite.  
(Dry Friction)

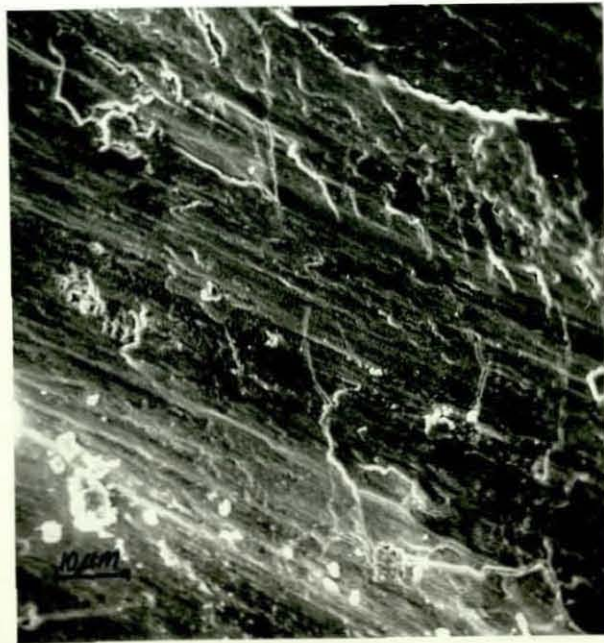


Fig.135 - SEM Micrograph for Compocast Worn Surface  
With 7½%wt Coarse Graphite.

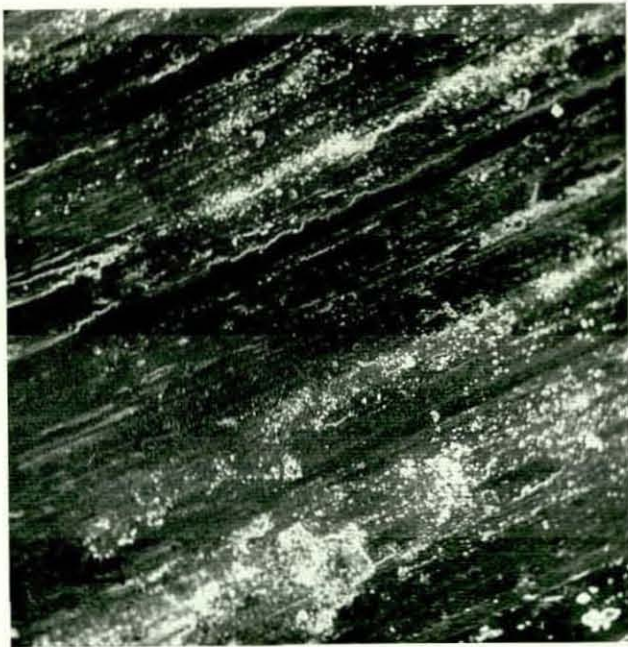


Fig.136 - SEM Micrograph for Compocast Worn Surface  
With 7½%wt Medium Fine Graphite.  
(Dry Friction)



Fig.137 - SEM Micrograph for Compocast Worn Surface  
With 7½%wt Medium Fine Graphite.

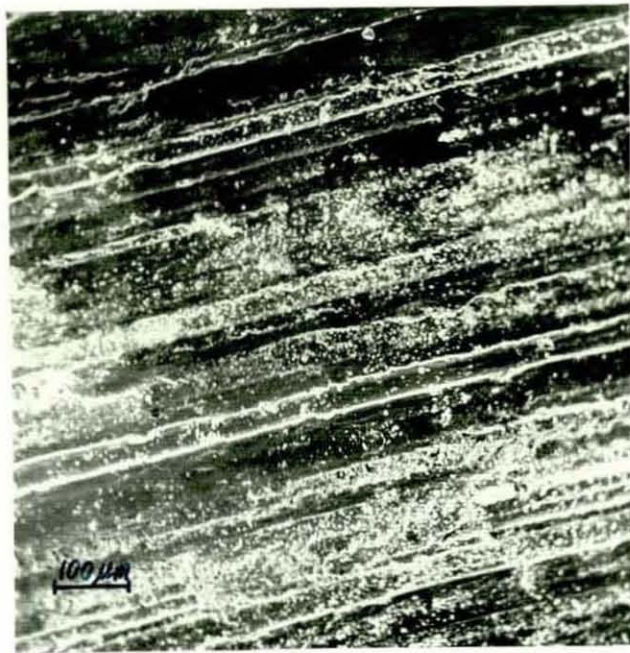


Fig.138 - SEM Micrograph for Compocast Worn Surface  
With 7½%wt Fine Graphite.

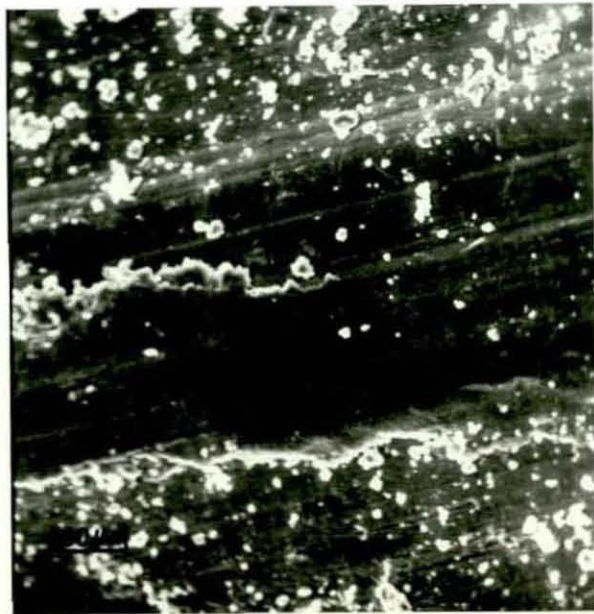


Fig.139 - SEM Micrograph for Compocast Worn Surface  
With 7½%wt Fine Graphite.

